

**Extracellular matrix-inspired surface coatings
functionalized with cargo lipids as a delivery system to
induce osteo- and chondrogenesis**

Dissertation

zur Erlangung des
Doktorgrades der Naturwissenschaften (Dr. rer. nat.)

der

Naturwissenschaftlichen Fakultät I – Biowissenschaften –

der Martin-Luther-Universität
Halle-Wittenberg,

vorgelegt

von Frau MSc. Yazmin Angelina, Brito Barrera

geb. am 28.01.1988 in Puebla, Mex

Gutachter: Prof. Dr. rer. nat. habil. Thomas Groth
PD Dr. Christian Schmelzer
Prof. Dr. Nuno Neves

Halle (Saale), 24.05.2023

To my family

Table of Contents

Abbreviations.....	5
Graphical abstract	7
Abstract	8
Zusammenfassung	10
Chapter 1: Introduction	13
Introduction.....	14
1. Basis of bone tissue: structure and functions	14
1.1. Bone remodeling and healing process.....	15
2. General overview of health situation and medical treatment	17
2.1 Evolution of orthopedic implants materials.....	18
2.2 The importance of osseointegration in implants.....	21
3. Surface modifications of implant materials	22
3.1 General overview Layer-by-Layer technique.....	25
3.2 Chemical and biological information of polyelectrolytes for multilayers.....	27
4. Mesenchymal stem cells for tissue engineering.....	31
4.1 Osteogenic differentiation of MSCs.....	33
4.2 Chondrogenic differentiation of MSCs.....	35
4.3 Role of dexamethasone and media supplements on chondrogenic and osteogenic differentiation	37
5. Modern technologies for drug delivery: nanoparticles.....	39

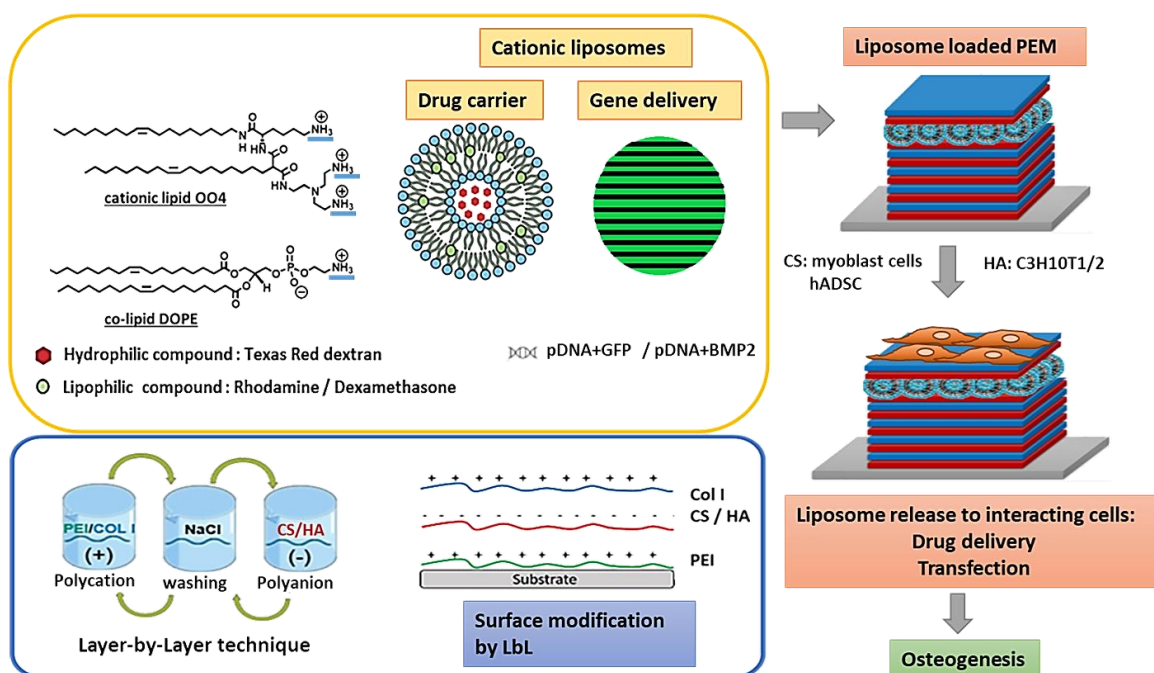
5.1 Overview of endocytic mechanisms for drug delivery	41
6. Survey of modern technologies for transfection of nucleic acids	41
6.1 Overview of cationic liposomes as a transfection system	43
7. Aim of this study	45
8. References	46
Chapter 2: Engineering osteogenic microenvironments by combination of multilayers from collagen type I and chondroitin sulfate with novel cationic liposomes	53
Chapter 3: Extracellular matrix-inspired surface coatings functionalized with Dexamethasone-loaded liposomes to induce osteo- and chondrogenic differentiation of multipotent stem cells	69
Chapter 4: Lipoplex-functionalized thin-film surface coating based on extracellular matrix components as local gene delivery system to control osteogenic stem cell differentiation	86
Summary and future perspectives	107
Acknowledgment	109
Publication list with declaration of self-contribution to research articles	111
Curriculum vitae.....	112
Selbstständigkeitserklärung.....	116

Abbreviations

ACAN	aggrecan
ADSCs	adipose-derived stem cells
ALP	alkaline phosphatase
ASC	ascorbic acid
BMP	bone morphogenetic protein
BSP	bone sialoprotein
Col I	collagen I
Cs	chondroitin sulfate
Dex	dexamethasone
DOPE	dioleoylphosphatidylethanolamine
ECM	extracellular matrix
FGF	fibroblast growth factor
FHL-2	four-and-a-half LIM-2
GAGs	glycosaminoglycans
GFP	green fluorescent protein
HA	hyaluronic acid
LbL	Layer by layer
LPX	lipoplexes
M-CSF	macrophage colony-stimulating factor
MDSCs	bone marrow-derived stem cells
MSCs	mesenchymal stem cells
NCPs	non-collagenous proteins
NPs	nanoparticles
OA	Osteoarthritis
OI	osseointegration
OO4	N-{6-amino-1[N-(9Z)-octadec-9-enylamino]-1-oxohexan-(2S)-2-yl}-N'-{2-[N,N-bis(2-aminoethyl)amino]ethyl}-2[(9Z)-octadec-9enyl]propandiamide
OPN	osteopontin
OSC	osteocalcin
OSX	osterix

pDNA	plasmid DNA
PEG	poly (ethylene glycol)
PEI	polyethyleneimine
PEM	polyelectrolyte multilayer system
PGA	polyglycolic acid
PGs	proteoglycans
PLA	poly lactic acid
RANKL	activator of nuclear factor- κ B ligand
RME	receptor-mediated endocytosis
qRT-PCR	quantitative real-time polymerase chain reaction
Runx2	runt-related transcription factor 2
Sox9	SRY-box 9 protein
TAZ	transcriptional co-activator with PDZ-binding motif
TCF/LEF-1	T-cell factor/lymphoid enhancer-binding factor
TGF-b1	transforming growth factor- b1
TSG-6	tumor necrosis factor-stimulated gene-6
WCA	water contact angle
Wnt	wingless-related integration site

Graphical abstract



Schematic illustration of the general overview of thesis chapters. The image shows the preparation of cationic liposomes using the cationic lipid OO4 and the zwitterionic co-lipid DOPE (protonation state at pH 4). The liposomes can be used as a carrier for hydrophilic, lipophilic drugs like dexamethasone (Dex) as well as plasmid DNA (pDNA). Due to the cationic charge, the liposomes can be embedded in polyelectrolyte multilayers (PEM), which are prepared from collagen I (Col) as polycation and chondroitin sulfate (Cs) and hyaluronic acid (HA) as polyanions using the Layer-by-Layer technique (LbL). Poly (ethylene imine) (PEI) was used for the initial modification of the substrate to achieve a positive surface charge. The liposomes embedded in the PEM can be internalized by cells growing on the modified substrate. This work was focusing on the physicochemical properties of the multilayers as well as the cell studies such as adhesion, metabolic activity, and cell differentiation. The Cs system used myoblast cells and the HA system used C3H10T1/2 for drug delivery of liposomes loaded with Dex. In the transfection part, the Cs system used human adipose-derived stem cells (hADSC) to transfect the plasmid DNA (pDNA) with green fluorescence protein and subsequently pDNA and bone morphogenetic protein 2 (BMP-2). Both systems were used to induce osteogenic differentiation.

Abstract

Biomimetic surface coatings can be combined with conventional implants to mimic the extracellular matrix (ECM) of the surrounding tissue to make them more biocompatible. The layer-by-layer technique (LbL) can be used for making surface coatings by alternating the adsorption of polyelectrolytes from aqueous solutions to form polyelectrolyte multilayers (PEM). In addition, cationic liposomes composed of (N-(6-amino-1-[N-(9Z)-octadec-9-enylamino]-1-oxohexan-(2S)-2-yl)-N'-{2-[N,N-bis(2-aminoethyl)amino]ethyl}-2-hexadecylpropanoamide) (OO4) and dioleoylphosphatidylethanolamine (DOPE) are promising systems for drug delivery and transfection system. Hence, two different approaches were combined to develop a functionalized surface coating: (i) a PEM surface coating that mimics the natural ECM of connective tissue by a combination of collagen type I (col) and glycosaminoglycans such as chondroitin sulfate (Cs) or hyaluronic acid (HA) and (ii) the immobilization of cargo-loaded liposomes using lipophilic and hydrophilic model compounds for drug delivery. This research presented the physicochemical characteristics of the multilayer films, such as surface zeta potential, thickness, layer growth, wettability, and topography. The characterization studies demonstrated a stable, uniform film with immobilization of the liposomes that can be taken up by myoblast cells (C2C12) even when covered with an additional bilayer of Cs and Col shown by studies with either hydrophilic or lipophilic model compounds. Subsequently, as a proof of concept, dexamethasone (Dex) was used as a lipophilic drug for potential local delivery at the defect site. This work has shown that the use of Dex embedded in liposomes in the Cs and Col system can be used to induce osteogenic in C2C12, and also Dex-embedded liposomes in HA and Col system can induce osteo and chondrogenic differentiation of C3H10T1/2 cells in situ. In both systems, the cell studies have shown good cell

adhesion which is important for the integration of implants related to cell growth and differentiation. The ability of the PEM-loaded Dex to induce osteogenic cell differentiation was observed qualitatively and quantitatively by positive histochemical staining of Alizarin red, fluorescence staining of osteo – chondrogenic markers, and quantification of osteogenic markers by qRT-PCR. In the last part, the liposomes were loaded with plasmid DNA (pDNA) with a green fluorescent protein (GFP) to form lipoplexes (LPX). The results showed a positive transfection efficiency of pDNA-GFP. Then, the liposomes were loaded with pDNA with bone morphogenetic protein 2 (BMP2), in order to develop a transfection system to increase the amount of growth factor BMP2 in human adipose-derived stem cells (hADSC) for osteogenic differentiation. PEM loaded with LPX using pDNA-BMP2 showed a positive transfection and the presence of hydroxyapatite after 24 days and positive staining of alizarin red which gives a hint of osteogenic differentiation. Then, osteogenic markers were quantified by qRT-PCR. For that reason, using cationic liposomes OO4/ DOPE is beneficial for the loading of pDNA-BMP2 to have an excellent transfection efficiency and promote osteogenic differentiation, avoid the use of direct growth factors, and reduce toxicity.

These findings indicate that designed OO4/DOPE-loaded PEMs have a high potential to be used as drug delivery or transfection system for implant coating in the field of bone regeneration and other applications.

Zusammenfassung

Biomimetische Oberflächenbeschichtungen können mit herkömmlichen Implantaten kombiniert werden, um die extrazelluläre Matrix (ECM) des umgebenden Gewebes nachzuahmen und sie biokompatibler zu machen. Die Layer-by-Layer-Technik (LbL) kann zur Herstellung von Oberflächenbeschichtungen verwendet werden, indem Polyelektrolyte aus wässrigen Lösungen abwechselnd adsorbiert werden, um Polyelektrolyt-Multischichten (PEM) zu bilden. Darüber hinaus sind kationische Liposomen, die aus (N-{6-Amino-1-[N-(9Z)-octadec9-enylamino]-1-oxohexan-(2S)-2-yl}-N'-{2-[N,N-bis(2-aminoethyl)amino]ethyl}-2-hexadecylpropandiamid) (OO4) und Dioleoylphosphatidylethanolamin (DOPE) bestehen, vielversprechende Systeme für die Verabreichung von Arzneimitteln und für Transfektionssysteme. Daher wurden zwei verschiedene Ansätze kombiniert, um eine funktionalisierte Oberflächenbeschichtung zu entwickeln: (i) eine PEM-Oberflächenbeschichtung, die natürliche ECM des Bindegewebes durch eine Kombination von Kollagen Typ I (Col) und Glykosaminoglykanen wie Chondroitinsulfat (Cs) oder Hyaluronsäure (HA) nachahmt, und (ii) die Immobilisierung von frachtbeladenen Liposomen unter Verwendung lipophiler und hydrophiler Modellverbindungen für die Wirkstoffabgabe. Im Rahmen dieser Forschungsarbeit wurden die physikochemischen Eigenschaften der Mehrschichtfilme wie Oberflächen-Zetapotenzial, Dicke, Schichtwachstum, Benetzbarkeit und Topografie untersucht. Die Charakterisierungsstudien zeigten einen stabilen, einheitlichen Film mit Immobilisierung der Liposomen, die von Myoblastenzellen (C2C12) aufgenommen werden können, selbst wenn sie mit einer zusätzlichen Doppelschicht aus CS und Col bedeckt sind, wie Studien mit hydrophilen oder lipophilen Modellverbindungen zeigten. Anschließend wurde als Konzeptnachweis Dexamethason (Dex) als lipophiles Medikament für eine mögliche

lokale Verabreichung an der Defektstelle verwendet. Diese Arbeit hat gezeigt, dass die Verwendung von in Liposomen eingebettetem Dex im CS- und Col-System zur Induktion der Osteogenese in C2C12 verwendet werden kann, und dass auch in HA- und Col-System eingebettete Dex-Liposomen die osteo- und chondrogene Differenzierung von C3H10T1/2-Zellen in situ induzieren können. In beiden Systemen haben die Zellstudien eine gute Zelladhäsion gezeigt, die für die Integration von Implantaten in Bezug auf Zellwachstum und -differenzierung wichtig ist. Die Fähigkeit des mit PEM beladenen Dex, eine osteogene Zelldifferenzierung zu induzieren, wurde qualitativ und quantitativ durch eine positive histochemische Färbung von Alizarinrot, eine Fluoreszenzfärbung von osteo-chondrogenen Markern und eine Quantifizierung osteogener Marker durch qRT-PCR beobachtet. Im letzten Teil wurden die Liposomen mit Plasmid-DNA (pDNA) mit einem grün fluoreszierenden Protein (GFP) beladen, um Lipoplexe (LPX) zu bilden. Die Ergebnisse zeigten eine positive Transfektionseffizienz von pDNA-GFP. Anschließend wurden die Liposomen mit pDNA mit Knochenmorphogeneseprotein 2 (BMP2) beladen, um ein Transfektionssystem zu entwickeln, das die Menge des Wachstumsfaktors BMP2 in humanen Stammzellen aus Fettgewebe (hADSC) zur osteogenen Differenzierung erhöht. PEM, die mit LPX unter Verwendung von pDNA-BMP2 beladen wurden, zeigten eine positive Transfektion und das Vorhandensein von Hydroxylapatit nach 24 Tagen sowie eine positive Färbung von Alizarinrot, was auf eine osteogene Differenzierung hindeutet. Anschließend wurden die osteogenen Marker mittels qRT-PCR quantifiziert. Aus diesem Grund ist die Verwendung von kationischen Liposomen OO4/DOPE für die Beladung mit pDNA-BMP2 vorteilhaft, um eine ausgezeichnete Transfektionseffizienz zu erzielen und die osteogene Differenzierung zu fördern, den Einsatz direkter Wachstumsfaktoren zu vermeiden und die Toxizität zu verringern.

Diese Ergebnisse deuten darauf hin, dass mit OO4/DOPE beladene PEMs ein hohes Potenzial haben, als Medikamentenverabreichungs- oder Transfektionssystem für die Implantatbeschichtung im Bereich der Knochenregeneration und für andere Anwendungen eingesetzt zu werden.

Chapter 1: Introduction

This cumulative thesis consists of three publications. This chapter represents a general introduction to the topic of this thesis. The three published papers are assembled as chapters 2-4 including a summary at the beginning of each chapter.

Introduction

1. Basis of bone tissue: structure and functions

The musculoskeletal system plays a key role in important functions in the human body, including transmitting forces from one part of the body to another, protecting organs, mineral storage, homeostasis, and controlling strain [1,2]. The skeletal tissues contain bone, cartilage, tendons, ligaments, and muscle [1]. Bone is a connective tissue that determines the complete structural stiffness and strength [3]. Bone plays a role in the support, protection, and movement of the body [1,4]. The composition of mature bone includes minerals, as well as an organic and inorganic matrix. The inorganic matrix is composed of calcium, and phosphorous that produce hydroxyapatite, magnesium, and sodium, and the main role is to provide bone strength, stiffness, and resistance. In addition, the organic matrix includes collagen type I, proteoglycans, glycoproteins, growth factors such as bone morphogenic proteins family, also interleukin 1 and 6, osteocalcin, and bone sialoprotein. The function of these factors is the mineralization and remodeling of the bone. Collagens are a group of proteins responsible for maintaining the structural integrity of the human body, and it is found in connective tissues, blood vessels, skin, and corneas [5]. Collagen type I is the most abundant collagen and is found in bone, skin, tendons, vasculature, etc. [5]

Cells are also a main component of the bone and they are classified into three types: osteoblasts, osteoclasts, and osteocytes [6]. The osteoblast is a cuboidal cell derived from mesodermal and neural crest progenitor cells and is responsible for the production of bone matrix components [7]. These cells have a strong alkaline phosphatase activity and they secrete proteins like collagen type I, non-collagenous proteins, and osteocalcin [8]. There are three stages of osteoblast formation: osteoprogenitor, preosteoblast, and osteoblast.

The first stage starts with the expression of the transcription factor SOX9 which shows the commitment to an osteoprogenitor. Subsequently, the expression of Runt-related transcription factor 2 (RUNX2) in the osteoprogenitor cell induces a preosteoblast formation and then matures to osteoblast [9]. Another important type of cell is the osteoclast. These cells are differentiated from hematopoietic cells through the interaction of macrophage colony-stimulating factor (M-CSF) and activator of nuclear factor- κ B ligand (RANKL) leading to the start of bone remodeling. They are usually found in contact with the calcified bone surface [6,10]. The process of the osteoclast attachment to the bone surface is through binding integrins that express these cells in the bone matrix [7]. In general, the integrins α 1 β 1 and α 2 β 1 bind to collagen types I and IV. In osteoclasts, α 2 β 1 integrins induce the attachment of the cell to the bone surface and it helps to select a specific zone to be resorbed, permitting the formation of an acidic environment necessary for bone degradation [11]. Osteocytes have morphological and functional activity depending on the cell age. When the osteocytes are at a young age, they have a more structural function. The important role of osteocytes is to organize bone maintenance through interactions between osteoblasts and osteoclasts. The osteocytes express receptor activator of RANKL, which promotes bone resorption that activates the osteoclasts [9]. However, older osteocytes are phagocytosed and digested during bone resorption [2,6,7].

1.1. Bone remodeling and healing process

During lifetime, the bone undergoes remodeling and constant homeostasis equilibrium from osteoblast and osteoclast [7]. Remodeling is the process of replacing old bone with new bone. This process contains five phases: activation, resorption, reversal, formation, and resting (Figure 1) [10]. During the activation process, there is a detection of remodeling signals such as damage, hormone activation, or direct mechanical strain of the bone. Here,

the osteocytes detect the physical signals and transfer them to biological signals to initiate bone remodeling [7,10]. Then, the resorption process continues with the migration of the preosteoclast to the bone surface where the cells are differentiated into osteoclasts [7,10]. The reversal phase starts with the transition from osteoclast to osteoblast. Here, the osteoclasts remove some parts of the bone matrix and this activity facilitates the deposition of the first layer of collagen and glycoproteins to help the adhesion of osteoblast [8]. Subsequently, in the formation phase which is the longest phase in the process due to the development of the new bone and mineralization, some proteins like osteocalcin, bone sialoprotein, osteopontin, and proteoglycans are involved in the process of maturation, mineralization, and activity [8,12]. Then, collagen type I is actively expressed. At the end, the ECM goes through different alterations in composition and organization to complete the mineralization part [8]. In the resting phase, the osteoblasts are completely differentiated from osteocytes while the osteocyte is secreting some inhibitor factors to decrease the degree of bone formation in order to have a balance between the bone mass and mineral homeostasis [8,12].

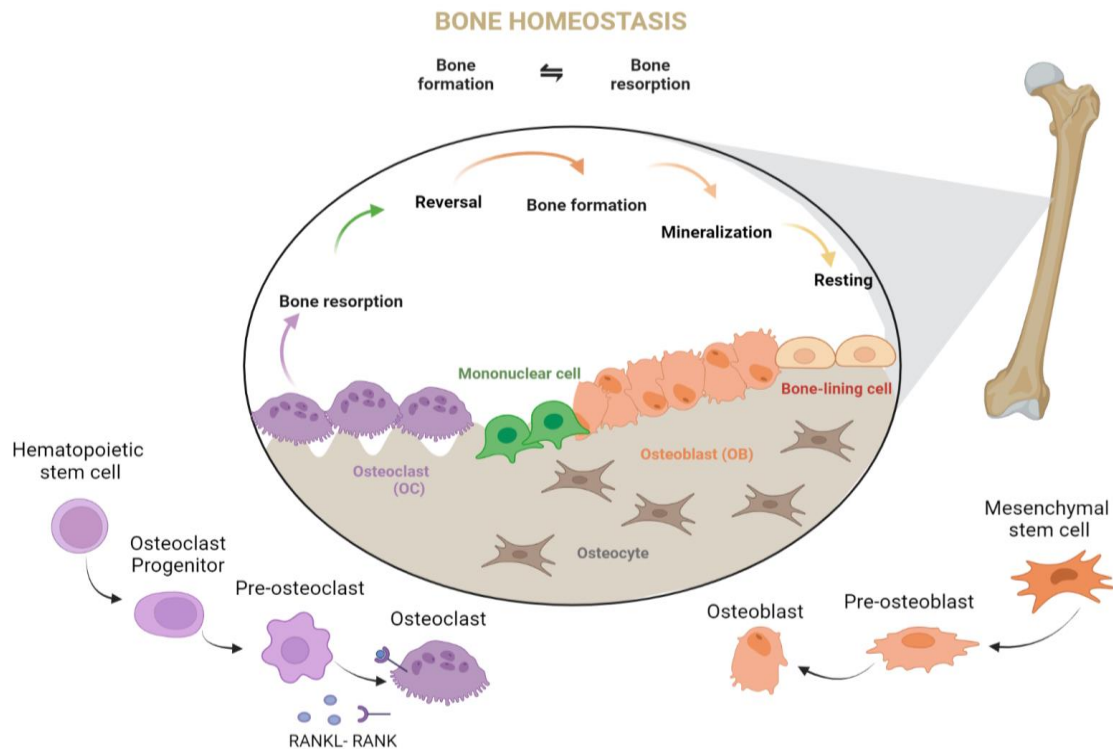


Figure 1. Illustration of bone homeostasis process through osteoclast (resorption of bone), osteoblast (bone mineralization and formation of osteocytes). Osteoclasts are derived from hematopoietic stem cells and osteoblasts are derived from bone marrow mesenchymal stem cells. Adapted from Metastasis to Bone Disrupts Bone Homeostasis by BioRender.com.

2. General overview of health situation and medical treatment

Bone studies are very important because of the extended list of diseases that affects this tissue, such as osteoporosis, osteoarthritis, osteomyelitis, etc. However, not only the diseases affect the bone tissue but also traumatic injury, orthopedic surgery, and tumors can induce bone defects [1].

Osteoporosis is the most common disease that can lead to bone fractures in women and people over 50 years old [13]. Around 10 million Americans suffer from this disease which seems to be similar in the UK [13]. Fractures can also affect children and young people, and it is estimated that around 1.5 million fractures occur every year [1,13,14]. The impact of the economic and clinical treatments of bone damage is increasing every year [14]. In the USA more than 1 million bone surgical procedures such as bone grafting, are done in

2005 and it is expected that this number will double in the next 25 years [1,13]. For all these reasons, researchers have turned their attention to creating new alternatives for less invasive treatments and more biocompatible techniques.

2.1 Evolution of orthopedic implants materials

Nowadays, the most effective method for bone damage treatment is the autologous bone or autograft, which promotes bone formation and stem cell differentiation to bone cells without an immune response. However, the disadvantage of this technique is the limited bone supply and donors [15]. Also, this technique can transmit other diseases or cause bacterial infections. Furthermore, the use of alternative materials for bone regeneration is considered a challenge because these materials should have specific mechanical and biological properties that are similar to the bone tissue properties, in order to avoid immune response and rejection of the implant [16]. Table 1 shows a summary of the most common materials that are used for orthopedic implants [17,18].

Table 1 Evolution of materials for bone implants [17,18]

Evolution of bone implants	Materials	Examples
First generation (Bio-inert)	Metals	Titanium or titanium alloys, stainless steel, cobalt-chromium alloys, magnesium, tantalum
Second generation (Bioactive)	Synthetic polymers	Poly methyl methacrylate, Teflon-type, Poly-glycolic acid (PGA), Poly-lactic acid (PLA)
	Synthetic and natural biodegradable polymers	Naturals: collagen, polyesters, calcium phosphates (corals, algae, bovine bone), calcium carbonate (natural or synthetic), calcium sulfates
	Ceramics	Alumina, zirconia, calcium phosphate (synthetic hydroxyapatite, silicate) Bioglass (silica or non-silica)
Third generation (Bioactive, Biomimetic)	Incorporation of soluble or insoluble factors into the materials	Soluble factors: growth factors, cytokines, hormones and chemicals Insoluble factors: extracellular matrix molecules, immobilized adhesion ligands

The first generation of biomaterials had the target to have a suitable combination of physical properties to replace the tissue without damaging the host. This generation includes metals. Stainless steel was the first successful material for substitutive joint prosthesis but stainless has low wear resistance which led to the introduction of new materials. The most common metal used for orthopedic implants is titanium [3]. However, the disadvantage of metals is the lack of cell adhesion and the risk of toxicity due to the accumulation or corrosion of the metal ion [19]. Also, their elastic modulus was an order of magnitude higher around ≤ 210 GPa than that of human bone which is around 20-30 GPa [3]. Due to its high modulus, the implant would carry the majority of the load in this situation, resulting in stress shielding of the adjacent bone. However, the lack of mechanical stimulation caused bone resorption, which led to implant failure and loosening [3,20].

The second generation of materials for bone implants are ceramics and polymers. Ceramics, especially alumina and zirconia are the most common materials in orthopedic implants [21]. The advantage of ceramics is the hardness, low roughness, and high degree of wettability that help to distribute the synovial fluid homogeneously between the implant surfaces [21]. On the other hand, ceramics are quite brittle and can break easily producing some microscopic debris that can activate macrophages resulting in bone resorption or embedding the fracture particles in the soft tissue [19,21]. An example of a new type of ceramic material is Bioglass. The Bioglass is designed as silica-based glasses and it was the first osseointegration material to have direct chemical bonding with the bone. However, a disadvantage of Bioglass is the low mechanical strength and reduced fracture resistance [22].

Synthetic polymers such as poly-glycolic acid (PGA) and poly-lactic acid (PLA) are also used as bone implants because of their tunable porosity and pore size. Nevertheless, their poor mechanical properties, as well as the high acid concentrations resulting from the

degradation of these polymers can affect cell differentiation and also provoke an inflammatory reaction [23]. But synthetic polymers offer the flexibility to adapt mechanical properties and degradation kinetics.

The second generation of materials also includes natural polymers. The advantage of natural materials is the good biocompatibility and biodegradability. In addition, some natural polymers can mimic the ECM and interact with the host tissue [24]. An example is collagen and hyaluronic acid, which are the most useful materials in orthopedics because they can induce osteogenic differentiation and improve cell attachment compared to synthetic polymers. However, there are some disadvantages such as the high cost of the used extraction and processing methods, as well as the dependence of the polymer properties on these methods [23,24].

Finally, the third generation of materials has the aim to include soluble or insoluble materials to induce cell adhesion, proliferation, and differentiation. Some of the soluble factors are growth factors and cytokines while the insoluble factors are ECM molecules and adhesive ligands [3]. During the evolution of the third generation, some appropriate physical characteristics of the materials were met such as high porosity and interconnectivity that induces cell interactions, oxygen and nutrients infiltration, and enhances vascularization [3]. Using biomaterials, it is possible to induce osteogenic differentiation through the introduction of osteogenic components like bone morphogenic proteins (BMP). Also, nanotechnology offers to control mechanical and biochemical microenvironments for cell delivery and cell differentiation [3]. For example, nanoceramics and nanocrystalline calcium phosphate show good degradation and enhance cell response in comparison with the normal size of calcium phosphate [1,3]. For that reason, nanomaterials are novel biomaterials for bone regeneration as alternatives to substitute grafts.

2.2 The importance of osseointegration in implants

The implant function is to promote the formation of natural bone which eventually fills the volume of the implanted scaffold as it degrades [25]. However, the bone implant materials ideally include an important number of criteria such as osteoinductive, osteoconductive, and osseointegration. Osteoinduction can be defined as the capacity of the implant to stimulate undifferentiated mesenchymal cells into preosteoblast [26,27]. Osteoconduction is the ability of the implant to promote cell attachment, proliferation, and migration across the implant surface and support bone growth on its surface [27]. Finally, long-term implants and osseointegration (OI) have been important for bone treatment. OI is a dynamic process that involves various cascade responses when there is a direct connection between the bone and the surface of the implant [28]. OI has been influenced by two aspects: environmental factors and surface and composition of materials [28]. First, the environmental factors include the host bone properties, concentration of osteogenic cells like osteoblast and osteoclast, and systemic illness, etc. Second, the type of material and surface coating influence the OI process and can enhance the environment and increase the OI [28].

Bone healing in contact with an implant contains a cascade of cellular responses. The first response is the inflammatory response, which starts when the implant has direct contact with the body and there is a release of soluble growth and differentiation factors and cytokines to form a blood clot [29]. Later, the blood clot is transformed by immune cells such as phagocytic cells, leukocytes, and macrophages [29]. The platelets change morphologically and biochemically as a response to the implant. The changes include cell adhesion, spreading, aggregation, and the generation of phosphotyrosine, increment of intracellular calcium, and hydrolysis of phospholipids. The presence of proteins absorbed on the surface helps the signaling for cell migration and proliferation [29]. The adsorption

of the proteins is influenced by the properties of the implant surface such as topography, roughness, and hydrophilicity [28,29]. The next step is the formation of the fibrin matrix that acts as a scaffold to help cell adhesion and migration [30]. After some days, angiogenesis takes place and the bone remodeling starts with mesenchymal stem cells [30]. These cells will be influenced by growth factors and cytokines that will promote osteogenic differentiation [28,29]. Here, the osteoblasts and MSCs deposit bone-related proteins and produce a non-collagenous matrix layer on the implant surface that will help to regulate the cell adhesion and bind minerals. Finally, the ECM is formed and present in the immature bone [30,31].

3. Surface modifications of implant materials

Recently, the demand for new alternatives for implants are increasing. The previous section mentioned different types of implant materials such as metals, ceramics, and polymers and also important criteria for bone implants [32]. Surface modification plays an important role because the surface of the implant is the first contact with the biological environment such as tissue, body fluids, bone, and blood [33]. Sometimes, the mechanical properties and biological responses of these materials need to be modified in order to be used as implants. This can be achieved by surface modification, which can improve criteria such as surface roughness and hydrophilicity [32,34]. For example, modifying the topography and roughness can improve cell growth, reduce bacterial adhesion or improve the lubrication properties of the implant [35]. Moreover, wettability can affect cell adhesion on the surfaces [33]. The cell attachment on the implant surface determines cell shape, which gives signals via the cytoskeleton to the nucleus resulting in the expression of specific proteins that will contribute to the cell phenotype. In addition, when the implant is attached, a complex system is initiated by the adhesion of some proteins like integrins (Figure 2). Also, surfaces having nanostructures in a well-controlled manner have shown

an effect on cellular adhesion and metabolism. For example, the surface of a prosthesis can be improved for better osseointegration with different surface modification methods like physical and chemicals in order to enhance antimicrobial properties, biocompatibility, biodegradation, and resistance while keeping the mechanical properties of the material [33].

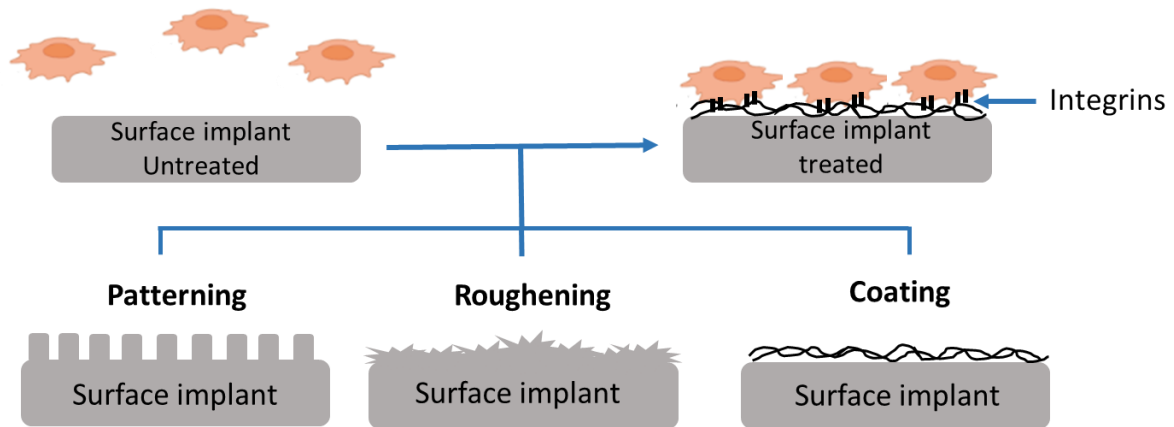


Figure 2. Schematic representation of surface modification and cell interaction

The surface modification methods can be classified into physical, chemical, and biological techniques. Table 2 shows examples of these modification methods.

Table 2. Surface modification methods for implant materials [32,34,37]

Surface modification	Techniques	General features
Mechanical	Polishing, grinding, machining, sandblasting, vacuum annealing	Potential to use different chemicals Improve the hydrophilicity Enhance the density and viscosity
Chemical	Thermal oxidation, hydrothermal treatment, anodic oxidation, sol-gel, acid etching	Enhance corrosion resistance Remove materials and modification of the roughness Not damage the mechanical properties
Physical	Laser treatment, physical vapor deposition, plasma spraying, lithography, Layer-by-Layer	Improve surface quality and biocompatibility Improve bone-implant contact Enhance cell adhesion Achieve complex and precise topography Increase the roughness
Biological	Immobilization of proteins, enzymes, peptides and glycans Layer-by-Layer	Creation of bio-inspired surfaces to enhance OI Natural composition, structure and physiological characteristics

In general, the physical and mechanical modifications use dry transformation techniques to change the surface's topography and morphology to produce good environments for bone implants. In this case, these methods can modify roughness hydrophilicity, surface tension, and bone affinity of the surfaces to improve cell adhesion, proliferation, and accelerate the osseointegration process [28,32,36]. Also, these techniques can remove surface contamination of the material by mechanical methods. For example, Goyal *et al* showed that increasing the roughness can increase the implant's surface area, and enhance cell migration and adhesion to the implant resulting in an enhanced osseointegration process [28,32,36].

The chemical modification changes the chemical properties of the surface and produces interactions between the cell surface and induces internal changes in the function and conformation of the structure of the cells [37,38]. This can be done by modifying the surface composition of the implant using oxidation, carbonization, or nitridation [37,38]. For example, anodic oxidation is a process in which an oxide film is generated by immersing

metal implants in an electrolyte bath. The oxide film on the metal goes through a repeated process of formation and disappearance. This technique is generally used to increase the corrosion resistance in titanium implants and produce a special formation of nanostructures on titanium implant surfaces [28]. The nanostructures enhance the bioactivity and improve the osseointegration process of the titanium [28,32]. However, these methods are expensive, causing chemical pollution and consuming a lot of power, etc [39].

The surface modification also includes biological methods. These methods include cell seeding and the addition of bioactive molecules such as proteins, and enzymes on the implant to make it more biocompatible [28]. These types of biological coatings can induce some biological responses such as effects on cell proliferation, adhesion, and differentiation which are important for bone formation and healing [32,40]. The biological methods are often used as a supplemental strategy to induce osseointegration[28]. However, the effects of the biological modification depend on some characteristics such as cell density, position, and the design of the implant [28,31].

3.1 General overview Layer-by-Layer technique

Nowadays, surface modification is not only to improve implant integration but also to create surfaces that respond to stimuli and contain active carriers for cell adhesion [33]. The Layer-by-layer (LbL) technique can be used as an implant coating to modify the surface in order to mimic ECM using natural or synthetic polymers [32].

The LbL is a versatile, simple, and cost-effective adsorption technique for the formation of multilayers composed of diverse materials such as polyelectrolytes with opposite charges in an aqueous solution (Figure 3) [41,42]. LbL was introduced by Decher to form a polymeric coating using anionic and cationic polyelectrolytes onto a positively charged surface [42]. LbL was developed based on ion pairing and electrostatic interaction of the charged polyelectrolytes. The intrinsic charge might be reduced on environmental

conditions [33]. In addition, other driving forces such as hydrogen bonding, hydrophobic interactions, and covalent coupling can also be involved in the multilayer formation [43]. The main advantage of LbL is that properties of multilayers can be modified in a wide range at nanometer scales, such as surface charge, thickness, wettability, and viscoelasticity by varying the properties of the adsorber material such as charge density, salt or buffer composition, ionic strength and pH [43]. For example, an increase in the molecular weight of the polyelectrolytes can induce a higher internal roughness, swelling, and dissociation response, or an increase in charge density also influences the thickness of the film [44]. Another modification can be done by external parameters such as light, electrical field, adsorption time, and the number of layers [42,44]. The substrates on different materials such as ceramics, metals, and polymers can be produced even with different geometries [38].

In addition, the LbL technique has been researched for various medical applications like drug and gene delivery [44]. Multilayer films can act as drug reservoirs to embedded with nanoparticles or active agents to preserve their activity, and protect the drug and delivery [45]. For example, it is possible to incorporate genetic material, and organic or inorganic nanoparticles between the layers or attach them to the surface [44]. Kotov and coworkers, researched about the bioactivity of multilayer film for biomaterial applications such as biosensors, drug delivery, superhydrophobic surfaces, etc. Kotov showed that LbL can be used as a scaffold for embedding growth factors, receptors, and ligands. In general, LbL represents an excellent technique suitable for coating implants and other biomedical applications [45–47].

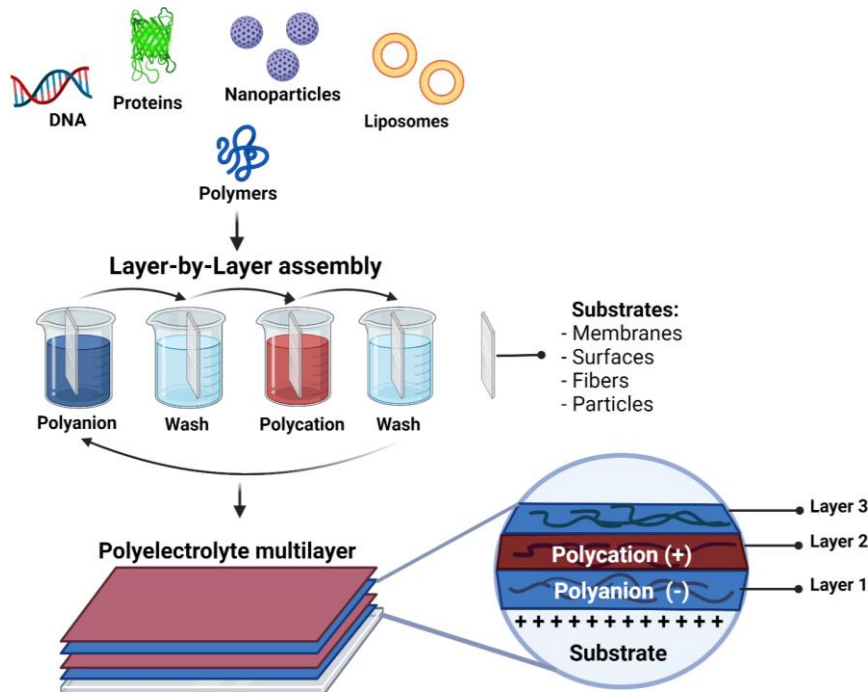


Figure 3. Schematic overview of Layer-by-Layer technique showing the layer materials and dip coating procedure. Created with BioRender.com.

3.2 Chemical and biological information of polyelectrolytes for multilayers

The development of multilayers can be done by many biopolymers and bioactive molecules. LbL has been used to mimic the ECM which makes the surface of implants more biocompatible. On the other hand, the multilayer can be formed with ECM proteins, polysaccharides, and other bioactive molecules in order to stimulate cell adhesion and proliferation [48]. Using these natural polymers one can develop multilayers with unique composition and help the mechanical and biochemical signals of the surface to stimulate a cellular response. The common examples of natural polymers are glycosaminoglycans (GAGs) including hyaluronic acid, chondroitin sulfate, and heparin. Also, proteins like collagen type I are used as natural biopolymers [47,48].

GAGs are polysaccharide chains made up of repeating disaccharide units linked by glycosidic bonds [49]. GAGs are considered as polyelectrolytes because of the presence of carboxylate and sulfate groups that gives them negative charges [49,50]. In the case of

proteins like collagen, the net charge depends on the isoelectric point and the pH of the solution. Basically, collagen is used as a polycation at acidic pH and can promote cell adhesion and osteogenic differentiation [50].

3.2.1 Chondroitin sulfate

Chondroitin sulfate (Cs) is a glycosaminoglycan that is composed of a repeating disaccharide made up of D-Glucuronic acid, and N-acetyl-d-galactosamine that is sulfated at the carbon 4 and 6 of the galactosamine (Figure 4) [51]. The molecular weight of the Cs is around 5-70 kDa. Cs is part of the connective tissue such as bone, ligaments, cartilage, and tendons. When Cs binds to a proteoglycan like aggrecan, which is bound to hyaluronan chains, it plays a role in the retention of water because of the high density of anionic groups and resistance to compression for cushioning and lubrication of the joints [49,52]. Cs also increases the synthesis of hyaluronan, glucosamine, and collagen II [49,51].

Using Cs in patients with osteoarthritis stimulates the synthesis of proteoglycans and inhibits the synthesis of proteolytic enzymes that reduces the catabolic activity of the chondrocytes. Moreover, Cs has anti-inflammatory activity to influence the signal processes in cells that can regulate inflammation, wound healing, and tumor development [49,51].

Cs has the ability to induce cell differentiation that can be useful for chondrogenic and osteogenic scaffolds due to strong interaction with growth factors such as BMP-2 [53].

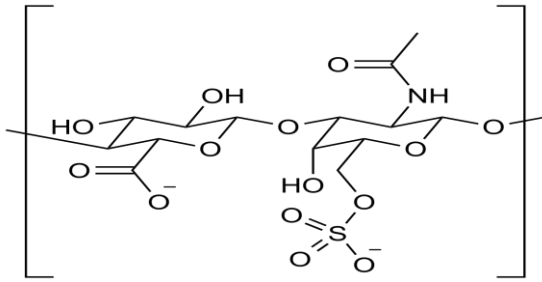


Figure 4. Chemical structure of chondroitin sulfate

3.2.2 Hyaluronic acid

Hyaluronic acid or hyaluronan (HA) is composed of units of glucuronic acid and N-acetylglucosamine monosaccharides alternated by β -1,3 and β -1,4 anhydro glycosidic bonds (Figure 5). HA is synthesized by membrane proteins called HA-synthases [51]. Especially, HA is the only non-sulfated GAG and it is not binding to a protein core. Moreover, HA is an important component of the ECM in cartilage due to its hydrogel-like elasticity and viscosity, high molecular weight, and moderate anionicity [49,51]. However, the molecular weight depends on the tissue and species. In humans, the highest concentrations of HA are found in the umbilical cord, synovial fluid, skin, and eye with a molecular weight of around 2×10^6 Da but decreasing with age progression [49]. Because of its high viscoelasticity, HA fills the intercellular space between other components like collagen, cell surroundings, and blood lymph vessels. In the extracellular space, HA is bound to hyaladherins. such as CD44 and tumor necrosis factor-stimulated gene-6 (TSG-6) [49,51]. HA plays a role in the inhibition of the formation and release of some prostaglandins, moreover, it enhances proteoglycan aggregation, synthesis and modulates the inflammation response [49]. There are a lot of commercially available products of HA, and some of them are used to treat osteoarthritis. In addition, HA is used to create new scaffolds such as hydrogels, microgels, or coatings for wound healing that

enhance the structural and biological properties due to its anionic nature and viscoelastic properties [51].

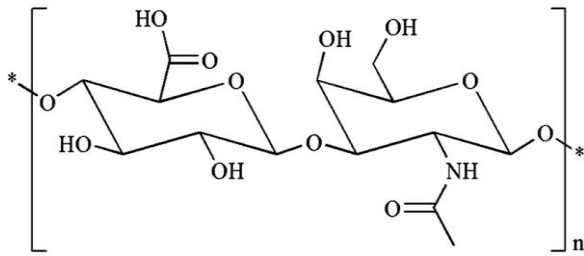


Figure 5. Chemical structure of hyaluronic acid

3.2.3 Collagen Type I

The ECM of the connective tissue is composed of a family of proteins called collagens. Collagen fibrils are composed of three polypeptide chains that give a triple-helix structure [54]. These chains can be homotrimeric or heterotrimeric depending on the collagen type, and each chain contains a polyproline II-like conformation [5,54]. The helix conformation of the collagen is formed by the repetition of some amino acids like glycine with the sequence Gly-X-Y, where X can be proline and Y hydroxyproline (Figure 6) [54]. In addition, there is a proteolytic cleavage of the propeptides due to the triple-helical collagen molecules that contain short telopeptides at each end and forms the fibrils. Furthermore, fibrillar collagen is secreted into the ECM as a soluble precursor named procollagen [5,54]. During procollagen synthesis, some enzymes and chaperones help the procollagen to fold and trimerize [54]. Collagen is found in skin, bone, cartilage, and tendon and has many types but the most common are I, II, III, and V. The role of collagen is to give structure and shear resistance and compress forces to the connective tissue [5,54]. The arrangement of the fibrils depends on the tissue. For example, in the cornea, the fibrils are arranged in complex three-dimensional form but for ligaments and tendons, the arrangement is parallel bundles [5].

Collagen type I is the most abundant collagen and is present in connective tissue except for hyaline cartilage. The amount of collagen type I in bone is around 95% of the content of collagens [5,54].

Collagen is used as a matrix or scaffold for tissue regeneration because of its biocompatibility. These scaffolds can control the delivery of bioactive substances like growth factors [5].

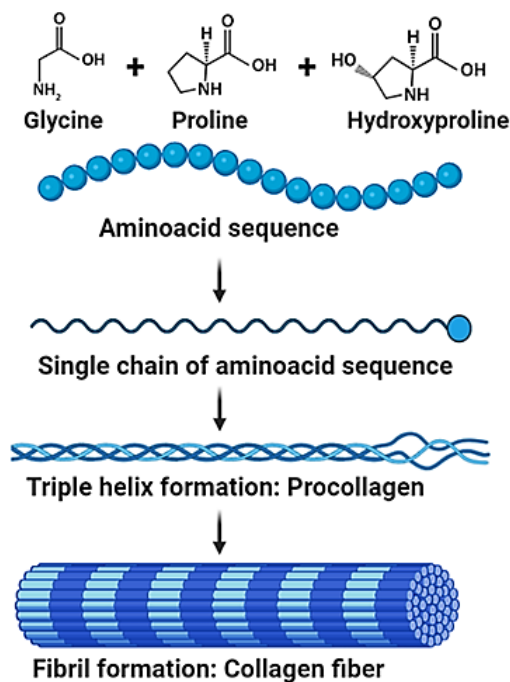


Figure 6. Schematic diagram showing the assembly of collagen type I into collagen fibrils. Created with BioRender.com.

4. Mesenchymal stem cells for tissue engineering

One of the most promising and recurrent studies in tissue engineering has concentrated on the use of stem cells, due to they can differentiate into all connective tissue phenotypes such as bone, cartilage, muscles, tendons, and ligaments [55].

The embryonic development mesenchyme contains stem cells that can differentiate into multiple cell lineages [55]. There are different types of stem cells: totipotent, pluripotent,

and multipotent stem cells. The first type is totipotent, these cells can establish a daughter cell line of any cell lineage in a given organism [56]. Then, there are the pluripotent stem cells that can self-renew and develop into three primary germ cell layers of the early embryo and then into the adult body [56]. The last type is multipotent stem cells, these cells are limited in that they can only produce daughter cells of specific tissues [56]. Mesenchymal stem cells (MSCs) are cells that have the ability to be self-renewing and their progeny provides growth to various mesenchymal tissues. MSCs have been isolated from cord blood, placenta, heart, amniotic fluid, adipose tissue, synovium, skeletal muscle, and bone marrow.

Both bone marrow and adipose tissues are considered the most common source to obtain MSCs, namely MDSCs and ADSCs, respectively [55,56]. These two types of cells can differentiate into cells and tissue of mesodermal origins, and there is no difference in immune phenotype or morphology. Nonetheless, ADSCs have the advantage to be more accessible than MDSCs. Also, ADSCs have shown excellent potential to differentiate in connective tissue [55,56].

In addition, the MSCs *in vivo* form niches where cells involve N-cadherins for cell-cell interaction that helps to maintain the stem cell state [55]. However, when the MSC is cultivated *in vitro*, they could have low cell-cell interaction, as a result, the integrins-based focal adhesion increases, and ECM molecules such as fibronectin, laminins, and collagen receptors, etc. are involved in the process [55].

MSCs can also secrete growth factors, chemokines, and cytokines that stimulate and regulate a local response to regenerate microenvironments and repair tissue. These molecules can act directly on themselves (autocrine response) or neighboring cells (paracrine response) [57]. Paracrine activity can be used to study the behavior of the cells. The paracrine factors form a complex network that gives stability and amplification of a

regenerative response [57]. One example is the growth factors secreted from MSCs, these factors are capable of inducing cell proliferation, migration, cytoprotection, and differentiation [57,58]. For that reason, novel researches aim to use stem cells for drug delivery complex as a vehicle to facilitate tissue regeneration.

During the last years, MSCs have demonstrated their therapeutic capacity and they are used in autologous tissue grafts that are considered as the gold standard for the reconstruction of bone tissue damage. Also, MSCs cells can be used in biocompatible scaffolds for implants to heal the defect without side effects or tissue damage [55].

Furthermore, MSCs can grow on a rigid polystyrene surface that can help to direct the cells into connective tissue but it is limited for myogenic differentiation. *In vivo*, these tissues have a range of stiffness from 0.1 to 100 kPa depending on the surface characteristics [58]. When MSC is cultured on a soft surface for enough time, it will guide the cells toward adipogenic differentiation, in contrast to a stiff surface which can guide them toward osteochondrogenic differentiation [58].

4.1 Osteogenic differentiation of MSCs

Osteogenesis is determined by a sequential cascade of a biological process that involves the recruitment of MSCs to bone remodeling, proliferation, lineage commitment, expression of some specific markers, collagen, and ECM mineralization [59]. The osteogenesis starts with the proliferation of MSCs and proceeds to pre-osteoblast, then the cells become mature and secrete ECM. Here, osteoblasts appear from the differentiation of osteogenic progenitor cells and are responsible for the mineralization from the beginning of bone formation until bone remodeling [60]. At the end, mineralization happens (Figure 7) [59]. During the osteogenic process, multiple factors participate, such as growth factor- β (TGF- β), bone morphogenic proteins (BMPs), Wnt/ β -Catenin and

fibroblast growth factor (FGF), etc., in order to differentiate an osteoblast progenitor to an osteoblast [59,61]. Many signaling pathways can induce conversion between osteogenesis and adipogenesis that are connected with two key transcription factors: Runx2 (osteogenic) and PPAR (adipogenic) [60]. During the differentiation, the Nel-like protein type I (NELL-1) inhibits adipose differentiation of MSCs while contributing to osteogenic differentiation [60]. Another signaling pathway is a transcriptional activator with a PDZ-binding motif (TAZ) which is a transcriptional modulator that induces osteogenic differentiation and inhibits adipogenesis [60].

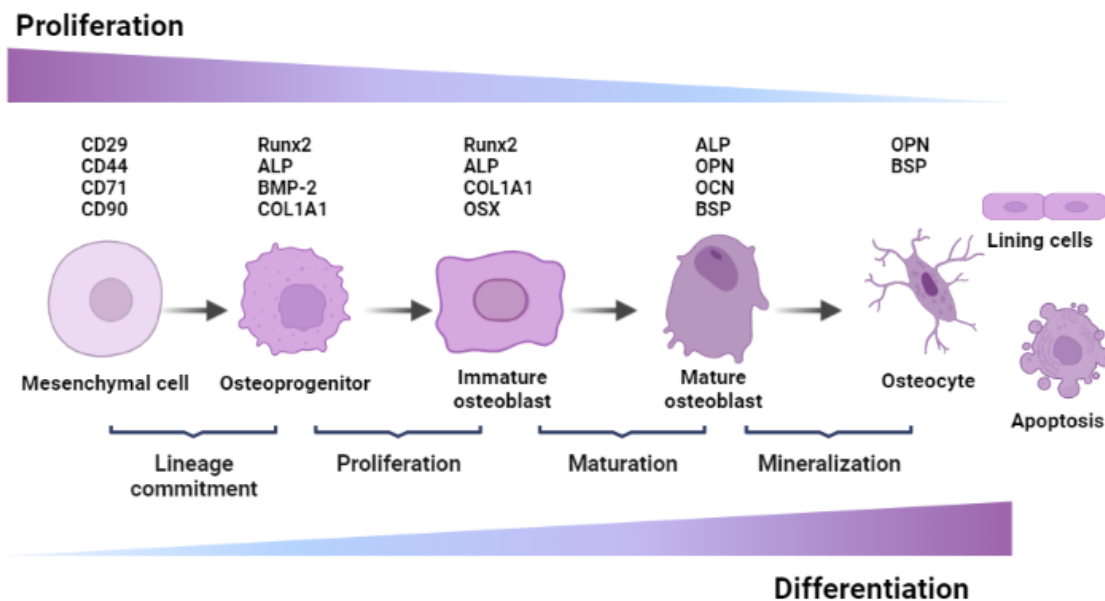


Figure 7. Schematic description of osteogenic differentiation phases from mesenchymal stem cells until osteocytes. Osteogenic markers are expressed during the different phases. Alkaline phosphatase (ALP), collagen I alpha I (COL1A1), Bone morphogenic protein-2 (BMP-2), Runt-related transcription factor 2 (Runx2), osterix (OSX), osteopontin (OPN), bone sialoprotein (BSP), osteocalcin (OCN). Created with BioRender.com.

BMP is a member of the TGF- β superfamily except for BMP-1 which is isolated from bovine bone extracts. It starts the signaling cascade of the osteogenic process by ligand binding to the heteromeric complex of types I and II serine/threonine kinase receptors on the cell surface [61]. Also, BMPs increase the transcription of core-binding factor-1/Runt-related

family 2 (Cbfa1/Runx2) that regulates osteogenic differentiation. The most important BMPs are BMP-2, -4, and -7 which are expressed in cartilage and bone [59,61]. Furthermore, the combination of BMPs with collagen and hydroxyapatite induces bone formation [60]. However, the osteoinductive effect of the BMPs is affected by the concentration [61]. In many clinical trials, it was shown that the growth factors are required in much higher dosages than in the physiological levels, in order to have an effect to induce osteogenesis. In general, some growth factors are synthesized by recombinant DNA in *E. coli* [62]. These factors are too sensitive and they might degrade or lose their bioactivity, stability, and efficiency easily, for example during the combination with drug delivery systems. Other disadvantages are the high cost, and the necessity to use large amounts [62]. Nowadays, new alternative methods are required to induce and enhance the efficacy of osteogenesis and bone regeneration. One novel alternative is to incorporate these molecules into scaffolds using liposomes. The advantage of liposomes is that they can retain the drug or growth factor at the site of interest in order to extend and maintain the biological activity of the molecule [63]. Another alternative is by transfection of the genes like Runx-2, BMP-2, -4, and -7 to promote osteogenic differentiation [61].

4.2 Chondrogenic differentiation of MSCs

During the formation of cartilage, various molecules provide signals to mesenchyme to produce the condensation of MSC. These cells produce a matrix consisting of collagen and proteoglycans. Chondrogenic differentiation is determined by various factors, including cell density, cell adhesion, and growth factors [64]. The aggregation of BMSCs is able to differentiate into chondrogenic progenitor cells. At that point, the chondroprogenitor cells convert to chondrocytes and these cells go through different processes and develop hypertrophic chondrocytes (Figure 8) [65]. Then, chondrocytes are progressively replaced by osteoblasts and it will form endochondral ossification. In addition, the condensation

allows the cell-cell and cell-matrix interaction via N-cadherins, neuronal cell adhesion molecule (N-CAM), gap junction, and integrins. However, not only the cell adhesion molecules promote chondrogenesis, but also the interaction with macromolecules of ECM are involved in the chondrogenic differentiation [65]. These macromolecules include collagen type II, hyaluronan, aggrecan (ACAN), and fibronectin. Also, some soluble proteins such as BMP, Wnt, FGF, and TGF are necessary for this process. BMPs and cartilage-derived morphogenetic proteins (CDMP or GDF-5) are members of the transforming growth factor β superfamily (TGF- β) which their functions are the formation of prechondrogenic condensation and change to chondrocytes [64,65].

The transcription factor SRY-box 9 protein (Sox9) is involved in the differentiation of BMSCs into chondrocytes [65]. The combination of Sox9 with collagen type II and ACAN activate its own gene expression and promote chondrocyte proliferation, and trigger the creation of ECM. Additionally, several experimental investigations have shown that Sox9 was present in large quantities in cartilage progenitor cells and chondrogenic cells, which is a prerequisite for retaining the phenotypic of chondrocytes [65]. As a result, Sox9 prevents chondrocytes from becoming pro-hypertrophic chondrocytes and does not take part in the subsequent differentiation of hypertrophic chondrocytes [65].

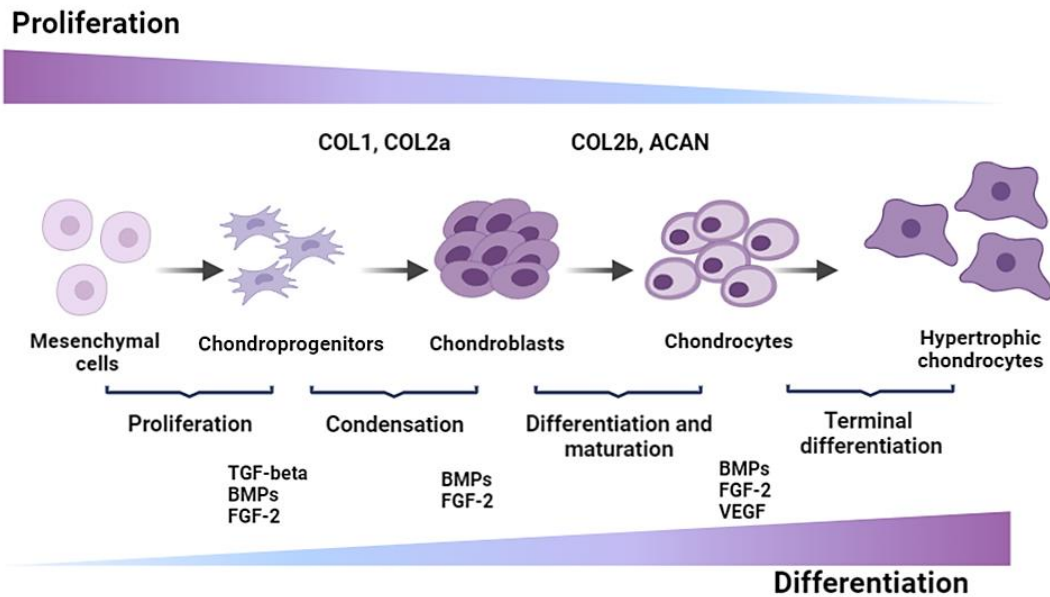


Figure 8. Schematic description of chondrogenic differentiation phases from mesenchymal stem cells until chondrocytes and hypertrophic chondrocytes. Chondrogenic markers are expressed during the different phases. Collagen I alpha I (COL1A1), collagen II alpha (COL 2a), aggrecan (ACAN). Created with BioRender.com.

4.3 Role of dexamethasone and media supplements on chondrogenic and osteogenic differentiation

MSCs in vitro can be differentiated by using media supplements such as dexamethasone, β -glycerolphosphate, and ascorbic acid (Asc). Dexamethasone is a synthetic glucocorticoid that is used as an anti-inflammatory drug [66]. Also, dexamethasone has been added as a media supplement for adipogenic, chondrogenic, and osteogenic differentiation, but the mechanism of how dexamethasone works in the differentiation is unclear. One possible mechanism of dexamethasone is the induction of cell differentiation by the WNT/ β -catenin pathway dependent on Runx2 expression [66]. Here, FHL2 is upregulated in response to a glucocorticoid like Dex. In the presence of an activator of the WNT signal, this activator will bind the FHL2 to β -catenin and transport it to the nucleus, where the β -catenin will bind to TCF/LEF-1 and starts Runx2 transcription [66]. However, there is another possible mechanism via the activity of the β -catenin-like molecule TAZ

(transcriptional co-activator with PDZ-binding motif). In this mechanism, TAZ recruits more components for the transcription and binds to the sequence of amino acids of Runx2 (Figure 9) [66]. For chondrogenesis, dexamethasone enhance the expression of Sox9 and activates the gene expression of Col2a1 and ACAN.

However, dexamethasone generates severe side effects, and it is reported that long use of steroids might cause or increase the risk of osteoporosis [66]. Tenenbaum and Heersche *et al.* demonstrated that the optimal concentration to induce osteogenic differentiation was 100nM [66]. Also, Hegeman *et al.* demonstrated that encapsulating this compound has beneficial effects on inflammatory diseases like osteoarthritis [63].

Asc is important for osteogenic differentiation because it is a cofactor for enzymes that hydroxylates the amino acids such as proline and lysine in pro-collagen, which is required for the formation of the helical structure of the collagen [66]. The main role of Asc is the secretion of Col I into the ECM. In general, the osteoblast binds to the ECM with both Col I and $\alpha 2\beta 1$ integrins that are specific for this type of collagen[66]. Then, the integrin ligand activates MAPK signaling, transporting the signal to the nucleus causing the activation of MAPK and phosphorylation Runx2 [66]. Another example of osteogenic media supplements is the β -Glycerolphosphate which is a source of the phosphate required for the production of hydroxylapatite and it can regulate the expression of osteogenic genes like osteopontin and BMP-2 [66].

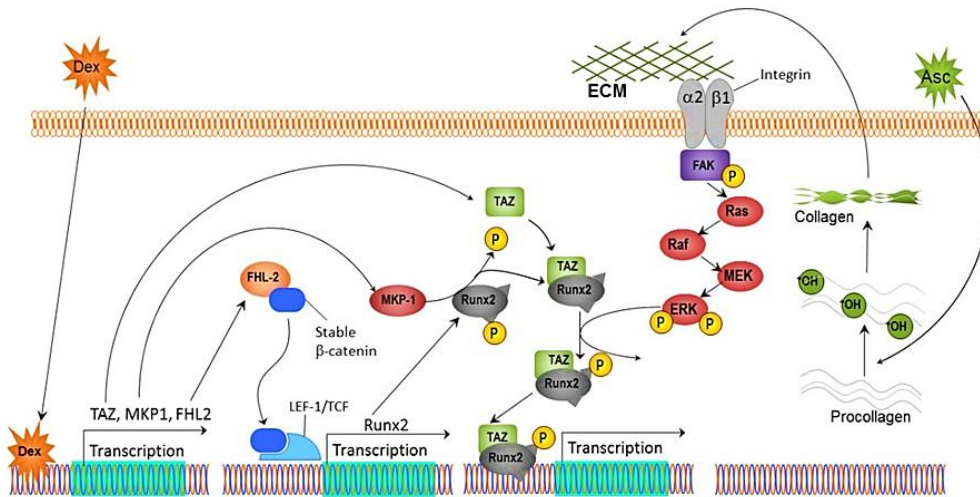


Figure 9. Schematic representation of the different possible pathways of the influence of dexamethasone in osteogenic differentiation. Reference (40)

5. Modern technologies for drug delivery: nanoparticles

Drug delivery systems permit to target a cargo in the body, decreasing the toxicity and the side effects. Drug delivery systems have many benefits in developing new alternatives for therapies, doses, and drug monitoring [67]. These benefits are attractive relative to the cost of creating a new drug. In general, the most common and novel drug delivery systems are nanocarriers such as: nanoparticles (NPs) made of metal and polymers, dendrimers, liposomes, and virus-like particles like adenoviral vectors [67,68].

Metal NPs are made of silver, gold, palladium, and titanium. These metal NPs have a reduced size and NPs can interact with the cell membrane. One advantage of metal NPs is the easy surface functionalization with active biomolecules through some interactions such as covalent bonding, hydrogen bonding, and electrostatic interactions [69]. Metal nanoparticles are getting attention for osteoinductive activity and their antimicrobial effects [69,70]. For example, Mahmoud et al showed that gold nanoparticles can promote the osteogenic differentiation of MSC via mitogen-activated protein kinase (MAPK) signaling which is important for osteogenesis [71].

Polymer NPs are formulated from natural and synthetic polymers with NPs sizes <100 nm, where the size of the NPs is important for systemic circulation. Examples of polymer materials are poly (ethylene glycol) (PEG) and poly (lactic acid) and poly (amino acids) [70]. NPs can be divided into two types depending on the morphology, referred as to nanocapsules and nanospheres. For example, nanocapsules contain an oily core to dissolve the drug and it will be covered with a polymeric shell, while nanospheres are formed with a polymeric network and the drug can be on the surface or inside [72].

Another type of drug delivery system is the dendrimer. Dendrimers are globular and symmetric macromolecules with highly branching architectures that make it possible to target ligands to be conjugated effectively [73,74]. The architecture of the dendrimers gives the possibility to functionalize the surface and change the biological and physicochemical properties. The dendrimers as drug delivery are used for anticancer therapies and diagnostic imaging [74]. For example, poly(amidoamine) (PAMAM) dendrimers (amino, hydroxyl, and carboxylate surface) demonstrated the ability to differentiate MSCs toward the osteogenic and adipogenic lineages [75].

Liposomes are a good imitation of the cell membrane and have the ability to mimic natural cell functions like the lipids that are enrolled in the transport of substances. The advantage of lipid carriers is a large amount of cargo, good stability, and the surface giving multiple options for targeting [67]. Liposomes are vesicular structures that can be made by self-assembly of lipids that contains hydrophilic head groups and hydrophobic tails [76]. Moreover, liposomes are in general a well-established cargo system and have many advantages over other nanoparticles, such as high load-carrying capacity (hydrophilic and lipophilic compounds), low toxicity, and versatile preparation and application [76]. Another advantage of liposomes is the release of cargo in select targeted cells or organs [67]. For that reason, local delivery of Dex using liposomes could be advantageous in therapies [63].

Monteiro et al showed the effect of Dex-loaded liposomes on hBMSCs. They showed that the liposomes with dexamethasone were able to stimulate an earlier induction of differentiation of hBMSCs into the osteogenic lineage [63].

5.1 Overview of endocytic mechanisms for drug delivery

Cells undergo the biological process of endocytosis to take in foreign objects, which can be molecules, nutrients, and signaling molecules. There are many pathways of endocytosis at the cell surface working at the same time. There are two possible categories of endocytosis [77]: the first classification is based on a specificity that is differentiated by receptor-mediated endocytosis (RME) which permits more rapid internalization of the targeted ligand in contrast to that of untargeted complexes [77,78]. Examples of this classification are: clathrin, caveolar, flotillin, and phagocytic pathways or non-specific ones like pinocytosis. The second classification is based on the mechanism of development of vesicles for cargos, including clathrin-dependent, caveolin-dependent, Rho-A-dependent, and flotillin-dependent endocytosis [78]. For example, when the object or macromolecule is taken by clathrin-dependent RME, it commonly goes through lysosomal degradation. On the other hand, in contrast, clathrin-independent RME internalization produces endosomal accumulation and no degradation [78]. For that reason, the NPs, and liposomes have the purpose to avoid the lysosomal pathway in order to protect the active compound from enzymatic degradation. In general, all the types of endocytosis except pinocytosis are possible ways for carriers to deliver the compounds into the cell [77,78].

6. Survey on modern technologies for transfection of nucleic acids

Transfection is a technique in which foreign nucleic acid can be added into the cells to modify the properties of the cells [79]. This technique can be used to study the gene products by increasing or inhibiting a specific gene expression in the cells. Transfection

has two different types: stable and transient [79]. Stable transfection is involving the genetic material with a specific marker gene in the genome of the cell to be expressed for a long period. In transient transfection, the transfected cells express the foreign gene for a limited time since it is not part of the genome [79]. There are three methods for the transfection process: biological, chemical, and physical. Furthermore, transfection methods are determined by cell type, transfection efficiency, toxicity, reproducibility, and the potentially provoked side effects [79]. Examples of the transfection methods together with their advantages and disadvantages are presented in table 3.

Table 3 Transfection methods for introducing genes in mammalian cells [79,83]

Group	Method	Advantage	Disadvantage
Physical	Microinjection	Easy method Avoids cytoplasmatic and lysosomal degradation	Requires well-isolate cells Presents technical and ethical issues
	Electroporation	High transfection system	Excessive cell death
	Biolistic particle delivery	Easy and transfer large sizes and amounts of DNA	Low integrity of delivered DNA Cell damage
Chemical	Cationic polymers	No viral vector	Chemical toxicity
	Calcium phosphate	Low cell death Simple and easy method	Transfection efficiency is low Low levels of transgene expression
	Cationic lipids	Good for in vivo and in vitro Carry large pieces of DNA Can be targeted Non-immunogenic Scale-up and standardization	Low transfection efficiency compared to viral systems Transient expression
Biological	Virus-base Adenovirus Retrovirus Adenoassociated virus Herpes simplex virus	High-efficiency Effective in vitro and in vivo	Immunogenicity Hazard for laboratory personnel Mutagenesis

The most common method used in transfection is virus-mediated transfection because of its high efficiency. Nonetheless, its major disadvantage is high toxicity and immunogenicity [79]. For that reason, modern methods like cationic liposomes are used for gene transfer (Figure 10). In these liposomes, DNA can be encapsulated into cationic lipids that interact electrostatically with DNA, promoting the formation of lipoplexes [80].

6.1 Overview of cationic liposomes as a transfection system

Cationic lipids contain a positive charge of one or more amines in the polar head groups. The presence of this positive polar head helps to bind anions in DNA. These cationic liposomes/DNA combinations are used for gene delivery [80]. The anionic liposomes, on the other hand, are more used in macromolecule delivery [81]. Some liposome characteristics such as membrane, charge, and size can influence how the liposome interacts with the cells. The main interaction mechanism between liposomes and cells is endocytosis [80]. In the case of gene delivery, the cationic liposomes/DNA (lipoplex) enters into the cell by endocytosis forming an endosome (Figure 10) [82]. Afterward, the destabilization of the endosome components starts to happen and in turn, the DNA is displaced from the cationic liposome and released into the cytosol (Figure 10) [80,82]. Liposomes are in general a well-established cargo system and have many advantages over other nanoparticles, such as high load-carrying capacity (hydrophilic and lipophilic compounds), low toxicity, and versatile preparation and application [76].

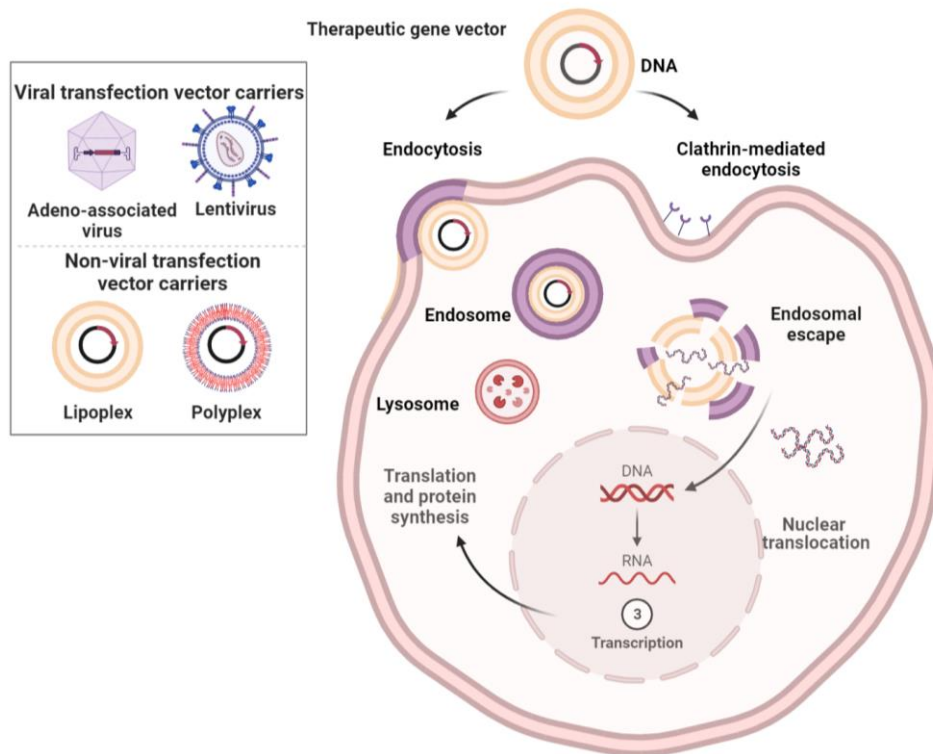


Figure 10. Illustration of transfection vectors carrier and representation of the main steps involved in the interaction of the lipoplexes with cell: endocytosis, cytoplasmic release, nuclear translocation, transcription, and translation. Adapted from Cancer Cell-Targeted Gene Therapy by BioRender.com.

There are some limitations using the liposomes such as toxicity at higher concentrations, and interactions with negatively charged molecules in serum, which can affect the stability of the liposome and its capacity to interact with the cells causing difficulties to reach the target tissues which decreases the transfection efficiency in the case of the cationic liposome [80]. For these reasons, new strategies must be used to develop functional (drug or transfection-eluting) films in a specific area at the interface of the artificial material (implants) and the biological tissues to avoid toxicity and damage.

7. Aim of this study

In this study, we combined two approaches, the ECM-mimicking environment, and the PEM-derived in situ drug delivery and/or transfection, to develop an ECM-mimicking surface coating to direct cell differentiation. We focused on a bone ECM-mimicking multilayer system consisting of Col and Cs, and a system of Col and HA loaded with liposomes or LPX composed of OO4/DOPE lipid composite. For drug delivery, the liposomes Dex-loaded was used to induce osteogenic and chondrogenic differentiation. For transfection, pDNA was used as a biologically active compound that encoded a BMP-2 sequence. These approaches were used to obtain a local delivery of Dex or pDNA-BMP-2 with the aim of initiating osteogenesis due to the paracrine effects of the cells. The work focused on three main aims: (i) A characterization of the material, in which we characterized the multilayer formation processes, especially the embedding of OO4/DOPE liposomes and lipoplexes, and the surface properties of PEMs. (ii) In addition, general cell studies such as cell adhesion, cell viability, and cell uptake including transfection were performed. (iii) We studied the ability of the system to induce osteogenic cell differentiation by gene expression analysis and histochemical and fluorescence assays. Overall, we present a new approach to engineering a bone ECM matrix-inspired surface coating made of collagen and glycosaminoglycans that represents a promising tool to develop multifunctional surface coatings for implant surfaces.

8. References

- [1] Porter J.R., Ruckh T.T., Popat K.C., (2009). Bone tissue engineering: A review in bone biomimetics and drug delivery strategies, *Biotechnology Progress*. 25,1539–1560. <https://doi.org/10.1002/btpr.246>.
- [2] Doblaré M., García J.M., Gómez M.J., (2004). Modelling bone tissue fracture and healing: a review, *Engineering Fracture Mechanics*. 71, 1809–1840. <https://doi.org/10.1016/j.engfracmech.2003.08.003>.
- [3] Yu X., Tang X., Gohil S.V., Laurencin C.T., (2015). Biomaterials for Bone Regenerative Engineering, *Advanced Healthcare Materials*. 4, 1268–1285. <https://doi.org/10.1002/adhm.201400760>.
- [4] Staines, K. A., Pollard, A. S., McGonnell, I. M., Farquharson, C., & Pitsillides, A. A. (2013). Cartilage to bone transitions in health and disease. *The Journal of endocrinology*, 219(1), R1. <https://doi.org/10.1530/JOE-13-0276>
- [5] Kruger T.E., Miller A.H., Wang J., (2013). Collagen Scaffolds in Bone Sialoprotein-Mediated Bone Regeneration, *The Scientific World Journal*. 2013, 812718. <https://doi.org/10.1155/2013/812718>.
- [6] Florencio-Silva R., Sasso G.R. da S, Sasso-Cerri E., Simões M.J., Cerri P.S., (2015). Biology of Bone Tissue: Structure, Function, and Factors That Influence Bone Cells, *BioMed Research International*. 2015, 421746. <https://doi.org/10.1155/2015/421746>.
- [7] Hadjidakis D.J., Androulakis I.I., (2006). Bone Remodeling, *Annals of the New York Academy of Sciences*. 1092 385–396. <https://doi.org/10.1196/annals.1365.035>.
- [8] Valdes-Flores Y., Orozco A., M. L., & Velzquez-Cruz, R. (2013). Molecular Aspects of Bone Remodeling. *InTech*. doi: 10.5772/54905.
- [9] Salhotra A., Shah H.N., Levi, M.T B.. Longaker, (2020). Mechanisms of bone development and repair, *Nat Rev Mol Cell Biol*. 21, 696–711. <https://doi.org/10.1038/s41580-020-00279-w>.
- [10] Raggatt L.J., Partridge N.C., (2010). Cellular and Molecular Mechanisms of Bone Remodeling, *Journal of Biological Chemistry*. 285, 25103–25108. <https://doi.org/10.1074/jbc.R109.041087>.
- [11] Boraschi-Diaz, I., Wang, J., Mort, J. S., & Komarova, S. V. (2017). Collagen type I as a ligand for receptor-mediated signaling. *Frontiers in Physics*, 5, 12. <https://doi.org/10.3389/fphy.2017.00012>
- [12] Kahla, R. B., & Barkaoui, A. (2021). *Bone Remodeling Process: Mechanics, Biology, and Numerical Modeling*. Academic Press.

- [13] Yousefi A.M., James P.F., Akbarzadeh R., Subramanian A., Flavin C., Oudadesse H., (2016). Prospect of Stem Cells in Bone Tissue Engineering: A Review, *Stem Cells International*. 2016, 6180487. <https://doi.org/10.1155/2016/6180487>.
- [14] Harvey, N., Dennison, E., & Cooper, C. (2010). Osteoporosis: impact on health and economics. *Nature Reviews Rheumatology*, 6(2), 99-105. <https://doi.org/10.1038/nrrheum.2009.260>
- [15] García-Gareta E, Coathup MJ, Blunn GW, (2015). Osteoinduction of bone grafting materials for bone repair and regeneration. *Bone*. Dec; 81:112-121. <https://doi:10.1016/j.bone.2015.07.007>.
- [16] Senra M.R., Marques M. de F.V., (2020). Synthetic Polymeric Materials for Bone Replacement, *Journal of Composites Science*. 4, 191. <https://doi.org/10.3390/jcs4040191>.
- [17] Navarro M, Michiardi A, Castaño O, Planell JA, (2008). Biomaterials in orthopedics. *J R Soc Interface*. Oct 6;5(27):1137-58. doi: 10.1098/rsif.2008.0151.
- [18] Fikai A., Andronescu E., Voicu G., Fikai A., Andronescu E., Voicu G., Fikai D., (2011). Advances in Collagen/Hydroxyapatite Composite Materials, *IntechOpen*. <https://doi.org/10.5772/13707>.
- [19] Tapscott D.C., Wottowa C., (2022). Orthopedic Implant Materials, in: *StatPearls*, StatPearls Publishing, Treasure Island (FL).
- [20] Bahraminasab, M., Sahari, B. B., Edwards, K. L., Farahmand, F., & Arumugam, M. (2013). Aseptic loosening of femoral components—Materials engineering and design considerations. *Materials & Design*, 44, 155-163. <https://doi.org/10.1016/j.matdes.2012.07.066>
- [21] Gallo J., Barry Goodman S., Lostak J., M. Janout, (2012). Advantages and disadvantages of ceramic on ceramic total hip arthroplasty: A review, *Biomed Pap Med Fac Univ Palacky Olomouc Czech Repub*. 156, 204–212. <https://doi.org/10.5507/bp.2012.063>.
- [22] Krishnan V., Lakshmi T., (2013). Bioglass: A novel biocompatible innovation, *J Adv Pharm Technol Res*. 4, 78–83. <https://doi.org/10.4103/2231-4040.111523>.
- [23] García-Gareta E., Coathup M.J., Blunn G.W., (2015). Osteoinduction of bone grafting materials for bone repair and regeneration, *Bone*. 81, 112–121. <https://doi.org/10.1016/j.bone.2015.07.007>.
- [24] Filippi M., Born G., Chaaban M., Scherberich A., (2020). Natural Polymeric Scaffolds in Bone Regeneration, *Front Bioeng Biotechnol*. 8, 474. <https://doi.org/10.3389/fbioe.2020.00474>.
- [25] Stewart C., Akhavan B., Wise S.G., Bilek M.M.M., (2019). A review of biomimetic surface functionalization for bone-integrating orthopedic implants: Mechanisms, current approaches, and future directions, *Progress in Materials Science*. 106, 100588. <https://doi.org/10.1016/j.pmatsci.2019.100588>.

- [26] Grzeskowiak, R. M., Schumacher, J., Dhar, M. S., Harper, D. P., Mulon, P. Y., & Anderson, D. E. (2020). Bone and cartilage interfaces with orthopedic implants: A literature review. *Frontiers in Surgery*, 7, 601244. <https://doi.org/10.3389/fsurg.2020.601244>
- [27] Albrektsson T, Johansson C. Osteoinduction, osteoconduction and osseointegration. *Eur Spine J*. 2001 Oct;10 Suppl 2(Suppl 2):S96-101. doi: 10.1007/s005860100282
- [28] Liu, Y., Rath, B., Tingart, M., & Eschweiler, J. (2020). Role of implants surface modification in osseointegration: A systematic review. *Journal of Biomedical Materials Research Part A*, 108(3), 470-484. <https://doi.org/10.1002/jbm.a.36829>
- [29] Jayesh R.S., Dhinakarsamy V., (2015). Osseointegration, *J Pharm Bioallied Sci*. 7 S226–S229. <https://doi.org/10.4103/0975-7406.155917>.
- [30] Mavrogenis, A. F., Dimitriou, R., Parvizi, J., & Babis, G. C. (2009). Biology of implant osseointegration. *J Musculoskelet Neuronal Interact*, 9(2), 61-71.
- [31] Shah, F. A., Thomsen, P., & Palmquist, A. (2019). Osseointegration and current interpretations of the bone-implant interface. *Acta biomaterialia*, 84, 1-15. <https://doi.org/10.1016/j.actbio.2018.11.018>
- [32] Zhu G., Wang G., Li J.J., (2021). Advances in implant surface modifications to improve osseointegration, *Mater. Adv.* 2, 6901–6927. <https://doi.org/10.1039/D1MA00675D>.
- [33] Costa R.R., Mano J.F., (2014), Polyelectrolyte multilayered assemblies in biomedical technologies, *Chem. Soc. Rev.* 43, 3453–3479. <https://doi.org/10.1039/C3CS60393H>.
- [34] Ting, M., Jefferies, S. R., Xia, W., Engqvist, H., & Suzuki, J. B. (2017). Classification and effects of implant surface modification on the bone: human cell–based in vitro studies. *Journal of Oral Implantology*, 43(1), 58-83. <https://doi.org/10.1563/aaid-joi-D-16-00079>
- [35] Henkel, J., Woodruff, M., Epari, D. et al., (2013). Bone Regeneration Based on Tissue Engineering Conceptions — A 21st Century Perspective. *Bone Res* 1, 216–248. <https://doi.org/10.4248/BR201303002>
- [36] Jemat A, Ghazali MJ, Razali M, Otsuka Y. (2015). Surface Modifications and Their Effects on Titanium Dental Implants. *Biomed Res Int*. 2015:791725. doi: 10.1155/2015/791725
- [37] Edgahi, M. A., Naghib, S. M., Emamian, A., Ramezanpour, H., Haghirsadat, F., & Tofighi, D. (2022). A practical review over surface modification, nanopatterns, emerging materials, drug delivery systems, and their biophysiochemical properties for dental implants: Recent progresses and advances. *Nanotechnology Reviews*, 11(1), 637-679. <https://doi.org/10.1515/ntrev-2022-0037>
- [38] Barfeie, A., Wilson, J., & Rees, J. (2015). Implant surface characteristics and their effect on osseointegration. *British dental journal*, 218(5), E9-E9. <https://doi.org/10.1038/sj.bdj.2015.171>

- [39] Gautam, S., Bhatnagar, D., Bansal, D., Batra, H., & Goyal, N. (2022). Recent advancements in nanomaterials for biomedical implants. *Biomedical Engineering Advances*, 100029. <https://doi.org/10.1016/j.bea.2022.100029>
- [40] Schneider, R., Facure, M. H., Chagas, P. A., Andre, R. S., dos Santos, D. M., & Correa, D. S. (2021). Tailoring the Surface Properties of Micro/Nanofibers Using 0D, 1D, 2D, and 3D Nanostructures: A Review on Post-Modification Methods. *Advanced Materials Interfaces*, 8(13), 2100430. <https://doi.org/10.1002/admi.202100430>
- [41] Kurapati, R., Groth, T. W., & Raichur, A. M. (2019). Recent developments in layer-by-layer technique for drug delivery applications. *ACS Applied Bio Materials*, 2(12), 5512-5527 <https://doi.org/10.1021/acsabm.9b00703>.
- [42] Shende, P., Patil, A., & Prabhakar, B. (2020). Layer-by-layer technique for enhancing physicochemical properties of actives. *Journal of Drug Delivery Science and Technology*, 56, 101519. <https://doi.org/10.1016/j.jddst.2020.101519>
- [43] Niepel, M. S., Kirchhof, K., Menzel, M., Heilmann, A., & Groth, T. (2015). Controlling Cell Adhesion Using pH-Modified Polyelectrolyte Multilayer Films. *Layer-by-Layer Films for Biomedical Applications*, 1-30. <https://doi.org/10.1002/9783527675869.ch1>
- [44] D.S. Linnik, Y.V. Tarakanchikova, M.V. Zyuzin, K.V. Lepik, J.L. Aerts, G. Sukhorukov, A.S. Timin, (2021). Layer-by-Layer technique as a versatile tool for gene delivery applications, *Expert Opinion on Drug Delivery*. 18, 1047–1066. <https://doi.org/10.1080/17425247.2021.1879790>.
- [45] Borges, J., & Mano, J. F. (2014). Molecular interactions driving the layer-by-layer assembly of multilayers. *Chemical reviews*, 114(18), 8883-8942. <https://doi.org/10.1021/cr400531v>
- [46] Ziyi Guo, Richardson J. J., Biao Kong, Kang Liang (2020). Nanobiohybrids: Materials approaches for bioaugmentation, *Science Advances*, 6, 12.
- [47] Yan, Y., Björnmalm, M., & Caruso, F. (2014). Assembly of layer-by-layer particles and their interactions with biological systems. *Chemistry of Materials*, 26(1), 452-460. <https://doi.org/10.1021/cm402126n>
- [48] Gribova, V., Auzely-Velty, R., & Picart, C. (2012). Polyelectrolyte multilayer assemblies on materials surfaces: from cell adhesion to tissue engineering. *Chemistry of Materials*, 24(5), 854-869. <https://doi.org/10.1021/cm2032459>
- [49] Köwitsch A, Zhou G, Groth T, (2018). Medical application of glycosaminoglycans: a review, *Journal of Tissue Engineering and Regenerative Medicine*. 12, e23–e41. <https://doi.org/10.1002/term.2398>.
- [50] Decher, G., Eckle, M., Schmitt, J., & Struth, B. (1998). Layer-by-layer assembled multi-composite films. *Current opinion in colloid & interface science*, 3(1), 32-39. [https://doi.org/10.1016/S1359-0294\(98\)80039-3](https://doi.org/10.1016/S1359-0294(98)80039-3)
- [51] Muzzarelli R.A.A., Greco F., Busilacchi A., Sollazzo V., Gigante A., (2012). Chitosan, hyaluronan and chondroitin sulfate in tissue engineering for cartilage

regeneration: A review, *Carbohydrate Polymers*. 89, 723–739. <https://doi.org/10.1016/j.carbpol.2012.04.057>.

[52] H. Sodhi, A. Panitch, (2021). Glycosaminoglycans in Tissue Engineering: A Review, *Biomolecules*. 11, 29. <https://doi.org/10.3390/biom11010029>.

[53] Andrews, S., Cheng, A., Stevens, H., Logun, M. T., Webb, R., Jordan, E., ... & Stice, S. (2019). Chondroitin sulfate glycosaminoglycan scaffolds for cell and recombinant protein-based bone regeneration. *Stem cells translational medicine*, 8(6), 575-585.

[54] Viguet-Carrin, S., Garnero, P., & Delmas, P. D. (2006). The role of collagen in bone strength. *Osteoporosis international*, 17(3), 319-336. <https://doi.org/10.1007/s00198-005-2035-9>

[55] Marion N.W., Mao J.J., (2006). Mesenchymal Stem Cells and Tissue Engineering, *Methods Enzymol*. 420, 339–361. [https://doi.org/10.1016/S0076-6879\(06\)20016-8](https://doi.org/10.1016/S0076-6879(06)20016-8).

[56] Rosenbaum, A. J., Grande, D. A., & Dines, J. S. (2008). The use of mesenchymal stem cells in tissue engineering: a global assessment. *Organogenesis*, 4(1), 23-27. <https://doi.org/10.4161/org.6048>

[57] Baraniak P.R., McDevitt T.C., (2010). Stem cell paracrine actions and tissue regeneration, *Regen Med*. 5, 121–143. <https://doi.org/10.2217/rme.09.74>.

[58] Pittenger, M. F., Discher, D. E., Péault, B. M., Phinney, D. G., Hare, J. M., & Caplan, A. I. (2019). Mesenchymal stem cell perspective: cell biology to clinical progress. *NPJ Regenerative medicine*, 4(1), 1-15. <https://doi.org/10.1038/s41536-019-0083-6>

[59] Infante, A., & Rodríguez, C. I. (2018). Osteogenesis and aging: lessons from mesenchymal stem cells. *Stem cell research & therapy*, 9(1), 1-7. <https://doi.org/10.1186/s13287-018-0995-x>

[60] Gong, F., Groth, T., Tu, C., Zhao, M., Huang, X., & Chu, J. (2021). Crosstalk between Macrophages and Mesenchymal Stem Cells Regulated by Biomaterials and Its Role in Bone Regeneration. *Advances in Materials Science and Engineering*, 2021. <https://doi.org/10.1155/2021/9954205>

[61] Grottkau, B. E., & Lin, Y. (2013). Osteogenesis of adipose-derived stem cells. *Bone research*, 1(1), 133-145. <https://doi.org/10.4248/BR201302003>

[62] Aravamudhan A., Ramos D. M., Nip J., Subramanian A., James R., Harmon M. D, X. Yu, Kumbar S. G. (2013), Osteoinductive Small Molecules: Growth Factor Alternatives for Bone Tissue Engineering, *Current Pharmaceutical Design*. 19 3420–3428.

[63] Monteiro N., Martins A., Ribeiro D., Faria S., Fonseca N.A., Moreira J.N., Reis R.L., Neves N.M., (2015). On the use of dexamethasone-loaded liposomes to induce the osteogenic differentiation of human mesenchymal stem cells, *J Tissue Eng Regen Med*. 9 1056–1066. <https://doi.org/10.1002/term.1817>.

[64] Jorgensen C., Gordeladze J., Noel D., (2004). Tissue engineering through autologous mesenchymal stem cells, *Current Opinion in Biotechnology*. 15, 406–410. <https://doi.org/10.1016/j.copbio.2004.08.003>.

- [65] Chen, H., Tan, X. N., Hu, S., Liu, R. Q., Peng, L. H., Li, Y. M., & Wu, P. (2021). Molecular mechanisms of chondrocyte proliferation and differentiation. *Frontiers in Cell and Developmental Biology*, 1063. <https://doi.org/10.3389/fcell.2021.664168>
- [66] Langenbach, F., & Handschel, J. (2013). Effects of dexamethasone, ascorbic acid and β -glycerophosphate on the osteogenic differentiation of stem cells in vitro. *Stem cell research & therapy*, 4(5), 1-7. <https://doi.org/10.1186/scrt328>
- [67] Tiwari G, Tiwari R, Sriwastawa B, Bhati L, Pandey S, Pandey P, Bannerjee SK, (2012). Drug delivery systems: An updated review. *Int J Pharm Investig*. Jan;2(1):2-11. doi: 10.4103/2230-973X.96920
- [68] Kaźmierczak, Z., Szostak-Paluch, K., Przybyło, M., Langner, M., Witkiewicz, W., Jędruchiewicz, N., & Dąbrowska, K. (2020). Endocytosis in cellular uptake of drug delivery vectors: Molecular aspects in drug development. *Bioorganic & Medicinal Chemistry*, 28(18), 115556.
- [69] Chandrakala, V., Aruna, V. & Angajala, G. (2022). Review on metal nanoparticles as nanocarriers: current challenges and perspectives in drug delivery systems. *emergent mater.* 5, 1593–1615. <https://doi.org/10.1007/s42247-021-00335-x>
- [70] Khan, I., Khan, M., Umar, M. N., & Oh, D. H. (2015). Nanobiotechnology and its applications in drug delivery system: a review. *IET nanobiotechnology*, 9(6), 396-400.
- [71] Mahmoud N.S., Ahmed H.H., Mohamed M.R., Amr K.S., Aglan H.A., Ali M.A.M., Tantawy M.A., (2020) Role of nanoparticles in osteogenic differentiation of bone marrow mesenchymal stem cells, *Cytotechnology*. 72, 1–22. <https://doi.org/10.1007/s10616-019-00353-y>.
- [72] Zielińska A, Carreiró F, Oliveira AM, Neves A, Pires B, Venkatesh DN, Durazzo A, Lucarini M, Eder P, Silva AM, Santini A, Souto EB. (2020). Polymeric Nanoparticles: Production, Characterization, Toxicology and Ecotoxicology. *Molecules*. Aug 15;25(16):3731. doi: 10.3390/molecules25163731.
- [73] Huang, X., Ma, Y., Li, Y., Han, F., & Lin, W. (2021). Targeted drug delivery systems for kidney diseases. *Frontiers in Bioengineering and Biotechnology*, 409.
- [74] Abbasi, E., Aval, S.F., Akbarzadeh, A. et al. (2014) Dendrimers: synthesis, applications, and properties. *Nanoscale Res Lett* 9, 247. <https://doi.org/10.1186/1556-276X-9-247>
- [75] Pires, R. F., Conde, J., & Bonifácio, V. D. (2020). Osteogenic Differentiation of Human Mesenchymal Stem Cells by the Single Action of Luminescent Polyurea Oxide Biodendrimers. *ACS Applied Bio Materials*, 3(12), 9101-9108. <https://doi.org/10.1021/acsabm.0c01315>
- [76] D.A. Balazs, WT. Godbey, (2011). Liposomes for Use in Gene Delivery, *J Drug Deliv*. 326497. <https://doi.org/10.1155/2011/326497>.
- [77] Kaźmierczak Z., Szostak-Paluch K., Przybyło M., Langner M., Witkiewicz W., Jędruchiewicz N., Dąbrowska K., (2020). Endocytosis in cellular uptake of drug delivery

vectors: Molecular aspects in drug development, *Bioorganic & Medicinal Chemistry*. 28 115556. <https://doi.org/10.1016/j.bmc.2020.115556>.

[78] Bareford, L. M., & Swaan, P. W. (2007). Endocytic mechanisms for targeted drug delivery. *Advanced drug delivery reviews*, 59(8), 748-758. <https://doi.org/10.1016/j.addr.2007.06.008>

[79] Kim, T. K., & Eberwine, J. H. (2010). Mammalian cell transfection: the present and the future. *Analytical and bioanalytical chemistry*, 397(8), 3173-3178. <https://doi.org/10.1007/s00216-010-3821-6>

[80] Simões S., Filipe A., Faneca H., Mano M., Penacho N., Düzgünes N., Pedroso de Lima M., (2005). Cationic liposomes for gene delivery, *Expert Opinion on Drug Delivery*. 2, 237–254. <https://doi.org/10.1517/17425247.2.2.237>.

[81] Kusuma G.D., Carthew J., Lim R., Frith J.E., (2017). Effect of the Microenvironment on Mesenchymal Stem Cell Paracrine Signaling: Opportunities to Engineer the Therapeutic Effect, *Stem Cells and Development*. 26, 617–631. <https://doi.org/10.1089/scd.2016.0349>.

[82] Khosravi, D. K., Mozafari, M. R., Rashidi, L., & Mohammadi, M. (2010). Calcium based non-viral gene delivery: an overview of methodology and applications.

[83] Dani, S. U. (1999). The challenge of vector development in gene therapy. *Brazilian Journal of Medical and Biological Research*, 32(2). <https://doi.org/10.1590/S0100-879X1999000200001>.

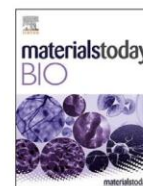
Chapter 2: Engineering osteogenic microenvironments by the combination of multilayers from collagen type I and chondroitin sulfate with novel cationic liposomes

The first paper aimed to show a novel cationic liposome called OO4 in combination with DOPE. These lipids contain high amounts of amino groups and are promising systems for drug delivery. Because of these amino groups, the cationic liposome can be used as polycationic for the development of multilayers using the Layer-by-Layer technique. This technique fabricates surface coatings by alternating adsorption of polyanions and polycations. This study aims to engineer a multilayer system made of Cs and Col by LbL technique with OO4/DOPE liposomes embedded in the terminal layers to create an osteogenic microenvironment. The advantage of using these polyelectrolytes is to mimic the ECM of the bone. Since liposomes are an excellent nanocarrier and suitable for endocytosis and the composition of PEM were used to promote osteogenic differentiation of C2C12 myoblasts as in vitro model. First, physicochemical studies of PEM were done to characterize layer growth, thickness, wettability, surface charge, and topography. The adhesion of myoblast cells was also evaluated whereby the benefit of a cover layer of Cs and finally Col I above the liposome layer was demonstrated. Then, the internalization of cargo-loaded liposomes from the PEM into C2C12 cells was studied using lipophilic (Rhodamine-DOPE conjugate) and hydrophilic (Texas Red labelled dextran) model compounds. Finally, as proof of concept, OO4/DOPE liposomes were loaded with Dex. Dex is a known compound that can induce osteogenic differentiation. Successful induction of osteogenic differentiation of C2C12 cells was shown using histochemical staining and quantification of alkaline phosphatase activity. The results presented in this article indicate that designed OO4/DOPE-loaded PEMs have a high potential to be used as a drug delivery system for implant coating in the field of bone regeneration and other applications.



Contents lists available at ScienceDirect

Materials Today Bio

journal homepage: www.journals.elsevier.com/materials-today-bio

Engineering osteogenic microenvironments by combination of multilayers from collagen type I and chondroitin sulfate with novel cationic liposomes



Y.A. Brito Barrera^a, G. Hause^b, M. Menzel^c, C.E.H. Schmelzer^c, E. Lehner^d, K. Mäder^d, C. Wölk^e, T. Groth^{a,f,*}

^a Department Biomedical Materials, Institute of Pharmacy, Martin Luther University Halle–Wittenberg, Heinrich Damerow Strasse 4, 06120, Halle (Saale), Germany

^b Martin Luther University Halle-Wittenberg, Biocenter, Weinbergweg 22, 06120, Halle (Saale), Germany

^c Department of Biological and Macromolecular Materials, Fraunhofer Institute for Microstructure of Materials and Systems (IMWS), Walter-Hülse-Strasse 1, 06120, Halle (Saale), Germany

^d Department Pharmaceutical Technology, Institute of Pharmacy, Martin Luther University Halle–Wittenberg, Kurt-Mothes Straße 3, 06120, Halle (Saale), Germany

^e Pharmaceutical Technology, Institute of Pharmacy, Faculty of Medicine, Leipzig University, 04317, Leipzig, Germany

^f Interdisciplinary Center of Materials Science, Martin Luther University Halle-Wittenberg, D-06099, Halle (Saale), Germany

ARTICLE INFO

Keywords:

C2C12 myoblasts
cationic lipids
chondroitin sulfate
collagen I
internalization
osteogenic differentiation
polyelectrolyte multilayer system

ABSTRACT

Cationic liposomes composed of a novel lipid (N-(6-amino-1-[N-(9Z)-octadec9-enylamino]-1-oxohexan-(2S)-2-yl)-N'-{2-[N, N-bis(2-aminoethyl) amino] ethyl}-2-hexadecylpropanamide) (OO4) and dioleoylphosphatidylethanolamine (DOPE) possess high amounts of amino groups and are promising systems for lipofection. Moreover, these cationic liposomes can also be used as a polycationic entity in multilayer formation using layer-by-layer technique (LbL), which is a method to fabricate surface coatings by alternating adsorption of polyanions and polycations. Since liposomes are suitable for endocytosis by or fusion with cells, controlled release of their cargo on site is possible. Here, a polyelectrolyte multilayer (PEM) system was designed of chondroitin sulfate (CS) and collagen type I (Col I) by LbL technique with OO4/DOPE liposomes embedded in the terminal layers to create an osteogenic microenvironment. Both, the composition of PEM and cargo of the liposomes were used to promote osteogenic differentiation of C2C12 myoblasts as in vitro model. The internalization of cargo-loaded liposomes from the PEM into C2C12 cells was studied using lipophilic (Rhodamine-DOPE conjugate) and hydrophilic (Texas Red-labeled dextran) model compounds. Besides, the use of Col I and CS should mimic the extracellular matrix of bone for future applications such as bone replacement therapies. Physicochemical studies of PEM were done to characterize the layer growth, thickness, and topography. The adhesion of myoblast cells was also evaluated whereby the benefit of a cover layer of CS and finally Col I above the liposome layer was demonstrated. As proof of concept, OO4/DOPE liposomes were loaded with dexamethasone, a compound that can induce osteogenic differentiation. A successful induction of osteogenic differentiation of C2C12 cells with the novel designed liposome-loaded PEM system was shown. These findings indicate that designed OO4/DOPE loaded PEMs have a high potential to be used as drug delivery or transfection system for implant coating in the field of bone regeneration and other applications.

Abbreviations: AFM, Atomic force microscopy; CLSM, Confocal Laser Scanning Microscopy; Col I, Collagen I; CS, chondroitin sulfate; Dex, Dexamethasone; DLS, Dynamic light scattering; DMEM, Dulbecco's modified Eagle's medium; DOPE, dioleoylphosphatidylethanolamine; ECM, Extracellular matrix; GAG, Glycosaminoglycan; LbL, Layer-by-Layer technique; OO4, (N-(6-amino-1-[N-(9Z)-octadec9-enylamino]-1-oxohexan-(2S)-2-yl)-N'-{2-[N, N-bis(2-aminoethyl) amino] ethyl}-2-hexadecylpropanamide); PEI, Polyethylenimine; PEM, Polyelectrolyte multilayer; PBS, Phosphate-buffered saline; SEM, Scanning electron microscopy; SPR, Surface plasmon resonance; TEM, Transmission electron microscopy; WCA, Water contact angle.

* Corresponding author. Department Biomedical Materials, Institute of Pharmacy, Martin Luther University Halle–Wittenberg, Heinrich Damerow Strasse 4, 06120, Halle (Saale), Germany.

E-mail address: thomas.groth@pharmazie.uni-halle.de (T. Groth).

<https://doi.org/10.1016/j.mtbio.2020.100071>

Received 22 April 2020; Received in revised form 15 July 2020; Accepted 16 July 2020

Available online 31 July 2020

2590-0064/© 2020 The Author(s). Published by Elsevier Ltd. This is an open access article under the CC BY-NC-ND license (<http://creativecommons.org/licenses/by-nc-nd/4.0/>).

Reprinted with permission from Materials Today Bio: Brito Barrera Y. A., Hause, G., Menzel, M., Schmelzer, C. E. H., Lehner, E., Mäder, K., ... & Groth, T. (2020). Engineering osteogenic microenvironments by combination of multilayers from collagen type I and chondroitin sulfate with novel cationic liposomes. *Materials Today Bio*, 7, 100071.

1. Introduction

Major problems that implants may cause have been related to poor healing related to recognition as foreign body with reduction or loss of function after device implantation [1]. These and other complications during the application of medical implants have fostered significant efforts in surface modification of biomaterials to achieve a well-defined and controlled interface between the material and host tissues [2]. Various studies have been focused on modifying the surfaces by physical and chemical means to improve biocompatibility and control cell behavior by establishing desired physicochemical properties, such as surface charge [3], wettability [4], topography [5], stiffness [6], and the presence of specific chemical groups on the surface [7].

Surface properties of scaffold materials are also critical in tissue engineering due to the adhesion and spreading controls functioning of cells including gene expression, proliferation, and differentiation [8,9]. However, tissue engineering goes beyond conventional biomedical implant technology because of degradable materials that are combined with cells and bioactive molecules to mimic the natural process of tissue regeneration [10,11]. Besides synthetic polymers such as polylactic acid, biopolymers such as polysaccharides (e.g. chitosan, hyaluronan, etc.) and proteins (e.g. collagens, gelatin, silk) have been used for making hydrogels, porous scaffolds, and coatings due to their biocompatibility, bioactivity, degradability, and often abundance [12]. Bioactivity of collagens and other proteins of the extracellular matrix (ECM) is due to their interaction with cell adhesion molecules, such as integrins followed by signal transduction processes [13]. On the other hand, polysaccharides in particular glycosaminoglycans (GAG) as class of animal glycans can address directly cellular receptors followed by signal transduction like hyaluronan-CD 44 ligation [14] or interact with matrix proteins and growth factors that lead to stabilization of growth factors and facilitate their binding to the corresponding cellular receptors as known for heparan sulfate with bone morphogenic proteins (BMPs) and corresponding BMP receptors [15]. Hence, ECM proteins like collagens from animal sources are used to make protein coatings on implants to guide cell attachment [16]. Moreover, combinations of GAGs with proteins like collagen I can be used for the formation of bioactive coatings, such as multilayers fabricated through layer-by-layer technique (LbL) [17].

The LbL technique is a method to fabricate coatings by alternating adsorption of polyanions and polycations, occurring via electrostatic or non-electrostatic interaction and is considered as a promising technique to modify material surfaces [18]. The LbL assembly can be realized by different methods such as dip-coating, spin-coating, and perfusion [18].

Since many biomolecules such as proteins and GAG represent polyelectrolytes, LbL can be used for biomedical applications due to inclusion of bioactive molecules [10,19]. Nowadays, biomaterials have been advanced through the design of biocompatible systems for controlled drug release in combination with the development of scaffolds in the area of tissue engineering [20]. The advantage of liposomes is that they can interact with cells through several mechanisms, such as endocytosis, fusion with the cell membrane, lipid exchange, and adsorption [21]. The use of liposomes as building blocks for LbL films has attractive aspects, including the ability to internalize a functional cargo, such as lipophilic or hydrophilic drugs or other bioactive compounds like DNA for transfection and controlled assembly of the liposome within LbL films without hampering the activity of functional molecules in the core or lipid part [22]. First approaches were made using natural phospholipids coated by poly-L-lysine to obtain a cationic surface enabling LbL deposition [23,24]. Nevertheless, the toxicity of poly-L-lysine represents a challenge for biomedical application [25]. An approach with negatively charged liposomes composed of phosphatidylserine or phosphatidylglycerol also allows LbL deposition of liposomes without stabilizing polymers [26]. Apart from the use of natural lipids, the use of novel synthetic lipids may represent an interesting strategy to modify liposomes' features toward better interaction with cells and embedding in LbL multilayer systems.

Malonic acid diamides are a group of peptide-mimicking cationic lipids, which are useful components to formulate liposomes with a positive surface charge, low cytotoxicity, and extremely high transfection efficiency [27,28]. These cationic liposomes can potentially be embedded in multilayer films based on LbL to retain these lipid containers after the localized release of a bioactive compound or alternatively, release the entire container with functional cargos from surfaces into the cells or surrounding tissue [22]. Liposomes have been considered as carrier systems, controlling the delivery of genetic material and other biomolecules, but little is known about their behavior as component of LbL multilayers, yet. Hence, this article investigates the deposition of novel cationic liposomes composed of (N-{6-amino-1-[N-(9Z)-octadec-9-enylamino]-1-oxohexan-(2S)-2-yl}-N'-{2-[N,N-bis(2-aminoethyl)amino]ethyl}-2-hexadecylpropandiamide) (OO4) and dioleoylphosphatidylethanolamine (DOPE) [29], a peptide-mimicking cationic amphiphilic of the malonic acid diamide family, onto polyelectrolyte multilayer (PEM) system. Col I and CS were used as polycations and polyanions, respectively, to mimic the ECM of bone as it was done in a previous study promoting osteogenic differentiation of mesenchymal stem cells [17,30]. The work focuses on characterization of multilayer formation process and surface properties of the resulting films

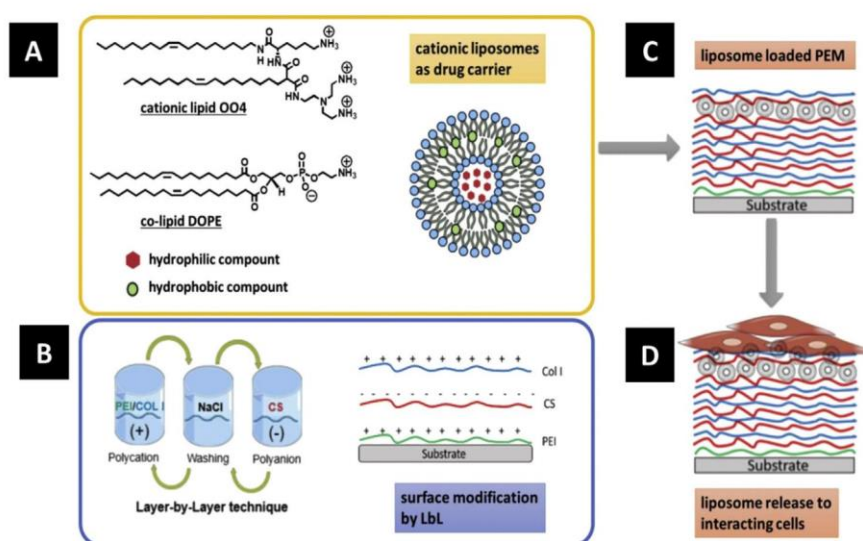


Fig. 1. A) Schematic illustration of the preparation of liposomes using the cationic lipid OO4 and the zwitterionic co-lipid DOPE (protonation state at pH 4) [27]. The liposomes can be used as a carrier for hydrophilic and lipophilic drugs. B) Due to the cationic charge [31], the liposomes can be embedded in polyelectrolyte multilayers (PEMs), which are prepared from collagen I and chondroitin sulfate using the layer-by-layer technique. Poly (ethylene imine) was used for the initial modification of the substrate to achieve a positive surface charge. C/D) The liposomes embedded in the PEM can be internalized by cells growing on the modified substrate.

including surface zeta potential, roughness, topography, and wettability. Besides studies on adhesion and viability of C2C12 myoblast cells on the films, also cellular uptake of liposomes from PEM loaded with hydrophilic and lipophilic fluorescence-labeled model substances was studied. Finally, a proof-of-concept study with liposomes loaded with dexamethasone to promote osteogenic differentiation of cells was performed. Fig. 1 summarizes the content of this work.

2. Materials and methods

2.1. Preparation of liposomes

Liposomes were prepared by film hydration procedure. The lipids OO4 and DOPE were dissolved in chloroform/methanol (8:2, v/v) in a round bottom flask and mixed to a molar ratio of 1:3 (cationic lipid/phospholipid). The solvent was evaporated for 1 h at 200 mbar. Then, 150 mM of NaCl with 10 mM acetic acid at pH 4 was added to final concentration of 1 mg/mL. Afterward, the lipid dispersion was incubated at 50°C and shaking gently for 30 min at 1,400 rpm (Eppendorf Thermomixer 5436) followed by sonication at 37 kHz and 50°C for 5 min. 1,2-dioleoyl-sn-glycero-3-phosphoethanolamine-N-(lissamine rhodamine B sulfonyl) ammonium salt (Avanti Polar lipids); Rhodamine-DOPE-loaded liposomes were prepared with the same method using a molar ratio of 1:3:0.05 ($n_{OO4}:n_{DOPE}:n_{Rhodamine-DOPE}$).

2.1.1. Loading of liposomes with dexamethasone

The liposomes were prepared with a concentration of 1 mg/mL total lipid (50 µg/mL dexamethasone) following the liposome preparation protocol explained in 2.2 using chloroform/methanol (8:2, v/v) stock solutions of OO4, DOPE, and dexamethasone combined to a molar ratio of 1:3:0.2 ($n_{OO4}:n_{DOPE}:n_{Dex}$). For determination of the encapsulation of dexamethasone we varied an ultracentrifugation protocol [32]. Briefly, 0.8 µL of the liposomes were diluted to 9 mL with 10 mM acetic acid buffer at pH 4 containing 150 mM of NaCl. Afterward the liposome dispersion was centrifuged for 4 h with 35,000×g using an ultracentrifuge (TL 100, Beckman Coulter GmbH, Krefeld, Deutschland). Afterward, 0.5 mL of the supernatant was freeze-dried and dissolved in 100 µL methanol for high-performance liquid chromatography (HPLC) analysis. A modified method from United States Pharmacopeia was used to quantify the amount of dexamethasone in the supernatant. A Jasco HPLC system with a PU-1580 Pump equipped with LG-1580-04 quaternary gradient unit, AS 1559 Intelligent Auto Sampler, UV 1559 intelligent UV/VIS Detector (all Jasco, Oklahoma City, USA), Purospher® Star RP-18 endcapped (5 µm) column (Merck Millipore, Billerica, Massachusetts, USA), operated at 40 °C, were used. Methanol was used as the mobile phase at a flow of 1 mL/min. A 20 µL of sample was injected and analyzed at $\lambda = 258$ nm. Data recording and processing were carried out with the software ChromNAV Ver.2 (Jasco, Oklahoma City, USA).

2.1.2. Loading of liposomes with Texas Red-labeled dextran

Liposomes were prepared as stated above (2.2) with the difference that the final concentration was 4 mg/mL and the hydration buffer contained additionally 0.4 mg/mL Texas Red dextran (Texas Red dextran [3,000 Da, lysine fixable] was purchased from Thermo Fisher Scientific). Afterward, the loaded liposomes were purified by size exclusion chromatography using PD-10 Columns (GE Healthcare) and 10 mM acetate buffer pH 4 with 150 mM of NaCl as elution buffer.

2.2. Characterization of liposomes

2.2.1. Dynamic light scattering

The size distribution was characterized by Zetasizer Nano ZS ZEN3600 (Malvern Instruments, Worcestershire, UK). The sample was measured three times; each run consisted 10 runs with a duration of 20 s

at 25°C. The viscosity $\eta = 0.8872$ mPa·s and the refractive index of 1.33 at 25°C were assumed, as has been described previously [33]. The Zetasizer software 7.12 was used for data evaluation.

2.2.2. Zeta potential measurements

The zeta potential measurements were carried out with the laser Doppler electrophoresis technique using Zetasizer Nano ZS ZEN3600 (Malvern Instruments, Worcestershire, UK). Three measurements were performed of 20 runs with a voltage of 50 V at 25°C. The viscosity $\eta = 0.8872$ mPa·s, dielectric constant $\epsilon = 78.5$ F/m and refractive index of 1.33 were assumed. The diffusion of aggregates was converted into the zeta potential using Smoluchowski equation $\zeta = \mu \eta / \epsilon$ (Zetasizer software 7.12) [33].

2.2.3. Transmission electron microscopy

For freeze-fracture analysis, the samples were firstly fixed with a propane jet freeze device JFD 030 (BAL-TEC, Balzers, Liechtenstein). Afterward, the samples were frozen fractured at -150 °C without etching with a freeze-fracture/freeze etching system BAF 060 (BAL-TEC, Balzers, Liechtenstein). The surfaces on the fractures were shadowed with platinum (2 nm layer, shadowing angle 45 degrees) and subsequently with carbon (20 nm layer, shadowing angle 90degrees). The replicas were floated into a sodium chloride solution (4% available chlorine) for 30 min, rinsed in distilled water for 10 min, washed in 30% acetone for 30 min, and finally rinsed in distilled water for 10 min. Thereafter, the replicas were placed on copper grids coated with a Formvar film for imaging [33].

Vitrified specimens for CryoTEM were prepared using a blotting procedure, performed in a chamber with controlled temperature and humidity using an EM GP grid plunger (Leica, Wetzlar, Germany). The sample dispersion (6 µL) was placed onto an EM grid coated with a holey carbon film (C^{flat} , Protochips Inc., Raleigh, NC, USA). Excess solution was then removed by blotting with a filter paper to leave a thin film of the dispersion spanning the holes of the carbon film on the EM grid. Vitrification of the thin film was achieved by the rapid plunging of the grid into liquid ethane held just above its freezing point. The vitrified specimen was kept below 108 K during storage, transferred to the microscope, and investigated.

Specimens were examined with a Libra 120 Plus transmission electron microscope (Carl Zeiss Microscopy GmbH, Oberkochen, Germany), operating at 120 kV. The microscope was equipped with a Gatan 626 cryotransfer system. Images were acquired using a BM-2k-120 dual-sens on-axis SSCCD camera (TRS).

2.3. Cleaning of substrata

Glass coverslips (\emptyset 12 mm, Menzel, Braunschweig, Germany) and silicon wafers (Silicon materials, Kaufering, Germany) were cleaned with a solution of NH_4OH (25%), H_2O_2 (35%), and micropure water (1:1:5, v/v/v) at 80°C for 15 min. Afterward, the samples were washed with micropure water (6 × 5 min) and dried with a stream of nitrogen. The gold-coated glass sensor for surface plasmon resonance (SPR, IBIS Technologies BV, Enschede, The Netherlands. 10×10 mm²) were treated by dipping into 0.5 M NaOH in 96% ethanol and followed by rinsing with ethanol (99%) and one last rinsing step with micropure water followed by drying with nitrogen.

2.4. Preparation of polyelectrolyte multilayers

Collagen type I from porcine skin (Mw ~ 100 kDa) was provided by Sichuan Mingrang Bio-Tech (Sichuan, China). Native CS A from the bovine trachea (Mw ~ 25 kDa) was provided by Sigma-Aldrich (Steinheim, Germany). Poly (ethylene imine) (Mw ~ 750 kDa) was provided by Sigma-Aldrich (Steinheim, Germany). Phosphate-buffered saline (PBS) was prepared according to the following formulation: 2.7 mmol/L KCl, 1.37 mmol/L NaCl, 1.4 mmol/L KH_2PO_4 , 4.3 mmol/L $Na_2HPO_4 \cdot 2H_2O$, pH

7.4. Sodium chloride and acetic acid 30% were purchased from Carl Roth GmbH (Karlsruhe, Germany).

The polyelectrolytes solutions were prepared as follows: PEI was dissolved in 0.15 M sodium chloride solution at a concentration of 5 mg/mL at pH 7.4. CS was dissolved in 0.15 M of sodium chloride at a concentration of 0.5 mg/mL. Collagen I was dissolved in 0.2 M acetic acid at a concentration of 2 mg/mL at 4 °C overnight. The final solution of Col I was obtained by diluting the stock solution in 0.2 M acetic acid supplied with 0.15 M sodium chloride at pH 4.

PEM were fabricated on cleaned glass coverslips, gold sensors, and silicon substrates depending on the type of experiment. PEI was used as the first layer to obtain the positive charge on the substrate followed by adsorption of CS as an anionic layer and then Col I as the cationic layer. The multilayer films were fabricated by immersing the glass coverslips in the polyelectrolyte solution for 15 min (PEI, CS) and 20 min (Col I) and one layer of liposomes for 2 h 30 min. By alternating adsorption of CS and Col I, PEM were build up to fourth bilayers named [CS, Col I]₄ CS, then the liposomes layer [CS, Col I]₄ CS-Lip, and followed by one bilayer [CS, Col I]₄ CS-Lip [CS, Col I]₁. Each adsorption step was followed by rinsing with 0.15 M sodium chloride solution at pH 4 (3 × 5 min).

2.5. Characterization of polyelectrolyte multilayer and surface properties

2.5.1. Ellipsometry

The thickness of the CS and Col I system was measured by a M – 2,000 V scanning ellipsometer (J.A Woollam Co. Inc., Lincoln, NE) at room temperature as previously described [5]. The measurements were performed at incident angles of linear polarized light of 60 degrees, 65 degrees, 70 degrees, and 75 degrees by M – 2,000 V scanning ellipsometer at ambient conditions, which means that PEMs were dry. The measurements were carried out within a wavelength range of $\lambda = 375\text{--}1,000$ nm. The data acquisition rate was about 5 s–10 s per full spectral scan, and the spot size was about $\sim 1\text{--}2$ mm². The experimental data were analyzed with the WVase32 software.

2.5.2. Surface plasmon resonance

The measurements were conducted with an IBIS-iSPR device (IBIS Technologies BV, Enschede, Netherlands). The gold sensor was coated with 11-mercaptoundecanoic acid from Sigma-Aldrich (Steinheim, Germany). The sensor mounted in a flow chamber was equilibrated with 0.15 M sodium chloride to establish a stable baseline. The solutions were injected at a flow rate of 3 $\mu\text{L/s}$ followed by rinsing with sodium chloride for 15 min. PEI was injected for 15 min, followed by CS for 15 min, Col I was injected for 20 min, and the liposomes solution for 150 min. PEM formation was continued until 13 single layers were formed. The average of the angle shifts values (m°) of each rinsing step was used for plotting the graphs.

2.5.3. Zeta potential measurements

The zeta potential of PEM was measured with a SurPASS electrokinetic analyzer (Anton Paar, Graz, Austria). Glass coverslip (10 × 20 mm²) was cleaned and coated with multilayers and mounted in the gap cell with double-sided tape. 1 mmol/L KCl solution was applied as the model electrolyte, and 0.1 mol/L NaOH was used for pH titration from pH 3.0 to 10 (acid-based pH). The flow rate of 100–150 mL/min at a maximum pressure of 300 mbar was adjusted to determine the zeta potential using the streaming. Each measurement was done in duplicate.

2.5.4. Atomic force microscopy

Atomic force microscopy (AFM, Nanowizard IV, JPK-Instruments, Berlin) in Quantitative Imaging Mode (QI) was performed to investigate the surface roughness and topography. Topographical images were recorded using silicon cantilever (qp-BioT, Nanosensors) in a standard liquid cell (JPK-Instruments) containing distilled water. A force map area of 5 × 5 μm^2 was recorded with a resolution of 512 × 512 pt^2 (pixel). Roughness analysis and calculation of the elasticity were performed

using the software JKP Data Processing V5.0.85 and Gwyddion (Gwyddion V2.49, 64-bit).

2.6. Cell culture

Cryopreserved C2C12 myoblasts were thawed and grown in Dulbecco's modified Eagle's medium (DMEM) supplemented with 10% (v/v) fetal bovine serum (FBS), and 1% antibiotic solution (penicillin/streptomycin), all provided by Biochrom AG (Berlin, Germany) in a humidified 5% CO₂/95% air atmosphere. Cells of almost confluent cultures were washed once with sterile PBS followed by treatment with 0.25% trypsin/0.02% EDTA at 37 °C for 3 min. Trypsin was neutralized with DMEM with 10% FBS, and the cells were re-suspended in DMEM after centrifugation at 250g for 5 min. Finally, the cells were seeded on PEM-coated glass coverslips at a concentration of 4 × 10⁴ cells mL⁻¹.

2.7. Viability assay and cell adhesion studies

C2C12 cells were seeded on glass coverslips coated with PEM coating liposomes, or Col I as terminal layers. Cultures were incubated for 24 h, 3 and 7 days, respectively, at 37 °C. After the incubation time the cell viability was determined by QBlue cell viability assay kit (Biochain, Hayward, USA). The cells were washed once with PBS to remove the medium. Then, 500 μL of Qblue solution with colorless medium (10:1) was added to each well and incubated at 37 °C for 3 h. Finally, 100 μL of supernatant from each sample was added to black 96 well plate, and the fluorescence intensity was measured at 544 nm excitation and 590 nm with plate reader.

On the other hand, C2C12 cells were seeded on glass coverslips coated with PEM coatings of either liposome 10th layer, or Col I as terminal layers to evaluate the cell adhesion. PEM-modified glass coverslips were placed into 24 well plates. The re-suspended cells were seeded on the samples in DMEM supplemented with 10% FBS. After incubation at 37 °C for 4 h, cells attached to the PEM were fixed with 4% paraformaldehyde solution (Sigma-Aldrich Chemie GmbH, Taufkirchen, Germany) for 10 min. After rinsing with PBS twice, the cells were permeabilized with 0.1% Triton X-100 in PBS (v/v) (Sigma-Aldrich Chemie GmbH, Taufkirchen, Germany) for 10 min. After rinsing with PBS, non-specific binding sites were blocked by incubation with 1% (w/v) bovine serum albumin (BSA, Merck, Darmstadt, Germany) in PBS at room temperature for 1 h. The focal adhesion protein vinculin was stained using a primary mouse antibody (1:100, Sigma) and a secondary Cy2-conjugated goat anti-mouse antibody (1:100, Dianova). The actin cytoskeleton was visualized by incubating the samples with Phalloidin CruzFluor 555 (1:1000, Santa Cruz Biotechnology, Heidelberg, Germany) at room temperature for 30 min. Cell nuclei were visualized by TO-PRO3 (1:500, Invitrogen, Darmstadt, Germany) incubating the samples for 30 min. The samples were washed with PBS and mounted with Mowiol 4–88 (Calbiochem, Darmstadt, Germany) containing 25 mg mL⁻¹ 1,4-diazabicyclo [2.2.2]-octane (Carl Roth GmbH & Co. Kg, Karlsruhe, Germany) and examined with confocal laser scanning microscopy (CLSM 701, Carl Zeiss Micro-Imaging GmbH, Jena, Germany) using 10 ×, 20 × objectives for quantification of cell adhesion and spreading, while a63 × oil immersion objective was used for higher magnification to visualize nuclei, actin cytoskeleton, and focal adhesions. Images were processed with the ZEN2012 software (Carl Zeiss). The analysis of images to quantify cell count and cell area was performed with Image J.

2.8. Studies on uptake of liposomes and cargo by cells

Quantitative analysis of the uptake of the liposomes was carried out with C2C12 cells plated on glass coverslips coated with PEM consisting terminal liposomes or Col I layers by flow cytometry. After 4 h, the medium was removed, and the samples were washed once with PBS. Afterward, cells were incubated with 0.25% trypsin/0.02% EDTA at 37 °C

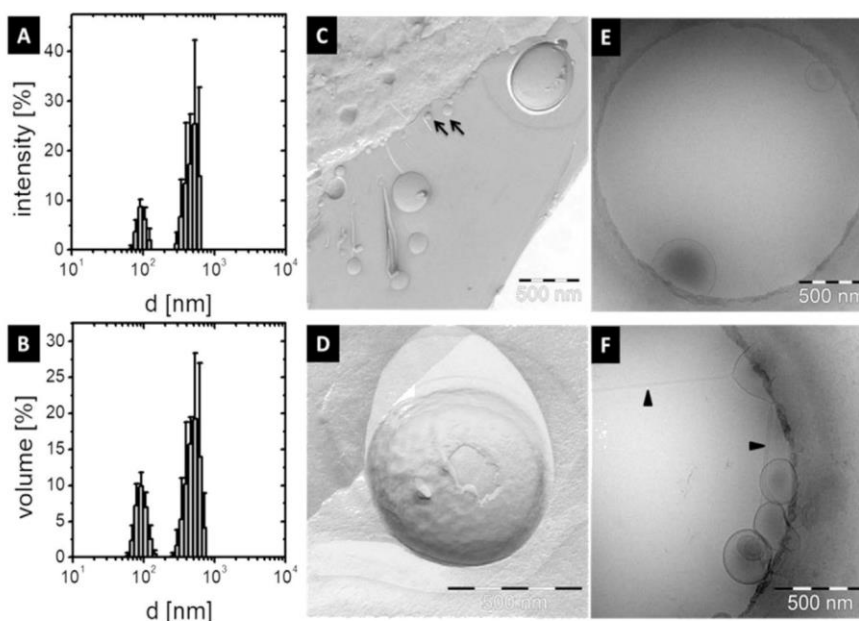


Fig. 2. Characterization of cationic liposomes in acetate buffer pH 4 (10 mM, 0.15 M NaCl). Intensity-weighted (A) and volume-weighted (B) size distribution curve (mean and standard deviation of three independent liposome preparations) measured by dynamic light scattering. Representative freeze-fracture TEM (C/D) and cryo-TEM (E/F) micrographs are shown. The bars indicate 500 nm. Arrows indicate small vesicles with a diameter below 100 nm and triangles lipid tubes.

for 3 min. The detached cell suspensions were centrifuged at $200\times g$ for 5 min, and the supernatant was carefully removed. Cells for imaging were diluted to a concentration of 1×10^6 cells in 60 μL per sample. Images were acquired using ImageStream® Flow cytometer (Merk, Darmstadt, Germany). The sample was measured with bright field at $60\times$ magnification, using AMNIS INSPIRED data acquisition software. The bright field was collected on channel 6, SSC on channel 2 (505–560 nm) and 5 (642–745 nm). Only 60 μL of sample was loaded, and 10,000 events meeting the cell classifier were acquired per file at 7 μm core diameter. A bright-field area vs. intensity side scatters plot was used to identify Texas Red and Rhodamine staining.

2.9. Differentiation studies: alkaline phosphatase assay and Alizarin Red-S staining

PEM-modified glass coverslips were placed into 24 well plates. The C2C12 cells were seeded on the samples in basal medium (DMEM supplemented with 10% FBS) (FBS, Biochrom) at a density of $4 \times 10^4 \text{ mL}^{-1}$ for 24 h. Then, osteogenic medium or basal medium with the following specifications were added to the samples: [CS, Col I]₆ (positive control) in **osteogenic medium** with DMEM, 2% FBS, 100 nM Dex, 50 $\mu\text{g}/\text{mL}$ ascorbic acid, and 10 mM β -Glycerophosphate, [CS, Col I]₆ (negative control) in **basal medium** of DMEM supplemented with 2% FBS only, [CS, Col I]₄-CS-Lip-[CS, Col I]₁ in osteogenic medium. [CS, Col I]₄-CS-Lip (DEX)-[CS, Col I]₁ loaded with Dex-containing liposomes in DMEM 2% FBS, 50 $\mu\text{g}/\text{mL}$ ascorbic acid and 10 mM β -Glycerophosphate (no dexamethasone was added to the medium).

Osteogenic medium composition was selected (DMEM 2% FBS, 100 nM Dex, 50 $\mu\text{g}/\text{mL}$ ascorbic acid, and 10 mM β -Glycerophosphate promoting osteogenesis of C2C12 cells [34]).

After 6 days, the cells were rinsed with PBS, and cell lysis was done using Triton X-100 for 30 min under shaking. Then, 100 μL of cell lysate was incubated with 1 mg/mL of *p*-NPP in 96 well plates and incubated for 90 min at 37°C to estimate expression of alkaline phosphatase (ALP) in C2C12 cells as indicator of osteogenesis. After the incubation time, the measurement of absorbance was done using a plate reader (Fluostar OPTIMA, BMG Labtech) set at 405 nm. At the same time, the BCA protein assay kit (Thermo Scientific, Rockford, IL, USA) was used according to

the manufacturer instruction to normalize ALP data to the protein amount, which corresponds to number of cells.

Furthermore, deposition of calcium phosphate as another indicator of osteogenic differentiation of C2C12 was studied. The cells were rinsed with PBS and fixed with 4% paraformaldehyde solution for 15 min. After rinsing with PBS twice, the cells were stained with Alizarin Red S (40 mM) for 30 min at RT. The cells were photographed with a transmitted light microscope after the staining (Nikon ECLIPSE Ti2, Tokyo, Japan) equipped with a CCD camera (DCIN, 12 V, EXT1/0, Tokyo, Japan). Afterward, the samples were rinsed with PBS again, and the presence of calcium deposits stained in red-orange color. For the quantification, the staining was extracted adding 10% acetic acid and neutralized with 10% ammonium hydroxide. The absorbance was measured at 570 nm with a plate reader.

2.10. Statistical analysis

All statistical analyses were performed with Origin 8G software. Means, standard deviations were calculated. Analysis of significance was performed by one-way ANOVA. A value of $p < 0.05$ was considered significantly different indicated by an asterisk. Further, box plots are shown where appropriate. The box indicates the 25th and 75th percentiles, the median (dash) and mean value (black square), respectively.

3. Results and discussion

3.1. Characterization of liposomes

The OO4/DOPE (1/3, n/n) liposomes were characterized regarding their size distribution, morphology, and surface charge at pH 4 in the presence of 0.15 M NaCl, the conditions of PEM formation. In Fig. 2A and B, the intensity- and volume-weighted size distribution curves are depicted, showing two size populations. The intensity-weighted curve results directly from the light scattering measurements, while the volume-weighted results (calculated from the intensity-weighted curve) are more representative than the other due to multimodal size distributions [35]. No particles with diameters above 1 μm were detected. The first size population appears at diameters between 70 nm and 100 nm,

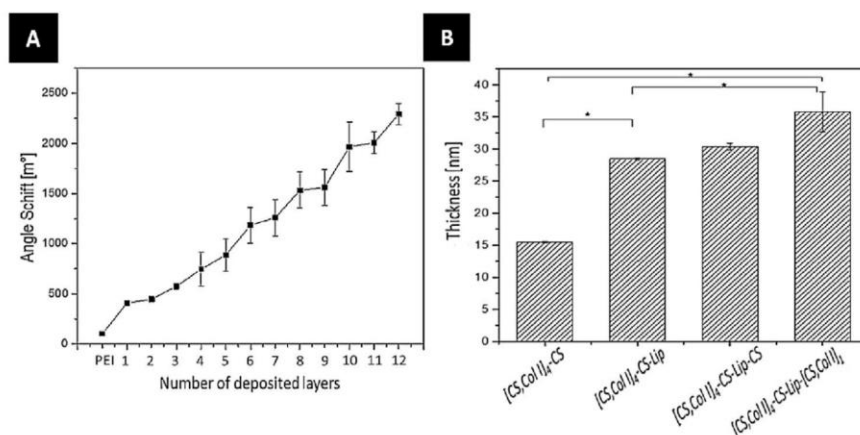


Fig. 3. A) Layer growth of polyelectrolyte multilayer (PEM) systems of [CS, Col I]₄-CS-Lip-[CS, Col I]₁ by surface plasmon resonance numbered as 1st layer to 12th layer. Odd layer numbers correspond to chondroitin sulfate (CS) coating and even layer numbers correspond to collagen I (Col I) coating except the 10th layer, which corresponds to liposomes (Lip); $n = 20$, mean \pm SD. B) Progression of the layer thickness of PEM after adsorption of the final layers of liposomes (Lip), CS and Col I by ellipsometry; $n = 10$, mean \pm SD, * $p \leq 0.05$.

and the second with diameter between 300 nm and 700 nm. The population with the larger diameter-size dominates in the intensity- and volume-weighted curves. To obtain information about the morphology of the liposome formulation, TEM was performed with samples treated by freeze-fracture and cryo-preparation (Fig. 2C–F). Freeze-fracture TEM showed liposomes with spherical shape (Fig. 2C and D). Also, small vesicles (Fig. 2C, arrows) next to larger ones with sizes > 300 nm were found that fit to the DLS measurements. However, no exact size determination is possible by this method because the fracture plane can be far away from the center of spherical liposomes. Indeed, the cryo-TEM micrographs show the unilamellar character of the liposomes (Fig. 2E and F). Moreover, tubes are present, which connect different vesicles (Fig. 2F, triangles). This tube formation is an effect of the OO4 lipid with its bulky head group, which can stabilize such highly curved structures [36]. It should be underlined that the tube formation represents not a disadvantage for the embedding process in PEM because not the shape but charge density is important for the adsorption of charged entities during PEM formation [37]. Therefore, zeta potential was measured to confirm

the overall charge that liposomes possess in the buffer used in LbL-based PEM formation. The average ζ potential of liposomes was 49.5 ± 4.8 mV. This result indicates a highly positive charged surface, useful as a polycationic component for multilayer formation, as it was shown previously by our group using cationic polymeric particles with a ζ potential of ≈ 30 mV [38]. A further advantage is that the positive charge also provides colloidal stability in suspension [39]. X-ray diffraction studies demonstrated that OO4/DOPE 1/3 forms non-correlated bilayers even at high lipid concentrations due to electrostatic repulsion [39]. This behavior causes the tendency to form spontaneously unilamellar vesicles. Since previous experiments demonstrated a high affinity of OO4 to membrane material of extruders, an extrusion step was declined to avoid changes of the OO4/DOPE ratio.

3.2. Characterization of multilayers

Multilayer formation of CS and Col I was studied with the optical technique of SPR. SPR was used to investigate the layer growth behavior

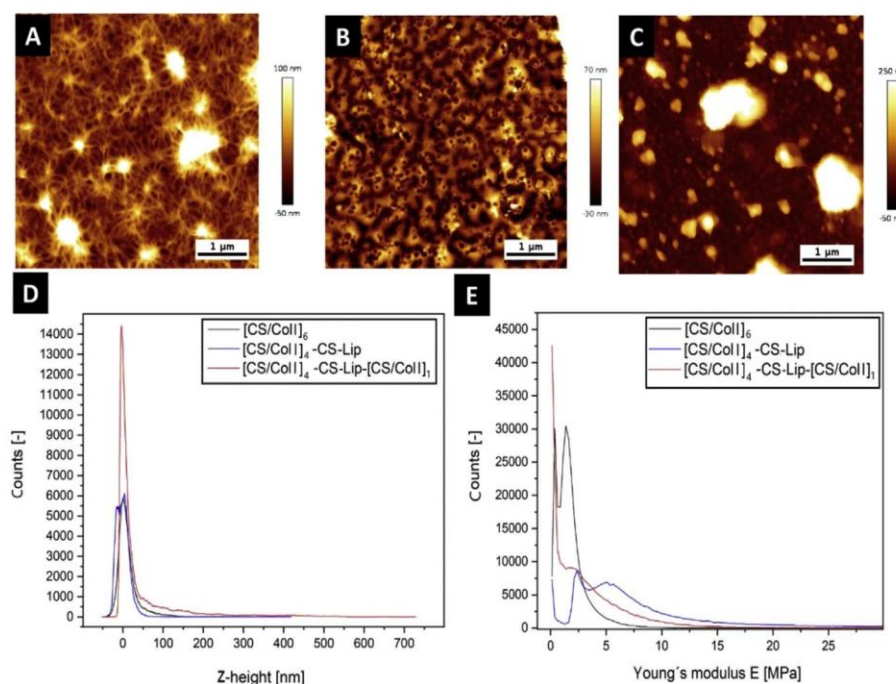


Fig. 4. A–C) Surface topography of (A) liposome-free CS and Col I multilayers of the sequence [CS, Col I]₆, (B) multilayers with embedded liposomes of layer-by-layer sequence [CS, Col I]₄-CS-Lip, (C) surface topography of [CS, Col I]₄-CS-Lip-[CS, Col I]₁, by atomic force microscopy [Scale bar: 1 μ m]. D) Topography height distributions curves of multilayers film. E) Distribution curves of E modulus with a force map of an area of $5 \times 5 \mu\text{m}^2$.

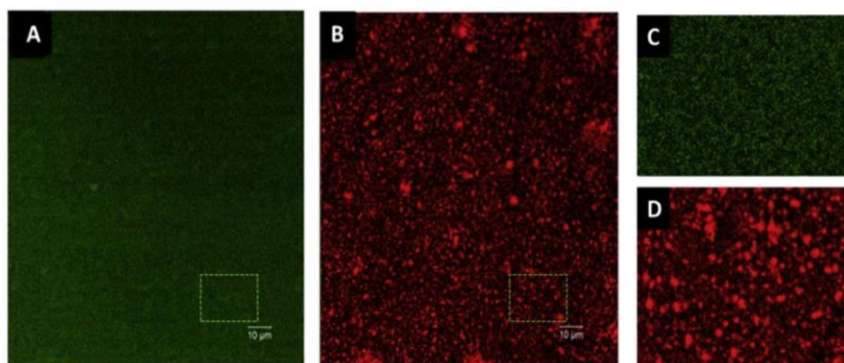


Fig. 5. A) Confocal laser scanning microscopy images of polyelectrolyte multilayer (PEM) system [CS, Col I]₄-CS-Lip-[CS, Col I]₁ CS was labeled with FITC (green), B) liposomes with Rhodamine-DOPE conjugated (red) on PEM [Scale: 10 μ m, 63 \times magnification]. C/D) Zoom of CS and liposomes distribution of the area in the white square.

also as an evidence for PEM formation. Fig. 3 (A) shows a linear growth behavior of PEM; every layer deposition increased the angle shift, which corresponds to an increase of the adsorbed mass [17,30]. It was observed that after the 6th layer, Col I contributed more to mass adsorption than CS, which is probably related to the higher molecular weight of Col I, which was well in line with previous studies [17]. Furthermore, the addition of liposomes as 10th layer (PEM sequence [CS, Col I]₄-CS-Lip) contributed significantly to mass deposition, which was evident by the largest angle shift of 500 m $^\circ$ compared with the other deposition steps in the LbL sequence shown in Fig. 3 (A). This is probably due to the large size of liposomes compared with that of the polyelectrolytes CS and Col I. To obtain also information on the layer thickness, ellipsometry on silicon substrate was applied to characterize the PEM as shown in Fig. 3 (B). The measurements were performed in duplicate of dry films; data were obtained from five different points on each sample with an area of 1–2 mm². The deposition of 9 polyelectrolyte layers (PEM sequence [CS, Col I]₄-CS) resulted in a dry film thickness of 15 nm. An increase in thickness by 40 nm was found after liposome adsorption (PEM sequence [CS, Col I]₄-CS-Lip), which is another evidence for the deposition of liposomes as part of PEM. The relatively low thickness increase after adsorption of liposomes compared with their size obtained in DLS and TEM measurements is probably due to their drying and shrinking. In addition, ellipsometry is providing an integral measure of thickness, which includes areas of higher (with adsorbed) and lower (without adsorbed liposomes) thickness. The final adsorption of a cover layer on the liposomes composed of CS and Col I (final PEM sequence [CS, Col I]₄-CS-Lip-[CS, Col I]₁) to an overall thickness of 45 nm. The results of ellipsometry confirmed the increase in mass deposition observed in SPR particularly after addition of liposomes. It should be noted that thickness of hydrated multilayers will exceed that of dry layers, but ellipsometry data revealed that the thickness increase of a single liposome layer is equivalent to that of the preceding 10 single layers of polyelectrolyte macromolecules, which illustrates the major contribution of adsorbed liposomes to the thickness of multilayer films.

Fig. 4 shows the results of AFM studies that shall shed a light on the topography of PEM with incorporated in comparison with the multilayer without liposomes. The deposited polyelectrolytes without liposomes showed a rather homogenous distribution in the scanned areas (Fig. 4A). The LbL sequence [CS, Col I]₆ was chosen for this experiment because the number of deposition steps is comparable with that of the liposome-loaded PEM. An assembling into a fibrous network was detected, which can be assigned to Col I. This indicates the fibrillization of the soluble Col I after its deposition, which is most probably due to an interaction with CS supporting arrangement of collagen fibers. Details have been discussed in our previous work [17,30]. Evaluation of AFM images after liposome adsorption [CS, Col I]₄-CS-Lip showed a remarkable change in surface topography as demonstrated in Fig. 4 (B). Flattened structures

appeared as an indication of presence and deformation of liposomes probably due to the strong electrostatic interaction with the preceding negative-charged CS layer. The spherical shape of liposomes was probably lost (with their flattening on the charged surface, resulting in the elevated structures). Fig. 4 (C) shows the topography after adsorption of the terminal CS, Col I bilayer. The images are quite different from previous liposome layer with larger aggregates that might indicate that the presence of liposomes in a kind of random distribution may provide nucleation sites for subsequent adsorption of CS and Col I, leading to an accumulation of these polyelectrolytes in certain areas. However, it is also visible that there is a rather granular morphology of multilayer as seen in previous studies with CS and Col I, when the protein was only used as terminal layer [40]. This means that the fibrillization of collagen is a process that requires the presence of multiple layers of the protein in the PEM.

Fig. 4 (D) shows height distribution curves of the highest and lower points in the measured area (5 \times 5 μ m²), which is another measure of overall roughness of the multilayer surface. Here, the highest frequency peak is found after the embedding of the liposomes, which can be taken as another evidence for their immobilization. It is also interesting to note that the preceding [CS, Col I]₆ and the final CS, Col I]₄-CS-Lip-[CS, Col I]₁ As supplemental information about the mechanical properties, Young's modulus (E) was measured. Fig. 4 (E) the E modulus of the sequence [CS, Col I]₆ was \sim 3 MPa. The mean E modulus after embedding the liposomes with sequence [CS, Col I]₄-CS-Lip shows the incidence of two peaks; the first peak was around \sim 4 MPa that indicates the presence of the previous layers as Col I. The second peak \sim 6 MPa resembles most probably the liposomes that can show extremely high E moduli after adsorption on surfaces as found in previous studies [41]. The adsorption of the terminal [CS, Col I] bilayer is represented by peak of \sim 4 MPa like the one of the initial [CS, Col I]₆ multilayers but with a wider distribution. This indicates also a complete coverage of the liposomes layer because of the similar value like the PEM before liposome adsorption. The description of the mechanical properties visualized in Figure D/E corresponds to the images that can be found in the supplemental information (S1).

From AFM, it was assumed that elevations and changes in the roughness of the [CS, Col I]₄-CS-Lip-[CS, Col I]₁ films represent liposomes. To prove that liposomes are embedded or part of multilayers CLSM studies were performed using FITC-labeled CS and Rhodamine-DOPE labeled OO4/DOPE liposomes for the formation of [CS, Col I]₄-CS-Lip-[CS, Col I]₁ PEM. Fig. 5(A) shows that a homogeneous distribution of FITC-CS was observed. Fig. 5(B) shows the distribution of Rhodamine-DOPE fluorescence across the PEM, indicating a successful incorporation of the positively charged labeled liposomes. The image indicates a homogenous distribution of liposomes over the whole area (see Fig. 5C and D), sometimes that may represent some aggregates. The

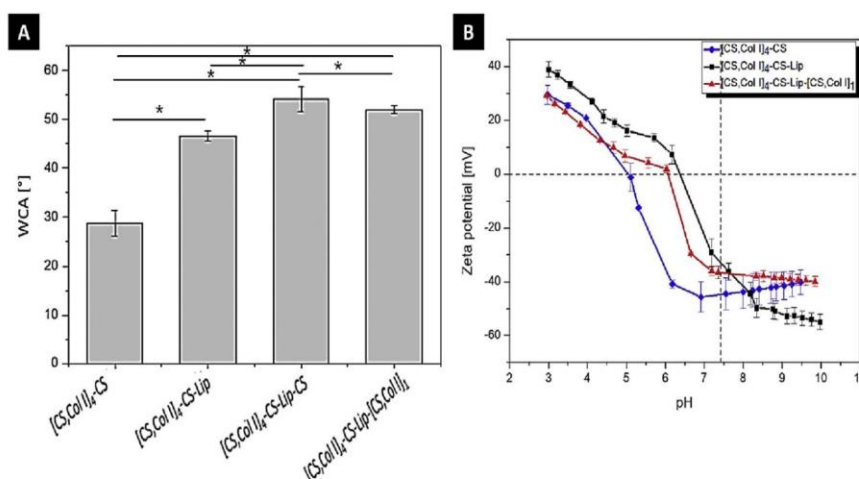


Fig. 6. A) Static water contact angle measurement during multilayer formation after nine layers. Results are means \pm SD of three independent experiments. B) Zeta potential measurements of the three different multilayers. Results are means \pm SD of two independent experiments.

dimensions of items are related to the size area of liposomes and fit to the area of the elevations found in AFM. Furthermore, the [CS, Col I]₄-CS-Lip PEM were prepared in a black, flat bottom 96-well plate to measure the loading degree by fluorescence measurements in a plate reader. It turned out that approximately 10% of the liposomes from the fluid phase were immobilized during the incubation process. Quantification of fluorescence yielded that approximately 15 $\mu\text{g}/\text{cm}^2$ liposomes are bound in a single well of 96 well-plate. The graphical evaluation of Fig. 5B provides the information that about 20% of the investigated film area are covered with Rhodamine-DOPE labeled liposomes. The image for the relative area can be found in the supplemental information (S2).

Surface wettability is an essential factor in the characterization of multilayers because the wetting properties control protein adsorption, and subsequently cell attachment [42]. In addition, wetting properties can be also used to follow the process of multilayer formation because of differences in wetting properties of the different polyelectrolytes [17,30]. Wetting characteristics of [CS, Col I]₄-CS-Lip-[CS, Col I]₁ films and intermediate processing steps are presented in Fig. 6A. The film with the sequence [CS, Col I]₄-CS (basal film for adsorption of cationic liposomes) is more hydrophilic with a WCA of 30°. CS is known to be a hydrophilic polysaccharide, therefore, the contact angle was lower in comparison to Col I [17]. After adsorption of liposomes, the WCA measurements of [CS, Col I]₄-CS-Lip yielded a higher contact angle of 45 degrees, which corresponds to moderately wettable surface. The CLSM experiments above demonstrated an incomplete coverage with liposomes (see Fig. 5), which indicates that both OO4/DOPE liposomes and uncovered CS contribute to this WCA value. With addition of a CS cover layer (PEM sequence [CS, Col I]₄-CS-Lip-CS), the WCA increased to 57°. Theoretically a decrease was expected after addition of a CS layer. The observed increase from 45° to 55° may result from a reorganization of the liposome (layer) after interaction with CS and is also a hint for intermingling structures of liposomes and CS on the surface of [CS, Col I]₄-CS-Lip-CS system. The final system [CS, Col I]₄-CS-Lip-[CS, Col I]₁ has a comparable WCA. These measurements revealed that the [CS, Col I]₄-CS-Lip-[CS, Col I]₁ represent a moderately wettable surface. In a previous work, we showed a WCA of $\approx 45^\circ$ for a [CS, Col I]₄ PEM system [30]. The slightly higher value of $\approx 50^\circ$ detected for the system [CS, Col I]₄-CS-Lip-[CS, Col I]₁ is probably related to intermingling of liposomes with the other two polyelectrolytes.

Zeta potential titration measurements were carried out because of the impact on surface charge on protein adsorption and cell adhesion [43]

but also to follow the changes in surface potential with the final adsorption steps of liposomes, CS and Col I. Fig. 6 (B) shows the changes of the zeta potential during the titration from acidic to basic pH for the basal PEM system [CS, Col I]₄-CS (CS before liposome attachment), [CS, Col I]₄-CS-Lip and the fully assembled liposome-loaded PEM system [CS, Col I]₄-CS-Lip-[CS, Col I]₁ that all resulted in a sigmoidal zeta potential curve.

The film with the terminal CS layer, [CS, Col I]₄-CS, has a point of zero charge (PZC) at pH 5 and shows a negative zeta potential with values around -40 mV at pH 6 lower, which shows the acidic character of the CS, because of the presence of sulfate groups and deprotonated carboxylic groups of CS that have a pKa value of around 3. Therefore, the surface charge is dominated by the terminal CS layer, which covers the film surface. The addition of cationic liposome, LbL sequence [CS, Col I]₄-CS-Lip, results in a PZC at higher pH values (around pH 6) due to the primary amino functions in the head group. In a previous work the pKa of OO4 was determined at pH 6 [27], this means that more than 99% of the lipid species are uncharged at pH ≈ 8 . The observed shift in the PZC also supports that liposomes were irreversibly adsorbed on the surface and do not desorbing during the washing steps with NaCl. However, the curve also demonstrates that the surface is only partially covered by the liposomes, only. Due to the amino groups of OO4 with a pKa value ≈ 6 a nearly neutral surface would be expected at pH values between 7 and 8 (90–99% neutral NH₂ groups), if the surface is dominated by the liposomes. If, we consider that the NH₂ species in DOPE has a pKa between 7 and 8 [44], a slightly negative zeta potential can be assumed at pH 8–9 (90–99% neutral NH₂ groups, and negatively charged phosphate). Hence, the zeta potential is with values between -40 and -60 mV highly negative at pH values above 7, an additional strong influence of the CS layer below can be assumed, a fact that is conform with the incomplete coverage of the film by liposomes confirmed by CLSM. For the final PEM, [CS, Col I]₄-CS-Lip-[CS, Col I]₁, a PZC at around pH 6 was detected. This value is slightly below the values determined for the liposome-terminated film [CS, Col I]₄-CS-Lip. Possibly, the fact is that the collagen contains less basic side groups such as lysine compared with the OO4/DOPE liposomes can explain this behavior. Nevertheless, additionally the influence of CS can be seen due to the zeta potential of ~ -40 mV above pH 7. Some authors suggested that the values of the zeta potential of the polyelectrolyte films not only reflect the outermost polyelectrolyte layer but as well the composition of the layers nearer to the surface [17], a

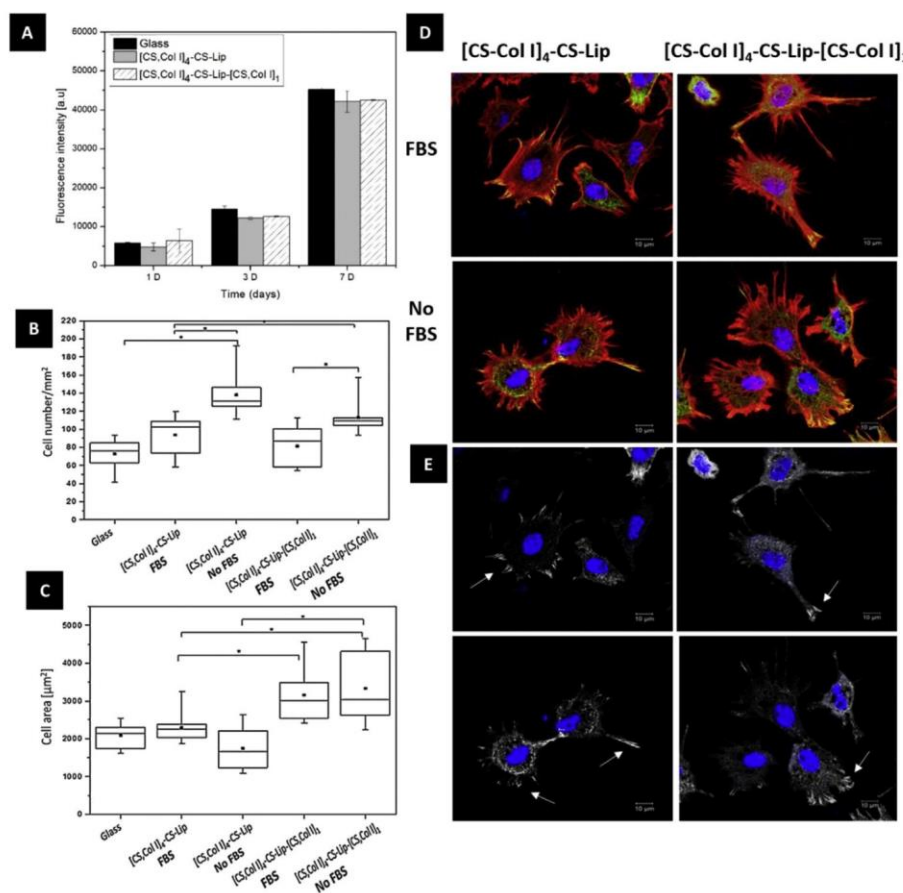


Fig. 7. A) Viability of C2C12 seeded in the presence or absence of bovine serum (FBS) on multilayers [CS, Col I]₄-CS-Lip and [CS, Col I]₄-CS-Lip-[CS, Col I]₁ measured by the QBlue assay for studying of viability of C2C12 cells after 24 h, 3 and 7 days (means \pm SD). B) Quantification of cell count per square millimeter and C) cell spreading area (μm^2) on each of the multilayers after 4 h (Box plots with whiskers, representing first and third quartiles, medians and means, respectively). (*) Statistically significant with p value ≤ 0.05 . D) Merged confocal laser scanning microscopy image of adherent C2C12 cultured on the different PEM after 4 h of incubation in serum and serum-free medium. The cells are stained for filamentous actin (red), vinculin (green), and nucleus (blue). [Scale: 10 μm , 63 \times magnification]. E) In the lower micrographs, white arrows show vinculin (white) positive focal adhesions for the same cells like above.

fact that fits with our observations. For that reason, it is the dominance of the CS on the PEM surface charge, which indicates that it is moderately present at the surface of the film or that there is an intermingled structures of the outer PEM layers.

3.3. Cell viability and adhesion studies on polyelectrolyte multilayer

PEM of Col I and CS were used to mimic the ECM of bone as it was done in a previous study promoting osteogenic differentiation of mesenchymal stem cells [17]. In this study, C2C12 mouse myoblast cells were used to study biocompatibility and osteogenic potential of the different PEMs because of their ability to differentiate either into myotubes or osteoblast [45]. First cell studies were designed to investigate the effect on viability and cell adhesion of the cationic liposomes embedded into PEM.

The viability of C2C12 on [CS, Col I]₄-CS-Lip and [CS, Col I]₄-CS-Lip [CS, Col I]₁ was studied after periods of 1, 3, and 7 days. Fig. 7A, shows the metabolic activity of C2C12 myoblast studied with Qblue assay that provides a measure of the quantity of viable, metabolic active cells on the different PEMs. The positive control (glass) shows a higher fluorescence intensity, compared with [CS, Col I]₄-CS-Lip and [CS, Col I]₄-CS-Lip-[CS, Col I]₁ after 3 and 7 days. Nevertheless, both PEMs express similar fluorescence intensities, which are not significantly different from the control. Also, the data show an increase of the fluorescence intensity with time due to the growth of cells that indicate a good biocompatibility of PEM also with the cationic liposomes, while a good biocompatibility of the terminal CS-Col I bilayer was expected as found in our previous studies [17]. These results demonstrate that none of the surfaces has any

toxic effect, owing to the liposome composition and biocompatible nature of the polyelectrolytes.

The cell adhesion studies were carried on to study cell spreading for the quantification of the cell area, cell number including visualization of actin filaments (red staining), focal adhesions like vinculin (yellow staining), and nuclei (blue staining). These studies are important since cell adhesion and spreading are tightly connected to cell differentiation due to chemical and mechanical signal transduction through focal adhesions including integrins and cell cytoskeleton [46]. C2C12 were seeded in the presence or absence of serum to study cell adhesion on the intermediate PEM with liposomes on terminal layer [CS, Col I]₄-CS-Lip and the final PEM [CS, Col I]₄-CS-Lip-[CS, Col I]₁. In Fig. 7B and C, the results show that there were significantly more cells adhering on [CS, Col I]₄-CS-Lip and [CS, Col I]₄-CS-Lip-[CS, Col I]₁ in the absence of serum, which indicates that adsorption of serum proteins such as albumin on the surface reduces cell adhesion slightly [47], possibly reducing the positive surface charge of liposome terminal layer or the interaction of cell surface integrins with collagen. The analysis of cell spreading data revealed a significantly higher spreading area for cells on [CS, Col I]₄-CS-Lip-[CS, Col I]₁ in the presence and absence of serum compared with C2C12 cells on films with liposomes as terminal layer. Indeed, the concept to add two layers more after [CS, Col I]₄-CS-Lip was not only to protect liposomes from degradation but also to improve the cell adhesion due to integrin-linked adhesion mechanism [7,13]. The advantage of using Col I as a terminal layer is that it provides structural support to cells and cell surface receptors that are important for cell-substrate interaction, for example, via integrin $\alpha 2\beta 1$ receptor of collagen I [48]. In Fig. 7D and E, the organization of the actin fibers in C2C12 seeded on [CS, Col

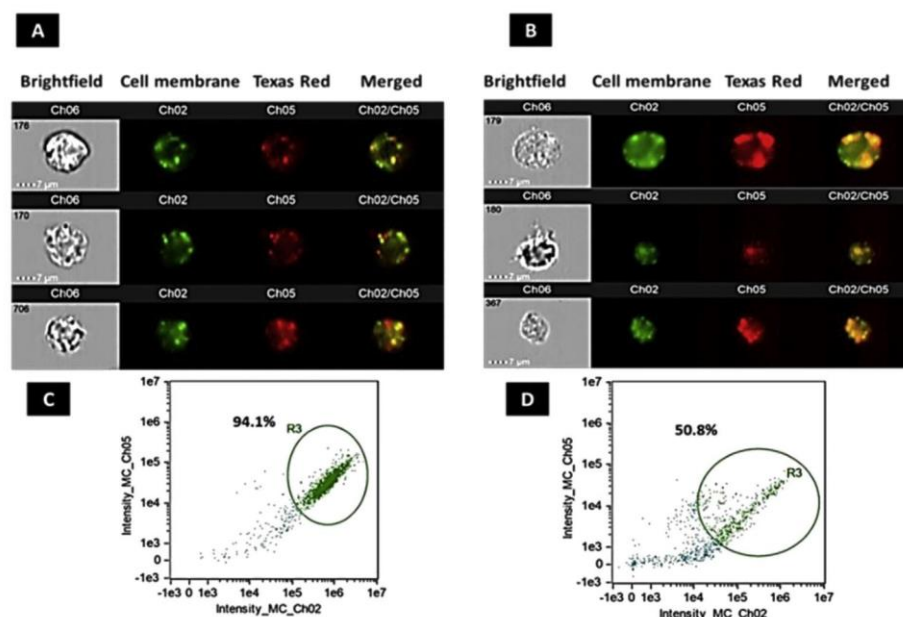


Fig. 8. A/B) Representative images captured by AMNIS ImageStream® Flow cytometer of cells seeded onto multilayers and liposomes with Texas Red dextran after 4 h. The first column shows bright field images of C2C12; the second column shows cell membrane with DiO staining (green); the third column shows liposomes with Texas Red (red); and the last one shows the internalization of Texas Red. [Scale: 7 μm , 60 \times magnification]. A/C) Polyelectrolyte multilayer with liposomes in the supernatant B/D) [CS, Col I]₄-CS-Lip-[CS, Col I]₁ liposomes with Texas Red dextran. C/D) Scatterplots of cell classification into a positive (R3) population.

I]₄-CS-Lip was oriented in an irregular form and organized mostly circumferentially independent whether FBS was present or not. In the case of [CS, Col I]₄-CS-Lip-[CS, Col I]₁ the organization of actin fibers was arranged longitudinally corresponding to higher cell spreading. Furthermore, the staining of vinculin at the end of actin fibers was present in C2C12 cells seeded on both surfaces indicating the presence of focal adhesions reflecting an integrin-mediated interaction with the surface (Fig. 7 E) [48]. The presented cell adhesion studies underline the beneficial effect of Col I as the terminal surface layer but also that the adsorbed liposomes possess an excellent biocompatibility as found in our previous studies [27,28].

3.4. Studies on endocytosis of liposomes labeled with model compounds

The question arose whether PEM-embedded liposomes can deliver a cargo into the cells growing on the modified surface. From our previous studies, it is known that cells have the capacity to rearrange PEMs consisting of CS and Col I mechanically and enzymatically [17], which means that liposomes even embedded underneath a terminal CS-Col I bilayer should be accessible to cells to be taken up by endocytosis. For that purpose, two model compounds were chosen, Rhodamine-DOPE, an amphiphilic compound, which was incorporated in the lipid bilayer of liposomes, and Texas Red dextran as a hydrophilic compound encapsulated in the liposomal aqueous core [49]. Imaging flow cytometry was

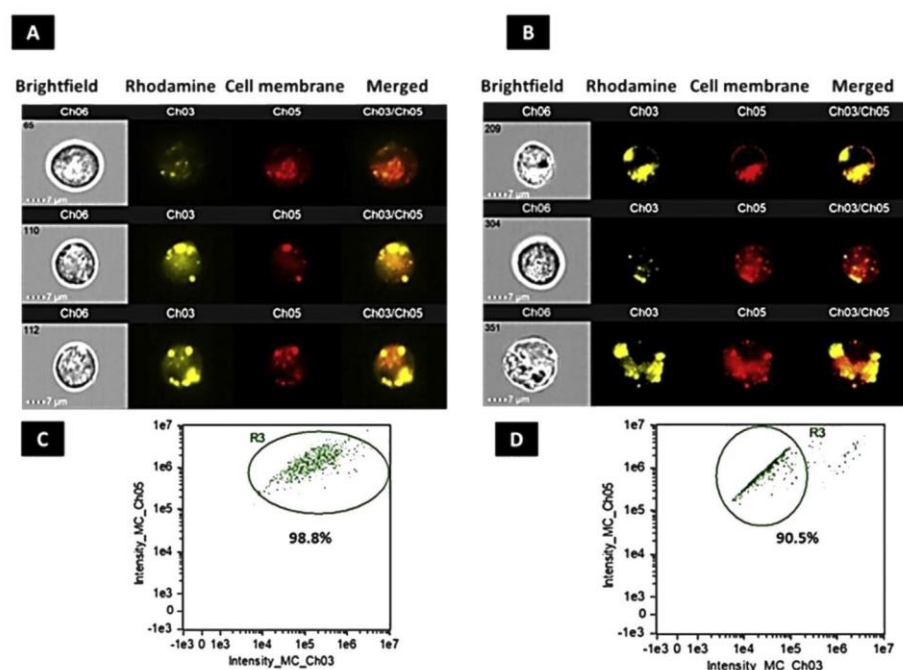


Fig. 9. A/B) Representative images captured by AMNIS ImageStream® Flow cytometer of cells seeded onto multilayers [CS, Col I]₆ supernatant and [CS, Col I]₄-CS-Lip-[CS, Col I]₁ with Rhodamine-DOPE conjugate after 4 h. The first column shows bright-field images of C2C12; the second column shows liposomes with Rhodamine-DOPE conjugate (yellow); the third column shows cell membrane with Cell Mask staining (red); and the last one shows the internalization of Rhodamine-DOPE conjugated. [Scale: 7 μm , 60 \times magnification]. A/C) polyelectrolyte multilayer (PEM) with liposomes in the supernatant B/D) Liposomes embedded in PEM [CS, Col I]₄-CS-Lip-[CS, Col I]₁. C/D) Scatterplots of cell classification into a positive (R3) population.

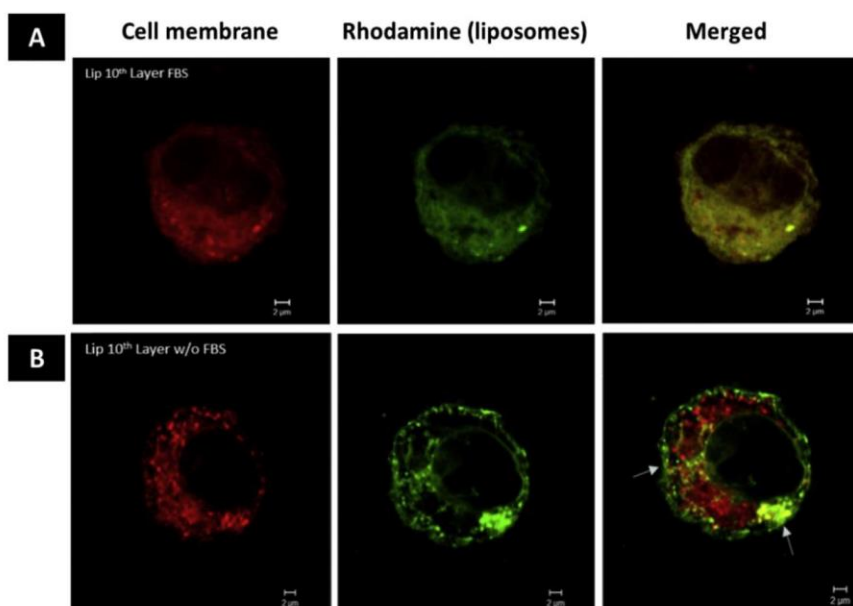


Fig. 10. Confocal laser scanning microscopy images of C2C12 cells growing on [CS, Col I]₄-CS-Lip-[CS, Col I]₁ in the presence of fetal bovine serum and under serum-free conditions. Cell membrane Cellmask Red (red), liposomes labeled with Rhodamine-DOPE conjugate (green). [Scale: 2 μm] Arrows point to co-localization sites of the liposomes.

used to investigate and quantify cells, which were labeled with one of the fluorescent labels after growing on [CS, Col I]₄-CS-Lip-[CS, Col I]₁ in comparison with cells growing on [CS, Col I]₆ with OO4/DOPE liposomes in the supernatant as a control. An association of the labeled compounds with the cells was taken as a strong indication of endocytic uptake of liposomes. Fig. 8 shows the quantification of Texas Red dextran-positive C2C12 cells. The micrographs visualized that a positive Texas Red signal is strongly associated with the cells (Fig. 8A and B). The intensity was shifted to higher values, indicated by the area (R3) after successful uptake of Texas Red dextran (Fig. 8C and D). The quantification of liposome uptake (Texas Red dextran-positive cells) indicated that

for cells that grow on the liposome-loaded PEM [CS, Col I]₄-CS-Lip-[CS, Col I]₁ 50.8% of the cells internalized liposomes (Fig. 8B, right diagram). However, for cells growing on a liposome-free PEM film [CS, Col I]₄ with liposomes in the supernatant, 94.1% C2C12 cells were Texas Red dextran-positive. The physical studies on multilayer formation indicated that structural rearrangement processes the liposomes when a further CS layer was added (see results of WCA studies). Therefore, some loss of the hydrophilic cargo seems to be possible after the adsorption of liposomes. Hence, the uptake result from adsorbed liposomes labeled with Texas Red-dextran seems to be encouraging because they demonstrate that a transfer of hydrophilic substances is possible with this system.

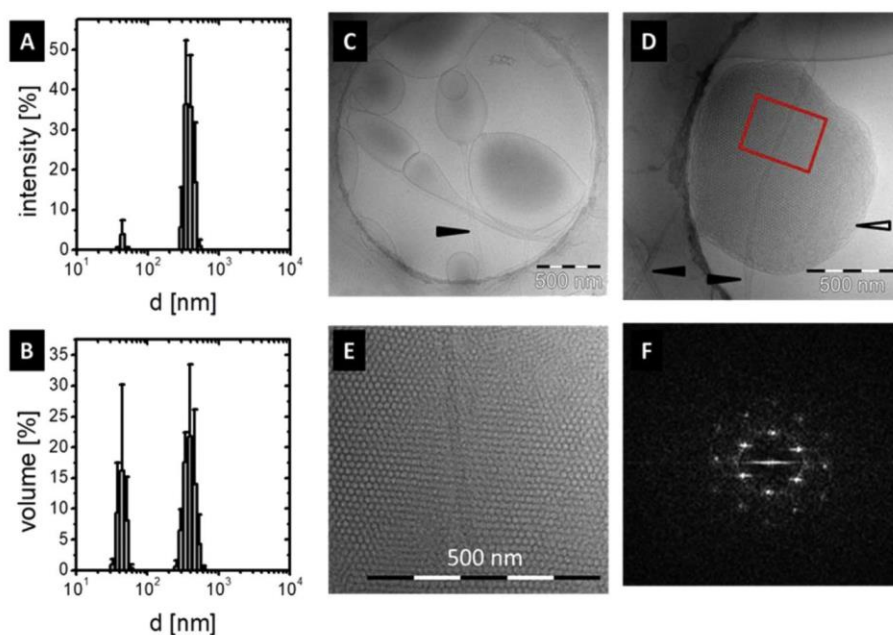


Fig. 11. Characterization of cationic liposomes in acetate buffer pH 4 (10 mM, 0.15 M NaCl) loaded with dexamethasone (2.5% m/m). Intensity-weighted (A) and volume-weighted (B) size distribution (mean and standard deviation of three independent liposome preparations) measured by dynamic light scattering. Representative cryo-TEM (C–E) micrographs are shown. The bars indicate 500 nm. Black triangles indicate lipid tubes and white triangles, cubosomes. E) is the zoomed image in the red labeled region of Figure D. F) shows the diffractogram gained by D due to Fourier transformation demonstrating the high order of the cubic structure.

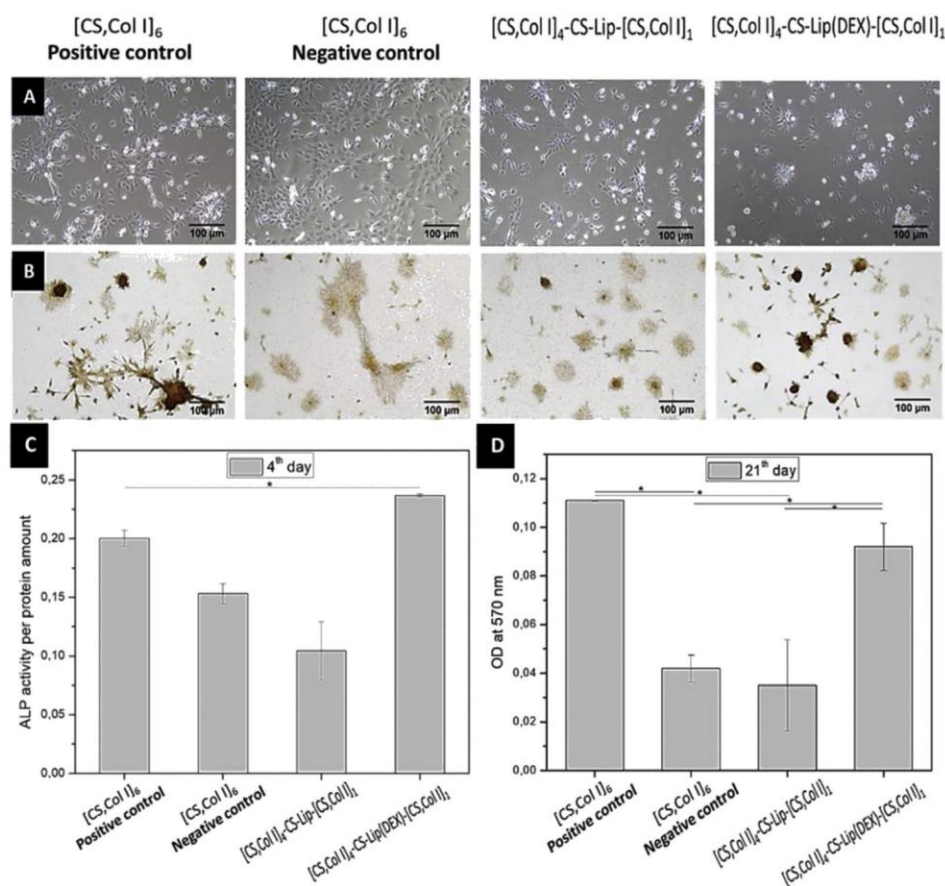


Fig. 12. Four systems are compared for osteogenic differentiation: [CS, Col I]₆ in osteogenic medium (positive control), [CS, Col I]₆ in basal medium (negative control), Dex-free liposomes [CS, Col I]₄-CS-Lip-[CS, Col I]₁ in osteogenic medium and loaded with Dex-containing liposomes [CS, Col I]₄-CS-Lip(Dex)-[CS, Col I]₁ in basal medium with (ascorbic acid and β -Glycerophosphate). **A)** Phase contrast images of C2C12 on the different systems after 4 days. **B)** Alizarin Red-S staining after 14 days [Scale: 100 μ m, 10 \times magnification]. **C)** Measurements of ALP activity in C2C12 cells seeded the different conditions in 24 well plates after 4 days of incubation. The measurements were normalized to the protein amount using the BCA assay. **D)** Measurement of Alizarin Red staining after 14 days of incubation.

Fig. 9 shows the uptake of Rhodamine-DOPE conjugate in C2C12 cells growing either on the liposome-loaded film [CS, Col I]₄-CS-Lip-[CS, Col I]₁ or [CS, Col I]₆ with liposomes in the supernatant. The Rhodamine-DOPE label was detected in C2C12 cells growing on both systems. The quantification of liposome uptake indicated that 90.5% of cells growing on [CS, Col I]₄-CS-Lip-[CS, Col I]₁ were Rhodamine-DOPE-positive (Fig. 9D), whereas 98.8% of cells growing on [CS, Col I]₆ with liposomes in the supernatant, were Rhodamine-DOPE positive (Fig. 9C). Consequently, an efficient uptake of liposomes can be assumed for both conditions.

Summarizing the observations above, it can be demonstrated that C2C12 cells efficiently internalize hydrophilic or lipophilic substances from liposomes embedded in [CS, Col I]₄-CS-Lip-[CS, Col I]₁ PEM. It cannot be differentiated with this experiment, if complete liposomes or only the cargo is taken up, although the first case is more reasonable. The results also indicate that uptake of cargo by C2C12 cells from liposomes in the supernatant is more efficient than from those embedded in multilayers, particularly regarding hydrophilic cargo. The small differences in the transfer of Rhodamine-DOPE between adsorbed and supernatant liposomes indicate that embedded liposomes remain accessible and can be taken up by adhering C2C12 cells. However, the postulated rearrangement of liposomes that is indicated by WCA and ellipsometry measurements might be connected to increased permeabilization of the lipid bilayer and partial loss of the hydrophilic cargo Texas Red dextran from the core of liposomes, while the lipophilic cargo Rhodamine-DOPE is an intrinsic part of the lipid membrane and remains in the hydrophilic environment. Hence, a different efficiency in the transfer of hydrophilic and lipophilic cargo can be expected.

To obtain more information if the cell-associated fluorescence found by flow cytometry analysis was related to internalization by or only association of liposomes with the cells, uptake experiments were performed

with C2C12 cells growing on [CS, Col I]₄-CS-Lip-[CS, Col I]₁ using Rhodamine-DOPE-loaded liposomes in the presence and absence of serum using CLSM. Bovine serum was added here to mimic the presence of plasma and subsequent adsorption of proteins on the PEM surface that may affect also the interaction of cells with embedded liposomes. Fig. 10 shows that in both cases, the label was found intracellularly in a granular distribution although more when FBS was absent proving the endocytosis of liposomes with transfer of the cargo into the cell.

3.5. Proof of concept study with dexamethasone-loaded liposomes

The previous results demonstrated clearly that the novel cationic OO4/DOPE liposomes embedded in a PEM system can be used for controlled release or transfer of components into cells. However, as a proof-of-concept that such transfer can also change cellular functions, the effect of the internalization of a lipophilic drug with effect on cell differentiation is studied here. For this purpose, dexamethasone (Dex) was incorporated in the lipid bilayer of liposomes to induce differentiation of C2C12 cells into osteoblasts [50]. The quantification of the loading capacity by HPLC demonstrated an efficient loading of 2.5% (m/m) of dexamethasone (loading efficiency of 54.0% and 54.3% in an experimental duplicate with a theoretical 5% (m/m) loading). The incorporation of dexamethasone in the lipid bilayer had only slight effects on OO4/DOPE liposomes. The size distribution curve (Fig. 11A and B) shows still a bimodal distribution comparable with drug-free OO4/DOPE liposomes (Fig. 2A and B). However, compared with the drug-free liposomes, the smaller population decreased in intensity. Consequently, a slight increase in the particle size was observed. The measured ζ potential decreased from 49.5 ± 4.8 mV to 44.1 ± 4.2 mV. However, it was still highly positive, which guarantees the adsorption during LbL multilayer

formation. Furthermore, large unilamellar vesicles and tubular structures were found (Fig. 11C) comparable with unloaded liposomes. Besides, these expected structures, cubosomes appeared, lipid nanoparticles consisting of continuous periodic membrane lattice structures in the inner core (Fig. 11D, white arrows, detail in Fig. 11E). These ordered 'membrane folding', which is connected with an increase of membrane area, allows a high degree of incorporation of lipophilic drugs compared with unilamellar liposomes of comparable size. The treatment of the cryo-TEM micrographs of the cubosomes with Fourier transformation resulted in a reflex pattern of multiple signals, which demonstrates the highly ordered symmetry of the cubic liquid crystalline phase inside the cubosomes (Fig. 11F) [51]. More details about the cubosomes can be found in the [supplemental information \(S3–S6\)](#).

Since, a successful incorporation of dexamethasone in OO4/DOPE liposomes could be shown, their effect after incorporation in [CS, Col I]₄-CS-Lip-[CS, Col I]₁ on osteogenic differentiation of C2C12 cells was studied regarding the enzymatic activity of ALP and deposition of calcium phosphate by histochemical staining with Alizarin Red. Indeed, this experimental model for osteogenesis of cells induced by other types of Dex-loaded liposomes was demonstrated previously, but applying them in supernatant [51]. The PEM with empty liposomes was chosen for comparison because CS and Col I containing multilayers may promote osteogenic differentiation of cells by mimicking the ECM composition of bone [17]. C2C12 were seeded on the different surfaces as described in the method section. Fig. 12A shows representative phase contrast micrographs of C2C12 cells on the different systems at day 4. It is visible that more cells were found on negative and positive controls that resemble [CS, Col I]₆ PEM with osteogenic and basal medium, while cell number on multilayers with embedded liposomes was slightly lower, which corresponds also to the studies with QBlue assay shown in Fig. 7A. Another interesting finding was that C2C12 cells tended to form aggregates when cultured on PEM with Dex-loaded nanoparticles [CS, Col I]₄-CS-Lip (DEX)-[CS, Col I]₁ (see Fig. 12A again, right micrograph). Alizarin Red-S staining was used to detect the formation of mineralized matrix by C2C12 cells after 14 days. In Fig. 12B, cells growing on [CS, Col I]₄-CS-Lip-[CS, Col I]₁ loaded with Dex-containing liposomes are characterized by stronger staining with Alizarin Red-S in comparison with the [CS, Col I]₄-CS-Lip-[CS, Col I]₁ film bearing drug-free liposomes and have a staining that is comparable with the positive control with dexamethasone in osteogenic medium. Quantitative measurements of osteogenic differentiation by ALP activity were done after 4 days and shown in Fig. 12C. An increase of ALP was found in samples where Dex-loaded liposomes were embedded [CS, Col I]₄-CS-Lip-[CS, Col I]₁ in comparison with the positive and negative control. It was also found that ALP was lower when cells were cultured on PEM with drug-free liposomes [CS, Col I]₄-CS-Lip-[CS, Col I]₁. Quantification of calcium phosphate by solubilizing bound Alizarin Red is shown in Fig. 12D. It is visible that deposition of calcium phosphate after 14 days was highest in cultures of cells on positive control, followed by cells growing on PEM with Dex-loaded PEM. Both negative control and PEM with drug-free liposomes had significantly lower values of Alizarin Red, which underlines the promoting effect of dexamethasone on differentiation of C2C12 myoblasts into osteoblastic cells.

The results indicate that dexamethasone can be taken up from liposomes embedded in PEM by adhering and growing C2C12 myoblasts cells. Therefore, such multilayer system such as [CS, Col I]₄-CS-Lip-[CS, Col I]₁ can help to avoid systemic effects, minimizing exposure of healthy or other tissues to the drugs having a local effect, only when used as a coating on implants or scaffold materials [10]. Here, the [CS, Col I]₄-CS-Lip(DEX)-[CS, Col I]₁ with Dex-loaded liposomes induced the osteogenic differentiation of C2C12 cells.

4. Conclusion

This work has shown that the LbL technique can produce multifunctional surface coatings to tailor the composition and

physicochemical properties of surfaces and permit controlled transfer of compounds. The characterization studies demonstrated a stable, relatively uniform film formation with immobilization of liposomes that could be taken up by cells even when covered with an additional bilayer of CS-Col I. Indeed, it was found that the transfer of lipophilic model compounds contained in the lipid bilayer was more efficient than that of hydrophilic contained in the core of liposomes, probably related to the reorganization of liposomes during adsorption of multilayers. It was also possible to demonstrate the functionality of this transfer of compounds by/through immobilized liposomes shown by the effect of a functional cargo like dexamethasone inducing osteogenic differentiation of C2C12 cells in situ. It should be considered that the suggested approach is applicable to a variety of cargos such as drugs, siRNA, mRNA and DNA for gene silencing, transient or permanent gene expression for in situ transfer avoiding potential problems in vivo like systemic toxicity, aggregation/interaction of liposomes with body fluids like blood and removal by the RES ending up in the liver, spleen, and other organs. Hence, the benefit of immobilization of liposomes in PEM is the increase in the uptake efficiency by increasing the local concentration close to the cell but probably also prolonging the half-life of the incorporated compounds. Results can be considered as a proof of concept of combination of LbL systems with liposomes to design the microenvironment of cells by the composition of multilayers and the kind of cargo to have the desired effects on the surrounding cells and tissues.

Author contributions

Y.A.B.B performed large part of surface characterization, studies with cells and writing of the manuscript; G.H. performed transmission electron microscopy, M.M. and C.E.H.S. carried out atomic force microscopy studies and made corresponding contributions to the manuscript. E.L. and K.M. performed high-performance liquid chromatography analysis of dexamethasone content of liposomes and made corresponding contributions to the manuscript. C.W. performed synthesis of lipids, preparation, and characterization of liposomes and was involved in conceptualization of the study and writing of the manuscript. T.G. was involved in conceptualization and writing of the manuscript. All authors were involved in reviewing and editing the final manuscript.

Funding

Y.A.B.B supported by the CONACYT-México and German Academic Exchange Service (DAAD). The work was supported by the Fraunhofer Internal Programs under Grant No. Attract 069–608203 (C.E.H.S.). The supported by the Deutsche Forschungsgemeinschaft (DFG) project-ID 396823779 (C.W.) is acknowledged. T.G. acknowledges the High-Performance Center Chemical and Biosystems Technology Halle/Leipzig and support by the European Regional Development Fund (ERDF).

Declaration of competing interest

The authors declare that they have no known competing financial interests or personal relationships that could have appeared to influence the work reported in this paper.

Acknowledgments

The authors thank the technical assistance of Mrs. Marlis Porobin for performing zeta potential measurements. We are very thankful to Dr. Alexander Navarrete Santos for his help during imaging flow cytometry measurements and data analysis.

Appendix A. Supplementary data

Supplementary data to this article can be found online at <https://doi.org/10.1016/j.mtbio.2020.100071>.

References

- [1] K.M.R. Nuss, B. von Rechenberg, Biocompatibility issues with modern implants in bone - a review for clinical orthopedics, *TOORTHJ* 2 (2008) 66–78, <https://doi.org/10.2174/1874325000802010066>.
- [2] S.P. Adiga, C. Jin, L.A. Curtiss, N.A. Monteiro-Riviere, R.J. Narayan, Nanoporous membranes for medical and biological applications, *Wiley Interdiscip Rev Nanomed Nanobiotechnol* vol. 1 (2009) 568–581, <https://doi.org/10.1002/wnan.50>.
- [3] G. Altankov, K. Richau, T. Groth, The role of surface zeta potential and substratum chemistry for regulation of dermal fibroblasts interaction, *Mater. Werkst.* 34 (2003) 1120–1128, <https://doi.org/10.1002/mawe.200300699>.
- [4] G. Altankov, F. Grinnell, T. Groth, Studies on the biocompatibility of materials: fibroblast reorganization of substratum-bound fibronectin on surfaces varying in wettability, *J. Biomed. Mater. Res.* 30 (1996) 385–391, [https://doi.org/10.1002/\(SICI\)1097-4636\(199603\)30:3<385::AID-JBM13>3.0.CO;2-J](https://doi.org/10.1002/(SICI)1097-4636(199603)30:3<385::AID-JBM13>3.0.CO;2-J).
- [5] M.S. Niepel, F. Almouhanna, B.K. Ekambaram, M. Menzel, A. Heilmann, T. Groth, Cross-linking multilayers of poly-L-lysine and hyaluronic acid: effect on mesenchymal stem cell behavior, *Int. J. Artif. Organs* 41 (2018) 223–235.
- [6] N. Brizuela Guerra, C. González-García, V. Llopis, J. Carlos Rodríguez-Hernández, D. Moratal, P. Rico, M. Salmerón-Sánchez, Subtle variations in polymer chemistry modulate substrate stiffness and fibronectin activity, *Soft Matter* 6 (2010) 4748–4755, <https://doi.org/10.1039/C0SM00074D>.
- [7] N. Faucheux, R. Schweiss, K. Lützow, C. Werner, T. Groth, Self-assembled monolayers with different terminating groups as model substrates for cell adhesion studies, *Biomaterials* 25 (2004) 2721–2730, <https://doi.org/10.1016/j.biomaterials.2003.09.069>.
- [8] M. Tanaka, Design of novel 2D and 3D biointerfaces using self-organization to control cell behavior, *Biochim. Biophys. Acta Gen. Subj.* 1810 (2011) 251–258, <https://doi.org/10.1016/j.bbagen.2010.10.002>.
- [9] N.J. Sniadecki, R.A. Desai, S.A. Ruiz, C.S. Chen, Nanotechnology for cell–substrate interactions, *Ann. Biomed. Eng.* 34 (2006) 59–74, <https://doi.org/10.1007/s10439-005-9006-3>.
- [10] R.R. Costa, J.F. Mano, Polyelectrolyte multilayered assemblies in biomedical technologies, *Chem. Soc. Rev.* 43 (2014) 3453–3479, <https://doi.org/10.1039/C3CS60393H>.
- [11] S.-H. Lee, H. Shin, Matrices and scaffolds for delivery of bioactive molecules in bone and cartilage tissue engineering, *Adv. Drug Deliv. Rev.* 59 (2007) 339–359, <https://doi.org/10.1016/j.addr.2007.03.016>.
- [12] I. Antoniac (Ed.), *Biologically Responsive Biomaterials for Tissue Engineering*, Springer, New York, 2013.
- [13] R.O. Hynes, Integrins: bidirectional, allosteric signaling machines, *Cell* 110 (2002) 673–687, [https://doi.org/10.1016/S0092-8674\(02\)00971-6](https://doi.org/10.1016/S0092-8674(02)00971-6).
- [14] S. Misra, V.C. Hascall, I. Atanelishvili, R. Moreno Rodriguez, R.R. Markwald, S. Ghatak, Utilization of glycosaminoglycans/proteoglycans as carriers for targeted therapy delivery, *Int. J. Cell Biol.* 2015 (2015) 25, 537560, <https://doi.org/10.1155/2015/537560>.
- [15] I. Matsuo, C. Kimura-Yoshida, Extracellular distribution of diffusible growth factors controlled by heparan sulfate proteoglycans during mammalian embryogenesis, *Phil. Trans. Biol. Sci.* 369 (2014) 20130545, <https://doi.org/10.1098/rstb.2013.0545>.
- [16] K.A. Davis, K.A. Burke, P.T. Mather, J.H. Henderson, Dynamic cell behavior on shape memory polymer substrates, *Biomaterials* 32 (2011) 2285–2293, <https://doi.org/10.1016/j.biomaterials.2010.12.006>.
- [17] M. Zhao, G. Altankov, U. Grabiec, M. Bennett, M. Salmeron-Sanchez, F. Dehghani, T. Groth, Molecular composition of GAG-collagen I multilayers affects remodeling of terminal layers and osteogenic differentiation of adipose-derived stem cells, *Acta Biomater.* 41 (2016) 86–99, <https://doi.org/10.1016/j.actbio.2016.05.023>.
- [18] J. Borges, J.F. Mano, Molecular interactions driving the layer-by-layer assembly of multilayers, *Chem. Rev.* 114 (2014) 8883–8942, <https://doi.org/10.1021/cr400531v>.
- [19] R.F. Mhanna, J. Vörös, M. Zenobi-Wong, Layer-by-layer films made from extracellular matrix macromolecules on silicone substrates, *Biomacromolecules* 12 (2011) 609–616, <https://doi.org/10.1021/bm1012772>.
- [20] N. Monteiro, A. Martins, R.L. Reis, N.M. Neves, Liposomes in tissue engineering and regenerative medicine, *J. R. Soc. Interface* 11 (2014) 20140459, <https://doi.org/10.1098/rsif.2014.0459>.
- [21] M. Çağdaş, A.D. Sezer, S. Bucak, Liposomes as Potential Drug Carrier Systems for Drug Delivery, *Appl. Nanotechnol. Drug Deliv.* (2014), <https://doi.org/10.5772/58459>.
- [22] S. Pavlukhina, S. Sukhishvili, Polymer assemblies for controlled delivery of bioactive molecules from surfaces, *Adv. Drug Deliv. Rev.* 63 (2011) 822–836, <https://doi.org/10.1016/j.addr.2011.03.017>.
- [23] M. Michel, D. Vautier, J.-C. Voegel, P. Schaaf, V. Ball, Layer by layer self-assembled polyelectrolyte multilayers with embedded phospholipid vesicles, *Langmuir* 20 (2004) 4835–4839, <https://doi.org/10.1021/la049736q>.
- [24] D.V. Volodkin, P. Schaaf, H. Mohwald, J.-C. Voegel, V. Ball, Effective embedding of liposomes into polyelectrolyte multilayered films: the relative importance of lipid–polyelectrolyte and interpolyelectrolyte interactions, *Soft Matter* 5 (2009) 1394–1405, <https://doi.org/10.1039/B815048F>.
- [25] T.G. Park, J.H. Jeong, S.W. Kim, Current status of polymeric gene delivery systems, *Adv. Drug Deliv. Rev.* 58 (2006) 467–486, <https://doi.org/10.1016/j.addr.2006.03.007>.
- [26] P.P. Campos, L.F. Fraceto, M. Ferreira, Layer-by-layer films containing emodin or emodin encapsulated in liposomes for transdermal applications, *Colloids Surf. B Biointerfaces* 162 (2018) 69–75, <https://doi.org/10.1016/j.colsurfb.2017.11.030>.
- [27] S. Tassler, D. Pawlowska, C. Janich, J. Giselbrecht, S. Drescher, A. Langner, C. Wölk, G. Brezesinski, Lysine-based amino-functionalized lipids for gene transfection: 3D phase behaviour and transfection performance, *Phys. Chem. Chem. Phys.* 20 (2018) 17393–17405, <https://doi.org/10.1039/C8CP01922C>.
- [28] C. Wölk, C. Janich, U. Bakowsky, A. Langner, G. Brezesinski, Malonic acid based cationic lipids - the way to highly efficient DNA-carriers, *Adv. Colloid Interface Sci.* 248 (2017) 20–34, <https://doi.org/10.1016/j.cis.2017.08.003>.
- [29] X. Zhang, L. Dai, A. Wang, C. Wölk, B. Dobner, G. Brezesinski, Y. Tang, X. Wang, J. Li, The directional observation of highly dynamic membrane tubule formation induced by engulfed liposomes, *Sci. Rep.* 5 (2015) 16559, <https://doi.org/10.1038/srep16559>.
- [30] M. Zhao, L. Li, C. Zhou, F. Heyroth, B. Fuhrmann, K. Maeder, T. Groth, Improved stability and cell response by intrinsic cross-linking of multilayers from collagen I and oxidized glycosaminoglycans, *Biomacromolecules* 15 (2014) 4272–4280, <https://doi.org/10.1021/bm501286f>.
- [31] S. Tassler, C. Wölk, C. Janich, B. Dobner, G. Brezesinski, Lysine-based amino-functionalized lipids for gene transfection: the protonation state in monolayers at the air–liquid interface, *Phys. Chem. Chem. Phys.* 19 (2017) 20271–20280, <https://doi.org/10.1039/C7CP03107F>.
- [32] U. Bhardwaj, D.J. Burgess, Physicochemical properties of extruded and non-extruded liposomes containing the hydrophobic drug dexamethasone, *Int. J. Pharm.* 388 (2010) 181–189, <https://doi.org/10.1016/j.ijpharm.2010.01.003>.
- [33] J. Giselbrecht, C. Janich, S.R. Pinnapireddy, G. Hause, U. Bakowsky, C. Wölk, A. Langner, Overcoming the polycation dilemma - explorative studies to characterise the efficiency and biocompatibility of newly designed lipofection reagents, *Int. J. Pharm.* 541 (2018) 81–92, <https://doi.org/10.1016/j.ijpharm.2018.02.029>.
- [34] F. Langenbach, J. Handschel, Effects of dexamethasone, ascorbic acid and β -glycerophosphate on the osteogenic differentiation of stem cells in vitro, *Stem Cell Res. Ther.* 4 (2013) 117, <https://doi.org/10.1186/scrt328>.
- [35] P.R. Majhi, A. Blume, Temperature-induced micelle-vesicle transitions in DMPc–SDS and DMPc–DTAB mixtures studied by calorimetry and dynamic light scattering, *J. Phys. Chem. B* 106 (2002) 10753–10763, <https://doi.org/10.1021/jp025849b>.
- [36] A. Zidovska, K.K. Ewert, J. Quispe, B. Carragher, C.S. Potter, C.R. Safinya, Block liposome and nanotube formation is a general phenomenon of two-component membranes containing multivalent lipids, *Soft Matter* 7 (2011) 8363–8369, <https://doi.org/10.1039/C1SM05481C>.
- [37] K. Glinel, A. Moussa, A.M. Jonas, A. Laschewsky, Influence of polyelectrolyte charge density on the formation of multilayers of strong polyelectrolytes at low ionic strength, *Langmuir* 18 (2002) 1408–1412, <https://doi.org/10.1021/la0113670>.
- [38] H. Al-Khoury, E. Espinosa-Cano, M.R. Aguilar, J.S. Román, F. Syrowatka, G. Schmidt, T. Groth, Anti-inflammatory surface coatings based on polyelectrolyte multilayers of heparin and polycationic nanoparticles of naproxen-bearing polymeric drugs, *Biomacromolecules* 20 (2019) 4015–4025, <https://doi.org/10.1021/acs.biomac.9b01098>.
- [39] S.F. Himmelstoß, T. Hirsch, Long-term colloidal and chemical stability in aqueous media of NaYF₄-type upconversion nanoparticles modified by ligand-exchange, *Part. Part. Syst. Char.* 36 (2019) 1900235, <https://doi.org/10.1002/ppsc.201900235>.
- [40] R. Anouz, A. Repanas, E. Schwarz, T. Groth, Novel surface coatings using oxidized glycosaminoglycans as delivery systems of bone morphogenetic protein 2 (BMP-2) for bone regeneration, *Macromol. Biosci.* 18 (11) (2018), e1800283, <https://doi.org/10.1002/mabi.201800283>.
- [41] O. Et-Thakafy, N. Delorme, C. Gaillard, et al., Mechanical properties of membranes composed of gel-phase or fluid-phase phospholipids probed on liposomes by atomic force spectroscopy, *Langmuir* 33 (21) (2017) 5117–5126, <https://doi.org/10.1021/acs.langmuir.7b00363>.
- [42] P.C.F. da Câmara, R.C. Balaban, M. Hedayati, K.C. Papat, A.F. Martins, M.J. Kipper, Novel cationic tannin/glycosaminoglycan-based polyelectrolyte multilayers promote stem cells adhesion and proliferation, *RSC Adv.* 9 (2019) 25836–25846, <https://doi.org/10.1039/C9RA03903A>.
- [43] J.H. Lee, H.B. Lee, A wettability gradient as a tool to study protein adsorption and cell adhesion on polymer surfaces, *J. Biomater. Sci. Polym. Ed.* 4 (1993) 467–481, <https://doi.org/10.1163/156856293x00131>.
- [44] S. Mochizuki, N. Kanegae, K. Nishina, Y. Kamikawa, K. Koichi, H. Masunaga, K. Sakurai, The role of the helper lipid dioleoylphosphatidylethanolamine (DOPE) for DNA transfection cooperating with a cationic lipid bearing ethylenediamine, *Biochim. Biophys. Acta Biomembr.* 1828 (2013) 412–418, <https://doi.org/10.1016/j.bbamem.2012.10.017>.
- [45] G. Sondag, S. Salihoglu, S. Lababidi, D. Crowder, F. Moussa, S. Abdelmagid, F. Safadi, Osteoactivin induces transdifferentiation of C2C12 myoblasts into osteoblasts, *J. Cell. Physiol.* 229 (2014), <https://doi.org/10.1002/jcp.24512>.
- [46] M.J. Dalby, A.J. García, M. Salmeron-Sanchez, Receptor control in mesenchymal stem cell engineering, *Nature Rev. Mater.* 3 (2018) 1–14, <https://doi.org/10.1038/natrevmats.2017.91>.
- [47] M. Mullaney, T. Groth, R. Darkow, R. Hesse, W. Albrecht, D. Paul, G. von Sengbusch, Investigation of plasma protein adsorption on functionalized nanoparticles for application in apheresis, *Artif. Organs* 23 (1999) 87–97, <https://doi.org/10.1046/j.1525-1594.1999.0x280.x>.
- [48] N. Davidenko, C.F. Schuster, D.V. Bax, R.W. Farndale, S. Hamaia, S.M. Best, R.E. Cameron, Evaluation of cell binding to collagen and gelatin: a study of the effect of 2D and 3D architecture and surface chemistry, *J. Mater. Sci. Mater. Med.* 27 (2016) 148, <https://doi.org/10.1007/s10856-016-5763-9>.
- [49] D. Needham, J.-Y. Park, A.M. Wright, J. Tong, Materials characterization of the low temperature sensitive liposome (LTSL): effects of the lipid composition (lysolipid

- and DSPE-PEG2000) on the thermal transition and release of doxorubicin, *Faraday Discuss* 161 (2013) 515–534, <https://doi.org/10.1039/C2FD20111A>.
- [50] N. Monteiro, A. Martins, D. Ribeiro, S. Faria, N.A. Fonseca, J.N. Moreira, R.L. Reis, N.M. Neves, On the use of dexamethasone-loaded liposomes to induce the osteogenic differentiation of human mesenchymal stem cells, *J. Tissue Eng. Regen. Med.* 9 (2015) 1056–1066, <https://doi.org/10.1002/term.1817>.
- [51] N. Tran, X. Mulet, A.M. Hawley, T.M. Hinton, S.T. Mudie, B.W. Muir, E.C. Giakoumatos, L.J. Waddington, N.M. Kirby, C.J. Drummond, Nanostructure and cytotoxicity of self-assembled monoolein–capric acid lyotropic liquid crystalline nanoparticles, *RSC Adv.* 5 (2015) 26785–26795, <https://doi.org/10.1039/C5RA02604K>.

Chapter 3: Extracellular matrix-inspired surface coatings functionalized with Dexamethasone-loaded liposomes to induce osteo- and chondrogenic differentiation of multipotent stem cells

In this paper, cationic liposomes composed of lipid OO4 and DOPE loaded with Dex were used as an entity in multilayer formation using LbL by alternating adsorption of polyelectrolytes such as HA as polyanion and Col I as polycation, which are compounds present in the ECM of bone. The addition of Dex is to promote bone and cartilage formation by inducing the proliferation and differentiation of mesenchymal stem cells to osteoblasts and chondrocytes. A polyelectrolyte multilayer system (PEM) was designed of HA and Col I with embedded cationic liposomes loaded with Dex into the terminal layers to achieve a local delivery and protection of this drug for induction of osteo- and chondrogenic differentiation of multipotent stem cells. Physicochemical studies were done to characterize layer growth, thickness, and surface properties of PEM and then evaluated cell adhesion. The surface properties of the PEM system show a positive zeta potential after liposome adsorption and a decrease in the wettability, both promoting cell adhesion and spreading of C3H10T1/2. Cell studies of C3H10T1/2 cells evaluated the advantage to use the liposomes embedded into the PEM against the use of liposomes in the supernatant and basal PEM. Osteo and chondrogenesis were evaluated by immunohistochemically staining and an upregulation of the expression of genes, which play a key role in osteogenesis (RunX2, ALP, Osteocalcin) and chondrogenesis (Sox9, aggrecan, collagen II), determined by qRT-PCR after 21 days. These results demonstrated that the liposome-loaded PEMs have a high potential for use as drug delivery systems for implant coatings because these coatings can promote bone and cartilage differentiation.



Contents lists available at ScienceDirect

Materials Science & Engineering C

journal homepage: www.elsevier.com/locate/msec

Extracellular matrix-inspired surface coatings functionalized with dexamethasone-loaded liposomes to induce osteo- and chondrogenic differentiation of multipotent stem cells

Yazmin A. Brito Barrera^a, Catharina Husteden^b, Jumanah Alherz^a, Bodo Fuhrmann^c, Christian Wölk^d, Thomas Groth^{a,c,e,*}

^a Department Biomedical Materials, Institute of Pharmacy, Martin Luther University Halle–Wittenberg, Heinrich-Damerow-Strasse 4, 06120 Halle (Saale), Germany

^b Medicinal Chemistry Department, Institute of Pharmacy, Martin Luther University Halle-Wittenberg, 06120 Halle (Saale), Germany

^c Interdisciplinary Center of Materials Science, Martin Luther University Halle-Wittenberg, D-06099 Halle (Saale), Germany

^d Pharmaceutical Technology, Institute of Pharmacy, Faculty of Medicine, Leipzig University, 04317 Leipzig, Germany

^e Laboratory of Biomedical Nanotechnologies, Institute of Bionic Technologies and Engineering, I.M. Sechenov First Moscow State University, 119991, Trubetskaya street 8, Moscow, Russian Federation

ARTICLE INFO

Keywords:

C3H10T1/2 cells
Cationic lipids
Hyaluronic acid
Collagen I
Dexamethasone
Osteogenic/chondrogenic differentiation
Polyelectrolyte multilayer system

ABSTRACT

Biomimetic surface coatings can be combined with conventional implants to mimic the extracellular matrix (ECM) of the surrounding tissue to make them more biocompatible. Layer-by-layer technique (LbL) can be used for making surface coatings by alternating adsorption of polyanions and polycations from aqueous solutions without need of chemical reactions. Here, polyelectrolyte multilayer (PEM) systems is made of hyaluronic acid (HA) as polyanion and Collagen I (Col) as polycation to mimic the ECM of connective tissue. The PEM are combined with dexamethasone (Dex)-loaded liposomes to achieve a local delivery and protection of this drug for stimulation of osteo- and chondrogenic differentiation of multipotent stem cells. The liposomes possess a positive surface charge that is required for immobilization on the PEM. The surface properties of PEM system show a positive zeta potential after liposome adsorption and a decrease in wettability, both promoting cell adhesion and spreading of C3H10T1/2 multipotent embryonic mouse fibroblasts. Differentiation of C3H10T1/2 was more prominent on the PEM system with embedded Dex-loaded liposomes compared to the basal PEM system and the use of free Dex-loaded liposomes in the supernatant. This was evident by immunohistochemical staining and an upregulation of the expression of genes, which play a key role in osteogenesis (RunX2, ALP, Osteocalcin (OCN)) and chondrogenesis (Sox9, aggrecan (ACAN), collagen type II), determined by quantitative Real-time polymerase chain reaction (qRT-PCR) after 21 days. These findings indicate that the designed liposome-loaded PEM system have high potential for use as drug delivery systems for implant coatings that can induce bone and cartilage differentiation needed for example in osteochondral implants.

Abbreviations: ALP, Alkaline Phosphatase; ACAN, aggrecan; AFM, Atomic force microscopy; ASC, ascorbic acid; BMP, bone morphogenetic proteins; CLSM, Confocal Laser Scanning Microscopy; Col, Collagen I; Dex, Dexamethasone; DMEM, Dulbecco's modified Eagle's medium; DOPE, dioleoylphosphatidylethanolamine; ECM, Extracellular matrix; FCS, Fetal calf serum; GAG, Glycosaminoglycan; β -Gly, β -Glycerophosphate; HA, Hyaluronic acid; RHAMM, hyaluronan-mediated motility; LbL, Layer-by-Layer; (MKP-1), Mitogen-activated protein kinase phosphatase 1; PBS, Phosphate-buffered saline; PEI, Polyethylenimine; PEM, polyelectrolyte multilayer system; qRT-PCR, Quantitative Real-time polymerase chain reaction; OO4, *N*-(6-amino-1-[*N*-(9Z)-octadec-9-enylamino]-1-oxohexan-(2S)-2-yl)-*N'*-(2-[*N,N*-bis(2-aminoethyl)amino] ethyl)-2-hexadecylpropanediamide; OCD, osteochondral defect; OCN, Osteocalcin; SN, supernatant; SPR, Surface plasmon resonance; TAZ, (transcriptional co-activator with PDZ-binding motif); WCA, Water contact angle.

* Corresponding author at: Department Biomedical Materials, Institute of Pharmacy, Martin-Luther-University Halle-Wittenberg, Heinrich-Damerow-Strasse 4, 06120 Halle (Saale), Germany.

E-mail address: thomas.groth@pharmazie.uni-halle.de (T. Groth).

<https://doi.org/10.1016/j.msec.2021.112516>

Received 27 August 2021; Received in revised form 19 October 2021; Accepted 22 October 2021

Available online 29 October 2021

0928-4931/© 2021 The Authors. Published by Elsevier B.V. This is an open access article under the CC BY license (<http://creativecommons.org/licenses/by/4.0/>).

1. Introduction

Bone and cartilages defects are common disorders affecting people of all ages. These defects are caused by trauma, tumors, infections, and congenital diseases [1,2]. One example are osteochondral defects (OCD) that affect both articular cartilage and subchondral bone as important components of joints in the body [2,3]. The articular cartilage protects the subchondral bone from contact pressure and permits low friction movements of the joint [3]. Commonly, the cartilage and subchondral bone undergo degeneration as the result of osteoarthritis, which requires often surgical interventions [2]. The more recent management of OC lesions does not only aim to relieving patients from pain and repairing damaged tissue but also restoring functionality of the joint [4]. Conventional therapies include drilling techniques, abrasion, micro fracture as well as transplantation of OC allografts and autologous chondrocyte implantation [5,6]. Unfortunately, severe OC defects often require total joint replacement implanting artificial joints made of metals, ceramics and durable polymers [4]. However, these materials are not bioactive, which may cause delayed healing or induction of inflammation as undesired effects [4]. Therefore, coating the implant surface – particularly the metallic parts that are inserted in the bone - with materials that promote engrafting like bioactive calcium phosphates or polymers has been suggested [4].

One of the techniques for surface coating of implants is the Layer-by-Layer technique (LbL) [7]. This surface coating method was established by Decher and coworkers [8] and is based on cycles of alternating adsorption of polyanions and polycations from aqueous solutions onto charged surfaces [8]. LbL has been widely used for various biomedical applications including tissue engineering, medical implants, regenerative medicines, and drug delivery [9–12]. For instance, multilayers made of biogenic polyelectrolytes such as collagen and glycosaminoglycans have been found to guide cell adhesion and function because they mimic partly the composition of extracellular matrix (ECM) of connective tissue [13].

Surface coatings based on LbL can be used to improve biocompatibility of implants but also to deliver a drug locally [14]. A limitation of pharmaceutical treatment of OC defects is that the systemic delivery of drugs is not leading to the desired local effect and it may have systemic side effects [15]. Hence, the advantages of a local delivery are to bring the agent to the target, reducing the drug amount, toxicity and other harmful local and systemic side effects [16,17]. Options to deliver a drug with an orthopedic implant or scaffold can be based on coating the drug on the implant surface or blending the drug with the biomaterials during production [15]. Nowadays, bone regeneration after complicated fractures or larger bone defects is achieved by use of growth factors like bone morphogenetic proteins (BMP), transforming growth factors, and growth hormones [15] to promote cell adhesion, proliferation, and differentiation [18]. However, a limitation of the current clinical use of growth factors like BMP-2, is the high cost and dosage used because of their fast degradation. Particularly the high dosage of growth factors like BMP-2 in mg scale in some clinical applications can have negative local and systemic side effects [19,20]. Therefore, local delivery of small quantities in microgram scale as suggested by Salmeron-Sanchez and coworkers [20] may provide a better solution for regeneration of bone.

On the other hand, nano-sized materials can be applied as systems for release of bioactive agents that can be used in regenerative medicine and treatment of cancer. Liposomes are interesting since they can carry different types of drugs because of their aqueous inner compartment and the hydrophobic part of the lipid bilayer. For example, liposomes have been applied for the delivery of dexamethasone (Dex) to regenerate bone [5,21]. They can be also applied for transfection of cells by the delivery of nucleic acids [22], since positively charged liposomes and lipoplexes can be efficiently internalized into cells. We could show recently that liposomes composed of dioleoylphosphatidylethanolamine (DOPE) and the ionizable lipid *N*-{6-amino-1[*N*-(9Z)-octadec-9-enylamino]-1-oxohexan-(2S)-2-yl}-*N'*-{2-[*N,N*-bis(2-aminoethyl)amino]

ethyl)-2[(9Z)-octadec-9-enyl]propandiamide (OO4) represent an excellent carrier for drug delivery in cells [23–25]. Overall, liposomes possess a very wide spectrum of application as drug-delivery systems for charged molecules [26], of anti-microbial agents [27], as vaccine carriers [28], transfection agents [29], and delivery of growth and differentiation factors such as BMP-2, TGF, and Dex [21,30]. In addition, liposomes can be used as component for formation of multilayers by LbL due to their inherent charge, which permits localized delivery of drugs avoiding systemic effects [31].

Previous studies combining vesicular structures with polyelectrolytes to fabricate multilayers (PEM) were made using phosphatidylcholine (PC) liposomes, doped with phosphatidylserine (PS) or phosphatidylglycerol (PG) and stabilized with poly-L-lysine (PLL) into PEMs composed of synthetic polymers [32,33]. However, these studies were focussed predominantly on the material science aspects. There are also previous investigations using PC liposomes embedded in different PEM systems to study their interactions with cells. For example, Graf et al. described efficient encapsulation of calcein-loaded PS-containing liposomes into PEMs fabricated from synthetic polymers and their delivery into cells [34]. Demuth et al. described a PEM based systems with embedded liposomes to deliver antigens into the skin via deposition on microneedles [35]. Further approaches created backpacks for cells loaded with echogenic liposomes which encapsulate doxorubicin as potential cancer therapy [36]. A very recent work describes the embedding of liposomes in multilayers as model for exosomes by LbL but used a dye for the evidence of transfer into cells [37]. However so far, no studies reported about the combination of liposomes with LbL for controlled release to engineer connective tissue have been reported.

In tissue engineering, mesenchymal stem cells (MSC) have been used for several years due to their potential to differentiate into various tissues such as muscle, fat, bone, and cartilage and others [38]. C3H10T1/2 is a mesenchymal stem cell line that was obtained from a mouse embryo and can differentiate into various phenotypic lineages such as adipocytes, chondrocytes and osteoblasts by different inductive mediators [39,40]. The phenotypic features and differentiation of MSC to bone and cartilage cells include markers, such as alkaline phosphatase, deposition of calcium phosphate, and the expression of various ECM proteins such as collagen type I (Col) and II, osteocalcin (OCN), proteoglycans like aggrecan (ACAN), and glycosaminoglycans (GAG), etc. [41]. Moreover, it involves the detection of specific transcription factors, which are known to control mesenchymal cell differentiation towards chondrogenic or osteogenic lineages [41]. The transcription factors, Runx2, Osterix, and β -catenin, regulate osteoblast differentiation. Sox family transcription factors like Sox9 regulate chondrocyte differentiation [42]. Further, mesenchymal progenitors are initially marked by expression of Sox9, followed by Runx2 leading to the development of osteoblast [36]. However, cells with Sox9 expression are bipotential and can also differentiate into chondrocytes [42]. The addition of an inductive mediator like Dex can influence both osteogenic and chondrogenic differentiation. [19,38]. Dex can activate β -catenin mediated transcription and this activation induces Runx2 expression and upregulates TAZ and MKP1 that also promote Runx2 activity [43,44]. For chondrogenesis, Dex enhance the expression of Sox9 and activates the gene expression of type II procollagen (Col2a1) and ACAN [45].

OC defects require repair of bone and cartilage together, which means that implant materials or scaffolds should induce osteogenesis in the bone and chondrogenesis in the cartilage part of the defect. Hence, we were interested in elucidating the potential of Dex-loaded cationic liposomes to induce both osteo- and chondrogenic differentiation in C3H10T1/2 cells. Two approaches were combined to develop a functionalized surface coating: (i) an LbL surface coating that mimics the natural ECM of connective tissue by combination of Col and HA in PEM system and (ii) the immobilization of Dex-loaded liposomes for potential local delivery at the defect site. This research presents the physico-chemical characteristics of the multilayer films, such as surface zeta potential, thickness, layer growth, and wettability. Cell studies with

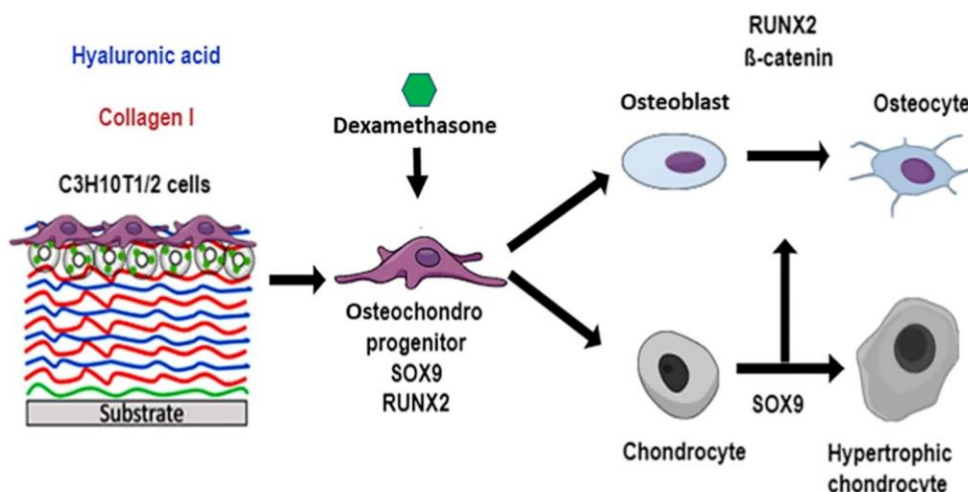


Fig. 1. Schematic illustration of the influence of the Dex in combination with polyelectrolyte multilayer in the regulation of osteoblast and chondrocyte differentiation by Sox9 and Runx2. During the process of osteoblast differentiation, Dex is an important compound for induction of mesenchymal stem cells to osteoblast lineage and clearly influences early stages of osteoblast differentiation as well as for chondrogenesis. Dex begins to play a key role in osteoblast differentiation by activating the Runx2-mediated and β -catenin pathways. For the period of chondrocyte differentiation initiated by Sox9-mediated mesenchymal condensation.

multipotent murine C3H10T1/2 cells evaluated the advantage of using liposomes loaded with Dex immobilized in PEMs to induce both osteogenic and chondrogenic differentiation (Fig. 1).

2. Materials and methods

2.1. Preparation of cationic liposomes

The lipid film hydration procedure was applied for the preparation of liposomes. Briefly, OO4 and DOPE lipids were separately dissolved in chloroform/methanol (8:2, v/v) to get stock solutions of 2 mg mL^{-1} . The stocks were mixed in the molar ratio 1:3 OO4/DOPE ($M_{\text{OO4}} = 860.39 \text{ g mol}^{-1}$, $M_{\text{DOPE}} = 744.03 \text{ g mol}^{-1}$). The solvent was evaporated, and the obtained thin lipid film was dissolved in water containing 0.15 M of sodium chloride (Carl Roth GmbH, Karlsruhe, Germany) and (0.1 M, final pH 4) acetic acid (Carl Roth GmbH, Karlsruhe, Germany) to obtain a lipid concentration of 1 mg mL^{-1} . For the film hydration at 50°C at 1400 rpm, an Eppendorf Thermomixer 5436 was used for 30 min followed by sonication using a bath sonicator at 37 kHz, 6 cycles for 3 min, while the last cycle was at 70°C for 4 min. The liposomes were prepared in batch sizes of 1 to 10 mL.

2.1.1. Loading of cationic liposomes with dexamethasone

The liposomes were prepared with a concentration of 1 mg mL^{-1} total lipid ($50 \mu\text{g mL}^{-1}$ Dex) following the liposome preparation protocol explained in previous studies [46] using chloroform/methanol (8:2, v/v) stock solutions of OO4, DOPE and Dex combined to a molar ratio of 1:3:0.2 ($n_{\text{OO4}}:n_{\text{DOPE}}:n_{\text{Dex}}$).

2.1.2. Characterization of liposomes

The size of liposomes was determined by dynamic light scattering (DLS) and zeta potential by laser Doppler velocimetry (LDV) using a Zetasizer Nano ZS ZEN3600 (Malvern Panalytical). DLS measurements were performed in half-volume cuvettes in three independent measurements consisting of 15 runs with a duration time of 20 s for each run at 25°C . The scattering angle was 173° . For the calculations, a viscosity $\eta = 0.8872 \text{ mPa s}$ and a refractive index of 1.33 were assumed and the autocorrelation function was evaluated by Zetasizer Software 7.13 (Malvern Panalytical). LDV was performed in a clear disposable folded capillary cell (DTS1060, Malvern Panalytical). Three independent measurements involving 30 runs with a voltage of 60 V were performed

at 25°C . For the calculations, the viscosity ($\eta = 0.8872 \text{ mPa s}$), dielectric constant ($\epsilon = 78.5 \text{ F m}^{-1}$) and refractive index ($n = 1.33$) of water were assumed. The mobility μ of the diffusing aggregates was converted into the ζ potential using the Smoluchowski relationship $\zeta = \mu \eta / \epsilon$ (Zetasizer Software 7.13).

2.2. Preparation of substrata

Before the deposition of polyelectrolyte multilayers on glass coverslips ($\phi 12 \text{ mm}$, VWR, Germany) and silicon wafers (Silicon materials, Kaufering, Germany), organic residues were eliminated after the RCA-1 method. This method suggests mixing the following solutions: ultra-pure water, ammonium hydroxide (Carl Roth GmbH, Karlsruhe, Germany), and hydrogen peroxide (Carl Roth GmbH, Karlsruhe, Germany) in the ratio of 5:1:1, respectively. The gold-coated glass sensor for surface plasmon resonance (SPR, IBIS Technologies BV, Enschede, Netherlands. $10 \times 10 \text{ mm}^2$) were treated by dipping into 0.5 M NaOH in 96% ethanol and followed by rinsing with ethanol (99%) and one last rinsing step with micro pure water followed by drying with nitrogen.

2.3. Glycosaminoglycan and collagen I solution preparation

The first solution required in the polyelectrolyte multilayer system was polyethylenimine (PEI). PEI ($M_w \sim 750 \text{ kDa}$) provided from Sigma-Aldrich (Steinheim, Germany) was dissolved in 0.15 M sodium chloride (Carl Roth GmbH, Karlsruhe, Germany) solution at a concentration of 2 mg mL^{-1} . A solution of sodium hyaluronate (HA) was used as a negatively charged polyelectrolyte for the multilayer assembly. Therefore, hyaluronic acid sodium salt ($M_w \sim 1.2 \text{ MDa}$) Kraeber & Co GmbH (Ellerbeck, Germany) was dissolved in 0.15 M sodium chloride solution at a concentration of 0.5 mg mL^{-1} . The positively charged Col was used as third solution. Col from porcine skin ($M_w \sim 100 \text{ kDa}$) was provided by Sichuan Mingrang Bio-Tech (Sichuan, China) and was dissolved in 0.2 M acetic acid (Carl Roth GmbH, Karlsruhe, Germany) in a concentration of 2 mg mL^{-1} as a stock solution and stored in a temperature of 4°C . Then, it was diluted with sodium chloride solution (0.15 M) to obtain a final concentration of 0.5 mg mL^{-1} . The pH value of all solutions was adjusted to pH 4.

2.4. Preparation of polyelectrolyte multilayers

PEM were fabricated on cleaned glass coverslips, gold sensor, and silicon substrates, respectively, depending on the method used afterwards. PEM were fabricated in 24 well plates with 500 μL volume of each solution. PEI was applied as the initial layer by incubation of 15 min to get a positively charged surface. The first layer was formed by the application of polyanion solution (HA solution) for 15 min. The second layer was the polycation solution (Col solution) incubated for 20 min. Each deposition step was followed by washing with 0.15 M sodium chloride for five minutes, *trice*. The application of HA and Col solutions alternated until the ninth layer for liposomes was added. Twelve layers were used for unloaded PEM system [HA/Col]₆ in experiments with liposome-free PEMs. For Lbl coatings with embedded liposomes, PEMs with the sequence [HA/Col]₄ were built like described above, followed by a HA layer to get the negative surface for adsorption of the positively charged Dex-loaded liposomes. For liposome deposition, the incubation time was 150 min. This layer was followed by deposition of an additional HA and Col layer to reach the final sequence [HA/Col]₄HA/Lip [HA/Col].

2.5. Characterization of polyelectrolyte multilayers and surface properties

2.5.1. Ellipsometry

The PEM systems were prepared on silicon wafers. The thickness of PEMs was estimated by the use of ellipsometry (M-2000 V scanning ellipsometer, J.A. Woollam Co. Inc., Lincoln, NE, USA) at room temperature. The measurements were taken at incident angles of 60, 65, 70, and 75 of linear polarized light to the normal surface. The data were analyzed using the software WVase32.

2.5.2. Surface plasmon resonance

The measurements were conducted with an IBIS-iSPR device (IBIS Technologies BV, Enschede, Netherlands). The gold sensor was coated with 11-mercaptopundecanoic acid (MUDA) (Steinheim, Germany), mounted in a flow chamber, and equilibrated with sodium chloride to obtain a stable baseline. Then, the polyelectrolyte solution was injected at a flow rate of 3 $\mu\text{L s}^{-1}$ followed by rinsing with sodium chloride for 15 min. PEI was added for 15 min, HA for 15 min, Col for 20 min and liposomes solution for 150 min until 13 layers were formed. The average of the shift values (m°) of each rinsing step was used for plotting the graphs and removing any unbound molecules.

2.5.3. ζ -Potential measurements

SurPASS electrokinetic (Anton Paar, Graz, Austria) was used to estimate the zeta-potential of PEM-coated glass substrates (10 \times 20 mm²). The samples were mounted on the gap cell with double-sided tape. The used model electrolyte was 1 mmol·L⁻¹ KCl in water (Carl Roth GmbH, Karlsruhe, Germany) solution. The pH titration solution from pH 3.0 to 10 (acid-based pH) was 0.1 mol·L⁻¹ sodium hydroxide (Carl Roth GmbH, Karlsruhe, Germany). The analyzer was adjusted during the measurement process to a flow rate of 100–150 mL·min⁻¹ at a maximum pressure of 300 mbar.

2.5.4. Water contact angle measurements

The wettability of the PEM was measured by static WCA using an OCA15+ device from Dataphysics (Filderstadt, Germany). The PEMs were prepared using glass cover slips. The sessile drop method was applied using 1 μL of water with the Ellipse-fitting method. The experiments were run in duplicates with five droplets per sample. Means and standard deviations were calculated.

2.5.5. Fluorescence microscopy of PEMs

PEMs were prepared according to the description in Section 2.4 using FITC-labeled HA and Rhodamine-DOPE labeled OO4/DOPE liposomes. The FITC-labelling of HA was done according to protocol published

[47]. The micrographs were taken with confocal laser scanning microscopy (CLSM 701, Carl Zeiss Micro-Imaging GmbH, Jena, Germany) using a 63 \times oil immersion objective. Images were processed with the ZEN2012 software (Carl Zeiss).

2.6. Cell culture conditions

Cryopreserved C3H10T1/2 murine cell line (ATCC; LGC Promochem, Molsheim, France) were thawed and grown in DMEM low glucose medium supplemented with 10% heat-inactivated fetal calf serum and 1% antibiotic solution (penicillin/streptomycin) solution all provided by Biochrom AG (Berlin, Germany). Cultured cells were grown at 37 $^{\circ}\text{C}$ in a humidified 5% CO₂/95% air atmosphere using a NUAIRE DH Autoflow incubator (NuAire Corp., Plymouth, Minnesota, USA). Cells of almost confluent cultures were washed once with sterile PBS, followed by treatment with 0.25% trypsin/0.02% EDTA (Biochrom) at 37 $^{\circ}\text{C}$ for 3 min. Trypsin was neutralized with DMEM with 10% FCS, and cells were re-suspended in DMEM after centrifugation at 250g for 5 min. Finally, the cells were seeded on PEM coated glass coverslips at different concentrations depending on the assay.

2.7. Cell adhesion and growth

2.7.1. Cell adhesion studies

C3H10T1/2 cells were seeded on glass coverslips coated with PEM that were placed into 24 well plates at a density of 20.000 cell·mL⁻¹ in DMEM supplemented with 10% FCS. After incubation at 37 $^{\circ}\text{C}$ for 4 h, cells attached to PEM were fixed with 4% paraformaldehyde solution (RotiHistofix, Carl Roth GmbH, Karlsruhe, Germany) for 10 min. After rinsing with PBS twice, the cells were permeabilized with 0.1% Triton X-100 in PBS (v/v) Sigma-Aldrich Chemie GmbH (Taufkirchen, Germany) for 10 min. After rinsing with PBS, nonspecific binding sites were blocked by incubation with 1% (w/v) bovine serum albumin (BSA, Merck, Darmstadt, Germany) in PBS at room temperature for 1 h. The vinculin was stained using primary mouse antibody (1:100, Sigma) and secondary Cy2- conjugated goat anti-mouse antibody (1:100, Dianova). Actin cytoskeleton was visualized by incubating the samples with Phalloidin CruzFluor 555 (1:1000, Santa Cruz Biotechnology, Heidelberg, Germany) at room temperature for 30 min. Cell nuclei were visualized by TO-PRO3 staining (1:500, Invitrogen, Darmstadt, Germany) incubating for 30 min. The samples were washed with PBS and mounted with Roti-Mount FluorCare (Carl Roth GmbH, Karlsruhe, Germany) and examined with confocal laser scanning microscopy (CLSM 701, Carl Zeiss Micro-Imaging GmbH, Jena, Germany) using 10 \times objective for cell counting, 20 \times objective for measurements of cell area and 63 \times oil immersion objective for visualization of focal adhesions, actin and nuclei. Images were processed with the ZEN2012 software (Carl Zeiss). The image analysis, such as cell count and cell area was performed with Image J. The quantification of vinculin-positive focal adhesions was done according to a protocol published previously [48].

2.7.2. Cell growth assay

Qblue assay was used as an indicator of cellular viability and cell growth. Cells were seeded at a density of 20.000 cell·mL⁻¹ in DMEM 10% FCS and incubated at 37 $^{\circ}\text{C}$ / 5% CO₂ for 24, 48, and 72 h for the first, second and third well-plate, respectively. QBlue reagent was mixed with colorless DMEM to produce a 10% (v/v) solution. The DMEM was removed from cells well-plate and the 10% solution of QBlue assay was added. The cells were incubated with 300 μL of the solution at 37 $^{\circ}\text{C}$ / 5% CO₂ for 3 h. After incubation, 100 μL was collected from each sample and transferred to 96 well-plates *trice*. The samples were analyzed using the microplate reader (FLUOstar OPTIMA, BMG LabTech, Germany) which was adjusted to a wavelength of 544 nm for excitation and 590 nm for emission.

Table 1
Primers of target and housekeeping genes.

Symbol	Name	Assay ID
Osteoblast		
ALP	Alkaline phosphatase	qMmuCEP0027961
RUNX2	Runt-related transcription factor-2	qMmuCEP0057696
NOG		
NOG	Noggin	qMmuCEP0058332
SP7	Osterix	qMmuCED0039982
Chondrocyte		
SOX9	Transcription factor SOX-9	qMmuCEP0053111
ACAN	Aggrecan	qMmuCEP0055269
COL1A1	Collagen type 1 alpha 1	qMmuCEP0052648
COL2A1	Collagen type 2 alpha 1	qMmuCEP0055155
Housekeeping gene		
RPLP0	60S acidic ribosomal protein P0	qMmuCEP0042968

2.8. Differentiation studies: osteogenesis

2.8.1. Alizarin red-S staining

C3H10T1/2 cells were seeded on PEM modified glass coverslips in 24 well plates at a density of $4 \times 10^4 \text{ mL}^{-1}$. The cells were cultured on glass in presence of **osteogenic medium** as a positive control (DMEM 10% FCS, 100 nM Dex, 50 $\mu\text{g mL}^{-1}$ ascorbic acid, and 10 mM β -Glycerophosphate), while the **basal medium** was DMEM with 10% FCS (negative control). The medium for the sample group was osteogenic medium without Dex. The Alizarin red (Carl Roth GmbH, Karlsruhe, Germany) staining was performed after 21 days as reported previously [46].

2.9. Differentiation studies: chondrogenesis

2.9.1. Safranin O staining

C3H10T1/2 cells were seeded on the samples placed into 24 well plates at high density of $1 \times 10^5 \text{ mL}^{-1}$. Here, the chondrogenesis requires high density to induce cell-cell interactions similar to the precartilaginous condensation [49]. The cells were incubated in presence of a **chondrogenic medium** as a positive control (DMEM 10% FCS, 100 nM Dex, 5 $\mu\text{g mL}^{-1}$ ascorbic acid) while **basal medium** was DMEM with 10% FCS (negative control). The medium for the samples group was chondrogenic medium in the absence of Dex.

The cells were prepared and fixed as described in Section 2.8. After

removing paraformaldehyde, samples were washed twice with distilled water and incubated in 1% acetic acid for 15 s. Subsequently, the samples were incubated for 15 min with 0.1% safranin O solution (Sigma-Aldrich, Steinheim, Germany). After the incubation time, the samples were washed with PBS and studied with a microscope equipped with a camera (Axiovert 100, Carl Zeiss, Oberkochen, Germany).

2.10. RNA extraction and quantitative real-time PCR

C3H10T1/2 cells were seeded on glass coverslips coated with PEM coatings as in the previous section. The re-suspend cells were seeded on the samples in DMEM supplemented with 10% FCS at a density of $5 \times 10^5 \text{ mL}^{-1}$ for osteogenic and $1 \times 10^6 \text{ mL}^{-1}$ for chondrogenic differentiation. The composition of media was the same as described above. To evaluate the osteogenic and chondrogenic differentiation, the cells were incubated for 14 days.

The RNA was extracted from samples using TRIzol method (Invitrogen, Darmstadt, Germany) according to the manufacturer's recommended procedure. First, cDNA was synthesized using an iScript Advanced cDNA Synthesis Kit for RT-qPCR (Biorad, Hercules, CA, USA) in 20 μL reactions, according to the manufacturer's instructions.

qRT-PCR was performed under standard enzyme and cycling conditions on a CFX Connect real-time PCR Detection System (Biorad, Hercules, CA, USA). Primer sets were pre-validated by PrimePCR Probe Assays from Biorad (Hercules, CA, USA) for osteogenic genes (ALP, RUNX2, Noggin, and Osterix) and chondrogenic genes (SOX-9, ACAN, collagen alpha 1, and collagen type 2 alpha 1). The housekeeping gene RPLP0 was also used in this study (Table 1). Data analysis was performed using the BioRad CFX Manager Software 3.0 (Hercules, CA, USA). The conditions of qRT-PCR were as follows: 95 $^{\circ}\text{C}$ for 30 s followed by 39 cycles at 95 $^{\circ}\text{C}$ for 15 s and 60 $^{\circ}\text{C}$ for 30 s. The relative expression levels for each gene were calculated and normalized to the housekeeping gene RPLP0 by the DDCT method ($2^{-\Delta\Delta\text{Ct}}$) [50].

2.11. Immunohistochemical staining

C3H10T1/2 cells were seeded on glass coverslips coated with PEM coatings as described in the previous section of differentiation studies. To study the osteogenic and chondrogenic differentiation, the cells were incubated for 21 days. After the incubation time, cells were fixed using 4% paraformaldehyde (Sigma-Aldrich) solution at room temperature for

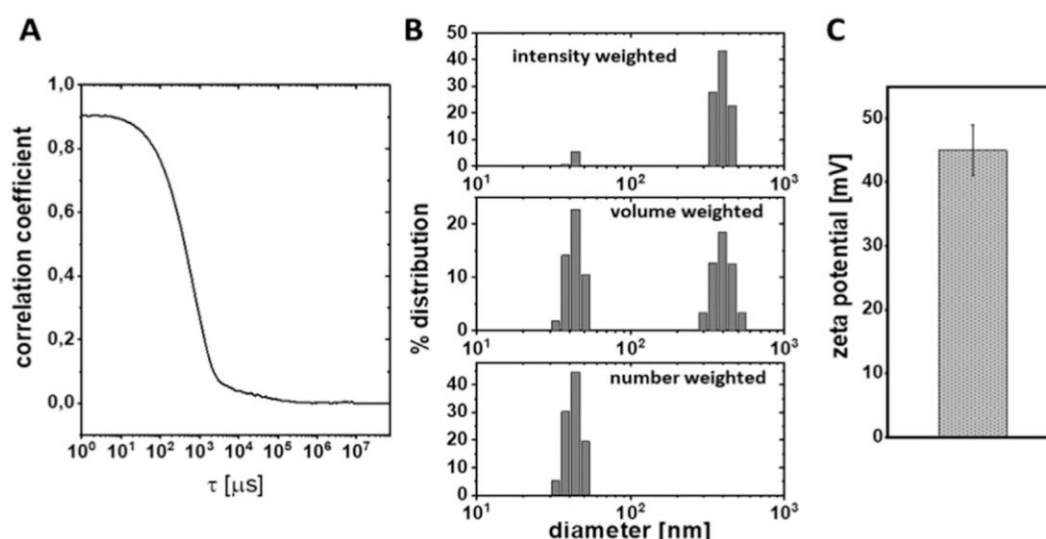


Fig. 2. Characterization of cationic liposomes loaded with Dex in acetate buffer pH 4 (10 mM, 0.15 M NaCl). (A) the correlation coefficient, (B) intensity, volume, and number weighted size distribution, (C) zeta potential (mean and standard deviation of three independent liposome preparations) measured by DLS and IdV.

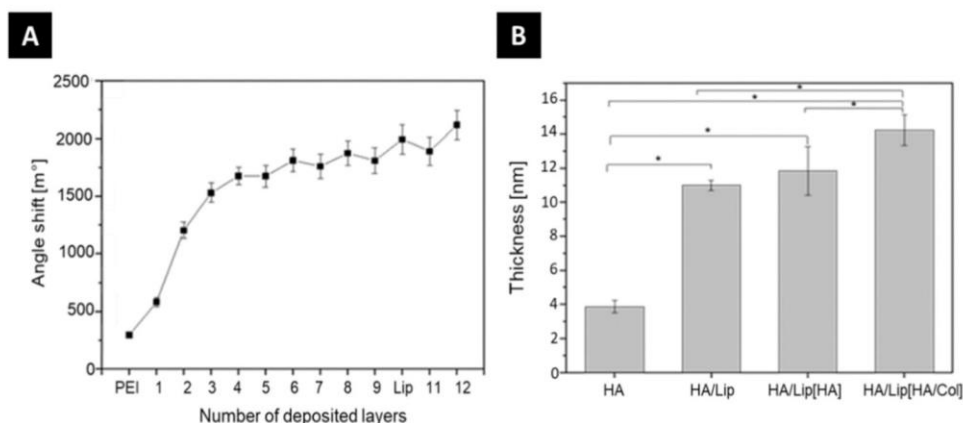


Fig. 3. (A) Layer growth of PEM systems of $[HA/Col]_4$ HA/Lip [HA/Col] by SPR numbered as 1 to 12 (1st layer to 12th layer). Odd layer numbers correspond to HA coating and even layer numbers correspond to Col coating except the 10th layer, which corresponds to liposomes loaded with Dex (Lip); $n = 20$, mean \pm SD. (B) Progression of the layer thickness of PEM sequence $[HA/Col]_4$ after adsorption of the additional layers of liposomes (Lip), hyaluronic acid (HA), and collagen I (Col) (see sequence details at the x-axis) determined by ellipsometry; $n = 10$, mean \pm SD, * $p \leq 0.05$.

15 min and washed three times with PBS. After permeabilization using 0.1% (v/v) Triton X-100 (Sigma-Aldrich) for 10 min, the non-specific binding sites were blocked with 1% bovine serum albumin solution (BSA, Carl Roth GmbH, Karlsruhe, Germany) in PBS at room temperature for 1 h. For visualization of chondrogenic markers, the cells were incubated with primary monoclonal antibodies raised against collagen type II (rabbit, Santa Cruz Biotechnology, Heidelberg, Germany) and a secondary antibody CY3 (anti-rabbit, Dianova, Hamburg, Germany) and ACAN (mouse, Santa Cruz Biotechnology, Heidelberg, Germany) and conjugated secondary CY2 (anti-mouse, Dianova, Hamburg, Germany). For detection of osteogenic markers, the cells were incubated with primary monoclonal antibodies raised against Col (mouse, Santa Cruz Biotechnology, Heidelberg, Germany) with secondary antibody anti-mouse (CY2) and (mouse, Santa Cruz Biotechnology, Heidelberg, Germany) with conjugated secondary anti-rabbit (CY3). The images were visualized using confocal laser scanning microscopy (CLSM 701, Carl Zeiss Micro-Imaging GmbH, Jena, Germany) using 20 \times and 63 \times oil immersion objectives. Images were processed with the ZEN 2008 software (Carl Zeiss).

2.12. Statistical analysis

All statistical analysis was performed with Origin 8G software. Mean, standard deviation, and analysis of significance were performed by one-way ANOVA (indicated as *). A value of $p < 0.05$ was considered as significantly different. Further, box-whisker diagrams are shown where appropriate. The box indicates the 25th and 75th percentiles, the median (dash), and the mean value (black square), respectively.

3. Results and discussion

3.1. Characterization of liposomes

The peptide-mimicking lipid OO4 bears ionizable amino functions and has an apparent pKa value of 6. The liposomes prepared solely from this lipid have a positive zeta potential over a wide pH range [51,52]. A positive charge of liposomes is needed for efficient embedding in LbL-based PEM formation. Here, the utilized liposomes are composed of a binary mixture of OO4/DOPE 1/3 (n/n). DLS and zeta potential measurements were performed to characterize the size and charge of the liposomes under conditions used for LbL. The results are presented in Fig. 2.

The autocorrelation function (Fig. 2A) demonstrates the high quality of DLS data with an intercept at 0.9, a sigmoidal decay of the signal, and

the absence of a noisy baseline which would indicate aggregation. The fitting of the autocorrelation function results in a bimodal size distribution curve (intensity weighted curve in Fig. 2B). The first size population is at diameter (d) \approx 40–50 nm and a second one at $d \approx$ 300–500 nm. The size differences between both populations make it difficult to get quantitative information because the scattering intensity is approximately proportional to d^6 . As such, the intensity distribution can be somewhat misleading, in that a small number of larger particles can dominate the distribution. Therefore, volume and number weighted size distribution curves were calculated, demonstrating that the 40–50 nm population is in a much higher quantity than expected from the intensity weighted curve [53]. In addition, zeta potential measurements show that the liposomes possess a positive surface charge required for immobilization on the PEM (Fig. 2C). DOPE is used as zwitterionic copolymer in the mixture to decrease the charge density of the liposomes. This becomes obvious comparing the high zeta potential of OO4 liposomes ($\zeta > 40$ mV) with the liposomes OO4/DOPE ($\zeta = 30$ mV) [24,51]. Furthermore, DOPE increases the fusogenic character of liposomes in acidic milieu and therewith triggers endosomal escape of payload after endocytosis, a phenomenon often discussed for lipid-mediated nucleic acid transfer [54].

3.2. Physical characterization of multilayers

SPR was used to investigate the layer deposition of PEM in situ. Fig. 3 (A) shows a linear growth behavior of PEM system until the third layer. During the further deposition steps, the layer growth was reduced pronouncedly. Every deposition step changes the angle shift, which corresponds to the adsorbed mass of each layer [13,55]. However, after the 4th layer the mass adsorption reached an equilibrium which was well in line with previous studies [56]. Furthermore, the addition of liposomes as the 10th layer (PEM sequence $[HA/Col]_4HA/Lip$) resulted in an additional mass deposition (angle shift increased from \sim 1700 to 2000 m^2). The deposition of a further bilayer of HA/Col causes a further small increase of angle shift, which indicates the deposition of both polyelectrolytes.

To obtain more information about liposome deposition, the PEM layer thickness was measured by ellipsometry. This measurement was conducted with duplicates of dry films on a silicon substrate at 5 different spots per film ($n = 10$). Fig. 3 shows an increasing thickness of PEM from 4.1 ± 0.2 nm for the sequence $[HA/Col]_4HA$ up to 14.2 ± 0.1 nm for the sequence $[HA/Col]_4HA/Lip[HA/Col]$ which is related to the increase of the number of layers of PEM. It is visible that the adsorption of liposomes makes the main contribution to the observed increase of

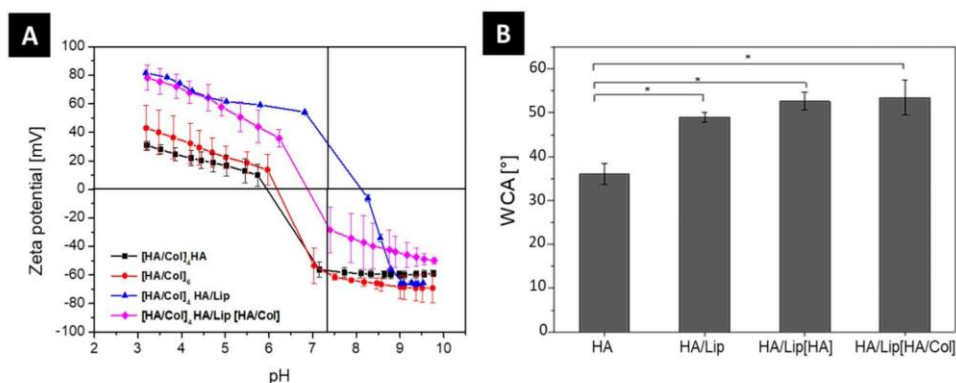


Fig. 4. A) Zeta potential measurements of the three different multilayers. Results represents means \pm SD of two independent experiments. B) Static water contact angle (WCA) measurement during multilayer formation. The x-axis demonstrate the film composition deposited on the basal part $[\text{HA/Col}]_4$. Results represent means \pm SD, $^*p < 0.05$ of three independent experiments.

PEM thickness. However, the relatively low thickness after adsorption of liposomes compared to their size obtained in DLS is a consequence of the drying procedure which results in the shrinking by the loss of the encapsulated aqueous core of liposomes [57]. Hence, it can be assumed that the thickness of hydrated multilayers is considerably larger compared to the thickness of dry layers because also HA tends to absorb water leading to swelling of PEM [58]. The ellipsometry results confirm the increase in mass deposition observed with SPR, particularly after liposomes were added.

Moreover, the surface topography was evaluated by atomic force microscopy (AFM). In previous studies, Zhao et al. showed the topography of HA/Col PEM which displayed a smooth surface with a small number of short collagen fibrils [13]. The AFM studies shown in Fig. S1 confirm the previous data showing a smooth surface with a roughness average (Ra) of 1.731 ± 0.721 nm and root mean square roughness (Rq) 2.914 ± 1.698 nm (see Table S1). After the deposition of the liposomes $[\text{HA/Col}]_4\text{HA/Lip}$ an increment of the roughness to Ra 17.96 ± 6.219 nm and Rq 23.55 ± 7.66 nm can be seen in Table S1. Also, the images in Fig. S1 provide evidence that the liposomes are immobilized on the surface visible by the presence of round structures covering the whole surface area. The roughness value for the sequence $[\text{HA/Col}]_4\text{HA/Lip}[\text{HA/Col}]$ are Ra 11.64 ± 2.647 nm and Rq 15.23 ± 3.389 nm. The values indicate the presence of the liposomes after deposition of additional bilayer where the liposomes changed their morphology and elongate diameter showing a rather flat structure on the surface due to the flexibility of liposomes and the strong Coulomb attractive force to

the deposited polyanion HA [46,57]. The structures are also maintained after deposition of an additional bilayer of HA/Col.

The knowledge of surface charge after each deposition step represents an important characterization of the buildup process of PEM [59]. Surface charge density, which corresponds to zeta potential, has also a pronounced effect on cell adhesion and fate [60]. Previous research has shown that PEM zeta potentials, particularly those made of hydrophilic biopolymers, reflect not only the charge distribution of the last polyelectrolyte layer but also of preceding ones due to the existence of swollen, conductive surface layers [61]. Fig. 4A shows the zeta potential of the final PEM and intermediate PEM assemblies as a function of pH value adjusted during the titration process. The pKa value of Col is around 5.5 [55]. Hence, it can be assumed that the Col is positively charged at low pH during titration and the charge will decrease continuously with increasing the pH value. In contrast, HA carries a negative net charge due to the presence of carboxylic groups with a pKa of 2.9 [62], which will further decrease the zeta potential when the pH value is increased during titration. The zeta potential of $[\text{HA/Col}]_6$ multilayers (curve with red points) shifts from positive values in the acidic to negatives potentials in the basic pH region. This indicates the contribution of both charged species, such as Col at low pH and HA at high pH to the zeta potential, related to the fact that not only the outermost layer but also inner layers of PEM contribute to the zeta potential as detected by Zimmermann & Werner [61,63]. The addition of a further layer of HA to $[\text{HA/Col}]_4$ (curve with black squares) decreases the zeta potentials slightly and indicates the contribution of the

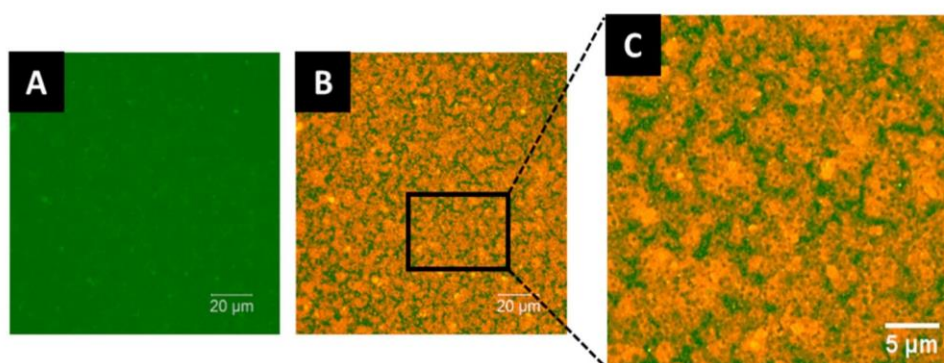


Fig. 5. CLSM images of PEM system after deposition of the liposomes: $[\text{HA-FITC/Col}]_4\text{HA/Lip}[\text{HA-FITC/Col}]$ HA was labeled using FITC (green), liposomes with Rhodamine-DOPE conjugated (red) on PEM. A) FITC fluorescence distribution, B) merged image of FITC fluorescence and Rhodamine-DOPE fluorescence C) detail (black square in B) merged image of HA and liposomes distribution of the area in the black square [scale 20 μm and 5 μm]. (For interpretation of the references to colour in this figure legend, the reader is referred to the web version of this article.)

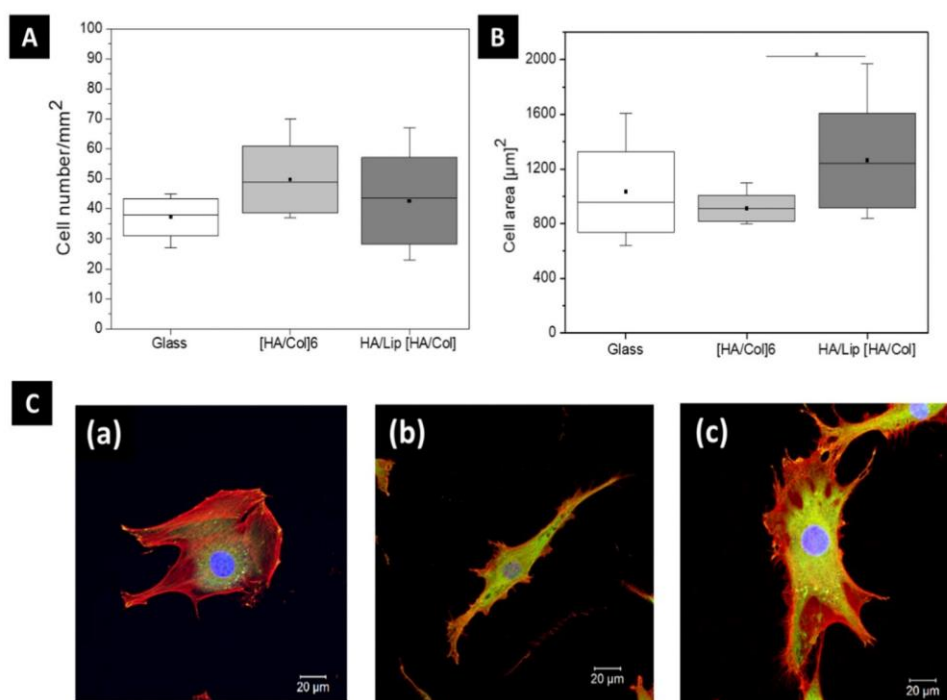


Fig. 6. A) Quantification of cell count per square millimeter B) Cell spreading area (μm^2) on each of the multilayers after 4 h; samples: Glass, [HA/Col]₆, [HA/Col]₄* HA/Lip [HA/Col] (Box plots with whiskers, representing first and third quartiles, medians and means). (*) statistically significant with a p -value ≤ 0.05 . C) Merged CLSM image of adherent C3H10T1/2 cultured on the different PEM after 4 h of incubation in serum and serum-free medium. (a) Glass, (b) [HA/Col]₆, (c) [HA/Col]₄ HA/Lip[HA/Col]. The cells are stained for filamentous actin (red), vinculin-positive focal adhesions (green), and nucleus (blue). [Scale 20 μm]. (For interpretation of the references to colour in this figure legend, the reader is referred to the web version of this article.)

polyanion HA to the potential. The adsorption of liposomes [HA/Col]₄HA/Lip (blue triangles) leads to a dramatic increase of zeta potentials with a huge shift of point of zero charge (PZC) from pH 6 to pH 8.5 which represents the positive charge of the cationic liposomes. The coverage of the liposome layer with an additional bilayer of HA/Col decreases the zeta potential again, but it remains still higher than that of the [HA/Col]₄ HA, which indicates that the liposomes underneath make still a contribution to the zeta potential of the system. The PZC of this system is 6.8, which means that both anionic and cationic species contribute to the potential. The zeta potential measurements show clearly that liposomes adsorb on the [HA/Col]₄HA multilayers and they remain also when an additional bilayer of HA/Col is immobilized on top of them.

On the other hand, surface wettability is another important factor that can affect the biological response to an implant because it affects protein adsorption and cell adhesion [64]. Fig. 4 (B) shows that [HA/Col]₄HA is hydrophilic with a WCA of $\sim 35^\circ$, which is related to the fact that HA is a hydrophilic polysaccharide [13]. After the adsorption of liposomes on PEM [HA/Col]₄HA/Lip, the WCA increased to a value of 50° , which corresponds to a moderately wettable surface due to the presence of amino groups, which make WCA in this range [65]. The subsequent [HA/Col]₄HA/Lip/HA displays an angle of $\sim 53^\circ$, and the final PEM [HA/Col]₄HA/Lip[HA/Col] was characterized by a WCA of $\sim 55^\circ$, demonstrating that the wetting properties of liposomes are also dominant after deposition the final bilayer, which indicates an intermingled structure of liposomes and polyelectrolytes in the outermost layer of the system [66].

Further evidence for the entrapment of liposomes in the PEM system is shown in Fig. 5 presenting micrographs made by CLSM. Fig. 5 A shows a uniform distribution of HA labeled with FITC in the PEM [HA-FITC/Col]₄HA/Lip[HA-FITC/Col] (green colour). Fig. 5B displays the distribution of Rhodamine-DOPE fluorescence across the PEM (orange

colour), with higher magnification in Fig. 5 C demonstrating the presence of labeled liposomes. The image depicts the distribution of liposomes over the entire area; however, the image indicates the presence of some liposomes aggregates and a partially homogeneous distribution, which could be due to interactions between the positive surface charge of the liposomes and the layer arrangement with carboxylic groups of HA and Col fibrils.

3.3. Adhesion and growth of C3H10T1/2 cells

C3H10T1/2 cells are a well-characterized model for in vitro differentiation of multipotent cells into osteoblasts, chondrocytes, and adipocytes [39,40]. The cell adhesion studies were carried out by the quantification of cell number and cell area including visualization of actin filaments (red staining), vinculin-positive focal adhesions (green staining), and nuclei (blue staining). These studies are important to understand how the PEM system properties influence cell adhesion, which may have also an effect on subsequent cell differentiation [67]. Fig. 6 A shows a higher number of cells on the PEM surfaces compared to the cells on glass used as a control after 4 h, which is due presence of cell receptors for HA and Col. Further, the cells seeded on PEM [HA/Col]₆ and [HA/Col]₄HA/Lip[HA/Col] show no significant difference probably due to similar composition of terminal layer (HA and Col). The quantification of the cell area (Fig. 6 B) demonstrated a significant higher spreading of cells on [HA/Col]₄HA/Lip[HA/Col] related to its higher WCA and zeta potential in contrast to the control and the basal PEM [HA/Col]₆. Fig. 6 C demonstrates the organization of the actin filaments on the different substrates. The cells on glass were characterized by a small aspect ratio of an irregular form and the actin filaments were organized mostly circumferentially. The cells cultured on the basal system [HA/Col]₆ had a longitudinal distribution of the actin filaments. However, the cells on [HA/Col]₄HA/Lip[HA/Col] displayed an

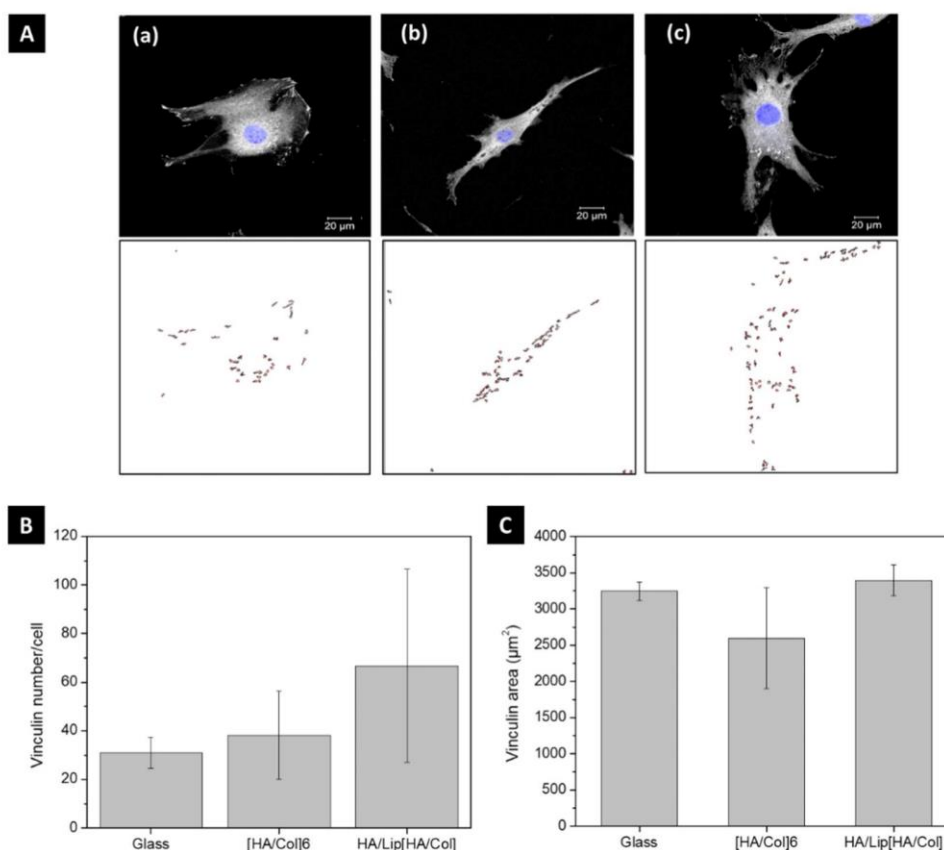


Fig. 7. A) Visualization of vinculin-positive focal adhesions in cells seeded on a) glass, b) [HA/Col]₆ and c) [HA/Col]₄HA/Lip[HA/Col]. B, C) Quantification of vinculin-positive focal adhesions number per cell and vinculin per cell area µm². vinculin-positive focal adhesions was quantified by Image J. Results represent means ± SD values, $n = 5$, $p \leq 0.05$.

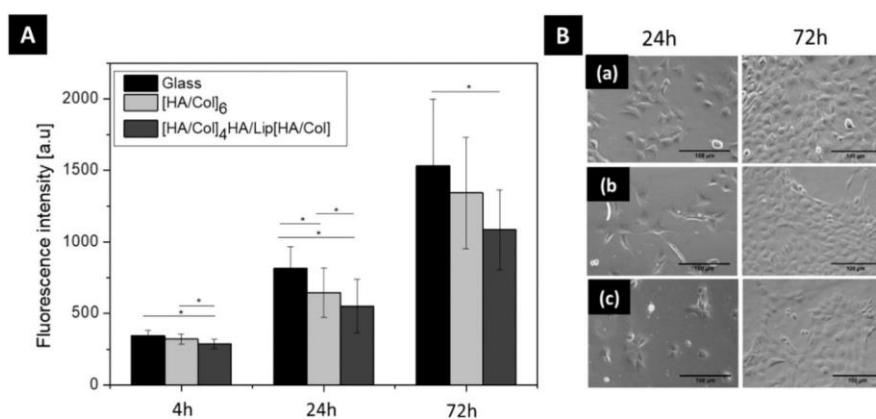


Fig. 8. A) Growth of C3H10T1/2 seed on glass and PEM system of [HA/Col]₆ and [HA/Col]₄HA/Lip[HA/Col] measured by the QBlue assay after 4 h, 24 h, and 72 h. B) Phase-contrast images of cell seeding on glass and multilayers after 24 h and 72 h. (a) Glass, (b) [HA/Col]₆, (c) [HA/Col]₄HA/Lip[HA/Col]. Scale bar 100 µm.

elongated and extended morphology which underlines that the embedded liposomes have a promoting effect on cell adhesion and spreading.

Fig. 7 displays the position of the vinculin-positive focal adhesions at the end of the actin filaments but also in central regions. Nevertheless, cell spreading was observed on both multilayers surfaces but the vinculin-positive focal adhesions amount was different. The PEM system

of [HA/Col]₄HA/Lip [HA/Col] showed a higher number and larger length of vinculin positive staining compared to the basal PEM [HA/Col]₆. Vinculin reinforces focal adhesion by crosslinking actin filaments to the structure molecules like talin [68]. This is an important step in cellular mechanics linking the cell to its substrate. Also, vinculin is recruited in integrin-mediated adhesions and the actin cytoskeletal network that is connected to the ECM. Therefore, the presence of

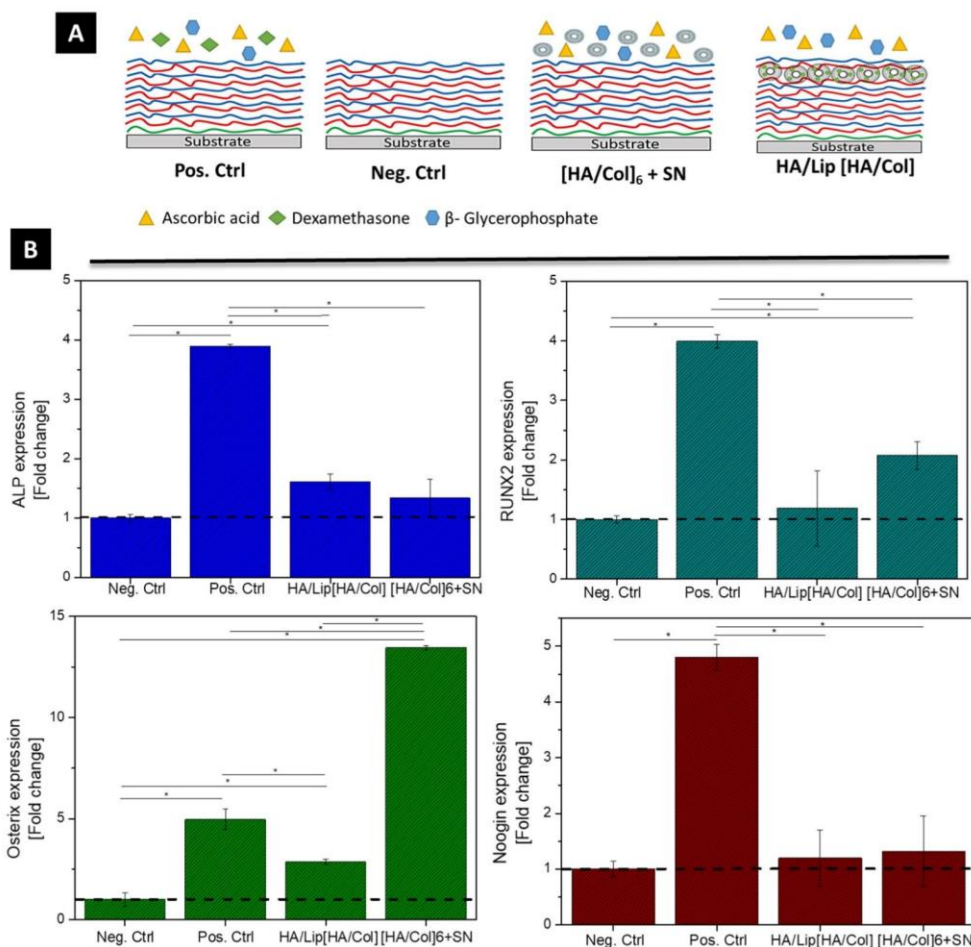


Fig. 9. A) Schematic illustration of the screened differentiation environments in the in vitro study. B) Relative expression of mRNA osteoblast markers (ALP, Runx2, Osterix, and Nogging) were determined after 14 days of incubation on PEM. qRT-PCR analyses were performed as described in the materials and methods. Data represent mean \pm SD values, $n = 5$, $p < 0.05$ and Scheffe-Post-Hoc test.

vinculin-positive focal adhesions in the samples gives an indication of integrin ligation and signal transduction processes [69].

Growth of C3H10T1/2 cells was studied by QBlue assay evaluating their metabolic activity to assure that cells can survive and multiply during longer culture for chondrogenic and osteogenic differentiation (Fig. 8). For this assay the samples were divided into three groups: the control group of C3H10T1/2 cells was seeded on glass slides and compared with cells growing on [HA/Col]₆ and on [HA/Col]₄HA/Lip [HA/Col]. In Fig. 8A it is shown that cells seeded on glass and both PEM system with liposomes showed similar metabolic activity after 4 h of incubation, which corresponds roughly to the results of adhesion studies. A significant increase within each group was detected with increasing time of culture certifying that cell can also grow on PEM as prerequisite for the differentiation studies. The positive control after 48 h and 72 h showed a higher fluorescence intensity, compared to [HA/Col]₆ and [HA/Col]₄HA/Lip [HA/Col]. As can be seen in the Fig. 8 B, cells were able to grow on all substrata over the time. However, the glass sample shows higher cell growth might due to the stronger substrate stiffness in comparison with the soft hydrated PEM systems where the HA has high water uptake capability and will decrease stiffness and roughness of the substratum [58,70]. It is well know that MSCs on soft substrates decrease the proliferative activity compared to cells grown on stiffer surfaces [71]. This consequence might not affect cell viability in vivo, but only their proliferative capacity [72].

Protein adsorption and cell adhesion are affected by the surface charge and wetting properties of the material [73,74]. For instance, negatively charged surfaces inhibit cell attachment, whereas positively charged surfaces stimulate [60]. The PEM system of [HA/Col]₄HA/Lip [HA/Col] showed positive zeta potential after the adsorption of the liposomes, where it is possible to observe a high cell area and a larger number of vinculin-positive focal adhesions compared to the basal sample [HA/Col]₆. In addition, the wettability of materials has been proven to have a considerable influence on cell growth and function [74]. The binding of liposomes and additional bilayer with Col a significantly increased WCA indicating a less hydrophilic surface. This reduction in the hydrophilicity decreases the hydration force of repulsion, promoting the cell adhesion process [50].

On the other hand, cell adhesion depends on the interactions of cells with their surrounding microenvironment, particularly ligands of different cell adhesion receptors [74]. HA and Col play important roles in the regulation of cell adhesion and spreading. For instance, HA can bind to a variety of cell surface receptors named hyaladherins, such as CD44 and RHAMM [75]. CD44 proteins are involved in a diversity of cellular functions, including growth and differentiation [75,76]. For Col, there are specific proteins that play a key role in this process, called integrins. The integrin family contains four collagen receptors such as $\alpha 1\beta 1$, $\alpha 2\beta 1$, $\alpha 10\beta 1$ $\alpha 11\beta 1$, whereas $\alpha 2\beta 1$ integrin is the main receptor for Col [77]. Therefore, both samples of PEM systems present a higher

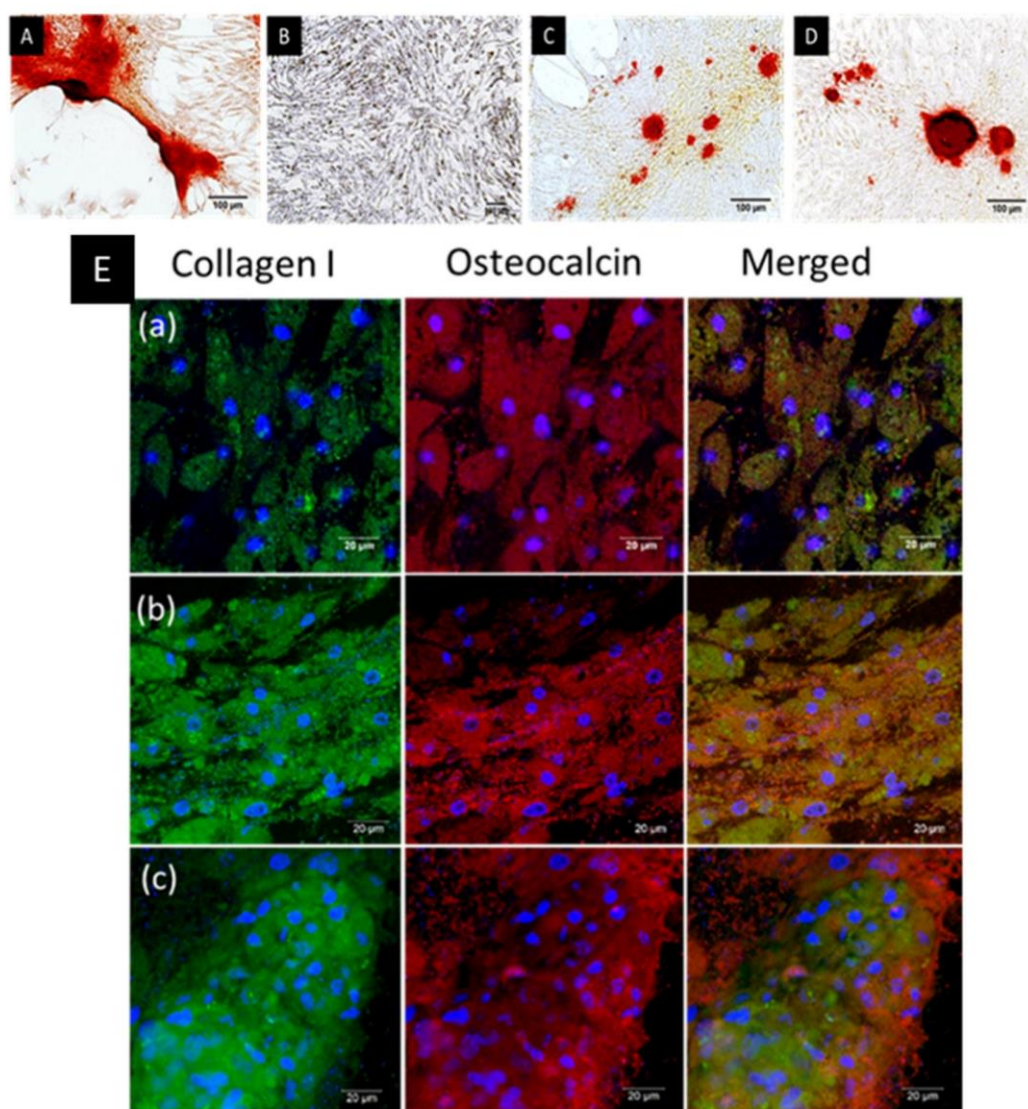


Fig. 10. Histochemical staining of C3H10T1/2 cells cultured on various test samples with basal medium and osteogenic medium. A) Positive control, [HA/Col]₆, B) Negative control, [HA/Col]₆ basal medium, C) [HA/Col]₆ and liposomes in the supernatant, D) [HA/Col]₄HA/Lip[HA/Col]. Alizarin red staining was performed after 21 days. Calcium deposits were staining in red [scale 100 μ m]. E) CLSM images of immunofluorescence staining of collagen I and osteocalcin of C3H10T1/2 cells cultured in osteogenic medium after 21 days. a) Positive control, [HA/Col]₆, b) [HA/Col]₆ and liposomes in the supernatant, c) [HA/Col]₄HA/Lip [HA/Col]. Collagen I (green fluorescence), osteocalcin (red fluorescence), nuclei (blue fluorescence) Scale bar 20 μ m. (For interpretation of the references to colour in this figure legend, the reader is referred to the web version of this article.)

number of vinculin-positive focal adhesions unlike the control (glass) due to the presence of fibrillary collagen as a terminal layer promoting the cell adhesion via integrin α 2 β 1 receptor of Col [52]. The benefit of integrin-binding surfaces is an enhanced cell adhesion and expansion [78]. For instance, integrins are of focal adhesion complexes that contain linker proteins to the cytoskeleton like, talin, and α -actinin and signaling transducers like vinculin and focal adhesion kinase [79]. These focal adhesions are involved in the adhesion process, function as the structural link between the cytoskeleton and ECM and activate signaling pathways to regulate transcription factors, involved in cell growth and cell differentiation [79,80].

3.4. Osteogenic differentiation of C3H10T1/2 cells

Previous studies confirmed that the cationic OO4/DOPE liposomes

embedded in a PEM system can be used for controlled release or transfer of compounds into cells [46]. To induce cell differentiation, Dex was incorporated in the lipid bilayer of the liposomes as described in the [Materials and methods section](#). Dex activates the expression of Runx2 which acts as an expression factor for procollagen [38]. Further, Dex in combination with ascorbic acid (ASC) and β -glycerophosphate (β -Gly) has shown to regulate the osteogenesis of mouse MSCs with mineralization in vitro [44]. To determine if there were levels of osteogenic markers due to Dex effects on cells, the relative quantification of mRNA was performed by qRT-PCR after 14 days in a growth medium with ASC and β -Gly. The different conditions are represented in [Fig. 9A](#). The qRT-PCR results ([Fig. 9 B](#)) demonstrated that Dex in the medium (positive control) or encapsulated in liposomes resulted in an upregulation of the gene expression of osteogenic markers (ALP, Runx2, osterix, and noggin) compared to the negative control, which was not treated with

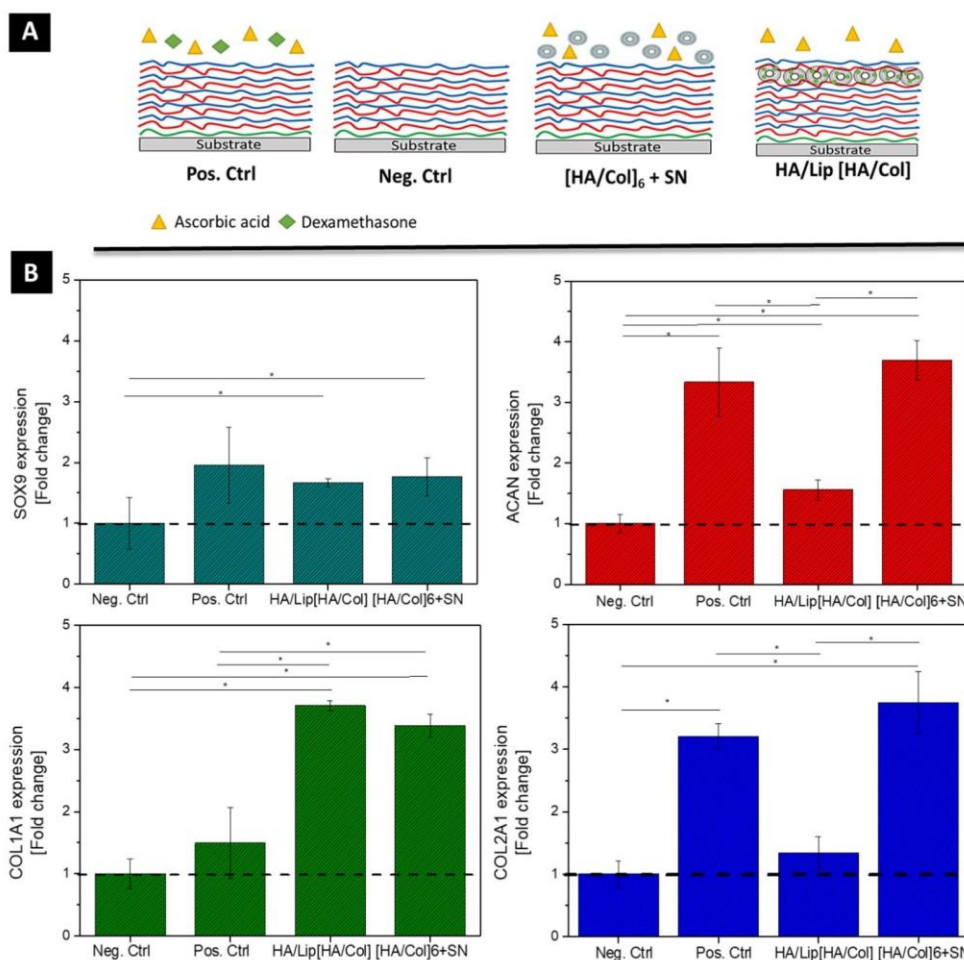


Fig. 11. A) Schematic illustration of the screened differentiation environments in the in vitro study. B) Relative expression of mRNA chondrogenic markers (Sox9, ACAN, COL1A1, and COL2A1) were determined after 14 days of incubation on PEM. qRT-PCR analyses were performed as described in the materials and methods. Data represent mean \pm SD values, $n = 5$, $p < 0.05$ and Scheffe-Post-Hoc test.

Dex. In addition, a higher level of ALP was found on the liposomes embedded into PEM. The high-level expression of ALP can be found because ALP is an early marker in osteogenesis and it promotes the formation of hydroxyapatite crystals in the bone matrix [81]. However, it is possible to observe an increase of other osteogenic markers like Runx2 and noggin (compared to negative control), but the expression of mRNA was lower compared to the positive control. Another important transcription factor is osterix. This transcription factor activates genes during the differentiation of pre-osteoblast to the final stage that is osteocytes [82]. In addition, Sox9, Runx2, and osterix play an important role in the decision by which the cells differentiate to osteoblast or chondrocytes [83]. The qRT-PCR shows increased expression levels in both systems with Dex-loaded liposomes. Further, the expression of the markers where the liposomes were added in the supernatant (SN) was high, which might be to the direct contact of the liposomes with the cell, compared to the liposomes embedded in the film. For that reason, to confirm the qRT-PCR results, the deposition of calcium phosphate at 21 days was studied by Alizarin red staining (Fig. 10 A).

This result is supported by the images obtained of C3H10T1/2 culture after histochemical staining by Alizarin Red S that interact with hydroxyapatite and results in red staining of mineralized nodules that corresponds to an ECM rich in calcium phosphates. These nodules were observed when cells were cultured in [HA/Col]₄HA/Lip[HA/Col] and liposomes in the supernatant [HA/Col]₆ + SN in presence of the

osteogenic medium. These results confirm the previous data of qRT-PCR.

Another method to evaluate the osteogenic differentiation was through immunofluorescence staining of Col and OCN after 21 days of incubation (Fig. 10E). The positive staining confirmed the presence of Col and OCN, which are specific protein markers synthesized by osteoblast during maturation [84]. The presence of markers was found in both of PEM systems [HA/Col]₄HA/Lip[HA/Col] and liposomes in the supernatant [HA/Col]₆ + SN. These results confirmed the protein production of osteogenic proteins at later stages but also supported that the liposomes with Dex can induce osteogenic differentiation.

On the other hand, connective tissues cells differ importantly in phenotype. The shape of MSC is involved in their specialized function, while at the same time drive to their multicellular organization [85]. For instance, cell spreading enables osteogenic matrix deposition during bone formation and these differences in cell morphology are due to the changes in the expression of the integrins, cadherins, and cytoskeletal proteins [67]. McBeath et al, demonstrated that cell spreading increased osteoblast differentiation in preosteoblastic progenitors [67]. Thus, previous results showed a high spreading presence in the PEM system [HA/Col]₄HA/Lip[HA/Col] in which not only the Dex is involved in the differentiation, but also the spreading phenotypes of cells are related to osteogenic differentiation. In contrast, for chondrogenesis, the cells need to grow at high densities where the cell spreading on the surface decreases but cell-cell contact and paracrine signaling increase [67].

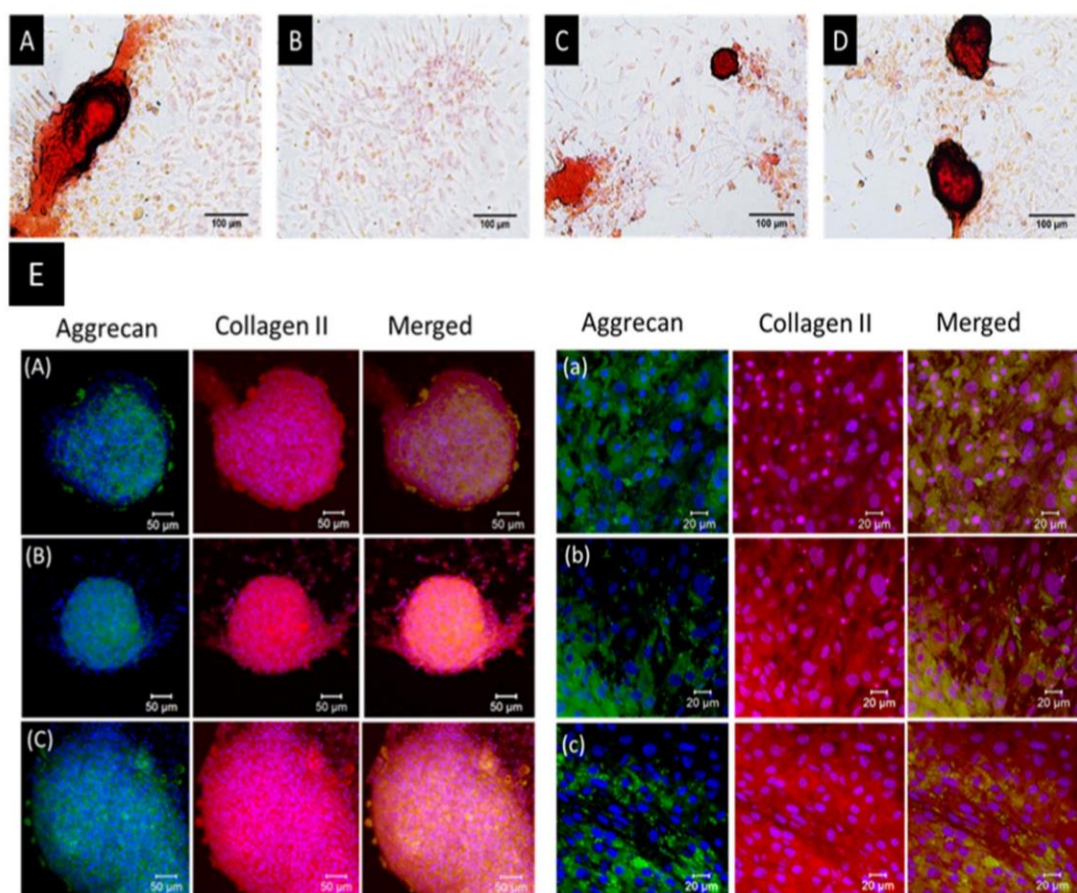


Fig. 12. Histochemical staining of C3H10T1/2 cells cultured on various test samples with basal medium and chondrogenic medium. A) Positive control, [HA/Col]₆, B) Negative control, [HA/Col]₆ basal medium, C) [HA/Col]₆ and liposomes in the supernatant, D) [HA/Col]₄ HA/Lip [HA/Col]. Safranin O staining was performed after 21 days. Accumulation of glycosaminoglycans was staining in red [scale 100 µm]. E) CLSM images of immunofluorescence staining of aggrecan and collagen II of C3H10T1/12 cells cultured in the chondrogenic medium after 21 days. A, a) Positive control, [HA/Col]₆, B, b) [HA/Col]₆ and liposomes in the supernatant, C, c) [HA/Col]₄ HA/Lip [HA/Col]. Aggrecan (green fluorescence), collagen II (red fluorescence), nuclei (blue fluorescence). Left images: scale bar 50 µm. Right images: scale bar 20 µm. (For interpretation of the references to colour in this figure legend, the reader is referred to the web version of this article.)

3.5. Chondrogenic differentiation of C3H10T1/2 cells

Dex not only induces the Runx2 expression but can also be involved in the expression of Sox9 for chondrogenesis. The orientation of chondrogenic differentiation is connected to osteogenesis since both processes share the transcription factor of Sox9 [42]. Some authors refer that Dex increases Sox9 expression in primary chondrocyte cultures, in which Sox9 controls collagen II a1 and ACAN gene expression [86]. However, the molecular mechanism by how Dex produces its effects is still unknown. The mesenchymal stem cells that go through chondrogenesis express proteins associated with hyaline cartilage such as ACAN and collagen type II [87,88]. For instance, hyaline cartilage is present on the articular surface of the bone with collagen type II as the main component of this cartilage, while fibro-cartilage is found on the meniscus containing fibers of Col [89]. The difference between these types of collagen is that Col forms heterotrimeric triple helices which are self-assembled and collagen type II forms homotrimeric molecules [90]. In addition, it is known that chondrogenic differentiation depends on cell density and the experimental system. Seeding the high density of cells can induce endochondral ossification due to the formation of dense cell-cell interaction regulated by N-cadherin's [49,91]. For that reason, chondrogenic markers such as Sox9, ACAN, Col, and collagen type II were measured by qRT-PCR after 14 days of incubation on the mRNA

level. Fig. 11 A shows the different conditions that were used to induce chondrogenic differentiation and the PEM systems. Fig. 11B shows the presence of these chondrogenesis markers Sox9, ACAN, Col, and collagen II in cells when they were exposed to Dex. Here, the Dex is immediately available for the positive control and the liposomes in the supernatant in comparison with the liposomes embedded into PEM. However, the PEM systems [HA/Col]₄HA/Lip[HA/Col] shows similar Sox9 values as the positive control and the liposomes in the supernatant [HA/Col]₆ + SN compared to the negative control. This result is an indicator that the cells were induced to undergo chondrogenesis. There were also increased mRNA values for ACAN and collagen type II for the PEM systems [HA/Col]₄HA/Lip[HA/Col], but the values of the positive control and the PEM system [HA/Col]₆ + SN were not reached. Col shows a high expression in both PEM systems, with liposomes in the SN and embedded in the PEM.

It is known that chondrogenesis can be stimulated in the presence of Dex and increase GAGs expression [88]. Therefore, histochemical staining with safranin O that detects acidic GAGs (e.g. hyaluronan, chondroitin sulfate, etc.) was done after 21 days. Fig. 12A–D shows the staining of the accumulation of GAGs and clusters with condensation of cells, which was positive for the control (positive) and both PEM systems with liposomes embedded or in the SN.

The study of chondrogenic markers by immunostaining revealed that

ACAN was uniformly distributed through the cell cluster and at the periphery, and collagen type II was accumulated also within the cluster in all the samples (Fig. 12). Here, the detection of ACAN and collagen type II confirmed the chondrogenic differentiation. In addition, previous studies demonstrate that the presence of HA and Col induces chondrogenic differentiation because of the partially mimic of ECM of bone and cartilage [39]. The mesenchymal progenitor shares Sox9 and the addition of induction supplements such as Dex and induce the differentiation to chondrogenic or osteogenesis. Further, transcription factor Sox9 can control the chondrocyte proliferation and the progression to hypertrophy chondrocytes and go through osteogenic lineage [42,92].

In literature it was demonstrated that chondrogenesis is induced when cells are seeded in high density in vitro because this mimics the condensation during cartilage formation. Interestingly, the low cell density causes high cell spreading to induce osteogenic differentiation, however, for chondrogenic differentiation the high cell density decreases the cell spreading and increase the number of cadherins, and trigger chondrogenesis [93]. For that reason, the advantage of the [HA/Col]₄HA/Lip[HA/Col] system is that the cells can differentiate into both osteogenic or chondrogenic pathways with minor changes in the conditions.

4. Conclusion

The LbL technique can be used to create multifunctional surface coatings that can modify the composition and physicochemical properties of implants surfaces with liposomes adsorption to allow the delivery of compounds like Dex. This technique can develop ECM-inspired surface coatings for osteochondral implants to induce bone and cartilage differentiation. In previous studies [40], the PEM system and Dex-loaded liposomes demonstrated a uniform and stable adsorption with a successful transfer into cells to induce cell differentiation. The benefit of the immobilization of liposomes in PEM with a cover bilayer of HA/Col is to protect them from degradation and spontaneous release of Dex, reducing the systemic effects and having a local delivery. The PEM made of HA/Col with embedded liposomes provides also good cell adhesion which is an important for integration of implants related to cell growth and differentiation. An important point is probably the effect of combining adhesive cues by the ECM-like composition of PEM with chemical cues like Dex to activate pathways for cell differentiation. Hence, differentiation of C3H10T1/2 cells was more prominent on the PEM system with embedded Dex-loaded liposomes compared to the use of free liposomes in the SN. Overall, the combination of multilayers mimicking the matrix of bone and cartilage in combination with Dex might be interesting for future studies as coatings for osteochondral implants.

CRediT authorship contribution statement

Brito-Barrera Y A: Conceptualization, Methodology, Visualization Investigation, Writing - Original Draft. **Husteden C:** Investigation, Visualization, Writing - Review & Editing. **Alherz J:** Investigation, Visualization. **Fuhrmann B:** Visualization, Supervision **Wölk C:** Conceptualization, Supervision, Validation, Writing - Review & Editing. **Groth T:** Conceptualization, Supervision, Project administration, Writing- Reviewing and Editing.

Funding

Y.A.B.B supported by the CONACYT-México and German Academic Exchange Service (DAAD). The support by the Deutsche Forschungsgemeinschaft (DFG) project-ID [396823779] to C.W. is greatly acknowledged. TG acknowledges the kind support by the Ministry of Science and Higher Education of the Russian Federation within the framework of state support for the creation and development of World-Class Research Centers "Digital biodesign and personalized healthcare"

[075-15-2020-926].

Declaration of competing interest

The authors declare that they have no known competing financial interests or personal relationships that could have appeared to influence the work reported in this paper.

Acknowledgments

The authors thank the technical assistance of Mrs. Marlis Porobin for performing zeta potential measurements.

Appendix A. Supplementary data

Supplementary data to this article can be found online at <https://doi.org/10.1016/j.msec.2021.112516>.

References

- [1] Y. Lu, W. Zhang, J. Wang, G. Yang, S. Yin, T. Tang, X. Jiang, Recent advances in cell sheet technology for bone and cartilage regeneration: from preparation to application, *International J. Oral Sci.* (2019), <https://doi.org/10.1038/s41368-019-0050-5>.
- [2] A.M. Yousefi, M.E. Hoque, R.G. Prasad, N. Uth, Current strategies in multiphasic scaffold design for osteochondral tissue engineering: a review, 2015, <https://doi.org/10.1002/jbm.a.35356>. Wiley Online Library.
- [3] W. Swieszkowski, B.H.S. Tuan, K.J. Kurzydowski, D.W. Huttmacher, Repair and regeneration of osteochondral defects in the articular joints, *Biomol. Eng.* 24 (2007) 489–495, <https://doi.org/10.1016/j.bioeng.2007.07.014>.
- [4] M. Navarro, A. Michiardi, O. Castano, J.A. Planell, *Biomaterials in orthopaedics*, 2008, <https://doi.org/10.1098/rsif.2008.0151>.
- [5] J.M. Oliveira, S. Pina, R.L. Reis, J. San Roman (Eds.), *Osteochondral Tissue Engineering: Challenges, Current Strategies, and Technological Advances*, Springer International Publishing, Cham, 2018, <https://doi.org/10.1007/978-3-319-76735-2>.
- [6] J.F. Mano, R.L. Reis, Osteochondral defects: present situation and tissue engineering approaches, *J. Tissue Eng. Regen. Med.* 1 (2007) 261–273, <https://doi.org/10.1002/term.37>.
- [7] P. Gentile, I. Carmagnola, T. Nardo, V. Chiono, Layer-by-layer assembly for biomedical applications in the last decade, *Nanotechnology* 26 (2015), 422001, <https://doi.org/10.1088/0957-4484/26/42/422001>.
- [8] G. Decher, J.D. Hong, J. Schmitt, Buildup of ultrathin multilayer films by a self-assembly process: III. Consecutively alternating adsorption of anionic and cationic polyelectrolytes on charged surfaces, *Thin Solid Films* 210–211 (1992) 831–835, [https://doi.org/10.1016/0040-6090\(92\)90417-A](https://doi.org/10.1016/0040-6090(92)90417-A).
- [9] P. Gentile, I. Carmagnola, T. Nardo, V. Chiono, Layer-by-layer assembly for biomedical applications in the last decade, *IOPscience* (2015), <https://doi.org/10.1088/0957-4484/26/42/422001>.
- [10] P. Gentile, M.E. Frongia, M. Cardellach, C.A. Miller, G.P. Stafford, G.J. Leggett, P. V. Hatton, Functionalised nanoscale coatings using layer-by-layer assembly for imparting antibacterial properties to polylactide-co-glycolide surfaces, *Acta Biomater.* 21 (2015) 35–43, <https://doi.org/10.1016/j.actbio.2015.04.009>.
- [11] W. Li, T. Guan, X. Zhang, Z. Wang, M. Wang, W. Zhong, J. Kong, The Effect of Layer-by-Layer Assembly Coating on the Proliferation and Differentiation of Neural Stem Cells, *ACS App. Mater. Interfaces* (2015), <https://doi.org/10.1021/am504456t>.
- [12] Y.T. Lai, E. Reading, G.L. Hura, K.L. Tsai, A. Laganowsky, F.J. Asturias, T.O. Yeates, Structure of a designed protein cage that self-assembles into a highly porous cube, *Nat. Chem.* (2014), <https://doi.org/10.1038/nchem.2107>.
- [13] M. Zhao, G. Altankov, U. Grabiec, M. Bennett, M. Salmeron-Sanchez, F. Dehghani, T. Groth, Molecular composition of GAG-collagen I multilayers affects remodeling of terminal layers and osteogenic differentiation of adipose-derived stem cells, *Acta Biomater.* 41 (2016) 86–99, <https://doi.org/10.1016/j.actbio.2016.05.023>.
- [14] H. Ai, S.A. Jones, Y.M. Lvov, Biomedical applications of electrostatic layer-by-layer nano-assembly of polymers 39 (2003) 23–44, <https://doi.org/10.1385/CBB:39:1:23>.
- [15] D.P. Pioletti, O. Gauthier, V.A. Stadelmann, B. Bujoli, J. Guicheux, P.-Y. Zambelli, J.-M. Boulter, Orthopedic implant used as drug delivery system: clinical situation and state of the research, *Curr. Drug Deliv.* 5 (2008) 59–63, <https://doi.org/10.2174/156720108783331041>.
- [16] B.S.G. Prasad, V.R.M. Gupta, N. Devanna, K. Jayasurya 5 (2014) 12.
- [17] G. Khang, J.M. Rhee, J.K. Jeong, J.S. Lee, M.S. Kim, S.H. Cho, H.B. Lee, Local drug delivery system using biodegradable polymers, *Macromol. Res.* 11 (2003) 207–223, <https://doi.org/10.1007/BF03218355>.
- [18] A. Aravamudhan, M.D. Ramos, J. Nip, A. Subramanian, R. James, D.M. Harmon, G. S. Kumar, Osteoinductive small molecules: growth factor alternatives for bone tissue engineering, *Curr. Pharm. Des.* 19 (2013) 3420–3428, <https://doi.org/10.2174/1381612811319190008>.

- [19] M. Yuasa, T. Yamada, T. Taniyama, T. Masaoka, W. Xuetao, T. Yoshii, S. Sotome, Dexamethasone Enhances Osteogenic Differentiation of Bone Marrow- and Muscle-Derived Stromal Cells and Augments Ectopic Bone Formation Induced by Bone Morphogenetic Protein-2, 2015, <https://doi.org/10.1371/journal.pone.0116462>.
- [20] V. Llopis-Hernández, M. Cantini, C. González-García, Z.A. Cheng, J. Yang, P. M. Tsimbouri, A.J. García, M.J. Dalby, M. Salmerón-Sánchez, Material-driven fibronectin assembly for high-efficiency presentation of growth factors, *Sci. Adv.* 2 (2016), e1600188, <https://doi.org/10.1126/sciadv.1600188>.
- [21] N. Monteiro, A. Martins, D. Ribeiro, S. Faria, N.A. Fonseca, J.N. Moreira, N. M. Neves, On the use of dexamethasone-loaded liposomes to induce the osteogenic differentiation of human mesenchymal stem cells, 2015, <https://doi.org/10.1002/term.1817>. Wiley Online Library.
- [22] C. Wölk, C. Janich, U. Bakowsky, A. Langner, G. Brezesinski, Malonic acid based cationic lipids – the way to highly efficient DNA-carriers, *Adv. Colloid Interf. Sci.* 248 (2017) 20–34, <https://doi.org/10.1016/j.cis.2017.08.003>.
- [23] S. Zhang, Y. Xu, B. Wang, W. Qiao, D. Liu, Z. Li, Cationic compounds used in lipoplexes and polyplexes for gene delivery, *J. Control. Release* 100 (2004) 165–180, <https://doi.org/10.1016/j.jconrel.2004.08.019>.
- [24] J. Giselbrecht, C. Janich, S.R. Pinnapireddy, G. Hause, U. Bakowsky, C. Wölk, A. Langner, Overcoming the polycation dilemma – explorative studies to characterise the efficiency and biocompatibility of newly designed lipofection reagents, *Int. J. Pharm.* 541 (2018) 81–92, <https://doi.org/10.1016/j.ijpharm.2018.02.029>.
- [25] X. Zhang, L. Dai, A. Wang, C. Wölk, B. Dobner, G. Brezesinski, J. Li, The directional observation of highly dynamic membrane tubule formation induced by engulfed liposomes, *Sci. Rep.* (2015), <https://doi.org/10.1038/srep16559>.
- [26] C.R. Dass, P.F. Choong, Targeting of small molecule anticancer drugs to the tumour and its vasculature using cationic liposomes: lessons from gene therapy, *SpringerLink*, 2006, <https://doi.org/10.1186/1475-2867-6-17>.
- [27] A. Kanazawa, T. Ikeda, T. Endo, Synthesis and antimicrobial activity of dimethyl- and trimethyl-substituted phosphonium salts with alkyl chains of various lengths, *Antimicrob. Agents Chemother.* (1994), <https://doi.org/10.1128/AAC.38.5.945>.
- [28] C. Barnier Quer, A. Elsharkawy, S. Romeijn, A. Kros, W. Jiskoot, Cationic liposomes as adjuvants for influenza hemagglutinin: more than charge alone, *Eur. J. Pharm. Biopharm.* 81 (2012) 294–302, <https://doi.org/10.1016/j.ejpb.2012.03.013>.
- [29] M.A. Mintzer, E. Simanek, E nonviral vectors for gene delivery, *Chem. Rev.* (2009), <https://doi.org/10.1021/cr800409e>.
- [30] V.E. Santo, M.E. Gomes, J.F. Mano, R.L. Reis, Controlled release strategies for bone, cartilage, and osteochondral engineering—part I: recapitulation of native tissue healing and variables for the design of delivery systems, 2013, <https://doi.org/10.1089/ten.teb.2012.0138>.
- [31] N. Patel 2 (2012) 7.
- [32] M. Michel, D. Vautier, J.-C. Voegel, P. Schaaf, V. Ball, Layer by layer self-assembled polyelectrolyte multilayers with embedded phospholipid vesicles, *Langmuir* 20 (2004) 4835–4839, <https://doi.org/10.1021/la049736q>.
- [33] D.V. Volodkin, P. Schaaf, H. Mohwald, J.-C. Voegel, V. Ball, Effective embedding of liposomes into polyelectrolyte multilayered films: the relative importance of lipid–polyelectrolyte and interpolyelectrolyte interactions, *Soft Matter* 5 (2009) 1394–1405, <https://doi.org/10.1039/B815048F>.
- [34] N. Graf, A. Tanno, A. Dochter, N. Rothfuchs, J. Vörös, T. Zambelli, Electrochemically driven delivery to cells from vesicles embedded in polyelectrolyte multilayers, *Soft Matter* 8 (2012) 3641–3648, <https://doi.org/10.1039/C2SM07272F>.
- [35] P.C. DeMuth, J.J. Moon, H. Suh, P.T. Hammond, D.J. Irvine, Releasable layer-by-layer assembly of stabilized lipid nanocapsules on microneedles for enhanced transcutaneous vaccine delivery, *ACS Nano* 6 (2012) 8041–8051, <https://doi.org/10.1021/nn302639r>.
- [36] R. Polak, R.M. Lim, M.M. Beppu, R.N. Pitombo, R.E. Cohen, M.F. Rubner 4 (18) (2015) 2832–2841, <https://doi.org/10.1002/adhm.201500604>.
- [37] V. Domínguez-Arca, R.R. Costa, A.M. Carvalho, P. Taboada, R.L. Reis, G. Prieto, I. Pashkuleva, Liposomes embedded in layer by layer constructs as simplistic extracellular vesicles transfer model, *Mater. Sci. Eng. C* 121 (2021), 111813, <https://doi.org/10.1016/j.msec.2020.111813>.
- [38] X. Ma, X. Zhang, Y. Jia, S. Zu, S. Han, D. Xiao, H. Sun, Y. Wang, Dexamethasone induces osteogenesis via regulation of hedgehog signalling molecules in rat mesenchymal stem cells, *Int. Orthop.* 37 (2013) 1399–1404, <https://doi.org/10.1007/s00264-013-1902-9>.
- [39] L. Zhao, G. Li, K.-M. Chan, Y. Wang, P.-F. Tang, Comparison of multipotent differentiation potentials of murine primary bone marrow stromal cells and mesenchymal stem cell line C3H10T1/2, *Calcif. Tissue Int.* 84 (2009) 56–64, <https://doi.org/10.1007/s00223-008-9189-3>.
- [40] C.M. Shea, C.M. Edgar, T.A. Einhorn, L.C. Gerstenfeld, BMP treatment of C3H10T1/2 mesenchymal stem cells induces both chondrogenesis and osteogenesis, *J. Cell. Biochem.* 90 (2003) 1112–1127, <https://doi.org/10.1002/jcb.10734>.
- [41] L. Han, A.J. Grodzinsky, C. Ortiz, Nanomechanics of the cartilage extracellular matrix, *Annu. Rev. Mater. Res.* 41 (2011) 133–168, <https://doi.org/10.1146/annurev-matsci-062910-100431>.
- [42] F. Long, Building strong bones: molecular regulation of the osteoblast lineage, *Nat. Rev. Mol. Cell Biol.* (2012), <https://doi.org/10.1038/nrm3254>.
- [43] O. Ghali, O. Broux, G. Falgayrac, N. Haren, J.P. van Leeuwen, G. Penel, P. Hardouin, C. Chauveau, Dexamethasone in osteogenic medium strongly induces adipocyte differentiation of mouse bone marrow stromal cells and increases osteoblast differentiation, *BMC Cell Biol.* 16 (2015), <https://doi.org/10.1186/s12860-015-0056-6>.
- [44] F. Langenbach, J. Handschel, Effects of dexamethasone, ascorbic acid and β -glycerophosphate on the osteogenic differentiation of stem cells in vitro, *Stem Cell Res Ther* 4 (2013) 117, <https://doi.org/10.1186/scrt328>.
- [45] I. Sekiya, P. Koopman, K. Tsuji, S. Mertin, V. Harley, Y. Yamada, K. Shinomiya, A. Nifuji, M. Noda, Dexamethasone enhances SOX9 expression in chondrocytes.
- [46] Y.A. Brito Barrera, G. Hause, M. Menzel, C.E.H. Schmelzer, E. Lehner, K. Mäder, C. Wölk, T. Groth, Engineering osteogenic microenvironments by combination of multilayers from collagen type I and chondroitin sulfate with novel cationic liposomes, *Mater. Today Bio.* 7 (2020), 100071, <https://doi.org/10.1016/j.mtbio.2020.100071>.
- [47] A. Köwitsch, M. Jurado Abreu, A. Chhalotre, M. Hielscher, S. Fischer, K. Mäder, T. Groth, Synthesis of thiolated glycosaminoglycans and grafting to solid surfaces, *Carbohydr. Polym.* 114 (2014) 344–351, <https://doi.org/10.1016/j.carbpol.2014.08.027>.
- [48] U. Horzum, B. Ozdil, D. Pesen-Okvur, Step-by-step quantitative analysis of focal adhesions, *MethodsX* 1 (2014) 56–59, <https://doi.org/10.1016/j.mex.2014.06.004>.
- [49] M. Sarem, O. Otto, S. Tanaka, V.P. Shastri, Cell number in mesenchymal stem cell aggregates dictates cell stiffness and chondrogenesis, *Stem Cell Res. Ther.* 10 (2019) 10, <https://doi.org/10.1186/s13287-018-1103-y>.
- [50] K.J. Livak, T.D. Schmittgen, Analysis of relative gene expression data using real-time quantitative PCR and the 2⁻ $\Delta\Delta$ CT method, *Methods* 25 (2001) 402–408, <https://doi.org/10.1006/meth.2001.1262>.
- [51] S. Tassler, B. Dobner, L. Lampp, R. Ziolkowski, E. Malinowska, C. Wölk, G. Brezesinski, DNA delivery systems based on peptide-mimicking cationic lipids—the effect of the co-lipid on the structure and DNA binding capacity, *Langmuir* 35 (2019) 4613–4625, <https://doi.org/10.1021/acs.langmuir.8b04139>.
- [52] S. Tassler, C. Wölk, C. Janich, B. Dobner, G. Brezesinski, Lysine-based amino-functionalized lipids for gene transfection: the protonation state in monolayers at the air–liquid interface, *Phys. Chem. Chem. Phys.* 19 (2017) 20271–20280, <https://doi.org/10.1039/C7CP03107F>.
- [53] J. Stetefeld, S.A. McKenna, T.R. Patel, Dynamic light scattering: a practical guide and applications in biomedical sciences, *Biophys. Rev.* 8 (2016) 409–427, <https://doi.org/10.1007/s12551-016-0218-6>.
- [54] I.S. Zuhorn, U. Bakowsky, E. Polushkin, W.H. Visser, M.C.A. Stuart, J.B.F. N. Engberts, D. Hoekstra, Nonbilayer phase of lipoplex–membrane mixture determines endosomal escape of genetic cargo and transfection efficiency, *Mol. Ther.* 11 (2005) 801–810, <https://doi.org/10.1016/j.yjmt.2004.12.018>.
- [55] M. Zhao, L. Li, C. Zhou, F. Heyroth, B. Fuhrmann, K. Maeder, T. Groth, Improved stability and cell response by intrinsic cross-linking of multilayers from collagen I and oxidized glycosaminoglycans, *Biomacromolecules* (2014), <https://doi.org/10.1021/bm501286f>.
- [56] M. Zhao, R. Anouz, T. Groth, Effect of microenvironment on adhesion and differentiation of murine C3H10T1/2 cells cultured on multilayers containing collagen I and glycosaminoglycans, 2020, <https://doi.org/10.1177/2041731420940560>.
- [57] C. Husteden, F. Doberenz, N. Goergen, S.R. Pinnapireddy, C. Janich, A. Langner, F. Szyrowatka, A. Repanas, F. Erdmann, J. Jedelská, U. Bakowsky, T. Groth, C. Wölk, Contact-triggered lipofection from multilayer films designed as surfaces for in situ transfection strategies in tissue engineering, *ACS Appl. Mater. Interfaces* 12 (2020) 8963–8977, <https://doi.org/10.1021/acsmi.9b18968>.
- [58] P.D. Ward, S.L. Thibault, S.D. Gray, Hyaluronic acid: its role in voice, *J. Voice* 16 (2002) 303–309, [https://doi.org/10.1016/S0892-1997\(02\)00101-7](https://doi.org/10.1016/S0892-1997(02)00101-7).
- [59] M. Michel, V. Toniazio, D. Ruch, V. Ball, Deposition mechanisms in layer-by-layer or step-by-step deposition methods: from elastic and impermeable films to soft membranes with ion exchange properties, *ISRN Mater. Sci.* 2012 (2012), <https://doi.org/10.5402/2012/701695>.
- [60] G. Altankov, K. Richau, T. Groth, The role of surface zeta potential and substratum chemistry for regulation of dermal fibroblasts interaction, in: *Mater. Sci. Eng. Technol.*, Wiley Online Library, 2003, <https://doi.org/10.1002/mawe.200300699>.
- [61] R. Zimmermann, O. Birkert, G. Gauglitz, C. Werner, *Electrosurface Phenomena at Polymer Films for Biosensor Applications*, 2003, <https://doi.org/10.1002/cphc.200200475>. Wiley Online Library.
- [62] J. Almodóvar, L.W. Place, J. Gogolski, K. Erickson, M.J. Kipper, layer-by-layer assembly of polysaccharide-based polyelectrolyte multilayers: a spectroscopic study of hydrophilicity, composition, and ion pairing, *Biomacromolecules* 12 (2011) 2755–2765, <https://doi.org/10.1021/bm200519y>.
- [63] M.S. Niepel, K. Kirchhof, M. Menzel, A. Heilmann, T. Groth, Controlling cell adhesion using pH-modified polyelectrolyte multilayer films, in: *Layer-by-Layer Films for Biomedical Applications*, John Wiley & Sons, Ltd, 2015, pp. 1–30, <https://doi.org/10.1002/9783527675869.ch1>.
- [64] G. Altankov, F. Grinnell, T. Groth, Studies on the biocompatibility of materials: Fibroblast reorganization of substratum-bound fibronectin on surfaces varying in wettability, 1996, [https://doi.org/10.1002/\(SICI\)1097-4636\(199603\)30:3<385::AID-JBM13>3.0.CO;2-J](https://doi.org/10.1002/(SICI)1097-4636(199603)30:3<385::AID-JBM13>3.0.CO;2-J). Wiley Online Library.
- [65] N. Fauchoux, R. Schweiss, K. Lützwow, C. Werner, T. Groth, Self-assembled monolayers with different terminating groups as model substrates for cell adhesion studies, *Biomaterials* 25 (2004) 2721–2730, <https://doi.org/10.1016/j.biomaterials.2003.09.069>.
- [66] M. Schönhoff, Layered polyelectrolyte complexes: physics of formation and molecular properties, *J. Phys. Condens. Matter* 15 (2003) R1781–R1808, <https://doi.org/10.1088/0953-8984/15/49/R01>.
- [67] R. McBeath, D.M. Pirone, C.M. Nelson, K. Bhadriraju, C.S. Chen, Cell shape, cytoskeletal tension, and RhoA regulate stem cell lineage commitment, *Dev. Cell* 6 (2004) 483–495, [https://doi.org/10.1016/S1534-5807\(04\)00075-9](https://doi.org/10.1016/S1534-5807(04)00075-9).

- [68] W.H. Goldmann, Role of vinculin in cellular mechanotransduction, 2016, <https://doi.org/10.1002/cbin.10563>. Wiley Online Library.
- [69] M. Bennett, M. Cantini, J. Reboud, J.M. Cooper, P. Roca-Cusachs, M. Salmeron-Sanchez, Molecular clutch drives cell response to surface viscosity, *PNAS* 115 (2018) 1192–1197, <https://doi.org/10.1073/pnas.1710653115>.
- [70] D.E. Discher, P. Janmey, Y. Wang, Tissue cells feel and respond to the stiffness of their substrate, *Science* 310 (2005) 1139–1143, <https://doi.org/10.1126/science.1116995>.
- [71] A.S. Mao, J.-W. Shin, D.J. Mooney, Effects of substrate stiffness and cell-cell contact on mesenchymal stem cell differentiation, *Biomaterials* 98 (2016) 184–191, <https://doi.org/10.1016/j.biomaterials.2016.05.004>.
- [72] A. Nolte, S. Hossfeld, B. Schroepel, A. Mueller, D. Stoll, T. Walker, R. Krastev, Impact of polyelectrolytes and their corresponding multilayers to human primary endothelial cells, *J. Biomater. Appl.* (2013), <https://doi.org/10.1177/0885328212437610>.
- [73] V. Gribova, R. Auzely-Velty, C. Picart, Polyelectrolyte multilayer assemblies on materials surfaces: from cell adhesion to tissue engineering, *Chem. Mater.* (2013), <https://doi.org/10.1021/cm2032459>.
- [74] T. Groth, Z.M. Liu, M. Niepel, D. Peschel, K. Kirchhof, G. Altankov, N. Fauchoux, Chemical and Physical Modifications of Biomaterial Surfaces to Control Adhesion of Cells, SpringerLink, 2010, https://doi.org/10.1007/978-90-481-8790-4_13.
- [75] M. Kiesel, M.M. Martino, M. Ventura, J.A. Hubbell, J. Hilborn, D.A. Ossipov, Improving the osteogenic potential of BMP-2 with hyaluronic acid hydrogel modified with integrin-specific fibronectin fragment, *Biomaterials* 34 (2013) 704–712, <https://doi.org/10.1016/j.biomaterials.2012.10.015>.
- [76] H. Ponta, L. Sherman, P.A. Herrlich, CD44: from adhesion molecules to signalling regulators, *Nat. Rev. Mol. Cell. Biol.* 4 (2003) 33–45, <https://doi.org/10.1038/nrm1004>.
- [77] J. Jokinen, E. Dadu, P. Nykvist, J. Käpylä, D.J. White, J. Ivaska, P. Vehviläinen, H. Reunanen, H. Larjava, L. Häkkinen, J. Heino, Integrin-mediated cell adhesion to type I collagen fibrils, *J. Biol. Chem.* 279 (2004) 31956–31963, <https://doi.org/10.1074/jbc.M401409200>.
- [78] P.J. Wrighton, J.R. Klim, B.A. Hernandez, C.H. Koonce, T.J. Kamp, L.L. Kiessling, Signals from the surface modulate differentiation of human pluripotent stem cells through glycosaminoglycans and integrins, 2014, <https://doi.org/10.1073/pnas.1409525111>.
- [79] J.D. Humphrey, E.R. Dufresne, M.A. Schwartz, Mechanotransduction and extracellular matrix homeostasis, *Nat. Rev. Mol. Cell. Biol.* 15 (2014) 802–812, <https://doi.org/10.1038/nrm3896>.
- [80] A.J. Garcia, Get a grip: integrins in cell–biomaterial interactions, *ScienceDirect* (2005), <https://doi.org/10.1016/j.biomaterials.2005.05.029>.
- [81] X. Wu, S. Ding, Q. Ding, N.S. Gray, P.G. Schultz, A small molecule with osteogenesis-inducing activity in multipotent mesenchymal progenitor cells, *J. Am. Chem. Soc.* 124 (2002) 14520–14521, <https://doi.org/10.1021/ja0283908>.
- [82] K.M. Sinha, X. Zhou, Genetic and molecular control of osterix in skeletal formation, *J. Cell. Biochem.* 114 (2013) 975–984, <https://doi.org/10.1002/jcb.24439>.
- [83] A. Cheng, P.G. Genever, SOX9 determines RUNX2 transactivity by directing intracellular degradation 25 (2010) 2680–2689, <https://doi.org/10.1002/jbmr.174>.
- [84] F. Jafary, P. Hanachi, K. Gorjipour, Osteoblast differentiation on collagen scaffold with immobilized alkaline phosphatase, *Int. J. Organ Transplant Med.* 8 (2017) 195–202.
- [85] J. Settleman, Tension precedes commitment—even for a stem cell, *Mol. Cell* 14 (2004) 148–150, [https://doi.org/10.1016/S1097-2765\(04\)00207-2](https://doi.org/10.1016/S1097-2765(04)00207-2).
- [86] I. Sekiya, P. Koopman, K. Tsuji, S. Mertin, V. Harley, Y. Yamada, K. Shinomiya, A. Nifuji, M. Noda, Dexamethasone enhances SOX9 expression in chondrocytes, *J. Endocrinol.* 169 (2001) 573–579, <https://doi.org/10.1677/joe.0.1690573>.
- [87] M.A. Pratta, W. Yao, C. Decicco, M.D. Tortorella, R.-Q. Liu, R.A. Copeland, R. Magolda, R.C. Newton, J.M. Trzaskos, E.C. Arner, Aggrecan protects cartilage collagen from proteolytic cleavage, *J. Biol. Chem.* 278 (2003) 45539–45545, <https://doi.org/10.1074/jbc.M303737200>.
- [88] H. Tanaka, C.L. Murphy, C. Murphy, M. Kimura, S. Kawai, J.M. Polak, Chondrogenic differentiation of murine embryonic stem cells: effects of culture conditions and dexamethasone, *J. Cell. Biochem.* 93 (2004) 454–462, <https://doi.org/10.1002/jcb.20171>.
- [89] A.C. Daly, S.E. Critchley, E.M. Rencsok, D.J. Kelly, A comparison of different bioinks for 3D bioprinting of fibrocartilage and hyaline cartilage, *Biofabrication* 8 (2016), 045002, <https://doi.org/10.1088/1758-5090/8/4/045002>.
- [90] M.K. Gordon, R.A. Hahn, Collagens, *Cell Tissue Res.* 339 (1) (2010) 247–257, <https://doi.org/10.1007/s00441-009-0844-4>.
- [91] M.S. Niepel, B.K. Ekambaram, C.E.H. Schmelzer, T. Groth, Polyelectrolyte multilayers of poly (l-lysine) and hyaluronic acid on nanostructured surfaces affect stem cell response, *Nanoscale* 11 (2019) 2878–2891, <https://doi.org/10.1039/c8nr05529g>.
- [92] L. Yang, K.Y. Tsang, H.C. Tang, D. Chan, K.S.E. Cheah, Hypertrophic chondrocytes can become osteoblasts and osteocytes in endochondral bone formation, *PNAS* 111 (2014) 12097–12102, <https://doi.org/10.1073/pnas.1302703111>.
- [93] L. Gao, R. McBeath, C.S. Chen, Stem cell shape regulates a chondrogenic versus myogenic fate through Rac1 and N-cadherin, *Stem Cells* 28 (3) (2010) 564–572, <https://doi.org/10.1002/steam.308>.

Chapter 4: Lipoplex-functionalized thin-film surface coating based on extracellular matrix components as a local gene delivery system to control osteogenic stem cell differentiation

An attractive strategy for bone tissue engineering is the use of smart biomaterials functionalized with biological cues to control cell proliferation and differentiation. Here, a gene-activated surface coating is presented based on the polyelectrolytes col I and Cs, two main biopolymers of the bone extracellular matrix, in combination with the incorporation of DNA/lipid-nanoparticles (lipoplex). The coating relies on layer-by-layer assembly technology, a process leading to the formation of PEM applicable to various material surfaces. The initial part of the study focuses on analyzing PEM formation and lipoplex deposition by surface-sensitive analytical methods that demonstrate a fibrillar structuring of collagen and homogenous embedding of lipoplexes. To gain the targeted biological activity, the immobilized lipoplexes encapsulate DNA encoding for osteogenesis-inducing bone morphogenetic protein 2 (BMP-2). Human adipose-derived mesenchymal stem cells were cultured on the gene-activated surface to study osteogenic differentiation *in vitro*, showing proliferation of the stem cells as well as efficient transfection, which induces cell differentiation towards the osteogenic lineage. Summarizing, the novel gene-functionalized and ECM-mimicking PEM represents a smart surface functionalization with great promise for tissue engineering constructs to control stem cell fate due to spatially induced expression of growth factor-encoding nucleic acid.

Lipoplex-Functionalized Thin-Film Surface Coating Based on Extracellular Matrix Components as Local Gene Delivery System to Control Osteogenic Stem Cell Differentiation

Catharina Husteden, Yazmin A. Brito Barrera, Sophia Tegtmeier, João Borges, Julia Giselbrecht, Matthias Menzel, Andreas Langner, João F. Mano, Christian E. H. Schmelzer, Christian Wölk,* and Thomas Groth*

A gene-activated surface coating is presented as a strategy to design smart biomaterials for bone tissue engineering. The thin-film coating is based on polyelectrolyte multilayers composed of collagen I and chondroitin sulfate, two main biopolymers of the bone extracellular matrix, which are fabricated by layer-by-layer assembly. For further functionalization, DNA/lipid-nanoparticles (lipoplexes) are incorporated into the multilayers. The polyelectrolyte multilayer fabrication and lipoplex deposition are analyzed by surface sensitive analytical methods that demonstrate successful thin-film formation, fibrillar structuring of collagen, and homogenous embedding of lipoplexes. Culture of mesenchymal stem cells on the lipoplex functionalized multilayer results in excellent attachment and growth of them, and also, their ability to take up cargo like fluorescence-labelled DNA from lipoplexes. The functionalization of the multilayer with lipoplexes encapsulating DNA encoding for transient expression of bone morphogenetic protein 2 induces osteogenic differentiation of mesenchymal stem cells, which is shown by mRNA quantification for osteogenic genes and histochemical staining. In summary, the novel gene-functionalized and extracellular matrix mimicking multilayer composed of collagen I, chondroitin sulfate, and lipoplexes, represents a smart surface functionalization that holds great promise for tissue engineering constructs and implant coatings to promote regeneration of bone and other tissues.

1. Introduction

Over the past few decades, the development of smart multifunctional biomaterials with the ability to control the behavior of stem cells on demand has become a powerful strategy in regenerative medicine and cell therapies.^[1,2] For instance, such stem cell-based therapies bear new chances to regenerate critical size bone defects from severe fractures or bone tissue loss after surgery. The osteogenic differentiation of mesenchymal stem cells is important for the healing of bone fractures and osteogenic diseases such as disorders of bone metabolism (osteoporosis).^[3-6] Various studies have determined characteristics and modifications of biomaterials that enable initiation of stem cell osteogenesis and represent promising approaches for clinical use. These approaches include materials that can mimic the bone microenvironment,^[7,8] materials with specific mechanical properties which stimulate bone tissue formation,^[9] and materials

C. Husteden, S. Tegtmeier, J. Giselbrecht, A. Langner
Institute of Pharmacy
Department of Medicinal Chemistry
Martin Luther University Halle-Wittenberg
Wolfgang-Langenbeck-Str. 4, 06120 Halle (Saale), Germany
Y. A. Brito Barrera, T. Groth
Institute of Pharmacy
Department of Biomedical Materials
Martin Luther University Halle-Wittenberg
Heinrich-Damerow-Str. 4, 06120 Halle (Saale), Germany
E-mail: thomas.groth@pharmazie.uni-halle.de

J. Borges, J. F. Mano
Department of Chemistry
CICECO – Aveiro Institute of Materials
University of Aveiro
Campus Universitário de Santiago, Aveiro 3810-193, Portugal
M. Menzel, C. E. H. Schmelzer
Department of Biological and Macromolecular Materials
Fraunhofer Institute for Microstructure of Materials and Systems (IMWS)
Walter-Hülse-Str. 1, 06120 Halle (Saale), Germany
C. Wölk
Institute of Pharmacy
Pharmaceutical Technology
Faculty of Medicine
Leipzig University
04317 Leipzig, Germany
E-mail: christian.woelk@medizin.uni-leipzig.de
T. Groth
Interdisciplinary Center of Materials Science
Martin-Luther-University Halle-Wittenberg
Heinrich-Damerow-Str. 4, 06120 Halle (Saale), Germany

 The ORCID identification number(s) for the author(s) of this article can be found under <https://doi.org/10.1002/adhm.202201978>

© 2022 The Authors. Advanced Healthcare Materials published by Wiley-VCH GmbH. This is an open access article under the terms of the Creative Commons Attribution License, which permits use, distribution and reproduction in any medium, provided the original work is properly cited.

DOI: 10.1002/adhm.202201978

which can release or control the activity of osteoinductive growth factors.^[10–12]

A straightforward strategy for the functionalization of biomaterials involves emulating the properties of the extracellular matrix (ECM) for the formation of an artificial microenvironment that enables a precise control of cell behavior and function.^[13] Due to interaction of ECM components with cell surface receptors such as integrins, ECM regulates cell proliferation, migration, and differentiation.^[14,15] Indeed, the ECM is a highly versatile and dynamic compartment that can support development, function, and regeneration of tissues and organs by modulating the production, degradation, and remodeling of its components.^[16] Therefore, the development of surface coatings mimicking the native ECM structure and function is of considerable interest to functionalize implant materials. In this context, a simple and versatile method that can effectively immobilize bio-functional molecules onto various materials and surfaces, with dynamic control of the surface topological and mechanical properties, is of upmost interest. The layer-by-layer (LbL) technology, well-known from the pioneering work by Decher et al. on the development of polyelectrolyte multilayers (PEMs) on solid surfaces by alternating deposition of oppositely charged polyelectrolytes, has evolved into a very simple and cost effective yet highly versatile and efficient surface modification and functionalization technology. LbL technique allows the production of multifunctional thin film coatings with precise control of the film composition, structure, properties, and functions at the nanoscale.^[17,18] A further advantage of LbL is that it can be performed by different methods such as dip-coating, spray coating, and spin-coating protocols allowing the coating of different materials and designs also in a time-saving manner.^[18] Indeed, PEMs have been broadly used as reservoir for either the surface immobilization or encapsulation of bioactive molecules, more precisely drugs and proteins, to engineer bio-functional materials by choice of polyelectrolytes and complexation conditions for regenerative medicine strategies.^[19–23] Type I collagen (Col) and chondroitin sulfate (Cs) are components of the ECM of bone. Col is the main organic component of the bone ECM and a perfect material in tissue engineering because of its excellent biodegradability, biocompatibility, and cell-attracting properties. In fact, Col has drawn much attention for biomaterial development due to the existence of binding sites for cell receptors, cytokines, and other ECM components.^[19,24–26] Cs is involved in cell recognition, intracellular signaling, and on the interaction between ECM components and cell-surface glycoproteins.^[27] As such, Cs can enhance bone regeneration; thus, being used for the functionalization of PEMs for improved mineral deposition and osteogenesis.^[28]

The functionalization of biomaterials with tissue relevant growth factors is also a promising strategy in tissue engineering. In the field of bone tissue engineering, the bone morphogenetic protein-2 (BMP-2) is a promising cytokine. Several studies have demonstrated that the growth factor BMP-2 can be applied to stimulate bone healing and improve osteogenesis/osteointegration.^[29–33] For example, recombinant BMP-2 is applied in the clinic for treatment of non-union bone injuries, open tibia fractures, and spinal fusion in FDA-approved systems for bone regeneration.^[8,34] However, due to some persistent issues, including the need of loading large amounts of the recombinant BMP-2 into the biomaterial, a burst release of supra-

physiological concentrations of BMP-2 as well as the risk of unregulated and ectopic bone formation in vivo, the current clinical utilization of BMP-2 has limitations,^[35] which forces the development of micro- or nanostructured delivery systems for BMP-2^[36] or novel gene-activated matrices.^[37]

To overcome the existing drawbacks of BMP-2 functionalized biomaterials, spatially limited acting in situ transfection systems gained attention to ensure a local cytokine production mediated by transfected cells. Surface-mediated transfection strategies are based on a concept in which viral or non-viral vectors embedded in matrix materials can promote a local, physiological, and/or sustained expression of a gene encoding for a therapeutic protein.^[38] By immobilizing plasmid DNA (pDNA) on surfaces, such as implants, surface-mediated gene delivery achieved remarkable transient cell transfection and therapeutic effects, both in vivo and in vitro.^[39,40] Despite their potential for tissue engineering, the use of viral vectors for gene delivery is limited by a high risk of immunogenicity and a certain risk for carcinogenicity. Therefore, current research is increasingly focusing on non-viral vectors.^[41] Promising new methods are studied to find non-viral vectors to achieve comparable gene transfer efficiency to viral vector equivalents. New transfection systems such as polymers, lipids, nanoparticles, and physical methods are studied to reduce cost, and increase safety and transfection efficiency.^[42,43] For example, Olden et al. used cationic polyplexes for gene delivery into primary human T cells.^[44] Non-viral gene delivery approaches have been specifically explored in cell-based therapies because of their desirable safety profiles and simplicity of the preparation process when compared to viral vectors.^[45] However, non-viral vectors are not suitable for systemic application in bone regeneration because DNA complexes carry the risk of transfection of undesired cell types and systemic side effects in vivo.

Previous studies have consistently demonstrated that electrostatic-driven LbL assembly is a powerful and simple technique to functionalize biomaterials with nucleic acids aiming for non-viral gene delivery.^[46–49] Thus, non-viral, surface-mediated gene delivery may represent an ideal strategy to control cell response in the close vicinity of an implant material avoiding any systemic complications in patients. Lipoplexes (LPX), a subtype of nucleic acid lipid nanoparticles, belong to the non-viral gene delivery systems. For example, in a proof-of-concept study by Holmes, Lipofectamine 2000-based LPX has been immobilized in PEMs and successfully transferred a model gene to typical screening cell lines (NIH3T3 fibroblasts and HEK293 kidney cells), but not to stem cells.^[50] However, we recently developed a LPX formulation composed of dioleoylphosphatidylethanolamine (DOPE) and the ionizable lipid *N*-{6-amino-1[*N*-(9*Z*)-octadec-9-enylamino]-1-oxohexan-(2*S*)-2-yl}-*N'*-{2-[*N,N*-bis(2-aminoethyl)amino]ethyl}-2[(9*Z*)-octadec-9-enyl]propan diamide (OO4), a lipid composite which demonstrated superiority in terms of efficient cellular uptake and DNA delivery in cell culture experiments, compared to Lipofectamine 2000.^[51,52] Moreover, we could show recently that surface coatings composed of either Col/Cs or Col/hyaluronic acid PEMs with dexamethasone (Dex) loaded OO4/DOPE liposomes could induce either osteogenic or chondrogenic differentiation of multipotent stem cells. This was related to the type of multilayer mimicking the composition of target ECM, such as bone or cartilage.^[53,54] Furthermore, we developed in a

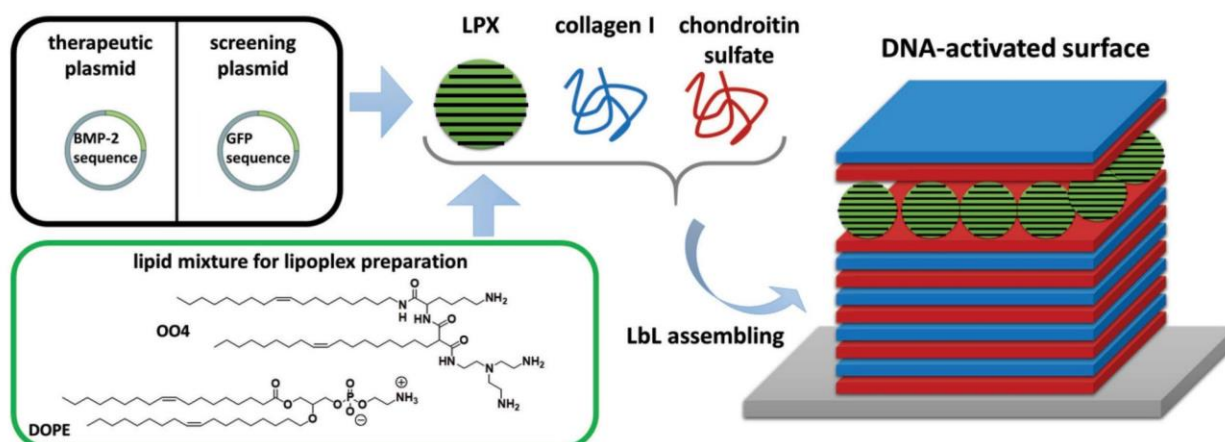


Figure 1. Schematic illustration of the DNA-activated bone-ECM-mimicking surface coating. The lipid components OO4/DOPE were formulated to cationic liposomes. The cationic liposomes were assembled with DNA encoding either of the reporter gene green fluorescent protein (GFP) or the therapeutic gene BMP-2, to LPX. LPX were assembled into DNA-activated surface coatings as tool for in situ transfection using the LbL technique.

proof-of-concept study, a strategy to incorporate LPX into PEMs composed of hyaluronic acid and chitosan and demonstrated the successful transfection of murine myoblasts and the epithelium of the chorion allantois membrane of the chicken embryo.^[48]

In the present study, we combined both approaches, such as the ECM-mimicking character of PEM and their ability to be used as carrier for in situ transfection, to develop a gene-activated ECM-mimicking surface coating to direct stem cells' fate. We focused on a bone ECM-mimicking PEMs consisting of Col and Cs loaded with LPX composed of OO4/DOPE lipid composite (see **Figure 1**). The DNA as biological active compound encoded a BMP-2 sequence to stimulate surface-mediated, transient expression of BMP-2 in human adipose-derived mesenchymal stem cells (hADSCs) to induce osteogenesis due to autocrine and paracrine effects of the cytokine. The work focused on three main objectives: 1) a material science part, in which we characterized the multilayer formation processes, especially the embedding of OO4/DOPE LPX and the surface properties of LPX-loaded PEMs. 2) In addition, general studies on cell proliferation, hADSCs attachment, and transfection were performed. 3) We studied the ability of the system to induce osteogenic stem cell differentiation by gene expression analysis and mineralization assays. Summarizing, we present a new approach to engineer a bone-ECM inspired gene-activated surface coating which allows controlling stem cells function, and consequently, represents a promising tool to develop multifunctional surface coatings for regenerative medicine strategies.

2. Experimental Section

2.1. Materials

If not stated otherwise, all chemicals were purchased from Sigma–Aldrich/Merck (Taufkirchen, Germany). Col was provided from Sichuan Mingrang Bio-Tech (Sichuan, China). The pDNA pCMV-GFP (3.5 kbp, 260 kDa) was acquired from Plasmid Factory (Bielefeld, Germany). The synthesis and characterization of the used cationic lipid OO4 was described in the authors' pre-

vious work.^[55] The phospholipids DOPE, 1,2-dioleoyl-*sn*-glycero-3-phosphoethanolamin-*N*-(7-nitro-2-1,3-benzoxadiazol-4-yl) (ammonium salt) (NBD-DOPE) ($\lambda_{\text{max}}^{\text{ex}} = 460 \text{ nm}$ and $\lambda_{\text{max}}^{\text{em}} = 535 \text{ nm}$), and 1,2-dioleoyl-*sn*-glycero-3-phosphoethanolamin-*N*-(lissamine rhodamine B sulfonyl) (ammonium salt) (Rho-DOPE) ($\lambda_{\text{max}}^{\text{ex}} = 560 \text{ nm}$ and $\lambda_{\text{max}}^{\text{em}} = 583 \text{ nm}$) were acquired from Avanti Polar Lipid, Inc. (Alabaster, AL, USA).

2.2. Methods

2.2.1. Preparation of Cationic Liposomes

For liposome preparation, lipids were separately dissolved in chloroform/methanol (8:2, v/v) as lipid stock. The stocks were combined in the desired molar ratio (OO4/DOPE 1/3 *n/n*, OO4/DOPE/Rho-DOPE 1/3/0.04 *n/n/n*, OO4/DOPE/NBD-DOPE 1/3/0.04 *n/n/n*) and the organic solvent was evaporated for 1 h at 200 mbar at a rotary evaporator. After formation of dry lipid film, a solution of 150 mM NaCl 10 mM acetic acid adjusted to pH4 was added to a final total lipid concentration of 1 mg mL⁻¹. Afterward, the lipid dispersion was incubated at 50 °C while shaking gently for 30 min at 1400 rpm (Eppendorf Thermomixer 5436) followed by sonication at 37 kHz and 50 °C for 5 min.

2.2.2. Plasmid DNA Isolation

pDNA with the human BMP-2 gene controlled by a human cytomegalovirus promoter controlled and containing a neomycin resistance gene (pCMV-BMP-2) was purchased from OriGene Technologies GmbH (Herford, Germany). It was cloned and amplified using *Escherichia coli* DH5 α safety strain (Invitrogen, Carlsbad, CA, USA). Plasmid purification was performed using a Plasmid Maxi Prep Kit (Qiagen, Venlo, Netherlands) according to manufacturer instructions, and the resulting pDNA (pDNA) was resuspended in MilliQ water. The pDNA concentration and

purity were measured using a UV spectrophotometer at 260 and 280 nm and gel electrophoretic analysis.

2.2.3. Lipoplex Formation

LPX were prepared by combining pDNA with OO4/DOPE 1/3 (*n/n*) liposomes to a N/P ratio (N = primary amines of the cationic lipids; P = phosphate groups of the nucleic acid) of 4 in sterile-filtered solution of 150 mM NaCl with 10 mM sodium acetate buffer solution (pH 4). pDNA was pipetted to the liposomes and gently mixed, followed by an incubation period of 15 min at room temperature.

2.2.4. Characterization of Lipoplexes and Liposomes

The size was determined by dynamic light scattering (DLS) and zeta potential by laser Doppler velocimetry (LDV) using a Zetasizer Nano ZS ZEN3600 (Malvern Panalytical, Malvern, UK) as described previously.^[53] Briefly, DLS measurements at a scattering angle of 173° consist of 15 runs with a duration time of 20 s for each. For size calculations, a viscosity $\eta = 0.8872$ mPa s and a refractive index of 1.33 were assumed. LDV was performed in a clear disposable folded capillary cell (DTS1060, Malvern Panalytical) with 30 runs at a voltage of 60 V. For data evaluation, the viscosity ($\eta = 0.8872$ mPa s), dielectric constant ($\epsilon = 78.5$ F m⁻¹), and refractive index ($n = 1.33$) of water were applied. Particle size distribution curves and zeta potential were calculated using Zetasizer Software 7.13 (Malvern Panalytical). All measurements were performed three times at 25 °C.

2.2.5. Preparation of Polyelectrolyte Multilayers

The polyelectrolytes solutions were prepared as follows: Polyethylenimine (PEI, $M_w \approx 750$ kDa) was dissolved in 0.15 M NaCl solution to a concentration of 5 mg mL⁻¹ at pH 7.4. Cs ($M_w \approx 25$ kDa) was dissolved in 0.15 M NaCl solution to a concentration of 0.5 mg mL⁻¹ at pH 4. Col ($M_w \approx 100$ kDa) was dissolved in 0.2 M acetic acid to a concentration of 2 mg mL⁻¹ (stirring overnight). The final solution of Col was obtained by diluting the stock solution in 0.2 M acetic acid supplied with 0.15 M NaCl at pH 4.

PEMs were assembled on surfaces (mainly glass coverslips, but also silicon wafers) cleaned using the RCA protocol.^[56] PEI was used as the first layer to obtain a positive charge on the substrate followed by adsorption of Cs as an anionic layer and afterward, Col as the cationic layer. PEMs were fabricated by immersing the glass coverslips or silicon wafers in the polyelectrolyte solution for 15 min (PEI, Cs) and 20 min (Col) and one layer of LPX for 2 h 30 min. Due to the different M_w of the polyelectrolytes, the larger Col molecules require more time for diffusion. For that reason, the adsorption time of Col was prolonged to 20 min following existing LbL protocols.^[57] By alternating adsorption of Cs and Col, a basal PEM consisting of four polyelectrolyte bilayers and a final Cs layer was fabricated [Cs/Col]₄Cs, followed by LPX adsorption [Cs/Col]₄Cs/LPX. Last, a Cs/Col cover layer was deposited to prepare the gene-activated PEM [Cs/Col]₄Cs/LPX/Cs/Col. Each adsorption step was followed by rinsing with 0.15 M NaCl solution at pH 4 (3 × 5 min).

2.2.6. Confocal Laser Scanning Microscopy to Study Lipid and DNA Deposition on PEM

A rhodamine-labeled lipid formulation of OO4/DOPE/Rhod-DOPE 1/3/0.04 (*n/n/n*) ($\lambda_{\max}^{\text{ex}} = 560$ nm; $\lambda_{\max}^{\text{em}} = 583$ nm) and Cy5 labeled pDNA ($\lambda_{\max}^{\text{ex}} = 649$ nm; $\lambda_{\max}^{\text{em}} = 670$ nm) was used to screen for LPX deposition on the PEMs.^[53] DNA was covalently tagged with Cy5 using the Label IT Nucleic Acid Labeling Kit from Mirus (Madison, WI, USA), according to the manufacturer's instructions. After production of [Cs/Col]₄Cs/LPX using the fluorescence-tagged LPX, the PEM was washed three times, and the Cs/Col cover layer was deposited to obtain the final construct [Cs/Col]₄Cs/LPX/Cs/Col for microscopical analysis. The films were fixed with Aquatex mounting medium (Merck, Darmstadt, Germany) and stored overnight at 7 °C to cure the mounting medium before examining the distribution of the fluorophores by confocal laser scanning microscopy (CLSM) (LSM 710, Carl Zeiss, Oberkochen, Germany).

For time dependent evaluation of DNA embedding in the PEMs, the LPX were prepared with Cy5 labeled pDNA and embedded in the PEMs. The PEMs were stored in phosphate-buffered saline (PBS) and Cy5 fluorescence was screened by CLSM at different time points using identical parameter settings for taking the micrographs. The fluorescence intensity was determined with 12 images per sample in triplicates using ImageJ.

2.2.7. pDNA Loading Efficiency on the PEM Studied With Gel Electrophoresis

DNA loading of PEMs was quantified by agarose gel electrophoresis using an established protocol for indirect quantification (see for visualization of method also Figure S1, Supporting Information).^[48] After basal PEM [Cs/Col]₄Cs preparation on coverslips in 24-well plates, the coverslips were rinsed with 0.15 M NaCl (pH 4) and then transferred into a new 24-well plate for the incubation with LPX. Various OO4/DOPE 1/3 (*n/n*) N/P 4 LPX concentrations (0.26 to 3.15 $\mu\text{g pDNA cm}^{-2}$) were used for incubation under gentle shaking for 2 h 30 min. Subsequently, the supernatant of each well was transferred into tubes for quantification of DNA in LPX, and PEMs were afterward washed twice with 0.15 M NaCl solution (pH 4). The washing solutions were also transferred into separate tubes for quantification of DNA in detached LPX. DNA quantification was performed by gel electrophoresis after releasing the DNA from LPX. Briefly, 50 μL supernatant/washing solution was mixed with 10 μL of blue/orange 6× loading dye (G190A) and 4 μL 1% heparin v/w. Heparin was used to release complexed DNA from LPX. Electrophoresis was performed on 1% agarose gel containing 0.308 $\mu\text{g mL}^{-1}$ Ethidium bromide in 1% Tris-acetate-EDTA buffer (pH 8) for 1 h at 90 V, while a 1 kb DNA ladder (G571A) (Promega, Madison, WI, USA) was used for size determination. Quantification was possible using a pDNA standard dilution series (0.01, 0.1, 0.2, 0.3, 0.5, and 0.8 $\mu\text{g pDNA}$) to obtain a calibration curve. The fluorescent DNA bands were quantified with a UVP UVsolo touch (Analytik Jena AG, Jena, Germany) for imaging and the software Vision-Works LS Analysis Software from Analytik Jena AG for fluorescence signal quantification. All samples were tested in triplicates. The sensitivity of the used method was <0.015 mg cm⁻².

2.2.8. Quartz Crystal Microbalance With Dissipation Monitoring

A Q-Sense Pro quartz-crystal microbalance with dissipation monitoring (QCM-D, Biolin Scientific, Gothenburg, Sweden) was used to monitor LPX deposition on PEMs in detail. Freshly cleaned gold-coated 5 MHz AT-cut quartz crystal sensors (QSX301 Gold, Q-Sense) were used as substrate for the build-up of the PEM thin films. The solutions were injected into a flow chamber with a mounted quartz crystal at a constant flow rate of 50 mL min⁻¹. The quartz crystal was excited at multiple overtones (1st, 3rd, 5th, 7th, 9th, 11th, and 13th, corresponding to 5, 15, 25, 35, 45, 55, and 65 MHz, respectively) and shifts in frequency (Δf_n) and energy dissipation (ΔD) were monitored in real-time. The frequency of each overtone was normalized to the fundamental resonant frequency of the quartz crystal substrate ($\Delta f_n/n$, in which n denotes the overtone number). An adsorption time of 6 min for each polyelectrolyte layer and an intermediate rinsing step of 4 min with acetate buffer 0.1 M pH 5.5 were established. LPX solution was injected and measured for 2 h in steady state without a constant flow to mimic deposition conditions of the film preparation mentioned above. The hydrodynamic thickness of the PEMs at each deposition cycle as well as at the end of the deposition cycles was estimated using the Voigt-based viscoelastic model implemented in the Q-Sense Dfind software (Broadfit function), assuming a fluid density of 1000 kg m⁻³, a layer density of 1000 kg m⁻³, and a fluid viscosity of 1 mPa s.

2.2.9. Water Contact Angle Measurements

Static water contact angle (WCA) measurements were analyzed at room temperature using an OCA15+ device from Dataphysics (Filderstadt, Germany). The sessile drop method was applied using 1 μ L of water with the Ellipse-fitting method. Reported contact angles represent mean values and standard deviation of five measurements per sample of duplicates.

2.2.10. Atomic Force Microscopy

Atomic force microscopy (AFM, Nanowizard IV, JPK-Instruments, Berlin, Germany) in combination with an inverted fluorescence microscope (Olympus IX71, Olympus, Olympus Europa, Hamburg, Germany) was performed in quantitative imaging mode (QI) to investigate the surface roughness and topography as well as record corresponding fluorescence images. Topographical images were recorded using a silicon cantilever (qp-BioT, Nanosensors, Neuchatel, Switzerland) in a standard liquid cell (JPK-Instruments) containing 0.15 M NaCl solution. A force map area of 5 \times 5 μ m² was recorded with a resolution of 512 \times 512 pixel². Post-processing and roughness analysis were performed using the software JPK Data Processing V5.0.85 and Gwyddion (Gwyddion V2.58, 64-bit).

2.2.11. Fluorescence Recovery After Photobleaching

FRAP (fluorescence recovery after photobleaching) experiments using CLSM were performed to evaluate the LPX mobility in the PEM. This technique was developed by Axelrod et al. (1976) as a

method to study mobility of substances for example proteins.^[58] In FRAP, a specific area is photobleached by intense laser light, removing fluorescence from this area, and screening afterward, the degree of fluorescence reappearance in this region. The used fluorophore for this study was NBD-DOPE. The fluorophore was used to prepare fluorescence tagged liposomes (OO4/DOPE/NBD-DOPE 1/3/0.04 n/n/n) which were applied for LPX formation with pCMV-GFP. The fluorescence tagged LPX were adsorbed to [Cs/Col]₄Cs basal PEMs for 2 h 30 min. The LPX-loaded PEM was finalized with an additional cover layer of Cs/Col to [Cs/Col]₄Cs/LPX/Cs/Col. FRAP studies of NBD-LPX loaded PEMs were performed using an LSM 710 confocal microscope. A magnification of 40 \times with an oil objective was used for that experiment. A defined area in the PEM was photobleached (laser 488 nm, 20 cycles with a laser line attenuator transmission 100%). After defined periods of time, the area was examined for NBD- fluorescence using the same setup parameters. Images were processed with the ZEN2012 software (Carl Zeiss). The analysis of images to quantify RFU was performed with Image J.

2.2.12. Cell Culture

Cryopreserved hADSCs (StemPro) were obtained from Thermo Fisher Scientific (Waltham, MA, USA) and thawed and grown in Dulbeccos's modified Eafless medium (DMEM) supplemented with 10% fetal bovine serum (FBS) and 1% antibiotic and anti-fungal solution at 37 °C (basal culture medium, BM) in a humidified 5% CO₂/95% air atmosphere. Cells of almost confluent cultures were washed once with sterile PBS followed by treatment with 0.25% trypsin/0.02% EDTA at 37 °C for 3 min. Trypsin was neutralized with DMEM with 10% FBS, and the cells were re-suspended in DMEM after centrifugation at 250 \times g for 5 min. Last, the cells were seeded on PEMs-coated glass coverslips with a cell density of 1 \times 10⁵ cells per mL. Cells used in this study were from passage P1-P6, and 50% of the culture media was changed three times a week.

For the purpose of osteogenic differentiation experiments, the pDNA pCMV-BMP2, which encodes for BMP-2, was used for LPX preparation. After the cells had reached 90% confluence, the medium was changed to induce the osteogenic differentiation. The cells were cultured in the osteogenic induction medium (OM) containing 0.1 μ M Dex, 10 mM sodium β -glycerophosphate (β -Gly), and 0.05 mM ascorbic acid-2-phosphate (ASC), in addition to BM as described above. For the positive control, the StemPro Osteogenic-Differentiation Kit from Thermo Fisher Scientific (Waltham, MA, USA) was used according to the manufacturer's protocol. This medium contains components and cytokines for an optimized osteogenic differentiation of hADSCs and other stem cells provided by the supplier. As negative control group, the cells received BM. In addition, hADSCs cultured on [Cs/Col]₆ in OM were used as LPX-free positive control. The cells were incubated for 24 or 28 days and medium was changed once a week. All samples were tested for mineralization and gene expression of osteogenic markers (see below).

2.2.13. Cell Adhesion Studies

Glass coverslips were coated with different PEMs composites: [Cs/Col]₆ (LPX free system), [Cs/Col]₄Cs/LPX (system with LPX

on surface), and [Cs/Col]₄Cs/LPX/Cs/Col/ (final LPX loaded PEM); placed in 24 well plates, hADSCs were seeded on the samples in DMEM at 37 °C for 4 h. Then, cells attached to PEMs were fixed with 4% paraformaldehyde solution for 10 min and rinsed twice with PBS for further studies. Cells were permeabilized with 0.1% Triton X-100 in PBS v/v (Sigma) for 10 min, rinsed with PBS, and nonspecific binding sites were blocked by incubation with 1% w/v bovine serum albumin (BSA, Merck, Darmstadt, Germany) in PBS at room temperature for 1 h. Vinculin was stained using monoclonal anti-vinculin clone hVIN-1 mouse ascites fluid antibody (1:200, Sigma–Aldrich, Germany); and a secondary goat anti-mouse IgG, Alexa Fluor 647 (1:1000, $\lambda^{\text{ex}}_{\text{max}} = 650 \text{ nm}$ and $\lambda^{\text{em}}_{\text{max}} = 583 \text{ nm}$, Thermo Fisher Scientific, Waltham, MA, USA). The actin cytoskeleton was stained with phalloidin-Atto 488 (1:50, $\lambda^{\text{ex}}_{\text{max}} = 500 \text{ nm}$ and $\lambda^{\text{em}}_{\text{max}} = 520 \text{ nm}$, Sigma–Aldrich, Germany) at room temperature for 30 min. Cell nuclei were stained by BOBO-1 Iodide (1:200, $\lambda^{\text{ex}}_{\text{max}} = 462 \text{ nm}$ and $\lambda^{\text{em}}_{\text{max}} = 481 \text{ nm}$, Invitrogen, Darmstadt, Germany), incubating the samples for 30 min. Before microscopic evaluation, samples were washed with PBS and mounted with Roti-Mount FluorCare (Carl Roth GmbH, Karlsruhe, Germany). Fluorescence micrographs were taken with a LSM 710 confocal microscope using 10 \times , 20 \times objectives for cell adhesion and spreading analysis. A 63 \times oil immersion objective was used to visualize nuclei, actin cytoskeleton, and focal adhesions. Images were processed with the ZEN2012 software (Carl Zeiss). The analysis of images to quantify cell count and cell area was performed with Image J.

2.2.14. Cell Proliferation Studies With QBlue Cell Viability Assay

hADSC cells were seeded on LPX-loaded PEMs with and without cover layer: [Cs/Col]₄Cs/LPX; [Cs/Col]₄Cs/LPX/Cs/Col. Cells seeded on clean glass coverslip and the LPX-free PEMs [Cs/Col]₆ were used as controls. Cultures were incubated at 37 °C for 24 h, 2 and 4 days, respectively. After the incubation time, the cell viability was determined by QBlue cell viability assay kit (Biochain, Hayward, NJ, USA). The cells were washed once with PBS to remove the medium. Then, 500 μL of Qblue solution with colorless medium (10:1) was added to each well and incubated at 37 °C for 3 h. Finally, 100 μL of supernatant from each sample was added to a black 96 well plate and the fluorescence intensity was measured at 544 nm excitation and 590 nm emission with plate reader (FLUOstar Omega, BMG Labtech, Ortenberg, Germany). All samples were tested in triplicates.

2.2.15. DNA Uptake Into Stem Cells

To visualize the DNA uptake from LPX-loaded PEMs, we prepared fluorescence-tagged LPX using Cy-5 ($\lambda^{\text{ex}}_{\text{max}} = 649 \text{ nm}$ and $\lambda^{\text{em}}_{\text{max}} = 666 \text{ nm}$) labeled pDNA-GFP (Label IT Nucleic Acid Labeling Reagents, pDNA-GFP labeled according to manufacturer's instructions) for the LPX preparation. After hADSCs were cultured for 48 h on the [Cs/Col]₄Cs/LPX/Cs/Col coating, cells were screened for Cy-5 positive structures while additional staining of nuclei and actin was performed for visualization of intracellular distribution of pDNA-GFP. For this purpose, the cells were fixed, permeabilized, and blocked as described above. The

order of cell staining was designed as follows: a) Phalloidin-Atto 488 (1:50) for staining filamentous actin and b) BOBO-1 (1:200) for staining the nucleus. All dyes were incubated for 30 min at room temperature and protected from light. PBS washing (three times, each 5 min) was performed after incubation with fluorescent dyes. Afterward, all samples were briefly washed with ultrapure water and mounted with Mowiol 4–88 containing 25 mg mL⁻¹ 1,4-diazabicyclo [2.2.2]-octane (Carl Roth GmbH, Karlsruhe, Germany), a mounting medium providing high fluorescence stability for storage at 4 °C in the dark. Samples were analyzed with a LSM 710 confocal microscope.

2.2.16. Flow Cytometry Measurements to Determine the Reporter Gene Expression

Cells with a cell density of 1×10^5 cells per mL were seeded on PEMs containing pDNA-GFP encapsulating LPX. After an incubation period of 24 h at 37 °C and 5% CO₂, the expression of the reporter gene encoding for green fluorescent protein (GFP) was measured by flow cytometry. Briefly, cells were detached with 0.05% trypsin/0.02% EDTA solution from the PEMs and centrifuged at 220 $\times g$ for 5 min, rinsed, and re-suspended in 500 μL of PBS containing 1% BSA. A BD Accuri C6 Plus flow cytometer (BD Bioscience, Franklin Lakes, NJ, USA) was used to analyze 10 000 cells per sample for GFP expression quantifying the relative fluorescence (GFP: $\lambda^{\text{ex}}_{\text{max}} = 488 \text{ nm}$ and $\lambda^{\text{em}}_{\text{max}} = 510 \text{ nm}$). Single cells were gated by size (FSC-H) and granularity (SSC). The calculated single cell population was gated to detect GFP-expressing by calculating the relative number of transfected cells and dead cells. The BD Accuri C6 Software was used for all data evaluation. All samples were tested in duplicate.

2.2.17. Mineralization Experiments

Alizarin-Red-Assay: After 24 days of the osteogenic differentiation experiments, calcium phosphate deposition was investigated by Alizarin Red S staining. Briefly, the samples were washed once with PBS and fixed with 4% paraformaldehyde for 10 min. After washing twice with distilled water, Alizarin Red S (2%, pH 4.2, Roth) solution was added into each well and incubated for 45 min under light exclusion at room temperature. Last, the excess dye was removed by washing with distilled water. Images were taken in transmission mode with a Nikon ECLIPSE Ti2, Tokyo, Japan equipped with a CCD camera (DCIN, Tokyo, Japan).

OsteoImage Kit: The commercial mineralization kit (OsteoImage, Lonza) was used to visualize the hydroxyapatite portion of bone-like nodules deposited by cells by measuring fluorescence measurement ($\lambda^{\text{ex}}_{\text{max}} = 495 \text{ nm}$ and $\lambda^{\text{em}}_{\text{max}} = 519 \text{ nm}$). This assay, as described by the manufacturer, uses a fluorescent staining reagent that binds specifically to the hydroxyapatite portion of the biomineralized structures. The intensity of the green fluorescence is proportional to the amount of hydroxyapatite in the sample. After 24 days of the osteogenic differentiation, samples were incubated with OsteoImage according to the manufacturer's instructions and examined with a LSM 710 confocal microscope.

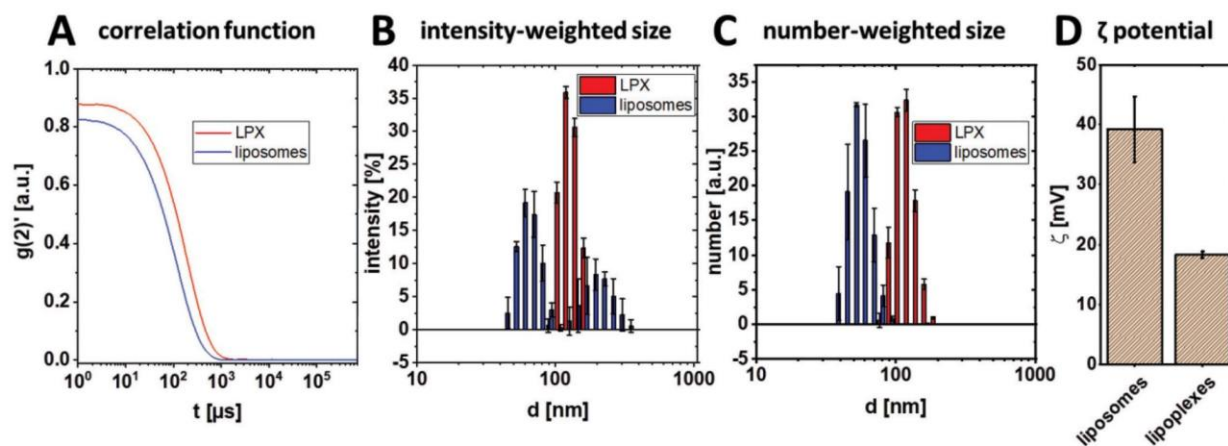


Figure 2. Correlation functions (representative of three measurements) A) of DLS measurements and the resulting B) intensity-weighted and C) number-weighted size distribution curves of OO4/DOPE liposomes (blue line) and LPX (0.1 μg pDNA, N/P 4) in 0.15 M NaCl containing 10 mM sodium acetate buffer at pH 4. D) Zeta potential results of OO4/DOPE liposomes and LPX. Results are means and standard deviations of three measurements (B–D).

2.2.18. Gene Expression Analysis

After 28 days of differentiation, the mRNA was extracted from samples using Aurum Total RNA Mini Kit spin columns from BioRad (Hercules, CA, USA) according to the manufacturer's recommended procedure. First, strand cDNA was synthesized using an iScript Advanced cDNA Synthesis Kit for RT-qPCR (real-time quantitative polymerase chain reaction, Biorad) in 20 μL reactions, according to the manufacturer's instructions. A CFX Connect RT-qPCR Detection System (Biorad) and pre validated primer sets PrimePCR Probe Assays from Biorad were used for gene expression analysis of the transcription factor Noggin (assay ID: qHsaCEP0054879), Collagen type 1 alpha 1 (Col1A1; assay ID: qHsaCEP0050510), Run-related transcription factor 2 (RunX2; assay ID: qHsaCEP0051329), Alkaline Phosphatase (ALP; assay ID: qHsaCEP0024224), and BMP-2 (assay ID: qHsaCIP0029912). RPLP0 (assay ID: qHsaCEP0041375) was used as housekeeping gene. Data analysis was performed using the BioRad CFX Manager Software 3.0. The following scheme was used for the RT-qPCR: 95 $^{\circ}\text{C}$ for 30 s followed by 39 cycles at 95 $^{\circ}\text{C}$ for 15 s and 60 $^{\circ}\text{C}$ for 30 s. The relative expression levels of each gene were calculated and normalized to the housekeeping gene RPLP0 using the DDCT method ($2^{-\Delta\Delta\text{Ct}}$).^[59]

2.2.19. Statistical Analysis

All statistical analyses were performed with Origin 8G software. If not stated otherwise, experiments were performed in triplicates ($n = 3$) and the results presented as means \pm standard deviation (SD). If the number of experiments n was different from 3, the value of n was given in the caption. Analysis of significance was performed by one-way ANOVA followed by Scheffé post hoc test with $\alpha = 0.05$. A value of $p < 0.05$ was considered as a significant difference and was indicated by an asterisk. Further, box plots are shown where appropriate. The box indicates the 25th and 75th

percentiles, the median (dash), and mean value (black square), respectively.

3. Results and Discussion

3.1. Characterization of Lipoplexes

The lipid formulation OO4/DOPE 1/3 (n/n) (hereinafter referred to as OO4/DOPE) was used to prepare LPX as transfection active component for the gene-activated surface coating. OO4 is a cationic peptide-mimicking amphiphile designed in our group^[43,55] and provided the positive charge for DNA complexation as well as PEMs assembly. DOPE is a commonly used co-lipid for lipid-based transfection agents. For efficient immobilization of LPX into PEMs via electrostatic interaction, a positive net charge was essential. DLS and zeta potential measurements were carried out to obtain information on particle size and charge of OO4/DOPE liposomes and, more substantially, of LPX under LbL preparation conditions. The data are presented in **Figure 2**. The autocorrelation function (Figure 2A) was characterized by intercepts at 0.9 for LPX (red) and 0.8 for liposomes (blue), a sigmoidal decay of the signal and the absence of a noisy baseline, indicating a good quality of DLS data for reasonable fitting. For the liposomes, the intensity-weighted size distribution showed a bimodal function, with a particle size population at diameter (d) ≈ 50 –100 nm and $d \approx 200$ –400 nm (Figure 2B). For multimodal size distributions, the intensity-weighted curve can be misleading because the scattering intensity is proportional to $\approx d^6$. Hence, small numbers of larger particles can dominate the distribution function. Therefore, the number-weighted size distribution curves were calculated (Figure 2C), showing that the 50–100 nm population was in a much higher quantity than expected from the intensity-weighted curve (compare blue size distribution curves). In contrast, LPX showed an unimodal size distribution with $d \approx 100$ –200 nm, in both intensity- and number-weighted curves (Figure 2B,C). The observed changes in particle size of LPX, compared to the liposomes, are probably due to the lipid

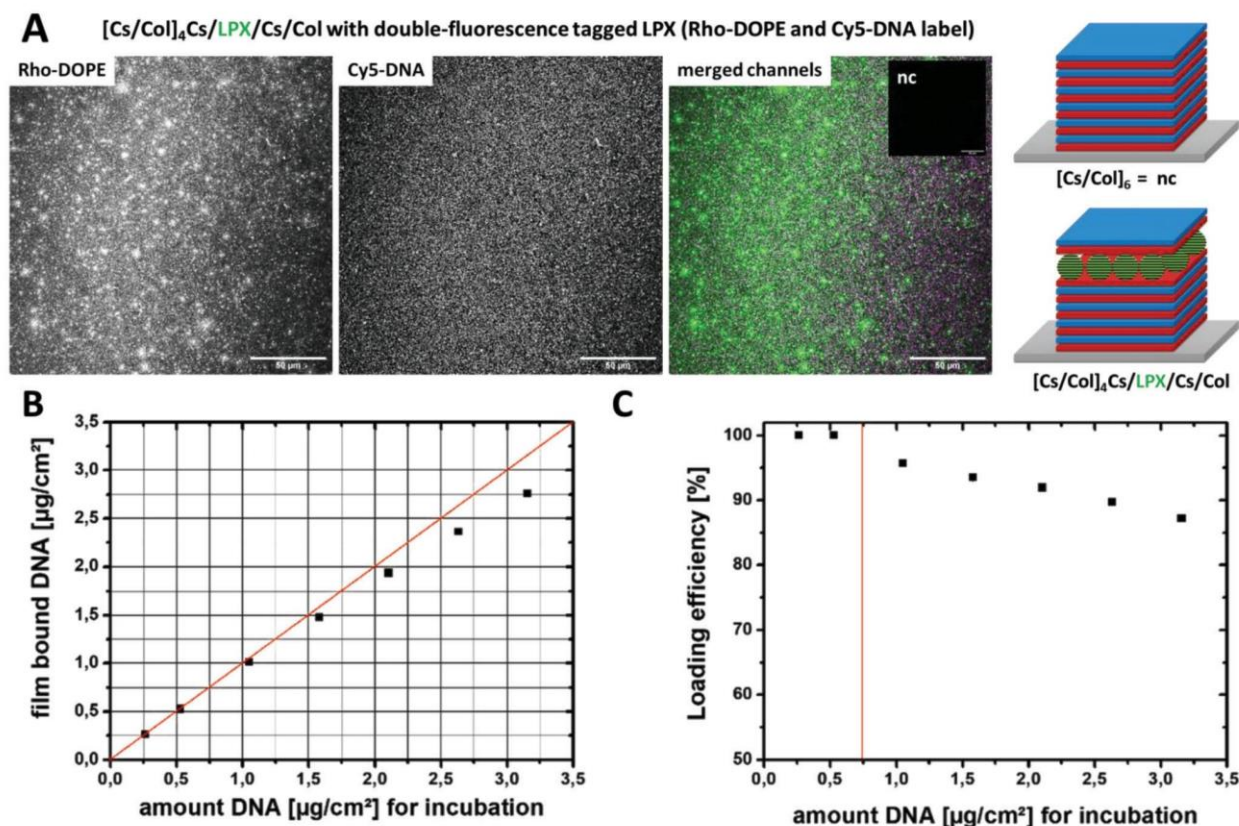


Figure 3. A) CLSM micrograph (40 \times magnification) of [Cs/Col]₄Cs/LPX/Cs/Col PEMs with fluorescent tagged LPX. The following fluorescence labels were used: Rho-DOPE as lipid label (left image in grey scale, green in the merged right image) and Cy5-labeled pDNA (middle image grey scale, magenta in the merged image right), which were used to visualize LPX attached to the PEMs. The inlay on the merged image (right), labeled with nc = negative control, was the LPX-free negative control [Cs/Col]₆ which was examined under the same conditions as proof for the absence of auto-fluorescence effects of the polyelectrolytes. The scale bars indicate 50 μ m. Images were analyzed using ImageJ. B) Schematic illustration of the PEM sequence codes [Cs/Col]₄Cs/LPX/Cs/Col (sample) and [Cs/Col]₆ (negative control). C) Film-bound amount of DNA in μ g cm⁻² in [Cs/Col]₄Cs/LPX/Cs/Col films as a function of the total DNA concentrations in the incubation medium (0.26–3.15 μ g cm⁻² LbL substrate). The calculation of the film-bound DNA was based on the indirect quantification of the non-bound DNA using agarose gel experiments presented in Figure S2, Supporting Information ($n = 3$). The red line shows the theoretical values of 100% binding efficiency. D) The calculated DNA loading efficiency from (C). Above is an LPX incubation with total DNA amount of 0.75 μ g cm⁻² PEM substrate (indicated by the red line); the loading efficiency decreases below 100%. (B,D) show the means \pm SD of triplicates. The bars indicate that the SD are below 0.04 μ g cm⁻²; and therefore, are not seen due to resolution of the graphs.

membrane reorganization process during the complex formation between DNA and the cationic liposomes, based on the templating effect of DNA.^[60,61] Comparing zeta potential measurements of liposomes and LPX, a decrease in the zeta potential from $\zeta \approx 38$ mV to $\zeta \approx 18$ mV was observed (Figure 2D) due to complex formation between the positively charged liposomes and the negatively charged DNA. Nevertheless, the positive net charge of the LPX for embedding into PEMs was proven.

3.2. Structural Characterization of PEMs with Focus on LPX Embedding

The embedding of LPX into PEMs composed of Cs and Col was demonstrated by CLSM using dual fluorescence-tagged LPX: The pDNA was covalently labeled with Cy5 and the lipid composite was modified with 1.25-mol% Rho-DOPE as fluorescence

label (Figure 3A). The images indicate a homogeneous distribution of the labeled DNA as well as the lipid in the PEM [Cs/Col]₄Cs/LPX/Cs/Col, considering the film curvature which leads to out-of-focus effects in the edge regions. Nevertheless, both channels do not fit in all details (merged images Figure 3A), an observation which can be explained by the fact that at a lipid-DNA loading ratio of N/P 4, some DNA-free cationic liposomes exist besides LPX.^[62] The LPX-free control [Cs/Col]₆ (Figure 3A, insert labeled with nc = negative control) shows no autofluorescence of the polyelectrolytes using the same experimental setup.

The DNA loading efficiency of [Cs/Col]₄Cs/LPX/Cs/Col films was determined in more detail. It was not possible to quantify DNA embedded in PEMs directly by gel electrophoresis or fluorescence passed assays in a reproducible manner. The appearance of colloids after disintegration of LPX-loaded PEMs, resulting in quenching and light-scattering effects,^[63] may explain this problem. Recently, we described a method for an indirect

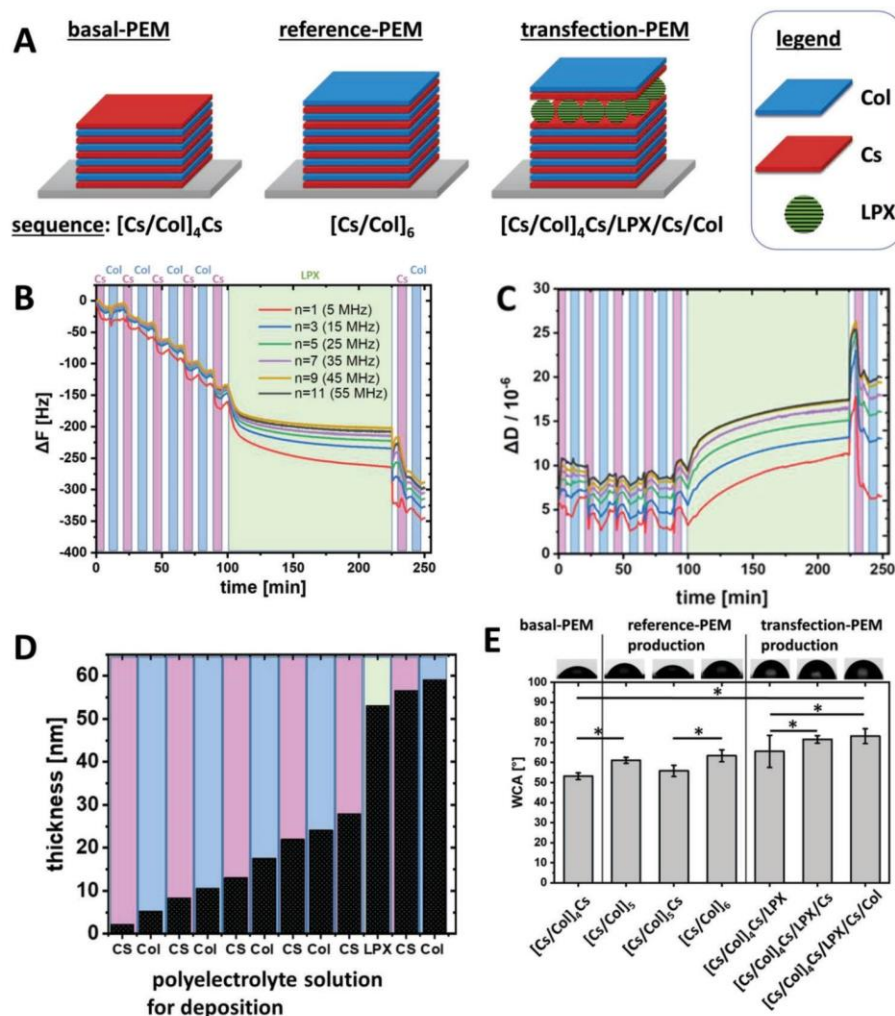


Figure 4. A) Schematic illustration of the LbL sequence codes of investigated PEMs. B–D) Build-up of $[\text{Cs}/\text{Col}]_4\text{Cs}/\text{LPX}/\text{Cs}/\text{Col}$ multilayered thin films onto Au-plated quartz crystal sensors via incubation with polyelectrolyte solutions to achieve LbL deposition. QCM-D monitoring of the normalized frequency (ΔF , panel B) and dissipation (ΔD , panel C) shifts. The frequency shifts of different overtones are presented. The dissipation shift is shown for the 7th overtone (35 MHz). The background color indicates the incubation/washing medium: magenta = Cs; blue = Col; green = LPX; white = washing buffer (B,C). Cumulative hydrodynamic thickness evolution for the $[\text{Cs}/\text{Col}]_4\text{Cs}/\text{LPX}/\text{Cs}/\text{Col}$ PEM production, obtained using the Voigt-based viscoelastic model (D). E) Static WCA measurement of intermediate and final PEM structures. The x-axis demonstrates the film composition deposited as sequence code. Results represent means \pm SD with $n = 10$; significance was tested using one-way ANOVA followed by Scheffé post hoc test, $\alpha = 0.05$, $*p \leq 0.05$.

quantification of DNA-LPX loading into PEMs by quantifying the fraction of DNA which was not incorporated in PEMs.^[48] For this purpose, the DNA of the supernatant and washing solutions, which was most likely complexed in LPX, was quantified via gel electrophoresis, a method which needed a pre-incubation with heparin to release all DNA from LPX (for details, see Figures S1 and S2, Supporting Information). The results are presented in Figure 3B,C. The incorporation of different amounts of DNA, from 0.26 to 3.15 $\mu\text{g cm}^{-2}$, was evaluated. Up to a loading amount of $\approx 0.75 \mu\text{g cm}^{-2}$, the LPX can be efficiently incorporated into the LbL system (loading efficiency of 100%, Figure 3C). PEMs with concentrations above 0.75 $\mu\text{g cm}^{-2}$ resulted in loading efficien-

cies below 100% (Figure 3C). In other studies on polyplex-loaded PEMs, a much lower DNA content of 25–30 ng cm^{-2} was described, showing that PEMs consisting of Cs and Col and loaded with LPX represent an excellent system for gene-activated PEMs.^[64] To evaluate whether LPX are desorbed from the PEM during subsequent rinsing steps, the washing solutions were also examined for DNA content, showing no burst release of adsorbed LPX or released DNA from the PEMs (for details, see Figure S2, Supporting Information).

QCM-D measurements were performed to monitor the material deposition during the LbL assembly process in situ. In **Figure 4B**, the frequency shift of different overtones is plotted.

The stepwise decrease of ΔF indicates the successful deposition of material, Cs, Col, or LPX, respectively, after each incubation step. Multilayer growth was thus proven for each deposition step. The interaction of the charged biopolymer or LPX with the oppositely charged surface was effective under the chosen assembly conditions with a pH value of 4 and 150 mM NaCl as electrolyte solution. The time to reach the adsorption equilibrium was much longer for LPX when compared to Cs and Col. Nevertheless, the time periods needed for deposition provide evidence that we reached the adsorption equilibrium with the PEM preparation protocol used in this study (Section 2.2.5). The following rinsing step did not result in an increase of ΔF ; thus, excluding the eventual desorption of adsorbed LPX. The evaluation of the dissipation changes demonstrated a pronounced increase in ΔD during LPX adsorption (Figure 4C, green area). Obviously, the plastic proportion in the viscoelastic behavior increased, concluding that the PEM gets softer and more hydrated due to the adsorption of LPX. The high ΔD value remained also after the deposition of the Cs and Col cover layers on the PEM film (final sequence [Cs/Col]₄Cs/LPX/Cs/Col). Obviously, the LPX dominated the film mechanics even with the outermost Cs/Col layers. Previous structural investigation has demonstrated that the LPX composed of OO4/DOPE are soft matter nanoparticles with a liquid crystalline substructure;^[65] consequently, a viscoelastic behaviour was expected. Furthermore, the cumulative hydrodynamic thickness evolution during the construction of the multilayer film was calculated from QCM-D data (Figure 4D). A linear increase of thickness was observed for the deposition of either Cs or Col. The thickness increase of ≈ 30 nm after LPX deposition was much higher compared to the biopolymers. Nevertheless, the DLS size distribution curves (Figure 2B,C) resulted in a main LPX diameter of 100–150 nm, a much higher value. Two facts may explain the discrepancy: 1) The LPX do not cover the whole area (we have evidence for that conclusion from CLSM micrographs; see also Figure 3A) combined with the fact that the QCM-D determined thickness is a mean thickness. 2) As mentioned above, LPX are soft matter nanoparticles, and a deformation and flattening of the LPX nanoparticles after adsorption on the surface can be expected.

The wetting behaviour of surfaces is an important parameter because moderate wettable surfaces with WCA $\approx 60^\circ$ promote protein adsorption and cell adhesion.^[66] Figure 4E shows the WCA of selected intermediates and the final construct of the DNA-activated PEM and the LPX-free reference PEM of comparable layer number. Starting from the basal-PEM [Cs/Col]₄Cs, which was the substrate for the LPX adsorption, a WCA of $\approx 53^\circ$ was measured, indicating a moderate wettability related to the presence of Cs as more hydrophilic molecule with carboxylic and sulfate groups.^[67] When LbL was continued with Col adsorption (sequences [Cs/Col]₃), a WCA of $\approx 61^\circ$ was detected, which is related to additional presence of amino groups in the protein which are less wettable than anionic groups. The alternating WCA lower for anionic Cs and higher for Col terminal layers indicates the dominance of these molecules in the outermost layer of PEMs.

The adsorption of LPX (PEMs sequence [Cs/Col]₄Cs/LPX) resulted in an increase of WCA to $\approx 66^\circ$ compared to the previous WCA of $\approx 53^\circ$ terminal Cs layer which is related to the cationic nature of the LPX. A further coating with Cs (PEM se-

quence [Cs/Col]₄Cs/LPX/Cs) caused an increase of WCA to 72° which may be related to some structural rearrangements of LPX upon contact with Cs which may be related to the presence of hydrophobic parts of lipid species, observed also in a previous study with liposomes.^[53] The terminal Col coating [Cs/Col]₄Cs/LPX/Cs/Col resulted in no significant change in WCA ($\approx 73^\circ$) which indicates some intermingling of LPX layer with Cs and Col in the terminal layer related also to the much larger size of LPX compared to both polyelectrolytes.^[54]

AFM was performed to study the surface topography and mechanical properties of the different PEMs (Figure 5). To investigate the elasticity and the force curve, the samples were compressed by the AFM tip and the force mapping mode was applied while the tip scanned a specific area of the sample.^[68] The force mapping mode measured the interaction forces such as adhesion or electrostatics and gives an idea regarding the stiffness and topography. The interest in testing mechanical properties and topography of surface coatings is related to their effect on cell behavior, such as spreading, proliferation, and differentiation.^[69,70] In addition, intermediate LbL process steps were investigated to learn more about the LPX deposition and the embedding process. The basal-PEM [Cs/Col]₄Cs, which was the substrate for LPX adsorption, showed a homogeneous nanofibrous network that can be assigned to Col deposition and fibrillation with a roughness of ≈ 12 nm (Figure 5A, Table 1). Previous studies demonstrated that Col/Cs PEMs are characterized by a fibrillary structure of Col.^[57,67,71] Due to its high charge density, Cs is known to promote the Col self-assembly to fibrils.^[72] After the adsorption of LPX, the surface topography changed showing a less organized fibrillary substructure (Figure 5B) but an increase of the roughness ≈ 23 nm (Table 1). Diffuse structures of different sizes were observed for the [Cs/Col]₄Cs/LPX film. In addition, the remaining fibrous structures appeared with a larger thickness of higher variability and more extended smeared structures (Figure 5B, arrowhead). The addition of a covering Cs layer induced the reappearance of the fibrillary topography with a roughness of ≈ 15 nm (Figure 5C, Table 1). The final DNA activated PEMs [Cs/Col]₄Cs/LPX/Cs/Col was characterized by an extended fibrillary structure, comparable to the basal-PEM (compare Figure 5A with Figure 5D; Figure S3, Supporting Information). The addition of the soft matter nanoparticles such as LPX might modify the arrangement of the Col fibers and it can influence the roughness. The behavior is also expressed by the roughness parameters shown in Table 1. R_a and R_q increased after LPX adsorption ([Cs/Col]₄Cs \rightarrow [Cs/Col]₄Cs/LPX) but decreased again to the initial values for the full PEMs. The same tendency can be seen in the waviness parameters $R3z$ ISO, W_a , and W_q (Table S1, Supporting Information).

Figure 5E presents the E_0 modulus distribution curves of the highest and lower points in the measured area. The sequence [Cs/Col]₄Cs was characterized by a broad distribution with a maximum value at $E_0 = 199$ kPa while a minimum value was seen above 50 kPa. The mechanical properties of the basal layer show the Col fibers with higher stiffness (maximum) than the surrounding area (minimum). It is known that highly negatively charged polysaccharides such as Cs have interfusing characteristics in PEMs and can act as a cross-linker for Col, supporting also the organization of fibrils and making these areas of PEMs stiffer.^[53] The adsorption of LPX reduced the stiffness of

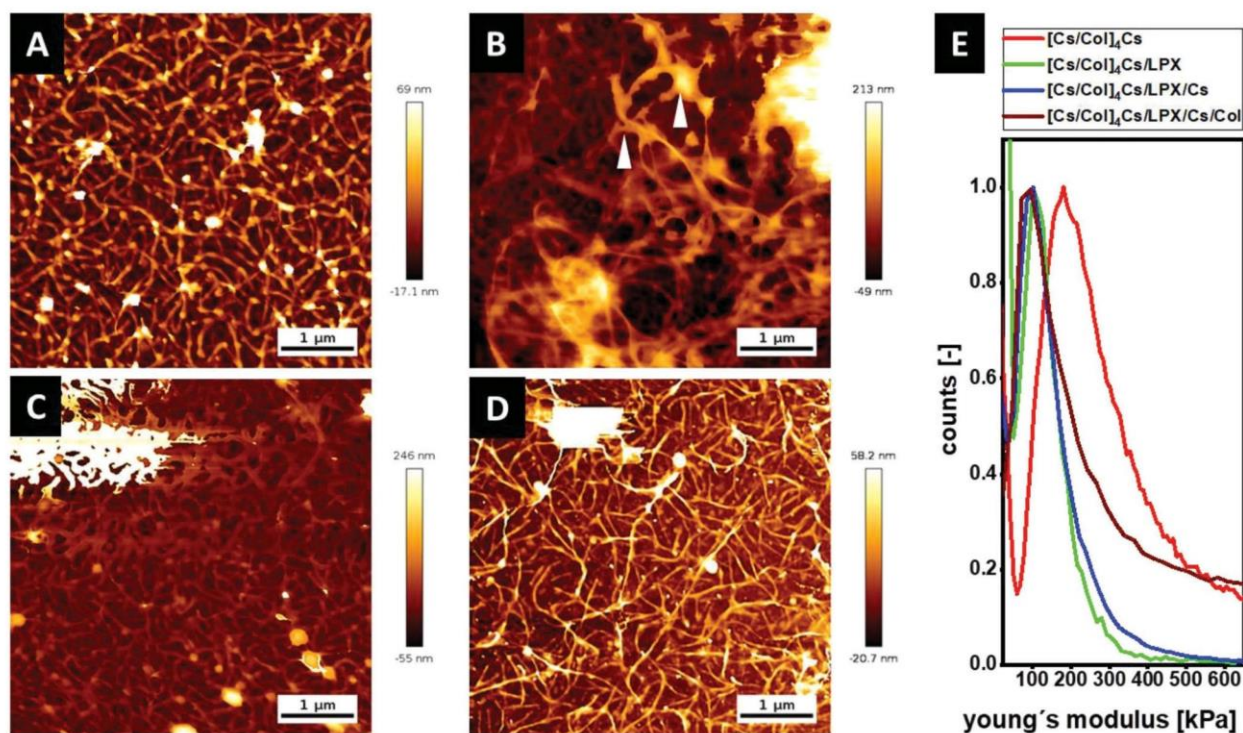


Figure 5. A–D) Topography images $[\text{Cs}/\text{Col}]_4\text{Cs}$ (A), $[\text{Cs}/\text{Col}]_4\text{Cs}/\text{LPX}$ (B), $[\text{Cs}/\text{Col}]_4\text{Cs}/\text{LPX}/\text{Cs}$ (C), and $[\text{Cs}/\text{Col}]_4\text{Cs}/\text{LPX}/\text{Cs}/\text{Col}$ determined by AFM [Scale bar $1\ \mu\text{m}$] (D). E) Distribution curves of Young's modulus (E_0) with a force map of a defined area (see also Figure S4, Supporting Information).

Table 1. Roughness parameters of area mean roughness (R_a), area root mean squared roughness (R_q) of PEMs sequences before and after LPX deposition. 1D roughness analysis, according to DIN EN ISO 4287, 4288, 3274, mean values \pm SD calculated from ten separate lines, $l_n = 5\ \mu\text{m}$, $D_c = 1\ \mu\text{m}$, cutoff filter: 0.02 measured by AFM.

	R_a [nm]	R_q [nm]	E modulus [kPa]
$[\text{Cs}/\text{Col}]_4\text{Cs}$	9.6 ± 0.9	12.2 ± 1.3	199.5 ± 6.3
$[\text{Cs}/\text{Col}]_4\text{Cs}/\text{LPX}$	18.6 ± 2.7	23.5 ± 3.3	111 ± 3.1
$[\text{Cs}/\text{Col}]_4\text{Cs}/\text{LPX}/\text{Cs}$	12.0 ± 1.8	15.5 ± 2.4	103 ± 3.5
$[\text{Cs}/\text{Col}]_4\text{Cs}/\text{LPX}/\text{Cs}/\text{Col}$	9.4 ± 1	12.8 ± 1.8	98 ± 4.5

the PEMs showing a shift of E_0 distribution curve to a maximum value of 111 kPa for $[\text{Cs}/\text{Col}]_4\text{Cs}/\text{LPX}$. An explanation is that LPX represent liquid crystalline soft matter particles, which can reduce the stiffness.^[65] It is interesting to note that further adsorption of Cs, and then, Col caused a further decrease of E_0 to 103 and 98 kPa, respectively. The lower E_0 values of PEM after LPX adsorption and the additional bilayer of Cs/Col are also related to an increased thickness of PEMs that will further reduce the E modulus of the coating due to swollen character of PEMs fabricated from biopolymers.^[73] Furthermore, this observation is also in line with the effect of the LPX observed for the ΔD values discussed in the QCM-D section above.

In summary of WCA and AFM studies, the complete PEMs $[\text{Cs}/\text{Col}]_4\text{Cs}/\text{LPX}/\text{Cs}/\text{Col}$ is characterized by moderate wettabil-

ity and a higher roughness promoting cell adhesion.^[74] What's more, a decrease in the stiffness of PEM was observed when LPX and the additional Cs/Col bilayer were added; the observed E modulus in the range of 100 kPa was still supporting cell attachment and spreading as found in other studies.^[69]

3.3. Mobility of LPX Incorporated in PEMs

Potential time dependent changes of the LPX layer in the PEMs $[\text{Cs}/\text{Col}]_4\text{Cs}/\text{LPX}/\text{Cs}/\text{Col}$ stored in PBS were studied using CLSM. Although because of their relatively large size and the electrostatic interaction with the polyanion Cs, a fast diffusion of LPX in the multilayer system was not expected. Nevertheless, two different experiments were performed to investigate if LPX have a certain mobility in PEMs. In the first experimental setup, Cy5 labelled DNA was used for the preparation of LPX which were afterward embedded in the PEMs. These samples were examined regarding the Cy5 fluorescence intensity at different time points of incubation in PBS by CLSM: directly after PEMs construction, as well as 24 h, 4 days, and 35 days after fabrication of PEMs. The results are shown in Figure 6A. A weak trend of a decrease in Cy5 fluorescence was observed, but all detected differences were not statistically significant. Therefore, it can be assumed that the DNA of the LPX remained entrapped in the PEMs within the time interval of 35 days. The large size of DNA (3.5 kbp, 260 kDa) in LPX and the complexation with the cationic lipids are certainly the reasons for the stability of the system.

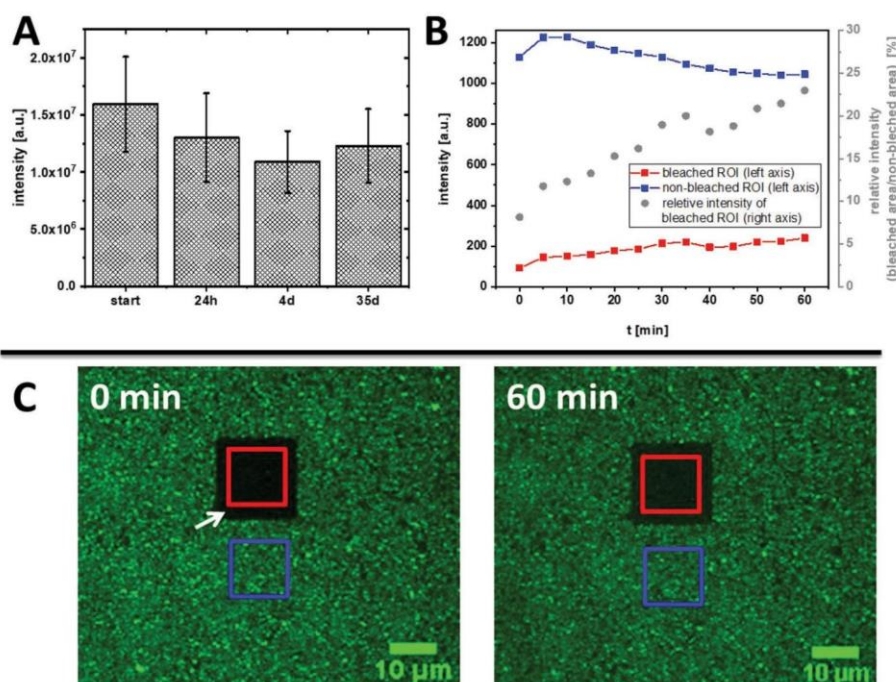


Figure 6. A) Fluorescence intensity of covalently labeled Cy5 DNA in LPX immobilized in PEM [Cs/Col]₄Cs/LPX/Cs/Col. CLSM-based intensity determination was done directly after the film construction (start) and after 1, 4, and 35 days. The results are given as means ± SD ($n = 36$). Significance was tested using one-way ANOVA followed by Scheffé post hoc test, $\alpha = 0.05$, $*p \leq 0.05$, no significant difference was found. B,C) Results of FRAP studies. Fluorescence intensity of NBD-DOPE was used as fluorescence probe in LPX (1 mol-% of the lipid composite). A defined area was bleached with high laser intensity and micrographs for intensity determination were taken in a period of 60 min after bleaching. Images were analyzed using ImageJ (B). CLSM images of [Cs/Col]₄Cs/LPX/Cs/Col loaded with NBD-labeled LPX directly (0 min) and 60 min after bleaching. The white arrow indicates the bleached region which appeared black due to successful fluorophore inactivation. The red square indicates the area applied to the fluorescence intensity determination of the bleached region in diagram (B); the blue square indicates the reference area of a non-bleached region (C).

In the second experimental setup, FRAP experiments were performed (Figure 6B,C). Here, the lipid components of LPX were fluorescence tagged. NBD-DOPE as efficiently bleachable fluorophore was used for the LPX preparation. Then, the PEM with embedded LPX was bleached at an area by applying high laser intensity (red box, Figure 6C). This photobleached area was examined for recovery of NBD fluorescence for 60 min. Indeed, a weak but steady increase in NBD fluorescence was detected in the bleached area. However, only $\approx 10\%$ of the intensity of the non-bleached reference area reappeared after 60 min (Figure 6B, red symbols). Note that the fluorescence in the control region was slightly decreasing (Figure 6B, blue symbols), an effect most-likely assigned to photo bleaching. This would imply that the calculated relative intensity change (Figure 6B, blue symbols) is biased, and the real reappearance is lower. Hence, only a small fraction of non-bleached fluorophores diffused into the bleached region, indicating that lipid components of LPX have certain mobility. Smaller molecules can diffuse in PEMs, as for example demonstrated for small model peptides.^[75]

Summarizing, it can be concluded that the DNA is stably entrapped in LPX which will also be evident by the subsequent transfection studies.

3.4. Cell Studies

3.4.1. Cell Adhesion and Proliferation of Mesenchymal Stem Cells on LPX-Loaded PEMs

Interaction of hADSCs with PEMs substrates was studied by staining nuclei used for cell counting, actin cytoskeleton used for cell spreading analysis, and the evaluation of focal adhesion (FA) as marker of cell-ECM contact points. Cells cultured on glass as positive control showed an extended phenotype with longitudinal organization of actin filaments and well-developed vinculin-positive FA in the cell periphery, indicating a normal behavior of these cells (Figure 7A, actin fibers shown in green). Cells cultured on LPX-free PEMs [Cs/Col]₆ were characterized by a longitudinal distribution of the actin filaments as well (Figure 7B, actin fibers shown in green). Many vinculin-positive FA were detected (Figure 7B, red signal in the merged image and signal in the lower single channel image). Cells on the intermediate PEM construct [Cs/Col]₄Cs/LPX were less extended, but also, a longitudinal organization of actin filaments was observed (Figure 7C, actin fibers shown in green). Slightly fewer and larger vinculin-positive FA were predominantly observed at the cell periphery (Figure 7C, red signal in the merged image and signal

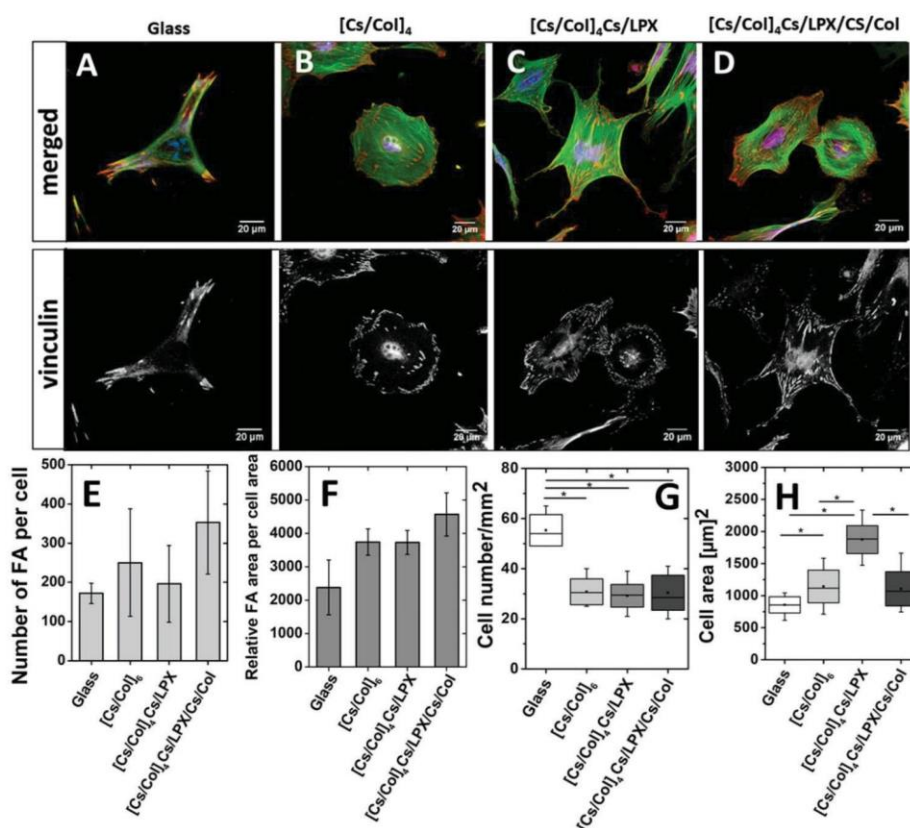


Figure 7. A–D) Merged CLSM image of adherent hADSCs cultured on the different PEMs after 4 h of incubation in serum. Glass slide (A), [Cs/Col]₆ (B), [Cs/Col]₄Cs/LPX (C), and [Cs/Col]₄Cs/LPX/Cs/Col (D). The cells were stained for filamentous actin (green), vinculin-positive FA (red), and nuclei (blue) in the merged images. The vinculin channel is shown separately in gray scale below the merged image. The scale bar represents 20 μm. E) Gives the quantification of vinculin-positive FA number per cell and F) relative vinculin-positive FA area per cell determined by Image J for representative six cells ($n = 6$; significance was tested using one-way ANOVA followed by Scheffé post hoc test, $\alpha = 0.05$, $*p \leq 0.05$, no significant difference was found). G) Quantification of cell count per square millimeter and H) cell spreading area (μm^2) on each of the PEMs after 4 h ($n = \text{ten images per condition}$). (Box plots with whiskers, representing first and third quartiles, medians and means. The star (*) indicates statistically significant differences using one-way ANOVA followed by Scheffé post hoc test, $\alpha = 0.05$, with a p -value ≤ 0.05 (F,G).

in the lower single channel image). Cells cultured on PEMs [Cs/Col]₄Cs/LPX/Cs/Col showed spread hADSCs with parallel arrangement of actin filaments (Figure 7D, green staining) and extended cell protrusions. Distinct vinculin-positive FA were observed at the cell protrusions and cell periphery (Figure 7D, red staining merged image and signal in the lower single channel image). The quantitative evaluation of FA showed no statistically significant differences between the positive control and PEMs; for both, the number of FA per cell and the relative area of vinculin positive FA. In addition, no statistical difference was found between the different PEMs. However, a trend to higher values was observed for PEMs [Cs/Col]₄Cs/LPX/Cs/Col (Figure 7E,F). The higher number of cells on the positive control in comparison to all PEMs shown in Figure 7G is probably related to the stiffness of glass that promotes cell attachment.^[76] On the other hand, the quantification of the cell area (Figure 7H) demonstrated that hADSCs on glass had a smaller cell area in contrast to [Cs/Col]₄Cs/LPX PEM that showed higher cell spreading (Figure 7H). The determined cell areas for the reference PEMs

[Cs/Col]₆ and [Cs/Col]₄Cs/LPX/Cs/Col were comparable and in between the values of glass and [Cs/Col]₄Cs/LPX PEM. As is known, cell spreading is a promoter of osteogenic differentiation so the PEMs made of Cs/Col may support osteogenesis of hADSCs.^[77] Moreover, the presence of Col as component of all PEMs can be considered as a promoter of mitogenic signal transduction through integrin receptors such as $\alpha 2\beta 1$ integrin, the main receptor for Col.^[59]

The proliferation of hADSCs was studied by QBlue assay evaluating metabolic activity of cells seeded on glass slides (positive control), PEMs [Cs/Col]₆, [Cs/Col]₄Cs/LPX, and [Cs/Col]₄Cs/LPX/Cs/Col. In Figure 8, it is shown that cells seeded on glass showed higher metabolic activity in contrast to PEMs, which relates to the results of adhesion studies. For all three surface coatings, a significant increase of the metabolic cell activity from day 1 to day 4 was observed (Figure 8) indicating cell growth with no differences among them on day 1. Comparing the cell growth on subsequent days, it was seen that [Cs/Col]₆ provided superior conditions while the presence of LPX in the

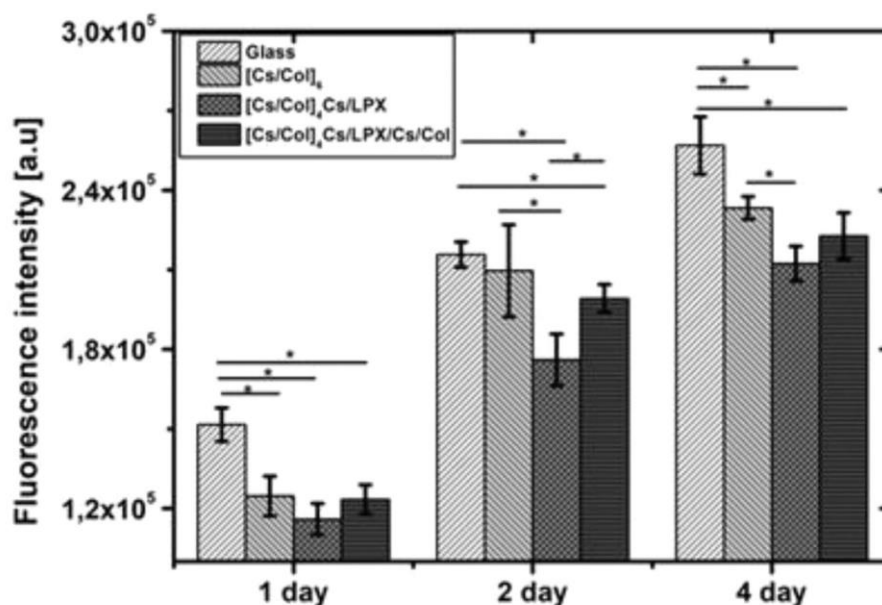


Figure 8. Growth of hADSCs seeded on PEMs sequence of glass slide (control), [Cs/Col]₆, [Cs/Col]₄Cs/LPX, and [Cs/Col]₄Cs/LPX/Cs/Col measured by the QBlue assay after 24, 48, and 96 h. The values represent means \pm SD with $n = 3$. The star (*) indicates statistically significant differences using one-way ANOVA followed by Scheffé post hoc test, $\alpha = 0.05$, with a p -value ≤ 0.05 .

two other systems had a slightly inhibiting effect on cell growth with significantly lower values comparing [Cs/Col]₄Cs/LPX with [Cs/Col]₆. This may be related to the cationic nature of LPX that may exert certain toxicity though adhesion studies did not provide any hints for that.^[51] Overall, all PEMs enabled attachment, spreading and growth of cells, as a prerequisite for subsequent cell differentiation studies.

3.4.2. Transfection Studies

Successful transfer of DNA from [Cs/Col]₄Cs/LPX/Cs/Col into hADSCs is essential for a clinical in situ transfection strategy. To study the cellular uptake, LPX were loaded with Cy5 labeled DNA. The fluorescent tagged LPX were embedded in the [Cs/Col]₄Cs/LPX/Cs/Col multilayer. Afterward, hADSCs were seeded onto the fluorescent tagged in situ transfection system and cells were evaluated after 2 days by CLSM (Figure 9). Cellular uptake of the Cy5 labeled DNA was demonstrated, showing a Cy5 fluorescence signal accumulated in the perinuclear region (Figure 9, yellow arrows). However, it is described in the literature that the Cy5 label preferentially tends to accumulate in mitochondria because of their higher mitochondrial membrane potential compared to normal cells, which is why DNA is hardly recognizable in the cell nucleus.^[78,79] The mechanism of LPX-uptake by cells from the PEMs [Cs/Col]₄Cs/LPX/Cs/Col is not understood in detail. However, a cell-mediated endocytosis can be assumed despite the presence of a cover layer because it was demonstrated previously that mesenchymal stem cells can actively remodel Col of Cs/Col-based PEMs.^[57] Moreover, we recently described successful endocytosis of liposomes from CS/Col-based PEMs into

C2C12 myoblasts adhering to the coating.^[54] It is further known that endocytotic uptake is the main route for LPX into cells.^[62,80] To proof efficient DNA transfer to the nucleus, reporter gene transfection experiments were also performed.

The DNA transfer activity of the gene-activated PEM was evaluated using a pDNA encoding for GFP as reporter gene (Figure 10). Besides the DNA-activated PEM [Cs/Col]₄Cs/LPX/Cs/Col, the intermediate PEM [Cs/Col]₄Cs/LPX (surface adsorbed LPX which were not protected by a cover layer) and the LPX-free reference PEM [Cs/Col]₆ with LPX in the supernatant, were used for comparison. These controls enable an assessment of the influence of the cover layer on the transfection on the one hand and whether embedding LPX in PEMs has an impact on the transfection efficiency on the other. After 24 h, the highest efficiency was detected for the system [Cs/Col]₄Cs/LPX ($\approx 16\%$ GFP positive cells), while the final PEM [Cs/Col]₄Cs/LPX/Cs/Col showed a slightly reduced efficiency ($\approx 12\%$ GFP positive cells). The control with LPX in the supernatant showed the lowest intensity. At 48 h after incubation, no significant differences were observed among the three groups and efficiency values of $\approx 17\text{--}20\%$ GFP positive hADSCs were detected. The immobilization of LPX seems to trigger a fast contact between LPX and cells, leading to higher efficiency of the systems with PEM bound LPX after 24 h. This kinetic effect levels off after 48 h. The results demonstrated that LPX immobilization had no diminishing effect on the efficacy of the LPX formulation in the time frame studied. In addition, the transfection efficacy of 20% was promising to proceed experiments with BMP-2 encoding DNA as autocrine and paracrine effects could be expected when 20% of the hADSCs growing on the PEMs express the gene of interest.^[81]

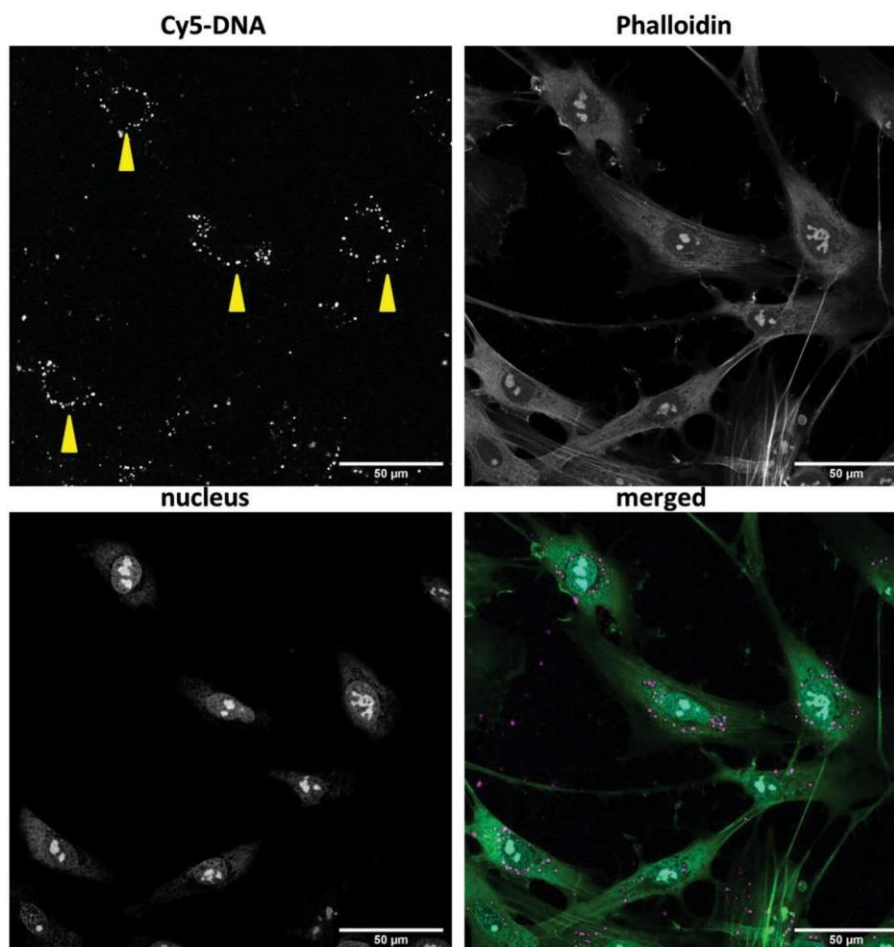


Figure 9. CLSM micrograph of transfected hADSCs after 48 h grown on [Cs/Col]₄Cs/LPX/Cs/Col with Cy-5 labeled DNA (merged image magenta). The cells are stained for filamentous actin with Phalloidin-Atto 488 (merged image green) and nucleus with BOBO-1 (merged image cyan). Images were taken at 40x magnification and evaluated with ImageJ. The bar represents 50 µm. Images are given as single channels and merged. The provided image is an optical cross section taken by CLSM analysis. An additional optical cross section at lower z-value near the PEMs surface is given in Figure S5, Supporting Information.

3.4.3. Osteogenic Differentiation of Mesenchymal Stem Cells on BMP-2-Gene Activated LPX-Loaded PEMs

In this section, the transfection-active surface coating [Cs/Col]₄Cs/LPX/Cs/Col was loaded with LPX with complex BMP-2-encoding DNA. Potentially, successful BMP-2 expression can lead to autocrine or paracrine BMP-2 effects by transfected cells. Gene expression analysis of specific osteoblast markers was performed by mRNA quantification. The expression of five osteogenesis-related genes (RunX-2, BMP-2, ALP, Col1A1 and Noggin) was quantified by RT-qPCR 28 days after hADSCs were seeded on [Cs/Col]₄Cs/LPX/Cs/Col (**Figure 11**). As medium for the experiments, we have chosen OM, which contained essential components for osteogenic differentiation: β -Gly serves as a source of phosphate in hydroxyapatite structures, Dex has an enhancing stimulus on BMP-2 effect, and ASC is an enhancer of collagen type 1 secretion.^[82,83] The following controls were chosen: cells cultured in BM on surfaces without PEM coating

were used as negative control due to the absence of inductors for osteogenic differentiation (**Figure 11**, non-coated; BM). As positive control, hADSCs were cultured on surfaces without PEM coating using the StemPro Osteogenic-Differentiation Kit provided by the supplier of the stem cells (**Figure 11**, non-coated; StemPro). StemPro has an optimized mix of supplements and cytokines to reliably induce differentiation to osteocytes. As further necessary control, hADSCs in OM growing on [Cs/Col]₆ in the absence of LPX were examined because of two reasons: 1) we know from our previous work that PEMs composed of ECM components can also trigger differentiation and want to estimate that effect^[53,54,57] and 2) due to the possibility to trigger osteogenic differentiation by Dex of the OM.^[84] Nevertheless, as biogenic glucocorticoids exert profound effects on bone and are essential for human osteoblast differentiation, we decided to keep Dex in the OM. The presence of BMP-2 in Dex containing OM has enhancing effects on the osteogenic differentiation of stem cells.^[85]

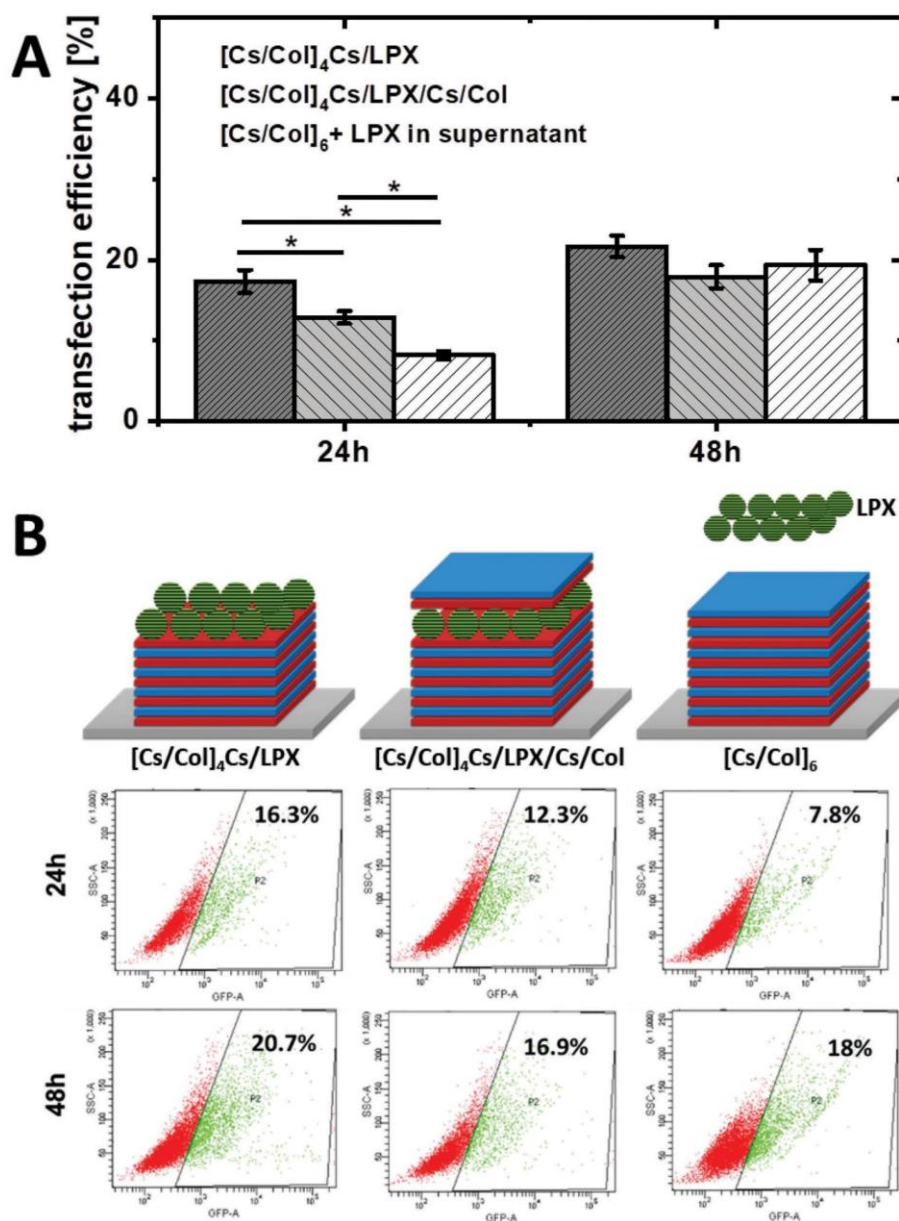


Figure 10. Transfection efficiency of the three examined PEMs sequences: [Cs/Col]₄Cs/LPX, [Cs/Col]₄Cs/LPX/Cs/Col, and [Cs/Col]₆ (LPX in supernatant). A) Transfection efficiency as fraction of GFP positive cells at 24 and 48 h after beginning of cell incubation. Error bars represent means \pm SD ($n = 3$), statistically significant differences using one-way ANOVA followed by Scheffé post hoc test, $\alpha = 0.05$, with a p -value ≤ 0.05 . B) Representative flow cytometry dot plots representing side scatter of cell light scattering (SSC-A) and the fluorescence intensity in the GFP-sensitive channel (GFP-A) of hADSCs seeded on [Cs/Col]₆ (LPX in supernatant), [Cs/Col]₄Cs/LPX, and [Cs/Col]₄Cs/LPX/Cs/Col. Green color corresponds to GFP positive cells with a higher fluorescence signal compared to the auto fluorescence of cells, and red color to the GFP-negative cells. The negative control of cells growing on [Cs/Col]₆ in the absence of LPX is presented in Figure S6, Supporting Information.

Analysis of the expression level of the mentioned osteogenic markers demonstrated that cells grown on BMP-2 gene-activated [Cs/Col]₄Cs/LPX/Cs/Col exhibited enhanced expression of all osteo-specific genes compared to the negative control (Figure 11). For BMP-2, [Cs/Col]₄Cs/LPX/Cs/Col showed a clearly increased expression by 15-fold. This observation demonstrated the suc-

cessful transfection and expression of the encoded gene in the DNA-activated PEMs. The positive control (non-coated; Stem-Pro) also showed a 5-fold increased BMP-2 expression but significantly lower compared to the [Cs/Col]₄Cs/LPX/Cs/Col multilayer. Osteogenic differentiation can also be associated with increased BMP-2 expression, which accelerates the differentiation

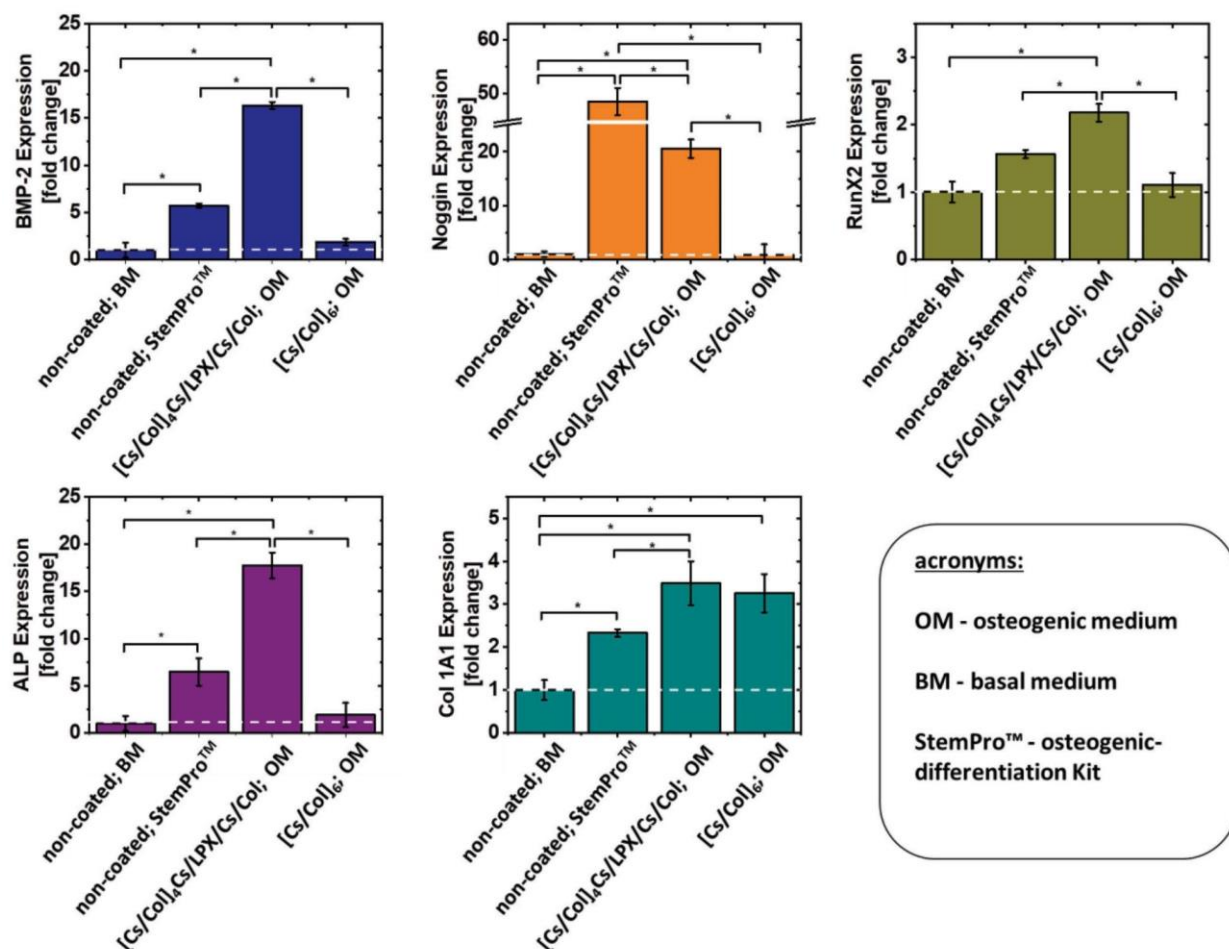


Figure 11. RT-qPCR analysis of representative osteogenic markers: BMP-2, ALP, Col 1A1, Noggin, and RunX2. The results represent the gene expression at day 28 of the osteogenic differentiation experiments. For the BMP-2 gene activated PEMs [Cs/Col]₄Cs/LPX/Cs/Col hADSCs were seeded on the multilayer in OM, containing β -Gly, Dex, and ASC but no BMP-2 or other cytokines). Multilayer film control without LPX hADSCs was grown on [Cs/Col]₆ in OM as medium to check for differentiation triggered by the two ECM components. For positive control, cells grew on non-coated wells and were treated with StemPro osteogenic-differentiation Kit from Thermo Fisher Scientific, containing supplements and cytokines for efficient osteogenic differentiation of hADSCs (non-coated; StemPro). For negative control, hADSCs grew on non-coated wells and were treated with BM (non-coated; BM). Results represent means \pm SD, with $n = 3$; statistically significant differences using one-way ANOVA followed by Scheffé post hoc test, $\alpha = 0.05$, with a p -value ≤ 0.05 .

process.^[86] The LPX-free PEM control film ([Cs/Col]₆; OM) showed no significant difference to the negative control (non-coated; BM) for the BMP-2 expression. As an antagonist of BMP-2, we investigated the expression of the osteogenic marker Noggin.^[87] Noggin was significantly upregulated for the positive control (non-coated; StemPro), and the transfection system [Cs/Col]₄Cs/LPX/Cs/Col also showed an increased expression of this marker (Figure 11). This was significantly higher for the positive control; although, the BMP-2 expression was significantly lower compared to the BMP-2 gene-activated PEM. It is known from literature that Noggin has a biphasic dose-dependent expression, and it has been reported that at lower BMP-2 concentrations (0.01 to 1 $\mu\text{g mL}^{-1}$), Noggin induction is enhanced. By contrast, induction of Noggin is diminished when BMP-2 concentrations are shifted from 1 to 50 $\mu\text{g mL}^{-1}$.^[88] This behavior could explain why the positive control has a lower BMP-2 ex-

pression but more than twice as much Noggin expression as cells growing on the [Cs/Col]₄Cs/LPX/Cs/Col multilayer. Nevertheless, this explanation remains speculative because the BMP-2 amount in our experiments was not quantified, a focus of ongoing research. The third marker, RunX2, is one of the most important transcription factors, which is especially important in the early phase of osteogenic differentiation as it is upregulated in pre-osteoblasts and downregulated in mature osteoblasts.^[89] For the sample [Cs/Col]₄Cs/LPX/Cs/Col and the positive control, RunX2 is upregulated. The BMP-2 gene-activated PEM has significantly higher RunX2 values compared to all controls (Figure 11). The same expression pattern is found for ALP (Figure 11), which is needed to generate phosphate ions from natural sources for the hydroxyapatite matrix of bone tissues. The significantly highest ALP expression is found in cells growing on the [Cs/Col]₄Cs/LPX/Cs/Col. The last screened marker was

Col1A1 because expression of the Col1A1 gene occurs mainly during the shift from early to mature stages of osteoblast maturation, when the osteoblasts start building the ECM.^[90] The [Cs/Col]₄Cs/LPX/Cs/Col, the positive control (non-coated; StemPro), and the LPX-free PEMs reference ([Cs/Col]₆; OM) show a significantly increased Col1A1 expression compared to the negative control (non-coated; BM) (Figure 11). That result can be expected for the [Cs/Col]₄Cs/LPX/Cs/Col and the positive control because the other osteogenic markers are also increased in the expression analysis. For the LPX-free [Cs/Col]₆ reference, Col1A1 is the only marker screened in this study which has statistically significant increase compared to the negative control (non-coated; BM). A closer look to the results for BMP-2, RunX2, and ALP expression of cells on LPX-free PEMs ([Cs/Col]₆; OM) shows a slight but non-significant increase of gene expression compared to the negative control (non-coated; BM). It is known from previous research that Col/Cs PEMs can promote osteogenic differentiation,^[57] which was why we have chosen these composites as main component for the DNA-activated PEM. Nevertheless, these studies demonstrated the additive effect of the ECM mimicking PEMs in combination with the in situ BMP-2 transfection.

To further evaluate osteogenic differentiation, all samples were tested for mineralization (Figure 12). At the final stage of osteoblast differentiation, the formation of mineralized nodules was a crucial phenomenon that indicates the maturation of osteoblasts. To evaluate this, Alizarin red staining was used to screen the degree of mineralization by visualizing calcium nodules after 24 days (stained red spots). Cells cultured on BMP-2 gene activated [Cs/Col]₄Cs/LPX/Cs/Col and positive control (non-coated, StemPro) developed large Alizarin positive nodules, a strong indication of hADSC undergoing osteogenesis. The poor performance of mineral nodules for hADSCs growing on [Cs/Col]₆ in OM may result from the lack of BMP-2, again demonstrating the enhancing effect of in situ BMP-2 transfection. As the bone ECM contains hydroxyapatite, a phosphate mineral with the composition Ca₁₀(PO₄)₆(OH)₂, a method for a mineral-specific staining provides more information than non-specific Alizarin staining. OsteoImage™, a commercially available hydroxyapatite specific fluorescence dye, was used to screen for these osteo-specific mineral deposition. The images from this staining confirm the results from alizarin red staining (Figure 12). Both the positive control (non-coated, StemPro) and the BMP-2 gene activated [Cs/Col]₄Cs/LPX/Cs/Col show pronounced hydroxyapatite structures after 24 days, which are absent in the negative control (non-coated, BM) and for hADSCs on [Cs/Col]₆ in OM. Concluding, the data from RT-qPCR are supported by these staining for the inorganic ECM components of bone tissue. The BMP-2 gene-activated PEM can induce osteogenic differentiation of hADSCs comparable to the positive control.

4. Conclusion

The main goal of this work was to develop a novel gene-functionalized ECM-mimicking multilayered thin film for implants coating. We demonstrated that it is possible to entrap LPX into PEMs composed of the bone ECM components Cs and Col

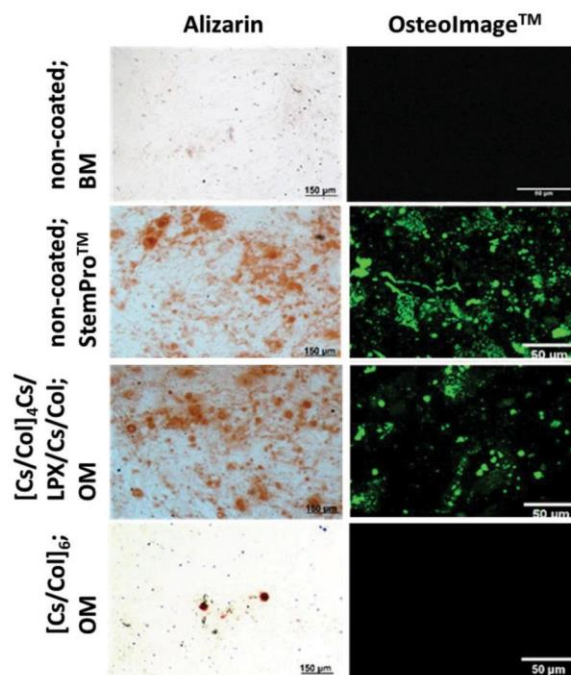


Figure 12. Histochemical (Alizarin) and fluorescence (OsteoImage™) staining for inorganic bone matrix at day 24 of the differentiation experiment. The alizarin staining appears for calcium structures red, while OsteoImage™ fluorescently stains hydroxyapatite with high specificity for CLSM investigation (here shown in green). To prove osteogenic differentiation with the developed PEMs, hADSCs were seeded on BMP-2 gene-activated [Cs/Col]₄Cs/LPX/Cs/Col in OM. PEMs without LPX was investigated with cells growing on [Cs/Col]₆ in OM. For positive control, cells grew on non-coated wells using the StemPro osteogenic-differentiation Kit to induce osteogenic differentiation. For negative control, hADSCs grew on non-coated wells using BM. Micrographs were taken for Alizarin staining at 10× magnification (bar represents 150 μm) and for OsteoImage™ staining at 40× magnification (bar represents 50 μm).

to engineer a nanoparticle functionalized thin film surface coating. The affinity of stem cells to the surface coating was proven as well as its ability of contact triggered transfection of cells growing on the gene-activated PEMs, triggering their differentiation into the osteogenic lineage. The transfection activity allows an in situ cytokine production which is spatially and temporally restricted due to the contact triggered transfection of cells with a non-viral gene delivery system, which only allows episomal gene uptake in cells resulting in a transient genetic modification. Hence, this PEM system is promising for clinical application as implant coating for bone tissue regeneration due to its camouflaging effect by mimicking bone ECM, providing an effective biological niche for osteogenic cell differentiation. The presented PEM-LPX system can also be used as an mRNA delivery system because mRNA also allows transient protein expression with promising opportunities for regenerative medicine.^[91] Therefore, this system is of high interest to develop novel alternatives for implant coating for future in vivo use in bone tissue regeneration and in other tissue engineering applications.

Supporting Information

Supporting Information is available from the Wiley Online Library or from the author.

Acknowledgements

C.H. and Y.A.B.B. contributed equally to this work. The authors are thankful for the help and support of Dr. Navarrete Santos during flow cytometry measurements and data analysis. Y.A.B.B. was supported by the Consejo Nacional de Ciencia y Tecnología (CONACYT-México) and Deutscher Akademischer Austauschdienst (DAAD) for funding. Furthermore, she received a grant from the International Graduate School AGRIPOLY supported by the European Regional Development Fund (ERDF) and Ministerium für Wissenschaft und Wirtschaft, Land Sachsen-Anhalt. C.H. was supported by DAAD which funded the exchange to University Aveiro. This work was funded by the Fraunhofer Internal Programs under Grant No. Attract 069-608203 (C.E.H.S.) and by the Programa Operacional Regional do Centro – Centro 2020, in the component FEDER, and by national funds (OE) through Fundação para a Ciência e a Tecnologia/Ministério da Ciência, Tecnologia e Ensino Superior (FCT/MCTES), in the scope of the project “SUPRASORT” (PTDC/QUI-OUT/30658/2017, CENTRO-01-0145-FEDER-030658). This work was developed within the scope of the project CICECO – Aveiro Institute of Materials, UIDB/50011/2020, UIDP/50011/2020 & LA/P/0006/2020, financed by national funds through the FCT/MEC (PIDDAC). The support by the Deutsche Forschungsgemeinschaft (DFG) project-ID 396823779 (C.W.) is acknowledged. J.B. gratefully acknowledges FCT for the individual Assistant Researcher contract (2020.00758.CEECIND).

Open Access funding enabled and organized by Projekt DEAL.

Conflict of Interest

The authors declare no conflict of interest.

Data Availability Statement

Research data are not shared.

Keywords

bone morphogenic protein 2, chondroitin sulfate, collagen I, human adipose-derived mesenchymal stem cells, lipoplexes, osteogenic differentiation, polyelectrolyte multilayers

Received: August 5, 2022

Revised: October 25, 2022

Published online:

- [1] R. A. Marklein, J. A. Burdick, *Adv. Mater.* **2010**, *22*, 175.
 [2] E. Piva, A. F. Silva, J. E. Nör, *J. Endod.* **2014**, *40*, S33.
 [3] P. Rosset, F. Deschaseaux, P. Layrolle, *Orthop. Traumatol.: Surg. Res.* **2014**, *100*, S107.
 [4] A. H. Undale, J. J. Westendorf, M. J. Yaszemski, S. Khosla, *Mayo Clin. Proc.* **2009**, *84*, 893.
 [5] V. Paspaliaris, G. Kolios, *Stem Cells Int.* **2019**, *2019*, 1730978.
 [6] X. Lin, S. Patil, Y.-G. Gao, A. Qian, *Front. Pharmacol.* **2020**, *11*, 757.
 [7] D. S. W. Benoit, M. P. Schwartz, A. R. Durney, K. S. Anseth, *Nat. Mater.* **2008**, *7*, 816.
 [8] J.-H. Hwang, U. Han, M. Yang, Y. Choi, J. Choi, J.-M. Lee, H.-S. Jung, J. Hong, J.-H. Hong, *Acta Biomater.* **2019**, *86*, 247.
 [9] M. B. Keogh, F. J. O'Brien, J. S. Daly, *Acta Biomater.* **2010**, *6*, 4305.
 [10] M. L. Macdonald, R. E. Samuel, N. J. Shah, R. F. Padera, Y. M. Beben, P. T. Hammond, *Biomaterials* **2011**, *32*, 1446.
 [11] C. Salvi, X. Lyu, A. M. Peterson, *Biomacromolecules* **2016**, *17*, 1949.
 [12] Y.-I. Chung, K.-M. Ahn, S.-H. Jeon, S.-Y. Lee, J.-H. Lee, G. Tae, *J. Controlled Release* **2007**, *121*, 91.
 [13] M. B. Rahmany, M. Van Dyke, *Acta Biomater.* **2013**, *9*, 5431.
 [14] B.-H. Luo, C. V. Carman, T. A. Springer, *Annu. Rev. Immunol.* **2007**, *25*, 619.
 [15] F. Gattazzo, A. Urciuolo, P. Bonaldo, *Bioch. Biophys. Acta* **2014**, *1840*, 2506.
 [16] R. O. Hynes, *Science* **2009**, *326*, 1216.
 [17] G. Decher, J.-D. Hong, *Macromol. Symp.* **1991**, *46*, 321.
 [18] J. Borges, J. F. Mano, *Chem. Rev.* **2014**, *114*, 8883.
 [19] A. M. Ferreira, P. Gentile, V. Chiono, G. Ciardelli, *Acta Biomater.* **2012**, *8*, 3191.
 [20] X. He, Y. Wang, G. Wu, *Appl. Surf. Sci.* **2012**, *258*, 9918.
 [21] S. Shu, C. Sun, X. Zhang, Z. Wu, Z. Wang, C. Li, *Acta Biomater.* **2010**, *6*, 210.
 [22] P. Gentile, I. Carmagnola, T. Nardo, V. Chiono, *Nanotechnology* **2015**, *26*, 422001.
 [23] V. Z. Prokopovic, A. S. Vikulina, D. Sustr, E. M. Shchukina, D. G. Shchukin, D. V. Volodkin, *ACS Appl. Mater. Interfaces* **2017**, *9*, 38908.
 [24] K. Gelse, *Adv. Drug Delivery Rev.* **2003**, *55*, 1531.
 [25] C. Dong, Y. Lv, *Polymers* **2016**, *8*, 42.
 [26] M. Büttner, S. Möller, M. Keller, D. Huster, J. Schiller, M. Schnabelrauch, P. Dieter, U. Hempel, *J. Cell. Physiol.* **2013**, *228*, 330.
 [27] N. S. Hwang, S. Varghese, H. J. Lee, P. Theprungsirikul, A. Canver, B. Sharma, J. Elisseeff, *FEBS Lett.* **2007**, *581*, 4172.
 [28] H. D. Kim, E. A. Lee, Y.-H. An, S. L. Kim, S. S. Lee, S. J. Yu, H. L. Jang, K. T. Nam, S. G. Im, N. S. Hwang, *ACS Appl. Mater. Interfaces* **2017**, *9*, 21639.
 [29] P. Cai, Z. Xue, W. Qi, H. Wang, *Colloids Surf. A* **2013**, *434*, 110.
 [30] T.-M. De Witte, L. E. Fratila-Apachitei, A. A. Zadpoor, N. A. Peppas, *Regener. Biomater.* **2018**, *5*, 197.
 [31] D. B. Asserson, H. Orbay, D. E. Sahar, *J. Craniofacial Surg.* **2019**, *30*, 703.
 [32] P. C. Bessa, M. Casal, R. L. Reis, *J. Tissue Eng. Regener. Med.* **2008**, *2*, 1.
 [33] P. C. Bessa, M. Casal, R. L. Reis, *J. Tissue Eng. Regener. Med.* **2008**, *2*, 81.
 [34] A. W. James, G. Lachaud, J. Shen, G. Asatrian, V. Nguyen, X. Zhang, K. Ting, C. Soo, *Tissue Eng., Part B* **2016**, *22*, 284.
 [35] A. Ramasubramanian, S. Shiigi, G. K. Lee, F. Yang, *Pharm. Res.* **2011**, *28*, 1328.
 [36] I. El Bialy, W. Jiskoot, M. Reza Nejadnik, *Pharm. Res.* **2017**, *34*, 1152.
 [37] R. E. De La Vega, A. Atasoy-Zeybek, J. A. Panos, M. Van Griensven, C. H. Evans, E. R. Balmayor, *Transl. Res.* **2021**, *236*, 1.
 [38] C. Jewell, D. Lynn, *Adv. Drug Delivery Rev.* **2008**, *60*, 979.
 [39] E. M. Saurer, C. M. Jewell, D. A. Roenneburg, S. L. Bechler, J. R. Torrealba, T. A. Hacker, D. M. Lynn, *Biomacromolecules* **2013**, *14*, 1696.
 [40] He Zhang, J.-J. Huang, J. Wang, Mi Hu, X.-C. Chen, W. Sun, Ke-F Ren, J. Ji, *ACS Biomater. Sci. Eng.* **2019**, *5*, 6610.
 [41] C. E. Thomas, A. Ehrhardt, M. A. Kay, *Nat. Rev. Genet.* **2003**, *4*, 346.
 [42] M. Rezaee, R. K. Oskuee, H. Nassirli, B. Malaek-Nikouei, *J. Controlled Release* **2016**, *236*, 1.
 [43] C. Wölk, C. Janich, U. Bakowsky, A. Langner, G. Brezesinski, *Adv. Colloid Interface Sci.* **2017**, *248*, 20.
 [44] B. R. Olden, Y. Cheng, J. L. Yu, S. H. Pun, *J. Controlled Release* **2018**, *282*, 140.
 [45] H. Kavanagh, S. Dunne, D. S. Martin, E. Mcfadden, L. Gallagher, J. Schwaber, S. Leonard, S. O'dea, *Cytotherapy* **2021**, *23*, 852.

- [46] V. Graceffa, *J. Genet. Eng. Biotechnol.* **2021**, *19*, 90.
- [47] H. Zhang, K.-F. Ren, H. Chang, J.-L. Wang, J. Ji, *Biomaterials* **2017**, *116*, 95.
- [48] C. Husteden, F. Doberenz, N. Goergen, S. R. Pinnapireddy, C. Janich, A. Langner, F. Syrowatka, A. Repanas, F. Erdmann, J. Jedelskaj, U. Bakowsky, T. Groth, C. Wolk, *ACS Appl. Mater. Interfaces* **2020**, *12*, 8963.
- [49] S. D. Hujaya, G. Marchioli, K. Roelofs, A. A. Van Apeldoorn, L. Moroni, M. Karperien, J. M. J. Paulusse, J. F. J. Engbersen, *J. Controlled Release* **2015**, *205*, 181.
- [50] C. A. Holmes, M. Tabrizian, *ACS Appl. Mater. Interfaces* **2013**, *5*, 524.
- [51] J. Giselbrecht, C. Janich, S. R. Pinnapireddy, G. Hause, U. Bakowsky, C. Wolk, A. Langner, *Int. J. Pharm.* **2018**, *541*, 81.
- [52] X. Zhang, L. Dai, A. Wang, C. Wolk, B. Dobner, G. Brezesinski, Y. Tang, X. Wang, J. Li, *Sci. Rep.* **2015**, *5*, 16559.
- [53] Y. A. Brito Barrera, C. Husteden, J. Alherz, B. Fuhrmann, C. Wolk, T. Groth, *Mater. Sci. Eng., C* **2021**, *131*, 112516.
- [54] Y. A. Brito Barrera, G. Hause, M. Menzel, C. E. H. Schmelzer, E. Lehner, K. Mäder, C. Wolk, T. Groth, *Mater. Today Bio* **2020**, *7*, 100071.
- [55] C. Wolk, S. Drescher, A. Meister, A. Blume, A. Langner, B. Dobner, *Chemistry* **2013**, *19*, 12824.
- [56] G. W. Gale, R. J. Small, K. A. Reinhardt, in *Handbook of Silicon Wafer Cleaning Technology*, 2nd ed. (Eds: K. A. Reinhardt, W. Kern), William Andrew Publishing, Norwich, NY **2008**, pp. 201–265.
- [57] M. Zhao, G. Altankov, U. Grabiec, M. Bennett, M. Salmeron-Sanchez, F. Dehghani, T. Groth, *Acta Biomater.* **2016**, *41*, 86.
- [58] D. Axelrod, D. E. Koppel, J. Schlessinger, E. Elson, W. W. Webb, *Biophys. J.* **1976**, *16*, 1055.
- [59] K. J. Livak, T. D. Schmittgen, *Methods* **2001**, *25*, 402.
- [60] B. A. Lobo, A. Davis, G. Koe, J. G. Smith, C. R. Middaugh, *Arch. Biochem. Biophys.* **2001**, *386*, 95.
- [61] E. Pozharski, R. C. Macdonald, *Biophys. J.* **2002**, *83*, 556.
- [62] N. Erdmann, C. Wolk, I. Schulze, C. Janich, M. Folz, S. Drescher, M. Dittrich, A. Meister, J. Vogel, T. Groth, B. Dobner, A. Langner, *Eur. J. Pharm. Biopharm.* **2015**, *96*, 349.
- [63] F. Caruso, H. Lichtenfeld, E. Donath, H. Möhwald, *Macromolecules* **1999**, *32*, 2317.
- [64] F. Meyer, V. Ball, P. Schaaf, J. C. Voegel, J. Ogier, *Biochim. Biophys. Acta, Biomembr.* **2006**, *1758*, 419.
- [65] S. Tassler, B. Dobner, L. Lampp, R. Ziolkowski, E. Malinowska, C. Wolk, G. Brezesinski, *Langmuir* **2019**, *35*, 4613.
- [66] N. Faucheux, R. Schweiss, K. Lützwow, C. Werner, T. Groth, *Biomaterials* **2004**, *25*, 2721.
- [67] M. Zhao, L. Li, C. Zhou, F. Heyroth, B. Fuhrmann, K. Maeder, T. Groth, *Biomacromolecules* **2014**, *15*, 4272.
- [68] N. Chen, B. Bhushan, *J. Microsc.* **2006**, *221*, 203.
- [69] A. J. Engler, L. Richert, J. Y. Wong, C. Picart, D. E. Discher, *Surf. Sci.* **2004**, *570*, 142.
- [70] B. K. Ekambaram, M. S. Niepel, B. Fuhrmann, G. Schmidt, T. Groth, *ACS Biomater. Sci. Eng.* **2018**, *4*, 1820.
- [71] R. Anouz, A. Repanas, E. Schwarz, T. Groth, *Macromol. Biosci.* **2018**, *18*, 1800283.
- [72] M. Sharabi, *Front. Mater.* **2022**, *8*, 793647.
- [73] J. Campbell, A. S. Vikulina, *Polymers* **2020**, *12*, 1949.
- [74] S. Cai, C. Wu, W. Yang, W. Liang, H. Yu, L. Liu, *Nanotechnol. Rev.* **2020**, *9*, 971.
- [75] D. Sustr, C. Duschl, D. Volodkin, *Eur. Polym. J.* **2015**, *68*, 665.
- [76] D. E. Discher, P. Janmey, Y.-L. Wang, *Science* **2005**, *310*, 1139.
- [77] R. Mcbeath, D. M. Pirone, C. M. Nelson, K. Bhadriraju, C. S. Chen, *Dev. Cell* **2004**, *6*, 483.
- [78] S. Lorenz, S. Tomcin, V. Mailänder, *Microsc. Microanal.* **2011**, *17*, 440.
- [79] A. R. Nödling, E. M. Mills, X. Li, D. Cardella, E. J. Sayers, S.-H. Wu, A. T. Jones, L. Y. P. Luk, Y.-H. Tsai, *Chem. Commun.* **2020**, *56*, 4672.
- [80] C. Janich, C. Wolk, F. Erdmann, T. Groth, G. Brezesinski, B. Dobner, A. Langner, *J. Controlled Release* **2015**, *220*, 295.
- [81] K. Yang, H.-J. Park, S. Han, J. Lee, E. Ko, J. Kim, J. S. Lee, J. H. Yu, K. Y. Song, E. Cheong, S.-R. Cho, S. Chung, S.-W. Cho, *Biomaterials* **2015**, *63*, 177.
- [82] F. Langenbach, J. Handschel, *Stem Cell Res. Ther.* **2013**, *4*, 117.
- [83] M. Yuasa, T. Yamada, T. Taniyama, T. Masaoka, W. Xuetao, T. Yoshii, M. Horie, H. Yasuda, T. Uemura, A. Okawa, S. Sotome, *PLoS One* **2015**, *10*, e0116462.
- [84] O. Ghali, O. Broux, G. Falgayrac, N. Haren, J. P. Van Leeuwen, G. Penel, P. Hardouin, C. Chauveau, *BMC Cell Biol.* **2015**, *16*, 9.
- [85] M. Jäger, J. Fischer, W. Dohrn, X. Li, D. C. Ayers, A. Czibere, W. C. Prall, S. Lensing-Höhn, R. Krauspe, *J. Orthop. Res.* **2008**, *26*, 1440.
- [86] G. Zheng, Z. Xie, P. Wang, J. Li, M. Li, S. Cen, S. A Tang, W. Liu, G. Ye, Y. Li, S. Wang, X. Wu, H. Su, Y. Wu, H. Shen, *Cell Death Dis.* **2019**, *10*, 350.
- [87] L. J. Brunet, J. A. McMahon, A. P. McMahon, R. M. Harland, *Science* **1998**, *280*, 1455.
- [88] C. Chen, H. Uludağ, Z. Wang, H. Jiang, *J. Cell. Biochem.* **2012**, *113*, 3672.
- [89] T. Komori, *Adv. Exp. Med. Biol.* **2010**, *658*, 43.
- [90] N. A. Twine, L. Chen, C. N. Pang, M. R. Wilkins, M. Kassem, *Bone* **2014**, *67*, 23.
- [91] E. R. Balmayor, *Curr. Opin. Biotechnol.* **2022**, *74*, 8.

Chapter 5:

Summary and future perspectives

This chapter will complete the study by summarizing the three main research findings about the research aims. It will also suggest opportunities for future perspectives.

This Ph.D. thesis has shown that the LbL technique can produce multifunctional surface coatings to adapt the composition and physicochemical properties of implant surfaces and permit the deposition of cationic liposomes composed of the co-lipid DOPE and the cationic lipid OO4 with a functional cargo. The characterization studies demonstrated a stable, uniform film with immobilization of the liposomes that can be taken up by myoblast cells (C2C12) even when covered with an additional bilayer of Cs and Col shown by studies with either hydrophilic or lipophilic model compounds. In addition, this work has shown that the use of dexamethasone embedded in liposomes in a Cs and Col system can be used to induce osteogenic in myoblast cells, and HA and Col system can induce osteo and chondrogenic differentiation of C3H10T1/2 cells in situ. In both systems, the cell studies have shown good cell adhesion which is important for the integration of implants related to cell growth and differentiation. The ability of the PEM-loaded Dex to induce osteogenic cell differentiation was observed qualitatively and quantitatively by histochemical staining of Alizarin red, fluorescence staining of osteo – chondrogenic markers, and quantification using qPCR. These results showed an increase in the osteogenic differentiation in contrast with the liposomes free in the medium. Furthermore, the PEM system can be used to functionalize various surfaces by adding pDNA in combination with liposomes (LPX) embedded into PEM. Here, the characterization studied showed a stable system and immobilization of the LPX on PEM. The characterization of these PEM with LPX demonstrated an increase of the layer thickness as well as the increase of the roughness

in the system, due to the re-arrangement of the collagen fibrils and the liposomes, similar results were found in the characterization of the liposomes embedded on previous PEMs. Also, human stem cells (hADSC) showed a high affinity to the surface coating as well as the transfection of the cells where the presence of plasmid encoding BMP-2 induced osteogenic differentiation.

The benefit of using col and Cs-HA is to mimic the ECM of the bone and have a biocompatible microenvironment. Also, the advantage of immobilization of the liposomes in PEM and adding the last cover bilayer is to protect them from degradation and spontaneous release of cargo, reducing the systemic effects and having a local delivery.

Results can be considered as a proof of concept of the combination of LbL systems with liposomes to design the microenvironment of cells by the composition of multilayers and the kind of cargo liposomes (e.g. osteogenic drugs, DNA) to induce differentiation of cells on implants. Additional experiments should focus on the evaluation of these PEM with embedded liposomes as a therapeutic potential of drug-delivering implant system *in vivo*, in order to analyze the inflammatory response and the osteoinductive properties of the coating in the bone remodeling process.

Acknowledgment

Foremost, I would like to express my sincere gratitude to my advisor Prof. Dr. T. Groth for the continuous support of my Ph.D. project, and his patience, motivation, hints, and constant encouragement throughout the learning process of this thesis. His guidance in this project helped me to grow not only professionally but also personally.

Many thanks to Dr. C. Wölk for been as a second supervisor during my Ph.D. project, I am grateful for his time and help in the preparation of liposome, reviewing the manuscripts, and providing important hints and comments. C. Husteden for her support.

I would like to acknowledge Prof Dr. Nuno Neves for his time in reviewing my thesis.

I would like to thank Dr. C. Schmelzer for his time in reviewing my thesis and also M. Menzel for their collaboration and attention in this project, and they allowed me to do some characterization experiments in Fraunhofer. Moreover, I am thankful to Dr. Navarrete Santos for his help and guidance in the flow cytometry experiments. Additionally, I want to thank Dr.-Ing. M, Niepel provided me with help and hints for using the confocal laser scanning microscope and his help in the surface plasmon resonance equipment. Also, I want to acknowledge Mrs. Porobin for her help and measuring the zeta potential and I am thankful for helping me not only in the laboratory but also in personal matters with the German language.

I could not have undertaken this journey without B. Ekambaram, M. Muhammad, and C. Willems that they were not only my colleagues, they are also my friends and my family. During the Ph.D., I met two more wonderful friends, Y. Lu, and H. Kindi and we worked together and we helped each other. All of them helped me not only in the laboratory but also outside it.

Special thanks to my friends M.E Perez, R. Gama, and Lis Ramirez for supporting me, listening, and motivating me during my Ph.D., and also no matter the distance, they always

bring me a part of Mexico. Also, to my friend M. Bassal, from the master to PhD, supporting me and listening, no matter the distance.

I am thankful to special persons F. Hans and J. Bierstedt to be all the time with me supporting in all aspects, listening, motivating me, making me happy when I needed it, and didn't leave me alone.

Words cannot express my deepest gratitude to my parents and sister for their support, advice, and motivation, for always being with me even in the distance, and for financial support when I needed it. I love them very much and thank you to believe in me, without them this dream would not have been possible. Also, to N. to be with me in the last part of my Ph.D.

Last but not least, I would like to acknowledge the CONACYT Mexico-DAAD for the financial support during my Ph.D. Also, I acknowledge the International Graduate School AGRIPOLY supported by the European Regional Development Fund (ERDF) and the Federal State Saxony-Anhalt for the financial support in the last part of my Ph.D.

Publication list with a declaration of self-contribution to research articles

1. Brito Barrera Y. A., Hause, G., Menzel, M., Schmelzer, C. E. H., Lehner, E., Mäder, K., ... & Groth, T. (2020). Engineering osteogenic microenvironments by the combination of multilayers from collagen type I and chondroitin sulfate with novel cationic liposomes. *Materials Today Bio*, 7, 100071.

My contribution was about 70%. I performed the synthesis, characterization, and measurements related to the multilayers and wrote the major part of the manuscript, except for part 3.1 Characterization of liposomes which was written by Dr. Wölk. The characterization of the liposomes was done by Dr. Wölk and Lehner from the group of Prof. Dr. K. Mäder. The AFM measurements were performed by M. Menzel from the group of Dr. Schmelzer at Fraunhofer Institute.

2. Brito Barrera, Y. A., Husteden, C., Alherz, J., Fuhrmann, B., Wölk, C., & Groth, T. (2021). Extracellular matrix-inspired surface coatings functionalized with dexamethasone-loaded liposomes to induce osteo- and chondrogenic differentiation of multipotent stem cells. *Materials Science and Engineering: C*, 131, 112516.

My contribution was about 60%. I performed the synthesis, characterization, and measurements related to the multilayers, and cell adhesion and wrote the major part of the manuscript. The characterization of the liposomes was done by Dr. Wölk. Ms. Alherz performed the differentiation studies. Husteden C. performed the qPCR studies.

3. Husteden, C., Brito Barrera, Y. A., Tegtmeyer, S., Borges, J., Giselbrecht, J., Menzel, M., ... & Groth, T. (2022). Lipoplex-functionalized thin-film surface coating based on extracellular matrix components as a local gene delivery system to control osteogenic stem cell differentiation. *Advanced Healthcare Materials*, 2201978.

My contribution was about 40% with the collaboration of Husteden, C with 40%. I performed the characterization and measurements related to the multilayers, cell adhesion, and transfection measurement and wrote half part of the manuscript. Characterization of liposomes which was written by Dr. Wölk. The FRAP and osteogenic differentiation experiment was done by Husteden, C. The AFM measurements were performed by M. Menzel from the group of Dr. Schmelzer at Fraunhofer Institute.

Curriculum vitae

Personal data

Name	Yazmin Angelina, Brito Barrera
Date and place of birth	28/01/1988 in Puebla, Mexico
Nationality	Mexican

Education

From August 2016 to present	<p>Ph.D. student in natural sciences in the field of Biomedical materials at Martin Luther University, Halle-Wittenberg, Germany</p> <p>Ph.D. topic: <i>Extracellular matrix-inspired surface coatings functionalized with cargo-loaded liposomes as drug/nucleic acid delivery system to induce osteogenesis</i></p> <p>Knowledge: Tissue engineering, controlled release, transfection, and biomaterials</p>
-----------------------------	--

October 2013- August 2016	<p>M.Sc. Pharmaceutical Biotechnology at Martin Luther University, Halle-Wittenberg, Germany</p> <p>Master thesis topic: <i>Development of cell spheroids for tissue engineering applications</i></p> <p>Knowledge: Tissue engineering, co-culture, spheroids</p>
---------------------------	---

August 2007- May 2012	<p>B.S. Pharmaceutical Sciences at the Universidad de las Américas Puebla, Mexico</p> <p>Bachelor thesis topic: <i>Synthesis of magnetic nanoparticles, surface functionalization and evaluation of toxicity in vitro</i></p> <p>Knowledge: nanomedicine for cancer treatment, controlled release, nanoparticles</p>
-----------------------	--

Professional experience

From November 2020 - July 2021	Research assistant at the Martin Luther University, Halle-Wittenberg, Germany
--------------------------------	---

February 2020	Staff in ESAO Winter School of the European Society for Artificial Organs (ESAO), Wittenberg. 113
	Supervisor of the master thesis in Pharmaceutical biotechnology of the student Mrs. J. Alherz at the Martin Luther University, Halle-Wittenberg Master thesis topic: Embedding of novel cationic liposomes to terminal layers of polyelectrolyte multilayer system of hyaluronic acid and collagen I to induce cell differentiation
November 2016	Collaboration project: <i>Endothelial and beta-cell composite aggregates for improved function of a bio-artificial pancreas encapsulation device</i> . MIRA Institute for Biomedical Technology and Technical Medicine, University of Twente, Enschede, Netherlands
January 2010 - May 2011	Scientist in the quality control laboratory of the pharmaceutical company, Janssen de México (Johnson & Johnson)

Knowledge

Languages

German: B1

B1: German language course at Martin Luther University, Halle-Wittenberg, Germany, 2020

A2: Goethe Certificate A2

German language course at the Carl Duisberg Center in Berlin, Germany, 2012

A1: German language at the Volkswagen Language Center, Puebla, Mexico, 2012

English: Advanced

Language exchange program at the University of Victoria British Columbia, Canada, 2011.

English language course at Interlingua Puebla, Mexico 2009-2012

Spanish: Native language

Publications

Lipoplex-functionalized thin-film surface coating based on extracellular matrix components as local gene delivery system to control osteogenic stem cell differentiation.

Husteden, C., Brito Barrera, Y. A., Tegtmeyer, S., Borges, J., Giselbrecht, J., Menzel, M., ... & Groth, T. (2022). *Advanced Healthcare Materials*, 2201978.

Extracellular matrix-inspired surface coatings functionalized with dexamethasone-loaded liposomes to induce osteo-and chondrogenic differentiation of multipotent stem cells.

Brito Barrera Y. A., Husteden, C., Alherz, J., Fuhrmann, B., Wölk, C., & Groth, T. (2021). *Materials Science and Engineering: C*, 112516.

Engineering osteogenic microenvironments by the combination of multilayers from collagen type I and chondroitin sulfate with novel cationic liposomes

Brito Barrera, Y. A., Hause, G., Menzel, M., Schmelzer, C. E., Lehner, E., Mäder, K., ... & Groth, T. (2020). *Materials Today Bio*, 100071.

Endothelial and beta-cell composite aggregates for improved function of a bioartificial pancreas encapsulation device.

Skrzypek, K., Brito Barrera, Y. A., Groth, T., & Stamatialis, D. (2018). *The International Journal of artificial organs*, 41(3), 152-159.

Cell viability and MRI performance of highly efficient polyol-coated magnetic nanoparticles.

Arteaga-Cardona, F., Gutiérrez-García, E., Hidalgo-Tobón, S., López-Vasquez, C., Brito-Barrera, Y. A., Flores-Tochihuitl, J., ... & Pal, U. (2016). *Journal of Nanoparticle Research*, 18(11), 345.

Conferences

- 2021 **Oral presentation:** *Development of osteogenic microenvironments using cationic liposomes embedded into a polyelectrolyte multilayer system.*
 Brito-Barrera YA, Menzel M., Schmelzer H. C., Wölk, C, Groth Th.
 31st Conference of the European Society of Biomaterials (ESB) together with 43rd Annual Congress of the Iberian Society of Biomechanics and Biomaterials (SIBB). Virtual
 5th-9th September 2021, Porto, Portugal
- Poster:** *Embedding novel cationic liposomes on the terminal layers of polyelectrolyte multilayer system to study the controlled release on myoblast cells.*
- 2020 Brito-Barrera YA, Wölk, C, Groth Th.
 ESAO Winter School 2020, 26th – 29th February 2020, Lutherstadt Wittenberg, Germany.
- 2019 **Oral presentation:** *Polyelectrolyte multilayer as a reservoir for novel cationic liposomes as a potential surface coating for medical implants for osteogenesis*
 Brito-Barrera YA, Wölk, C, Groth Th.
 46th Congress of the European Society for Artificial Organs (ESAO), 3rd – 7th September 2019, Hannover, Germany
- Oral presentation:** *Use of cationic liposomes embedded into polyelectrolyte multilayer system for controlled release*
 Brito-Barrera YA, Wölk, C, Groth Th
 10th International Congress in Nanotechnology in Medicine and Biology BioNanoMed, 15th – 17th April 2019, Graz, Austria
- Poster:** *Embedding novel cationic liposomes on the terminal layers of polyelectrolyte multilayer system to study the controlled release on myoblast cells*
 Brito-Barrera YA, Wölk, C, Groth Th
 Controlled Release Society, Local Chapter Meeting Leipzig, 7th – 8th March 2019, Leipzig, Germany
- Poster:** *Use of cationic Liposomes Embedded onto Polyelectrolyte Multilayer Systems for Controlled Release*
 Brito-Barrera YA, Wölk, C, Groth Th
 Controlled Release Society, Local Chapter Meeting Halle, 1st – 2nd March, 2018, Halle (Saale), Germany

- 2018 **Poster:** *Use of Cationic Liposomes Embedded onto Polyelectrolyte Multilayer Systems for Controlled Release.*
Brito-Barrera YA, Wölk, C, Groth Th
45th Congress of the European Society for Artificial Organs, 12th - 15th September 2018, Madrid, Spain
- Oral presentation:** *Use of cationic Liposomes Embedded onto Polyelectrolyte Multilayer Systems for Controlled Release*
Brito-Barrera YA, Wölk, C, Groth Th
Comprehensive Summer School on Tissue Engineering, 18th - 23rd June 2018 Trento, Italy
- 2017 **Poster:** *Development of an in situ transfection system for regeneration of bone*
Brito-Barrera YA, Wölk, C, Groth Th
44th Congress of European Society for Artificial Organs, 06th - 09th September, 2017, Vienna, Austria
- 2016 **Poster:** *Development of cell spheroids for tissue engineering applications*
Brito-Barrera YA, Groth Th
Mexican Week of Science and Technology, Embassy Mexico, 04th - 06th July, 2016, Berlin, Germany (Poster)

Selbstständigkeitserklärung

Hiermit erkläre ich gemäß § 5 der Promotionsordnung der Naturwissenschaftlichen Fakultät I der Martin-Luther-Universität Halle-Wittenberg, dass ich die Ergebnisse der vorliegenden kumulativen Dissertationsarbeit

Extracellular matrix-inspired surface coatings functionalized with cargo lipids as a delivery system to induce osteo-, chondrogenesis

am Institut für Pharmazie in der Arbeitsgruppe Biomedizinische Materialien unter Anleitung von Prof. Dr. rer. nat. habil. Thomas Groth selbständig erarbeitet und die Dissertation ohne fremde Hilfe verfasst habe.

Weiterhin erkläre ich, dass ich keine anderen als die von mir angegebenen Quellen und Hilfsmittel zur Erstellung meiner Dissertation verwendet habe. Den benutzen Werken wörtlich oder inhaltlich entnommene Stellen sind als solche gekennzeichnet.

Ferner erkläre ich, dass ich mich mit der vorliegenden Dissertationsarbeit erstmals um die Erlangung eines Doktorgrades bewerbe.

Halle (Saale), den 22.December 2022

MSc. Yazmin Angelina, Brito Barrera